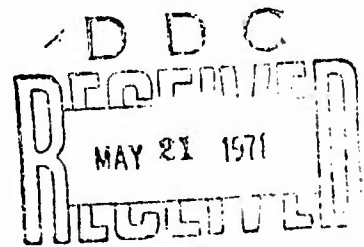AD723349

THE SHOCK AND VIBRATION BULLETIN

Part 4
Vibration

DECEMBER 1970

A Publication of
THE SHOCK AND VIBRATION
INFORMATION CENTER
Naval Research Laboratory, Washington, D.C.

Office of
The Director of Defense
Research and Engineering

D D C
RECEIVED
MAY 21 1971
C

DISCLAIMER NOTICE
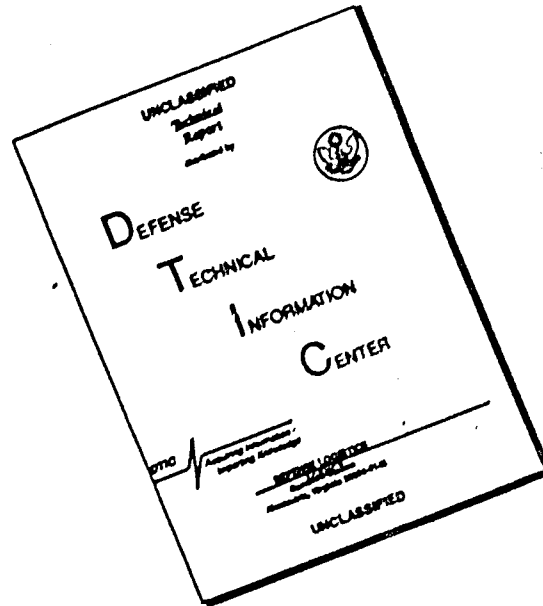
THIS DOCUMENT IS BEST
QUALITY AVAILABLE. THE COPY
FURNISHED TO DTIC CONTAINED
A SIGNIFICANT NUMBER OF
PAGES WHICH DO NOT
REPRODUCE LEGIBLY.

SYMPOSIUM MANAGEMENT

THE SHOCK AND VIBRATION INFORMATION CENTER

William W. Mutch, Director
Henry C. Pusey, Coordinator
Rudolph H. Volin, Coordinator
Edward H. Schell, Coordinator
Katherine G. Jahnel, Clerk Typist

Bulletin Production

Graphic Arts Branch, Technical Information Division,
Naval Research Laboratory

THE
SHOCK AND VIBRATION
BULLETIN

DECEMBER 1970

A Publication of
THE SHOCK AND VIBRATION
INFORMATION CENTER
Naval Research Laboratory, Washington, D.C.

The 41st Symposium on Shock and Vibration was
held at the Air Force Academy, Air Force Academy,
Colorado, on 27-29 October 1970. The U.S. Air Force
was host.

Office of
The Director of Defense
Research and Engineering

CONTENTS

PAPERS APPEARING IN PART 4

Vibration

PAPERS APPEARING IN PART 1
Part 1 - Classified
(Unclassified Titles)

DYNAMIC RESPONSE OF ABOVE-GROUND TARGETS TO A BLAST WAVE
P. N. Mathur, D. M. Rogers, R. H. Lee, and J. W. Murdock, The Aerospace Corporation, San Bernardino, California

v

PAPERS APPEARING IN PART 5

Shock

VIBRATION

SURVEY OF SPACE VEHICLE VIBRATION
ANALYSIS AND TEST TECHNIQUES

W. Henricks, R. J. Herzberg, B. G. Wrenn
Lockheed Missiles & Space Company
Sunnyvale, California

A space vehicle must survive a variety of environments during the launch, ascent and orbital sequences of its flight. One of the principal environments is the dynamic environment. Its prediction, related analysis and test procedures, test philosophy, recent experience and current results are discussed. Current areas of considerable interest in the industry are the analytical techniques for high frequency (>100 Hz) random vibration and the attendant current state-of-the-art testing techniques. These areas will receive particular attention with special emphasis on recent test results. The mission requirements of the space vehicles will not be discussed. Only the technology problems associated with the analysis and testing of space vehicle configurations is surveyed.

INTRODUCTION

This survey paper will discuss the dynamic environments that induce high frequency (>100 Hz) random vibration in a space vehicle and components thereof. Particular emphasis will be given to current state-of-the-art problem areas in both analysis and testing. No attempt will be made to provide an extensive bibliography as an excellent one already exists in the work of Lyon [1]. The methods employed will be discussed in detail only when such detail is not a repetition of that found in Ref. [1]. Further, some of the current work has not yet appeared in the open literature and hence the paper will present some new results as well. It should be further pointed out that there exists a variety of approaches and philosophies as to the particular analysis and testing techniques to be utilized. This paper presents our approach to the problem. This approach has been successful for Lockheed Missiles & Space Company (LMSC) and we believe it to be a viable one.

The area to receive particular attention is the high frequency vibration induced in the vehicle and its components by the inflight fluctuating pressure fields. This high frequency vibration service environment will be discussed in outline form in sufficient depth to establish the significance of the various sources relative to design analysis and ground test planning. Ground testing will then be categorized according to test objectives (e.g., development, qualification, acceptance, etc.), by test procedure (e.g., acoustic excitation or shaker excitation) and by level of assembly (e.g., component, subassembly, complete assembly and flight system).

The impact of new methods of testing, especially large scale acoustic testing, is presented together with a discussion of the recent advances in data usage made possible by the availability of on-line digital computers. Decisions can now be made during the test program rather than several weeks later. Selected examples of recent LMSC experience are presented.

The paper includes analysis techniques, recent test correlation and flight data. An explanation of totally broadband random versus random sweep random shaker type excitations (primarily for equipment testing) will be developed. The concept of the statistical method used for evaluating the zonal vibrational behavior will also be discussed. In addition, an application of peak counting will be presented. This technique affords a method for objectively evaluating the cumulative random vibration exposure (by introducing time as a parameter) that a given piece of equipment experiences. The paper concludes with some recent results of analysis and testing.

PHILOSOPHY OF TESTING

Structural dynamic testing programs are important and frequently costly portions of the engineering effort associated with the design and manufacture of spacecraft systems. The basic intent of such testing is to provide the cognizant program management with the highest practical confidence that their spacecraft-booster system will not suffer flight malfunction due to vibratory effects induced in the vehicle structure and components. In order for the testing to be effective, it is necessary that there be minimum risk of producing laboratory failures which are not representative of potential flight failures. Hence every effort must be made to assure that the proposed structural dynamic test is the best possible state-of-the-art simulation of the anticipated flight environment.

In an effort to obtain the best possible state-of-the-art simulation, the following three test

1

characteristics are desirable.

1. Frequency distribution – the vibrational energy should be distributed in all frequency bands of interest in a manner that simulates the service environment.

2. Spatial distribution – the vibrational energy should be distributed throughout the structure in a manner that simulates the service environment.

3. Control – the vibrational energy must be controlled to prevent unrealistically high levels at any point on the structure.

A brief discussion of shaker versus acoustic testing, for acoustically and aerodynamically induced random vibration, follows:

Shaker Excitation

The response at points on a structure that is excited at one or more locations, by shakers, will show large fluctuations in level between frequency bands. These fluctuations will, in general, exceed those of the service environment. This is caused by several factors. The excitation cannot efficiently excite nonresonant response in the structure with the consequence that the structural response is dominated by individual modes. If attention is restricted to a single point, these fluctuations can be minimized by varying the force delivered by the shaker. However, this presents serious control problems because of the high amplifications that are typical of structural resonances. It is then necessary to notch the test level in the vicinity of a resonance. However, since small differences in material properties and assembly procedures can shift the structural resonant frequencies, the frequency notches may be so wide as to compromise general test confidence.

In addition to large fluctuations between the frequency bands, shaker excitation can also induce large differences between different points on the structure. This phenomena is also associated with the single mode response pattern of shaker testing. Those points on the structure near nodal regions of the particular mode being excited can be expected to show very little response relative to those regions near anti-nodes. This not only compromises test confidence insofar as the nodal regions are concerned, but also presents control problems. A large number of structural points must be monitored to insure that no large anti-nodal response regions are overlooked when establishing the control levels.

Another cause of spatial variation of the vibrational energy is related to the apparent increase in structural damping with frequency. For spacecraft type structures, it is reasonable to expect great difficulty in delivering significant energy above 500 Hz to areas distant from the shaker locations without seriously overexciting regions near the shakers.

Acoustic Testing

The important difference between shaker and acoustic testing is the difference between the spatial distributions of the forcing functions. When acoustic excitation is used, it can be shown, through analysis of the joint acceptance functions of the structure, that there is a greater diffusion of vibratory energy at a specific point as well as between different points on the structure. This minimizes the dominance of individual structural modes and explains generally why acoustic fields are more efficient at exciting the non-resonant response. All of this only reflects what is obvious and apparent a priori. That is, the acoustic excitation is in reality a forcing function exciting each and every point on the structure (an infinite number of points) whereas shaker testing is limited to a finite (and usually small) number of discrete forcing functions. This, combined with the fact that acoustic testing is a much better simulation of the actual flight environment, explains why acoustic testing is getting more popular.

However, where individual components of the spacecraft are concerned, random vibration shaker testing is, in general, the best possible test. The inputs for the shaker test of components comes from acoustic testing of larger subassemblies and systems.

ROLE OF ACOUSTIC TESTING

Acoustic tests (as well as other testing) generally fall into the following three types:

1) development tests
2) qualification tests
3) flight acceptance tests

The intent of acoustic development testing is to provide information on those aspects of the component, bracketry and structural design which cannot be adequately handled by analysis. Such testing frequently utilizes engineering models of structural assemblies (e.g., mass simulated components). Acoustic testing of a flight type non-operational spacecraft system, at the complete assembly level, has been found to be a valuable tool for uncovering bracketry deficiencies. Such testing also serves to verify the component random vibration qualification specifications and helps develop consistent acoustic flight acceptance test procedures and levels.

Acoustic qualification tests are tests designed to prove the ability of the spacecraft system to withstand the anticipated inflight fluctuating pressure induced random vibration. The optimum test in this instance would utilize a test article which is flight identical and operational as a system. Because of uncertainties in predictions of the actual flight environment, and to cover normal variations in vehicle and flight fluctuating pressure characteristics, this type of testing is accomplished at levels which constitute an over-test vis-a-vis the best possible flight predictions. Failures uncovered during such testing are considered design defects and generally result in corrective redesign.

Flight acceptance tests are intended to uncover system peculiar defects associated with manufacturing and assembly procedures. They are generally performed on the actual flight vehicles prior to launch. Since these are preceded by the qualification test, the vehicle design is presumably adequate, and failures are normally remedied by rework of installations or replacement of defective components rather than by redesign of the system. It is extremely important that this type of testing be carefully planned and controlled, since the risk of creating incipient damage and thereby degrading the spacecraft performance always exists and must be kept to an absolute minimum. Acoustic acceptance testing is a valuable tool for gaining confidence in spacecraft performance.

The preceding discussion has dealt with acoustic testing of entire spacecraft systems or major subassemblies thereof. For individual pieces of equipment, it is desirable that the levels monitored (during systems testing) envelope the most extreme flight environments in all frequency bands. The actual test levels which are normally used, however, are somewhat lower than this most extreme envelope. This is so because of the excessive costs associated with designing all components to pass the maximum envelope environment. Acoustic development testing of spacecraft structural systems is very helpful in resolving the vibration environment at the component level. High response installations can be identified (i.e., those installations that respond at levels exceeding the component random vibration qualification levels) and corrective action (e.g., incorporation of vibration isolation mounts) taken. As an example of the above concept, Figure 1 shows random vibration levels on a component installation which were uncovered during a system level acoustic development test. The original levels substantially exceeded the qualification level for this component. Corrective action consisted of the relatively simple incorporation of rubber isolation washers and the resultant vibration was thereby reduced to acceptable levels. The component subsequently performed without malfunction during flight.

DISCUSSION OF SPACECRAFT FLIGHT ENVIRONMENTS

Atmospheric operation of space vehicles will be accompanied by fluctuating pressure sources on the external vehicle surfaces. This service environment is generated by such sources as engine exhaust noise, boundary layer turbulence, separated flow, base pressure fluctuations and oscillating shock waves. The various characteristics of interest for these environments are the distributions of pressure levels over the vehicle surface, frequency distributions, impingement angles, convection speeds and the spatial extent of a correlated fluctuating pressure field. These fluctuating pressure sources can be separated into either an acoustic, or an aerodynamic environment. By acoustic is meant pressure fluctuations that propagate with the speed of sound and are appropriately described by ordinary acoustic theory. The aerodynamic pressure fluctuations encompass a broader environment that includes turbulent boundary layer, separated flow, oscillating shock waves, etc. In addition to the random

vibration response induced by the fluctuating pressure distributions, there is also present the induced random response due to the mechanical excitation of the engines.

The acoustic environment (Fig. 2) exists during the short interval of time that the space vehicle is in the immediate vicinity of the launch pad. While it has been possible to obtain some analytical predictions of this environment, a sufficient body of measured data also exists so that a reasonable definition can be made of this environment. The important characteristics of this environment depend on the total power generated by the engine, efflux velocity of the exhaust issuing from the engine nozzle, the diameter of the nozzle exit plane, and the design of the launch pad flame buckets and exhaust tunnels. The spatial distribution of the overall sound pressure level over the length of the vehicle decreases as the measurement station moves forward of the engine exhaust.

The frequency spectrum typically peaks at approximately 100-500 Hz and rolls off rather rapidly with time. Due to this external environment, the internal equipment of the vehicle experiences a severe acoustically induced random vibration with significant energy distribution over a wide portion of the frequency spectrum. The power spectral density of the acceleration response is highly dependent upon localized installations and small changes can significantly shift the distribution of energy that a given piece of equipment experiences.

For upper stage space vehicles, the aerodynamic pressure fluctuations (Fig. 3) over local external surfaces, during flight through the transonic regime, can be in the order of 20dB higher than the liftoff acoustic environment. Such excitation is usually associated with oscillating shock-separated flow interactions. This aerodynamic environment is very difficult to predict and many features of it are clouded by uncertainties. Predictions are analytically cumbersome and an appropriate body of data does not exist to give a completely sufficient empirical definition. There are several approaches that can be taken to obtain further information on this environment; additional theoretical studies, wind tunnel tests on models and flight measurements on vehicles. As a practical matter, a combination of all three approaches is usually used. Theoretical and windtunnel studies establish such general features as overall levels and spectral shapes, while flight measurements are used to corroborate these features. The intensity of the aerodynamic pressure fluctuations can generally be correlated with the dynamic pressure, q, of the space vehicle, ranging from 0.6 to 20 percent of q. Maximum levels will occur between the Mach 0.8 and maximum dynamic pressure conditions depending on the location behind the nose of the shroud, as well as on the geometry of the shroud itself. The frequency content of the aerodynamic excitation depends on the type of flow being considered, but generally shows more of the total energy concentrated at higher frequencies when compared to the acoustic excitation at lift-off.

It is the external fluctuating pressure sources described above, coupling with the surfaces of the

shroud, that combine with the acoustic and mechanical transmission paths to establish the environment of a shroud enclosed spacecraft. The acoustic transmission path becomes very important when considering the aerodynamic induced environment since it is known to be primarily a direct function of density of the space enclosing the spacecraft. The implication here is that high external aerodynamic pressure fluctuations do not necessarily result in a high spacecraft acoustic environment. To establish the internal environment of the shroud and spacecraft, a very careful study must be made of the booster and launch pad to be used, the trajectory and type of shroud to be flown, and the dynamic characteristics of the spacecraft itself.

Mechanical excitation includes a random vibration environment that is transmitted from the engine and its associated pumping machinery through the primary and secondary vehicle structures and skins to the equipment. The response spectrum of the equipment is broad and the excitation exists during the entire engine burn sequence and as such its effect must be considered with the liftoff and transonic environments.

ANALYTICAL PROCEDURES FOR DETERMINATION OF STRUCTURAL RESPONSE TO ACOUSTICS

The analytical procedures presently available for the calculation of fluctuating pressure field induced structural response and noise reduction fall into two broad categories: the direct modal superposition technique and the methods of statistical energy analysis.

Direct Modal Superposition Approach

This method is only practical in the lower frequency bands where the structural-acoustic system has a small number of modal frequencies. A wide range of random response problems have been attacked by this method. The basic approach has developed directly from the conventional methods of structural vibration analysis. The normal modes of the structure are generated by finite element, finite difference, analytical methods, or by a ground vibration survey. The response is then taken as a superposition of these modes and linear random process theory is utilized to develop RMS values and power spectra for response quantities of interest. The response expressions are usually specified in terms of modal transfer functions and the excitation field cross-power spectral density. This latter quantity is difficult to obtain for certain pressure fields of interest (e.g., oscillating shock and separated flow, especially in the higher frequency bands). Other difficulties arise in the higher frequency bands (i.e., these bands usually contain large numbers of modes each of which will be more costly to define either by numerical calculation or by measurement). As a result of these difficulties considerable effort has been expanded on the development of the alternate procedures of statistical energy analysis.

Statistical Energy Analysis

This method of attack was motivated in part by the statistical analysis of room acoustics and, in like

fashion, generates a response power spectrum which is an average over a portion of the acoustic-structural system. Such averages best characterize the response when the fields of structural vibration and acoustic pressure can be considered reverberant. In an application of statistical energy analysis, the modes of the acoustic-structural system are divided into groups in which each mode of a particular group is coupled in a similar fashion to all of the modes of one of the other groups. For example, the resonant modes of a shroud in a specified frequency band might be divided into the group of acoustically fast modes (well coupled to the modes of the internal sound field) and a group of acoustically slow modes (poorly coupled to the internal sound field). Each modal group is characterized by an energy variable, the average energy per mode, which can be directly related to the aforementioned space and frequency band averaged response power spectra. A power balance equation, involving the energy variables, may be written for each modal group. The result is a set of linear nonhomogeneous algebraic equations in the energy variables, where the average (for a frequency band) resonant and nonresonant power inputs to the system constitute the inhomogeneous or forcing terms. This method, originally applied to reverberant acoustic field excited structures, may be extended to general random pressure field excitation (e.g., a turbulent boundary layer pressure field). The elements of the matrix of coefficients of the energy variables in the set of power balance equations is composed of modal group average modal densities and dissipation loss factors as well as average coupling loss factors between the modal groups. An advantage of statistical energy analysis is that expressions for averaged system parameters such as group modal densities and inter-group coupling loss factors calculated for simple systems may be applied in some cases to more complex systems. Response and noise transmission characteristics predicted by statistical energy analysis for rather complex systems agree well with measured data for the case of spacecraft acoustic path excitation (no coupling between groups of structural modes). Agreement is less favorable, however, for the case of spacecraft mechanical path excitation due to uncertainties in the coupling loss factors between groups of structural modes.

Although each of the above response prediction techniques has inherent limitations, they serve to identify the pertinent system parameters and to predict gross response trends and thus provide a basis for rational test planning.

LABORATORY ACOUSTIC TESTING TECHNOLOGY

Failures and techniques for the laboratory acoustic testing of full size spacecraft have evolved rapidly during the past ten years. Although this type of testing is a relative newcomer to the aerospace testing field, it has established itself as a useful and practical engineering tool.

The types of acoustic fields that can be generated in commercial testing facilities are basically divided into three categories:

1. Reverberant

4

2. Direction radiation

3. Progressive wave

These are illustrated in simplified fashion in Figure 4.

Reverberant field testing consists of introducing acoustic energy into a room possessing highly reflective walls. The field developed is intended to be diffuse in that the spectral content is approximately equal at any location within the room. The actual acoustic fields generated in reverberant chambers can be considered diffuse only above a chamber peculiar lower frequency limitation. The larger the room, the lower this frequency becomes. This is an important consideration when planning acoustic tests in reverberant chambers. This type of testing is the one most commonly used for testing spacecraft.

In specifying a reverberant acoustic test, the random nature of the acoustic field over space (as well as over time) must be considered. Thus for example it is somewhat ambiguous to specify that the acoustic spectra should be 150 · 2 dB throughout the test chamber. The random nature of the sound field makes it necessary to consider the probable deviations in sound intensity throughout the chamber volume. It would be more realistic to specify either: 1) a permissible spatial standard deviation of the sound level, or 2) a requirement that the mean sound level fall within some interval with a given confidence level. The spatial uniformity of the acoustic field generated in LMSC's 200,000 ft³ reverberant cell is shown in Figure 5.

Two methods for varying the space-time correlation of the test acoustic field have been investigated and are in limited use. These are local reinforcement of the reverberant field by use of direct radiation of the noise generator on the test specimen, and development of a progressive wave field over the specimen surface. Both techniques make possible limited duplication of the convecting and decaying fluctuating pressure fields encountered in flight. The spatial correlation functions in each case differ from flight. Direct radiation fields have greater correlation over the specimen surface than flight in the region of high intensity, and they are nonconvecting. The progressive wave environment does possess a convecting characteristic, however the speed of convection and decay of the field differ from those of flight.

Progressive wave testing consists of developing a field of plane wave acoustics propagating along a duct and passing over the test specimen surface. The waves are then either allowed to expand into a large area or be absorbed in an anechoic termination. Although this type of testing has certain attractive advantages, such as minimum power requirements, it is highly specialized in its application to spacecraft systems.

Direct radiation testing, however, shows distinct potential advantages over purely reverberant testing and LMSC has incorporated the capability for direct radiation testing in its acoustic facility.

The general concept of direct radiation testing is illustrated on Figure 6. The intent is to develop an acoustic field that varies in spatial intensity over the test specimen surface and thereby more nearly simulates the nonuniform flight environment associated with shock/boundary layer interaction. This approach has been studied in detail and the capability now exists for such testing.

STATISTICAL DATA EVALUATION TECHNIQUES FOR DERIVATION OF COMPONENT TEST SPECIFICATIONS (CURRENT METHOD)

A statistical treatment of vibration response data provides the only viable approach when dealing with an excitation phenomenon that is not only random in nature, but which also excites a complex structural assembly that exhibits such a variation in its local dynamic properties that a precise description of the overall structural response characteristics cannot be made. Such statistics are extremely useful for analyzing the response of equipment sections for a given type excitation, and for establishing significant trends.

Typically, a statistical derivation begins with assembling acceleration spectra for equipment or structural installations that are considered to have similar dynamic characteristics. The appropriate selection of data from these zones is important for establishing meaningful data trends. Each zonal acceleration spectrum is divided into narrow frequency bands, such as one-third octaves, and a weighted average vibration level recorded for each band. The values obtained for a given zonal frequency band are then fitted into a statistical model. The statistical model used can be that of an assumed distribution. A log-normal distribution seems to provide an adequate fit of the vibration data obtained from complex structures under a wide variety of circumstances. Other distributions can also be assumed if they appear to give a better description of the data. Also, when sufficient data exists, the data can be used directly as the appropriate statistical model. A percentile estimate is then selected and the value of this estimate for each frequency band is used to construct a statistical spectrum. The above described derivation is illustrated in Figure 7.

The percentile estimate of the distribution that is selected depends upon the type of analysis being made. The median spectrum is usually used to establish trends based on the fact that many data points influence the shape of this spectrum. Higher percentile estimates of the distribution can be influenced significantly by only a few extremely high or low values; however, if the median spectrum has high values for certain frequency bands it is reasonable to expect that a disproportionate amount of energy is centered there. This must also be considered when a determination is being made as to whether to use a broadband random test, a random swept random, or a random swept sine test. The manipulation of the data to obtain these types of test specifications is shown in Figure 8.

The broadband test level is typically obtained by constructing a weighted envelope of the 95th

percentile spectra and the peak acceleration levels. The broadband level, for random swept random testing, is typically obtained by taking the energy distribution of the 50th percentile spectra appropriately ratioed to obtain an energy level corresponding to the 95th percentile overall Grms level. The random swept sine background level is obtained in a similar manner. The sweep level is obtained from the 95th percentile of the statistical spectra. The bandwidth of the random sweep is adjusted to adequately account for the width of the energy spikes that protrude above the adjusted background level. Normally the sweep bandwidth is 50 Hz.

For response spectra having only a discrete number of narrow peaks, the random swept sine or the random swept random tests have an overall energy level much lower than the broadband random test. Hence, the swept sine and swept random concept has a much lower chance of causing an unrealistic failure to occur. These considerations may be overweighed, however, if the manufacturer does not have the testing capability to conduct sweep type testing. Then the cost of shipping the component to a better equipped test facility must be weighed against a higher level test and greater probability of an unrealistical failure.

The acceleration response spectra for the liftoff, transonic and engine burn conditions are compiled from data taken during acoustic testing, engine hot fire testing, prior tests on similar structures, flight test results, etc.

STATISTICAL DATA EVALUATION TECHNIQUES FOR DERIVATION OF COMPONENT TEST SPECIFICATIONS (NEW METHOD)

The method for deriving test specifications discussed in the previous section does not explicitly account for the time history differences in the various environments encountered by the spacecraft. For example, a perusal of Figures 2 and 3 will show that the rolloff of the transonic levels is much slower than those at liftoff. Hence a mere comparison of the levels of the response is incomplete. A more consistent approach objectively combines the level as well as the time. This is accomplished through the utilization of a technique referred to as peak counting. While this technique is certainly not new, we feel that its application to the development of component specifications for entire spacecraft systems has value.

The peak count method affords a means for objectively evaluating the cumulative random vibration exposure. It implicitly assumes that equipment damage potential is linearly related to the cumulative peak distribution. The peak count method explicitly introduces time as a parameter. It accumulates the total random vibration exposure that a qualification unit experiences (e.g., development, qualification, reliability testing) and compares it to what a flight unit experiences (e.g., box acceptance, system level acoustic acceptance, worst case flight environment). If a given box possesses a sufficient positive margin (demonstrated capability exceeds exposure of flight units), the unit is considered flightworthy. If not, remedial matters must be

considered.

Two basic assumptions are made in the development of this approach. First, it is assumed that a broadband random signal, whose PSD amplitude varies with frequency, can be treated on a narrow band basis; and second, that the signals being analyzed can be described as an ergodic random process whose instantaneous amplitude is normally (Gaussian) distributed.

If both of these assumptions are valid, it follows then that the peak distribution, in any given narrow band, is Rayleigh distributed. A review of recent flight data indicates the validity of the assumptions employed (e.g., Fig. 9). Some scattering of the data in this figure is noted at the high sigma values for the liftoff environment. This is probably due to the rapid change in the overall levels for this flight event. The applications of the peak count method are less developed than the statistical method formerly discussed. It has been used to verify margins. However, the methods for developing new test specifications (if margins are negative or inadequate) are not fully developed. The method is schematically illustrated in Fig. 10.

ACOUSTIC TESTING CAPABILITY

The acoustic facility recently constructed at LMSC provides the largest and most versatile vehicle test capability available for high intensity acoustic testing. The facility has been designed not only to accommodate large space vehicles but also to provide the flexibility of performing acoustic tests on vehicle sections or subsystems with the incorporation of two smaller test cells within the complex. The physical characteristics of the test cells are shown in Figure 11.

The noise generators consist of twelve Ling EPT 200 transducers and four Wyle Laboratories WAS 3000 transducers rated for a maximum of 240,000 watts of acoustic power when operated into an anechoic termination. The Ling transducers were acquired to provide as much high frequency spectral control as possible and the Wyle units to generate low frequency acoustic power. Exponential horns with low frequency cutoffs varying from 44 to 350 Hz are available to provide maximum spectral shaping capabilities. The transducers are operated with gaseous nitrogen. A simplified illustration of the operation is presented in Figure 12.

An important aspect is the facility's Data Acquisition and Control System. A block diagram of the system is presented in Figure 13. The basic system is designed to acquire real time data from up to 140 piezoelectric transducers and 112 resistive strain gages.

RECENT RESULTS (ACOUSTIC TEST SIMULATION OF THE EXTERNAL SPACECRAFT ASCENT ENVIRONMENT)

In an effort to determine the ascent environment and the induced random vibration response of a spacecraft within a shroud, an instrumented shroud and spacecraft were exposed to acoustic

6

excitation representative of the flight fluctuating pressure fields. This section describes how this external service environment was defined and how it was then simulated in the test laboratory.

From previous flight experience, it was known that the acoustic environment generated at lift-off would be the most significant service environment over the aft section of the shroud; and for the forward section, aerodynamic fluctuating pressure fields generated by a terminal shock wave interacting with the boundary layer beneath t would dominate. While the lift-off environment could be defined from actual launch pad measurements, it was considered necessary to further define the aerodynamic environment through wind tunnel testing.

Wind tunnel tests were conducted in the 16-foot Propulsion Wind Tunnel at the Arnold Engineering Development Center, Tullahoma, Tenn. As part of this test, aerodynamic pressure fluctuations and static pressure measurements were obtained on three nose-cylinder combinations; a blunted 15° nose-cylinder, a 25°-10° biconic nose-cylinder, and a 25°-10° biconic nose with a corrugated cylinder. These configurations are illustrated in Figure 14. While the biconic corrugated model was the configuration of primary concern, the 15° cone-cylinder served as a simple baseline configuration to which the data from the more complicated biconic configuration could be compared. The biconic smooth model was used to evaluate the effect of the external corrugations on the aerodynamic fluctuating pressure field. The diameter of the wind tunnel models was 1.8 feet, representing an 18% modeling of the full scale configuration and a 1% blockage of the test section. The models were extensively instrumented with fluctuating pressure pickups utilizing some fifty-five 1/16 inch diameter Kulite and seventy 1/8 inch diameter Kistler microphones.

Wind tunnel test runs were made at discrete Mach numbers between 0.6 and 1.4, and the angle of attack was varied between 0 and ± 10 degrees. Because of the large model size, it was possible to keep the Reynolds number and associated wing tunnel dynamic pressure fairly typical of the actual flight condition at most Mach numbers. The most severe shock induced fluctuating pressure levels occurred at M 0.8 with an angle of attack of 3 degrees (Figure 15). Vortices generated upstream by the shock wave on the nose cone caused the terminal normal shock at the cone-cylinder intersection to ripple (Figure 16). The longitudinal range of the terminal shock, which corresponds to the maximum noise peaks, is shown in Figure 17. Typical spectra in the vicinity of the terminal normal shock are presented in Figure 18. Under the local separation bubble, the shock dominates the spectra which consequently shows more low frequency content. In the turbulent boundary layer behind the shock generated noise peaks, the fluctuating pressure levels did not exceed 145 dB.

The effect of the nose configuration and corrugations is illustrated in Figures 19 and 20. The 25°-10° biconic nose causes a significant reduction in the terminal normal shock pressure fluctuations relative to the 15° cone cylinder, but adds a region

of high excitation aft of the cone-cone shoulder. The corrugated skin configuration considerably alters both the level and the shape of the fluctuating pressure distributions. The terminal normal shock stands farther aft on the corrugated model, and not only is the shock noise greater for the corrugated configuration, but an additional fluctuating pressure peak occurs near the leading edges of the corrugations.

Figure 21 presents the most significant features of the final ascent service environment. Except over the nose cone and in the immediate vicinity of the nose cone - shroud cylinder intersection, the liftoff acoustic field is dominant. Figure 22 presents typical spectra for liftoff and transonic flight. The liftoff spectra was obtained from a 95th percentile estimate of the actual launch pad measurements. The transonic spectra was obtained by Strouhal scaling of a worst case envelope of the wind tunnel test results.

At present much effort is being expended by the Aerospace industry in establishing criteria for simulating the flight fluctuating pressure fields in an acoustic test cell. To establish an equivalence for a given flight vehicle system, consideration must be given to the frequency content, spatial correlation and spatial sound-pressure level distribution of the external fluctuating pressure field. In most instances, the spatial correlation and sound-pressure level distribution of the test environment is fixed by the nature of the test chamber; equivalence between flight and test conditions must then be established through control of the frequency content of the acoustic environment generated. The problem of establishing complete equivalence will be greatly simplified if the local sound-pressure level variations in the flight environment can be reproduced in the test chamber; for then only one uncontrolled acoustic function remains, the spatial correlation. Flight data indicates that this function can to some extent be accounted for in the frequency domain be increasing the high frequency content of the acoustic test environment. This increase can then be catered to as facility capability permits.

For the reasons given above a direct radiation-reverberant test mode was chosen as a means for improving the simulation of the flight fluctuating pressure fields in the test laboratory, refer to Figure 6. The local reinforcement given by the direct field is utilized to simulate the shock disturbed pressure fluctuations, and the associated reverberant field simulates the pressure fluctuations aft of this area. In theory it would be possible to conduct two tests to simulate the flight environment, one to simulate the liftoff condition and the other to simulate that of transonic flight. However, for practical reasons testing is carried out for the liftoff and transonic environments simultaneously. In Figures 23 and 24 the acoustic field of a direct radiation - reverberant test is compared to the flight fluctuating pressure fields it was intended to simulate. A comparatively good simulation was obtained of the desired spectrums but the area of reinforcement provided by the direct field was broader than that expected in flight. This difference in the area of reinforcement encountered in

7

flight and in the test chamber can be partially compensated for by altering the test sound-pressure level in such a way that the force delivered to the vehicle is equal for both cases. It should be recognized that this acoustic testing technique is comparatively new and still needs verification through actual flight experience.

RECENT RESULTS (THEORETICAL METHODS AND EXPERIMENTAL VERIFICATION)

This section will review some results of theoretical approaches that help define the internal inside shroud acoustic environment and the spacecraft equipment response. These theoretical methods are invaluable in helping to ascertain the overall trends. A knowledge of these trends, when combined with available experimental data, provides the best approach for the determination of the acoustic environments and equipment responses.

Results will be presented using two theoretical approaches; Statistical Energy Analysis and Modal Superposition. The results from the statistical energy analysis will be discussed first.

The statistical energy approach for calculating structural response to a diffuse acoustic field was first developed by Lyon and other workers at Bolt Beranek and Newman. Using this method, LMSC derived a set of equations which predict the noise reduction and response of concentric cylinders. The purpose of adopting the concentric-cylinder model was to simulate a space vehicle enclosed by a shroud. The model used for the derivation of the equations is shown in Figure 25. Here (1) is the external acoustic field, (2) is the outer cylinder, (3) is the internal acoustic field, (4) is the inner cylinder and (5) is the volume of the inner cylinder. To examine how well the derived environmental estimates compared to experimental data, two cylinders with the following physical properties were tested. The outer cylinder was five feet in diameter, five feet in length, and had a skin thickness of .04 inch. The inner cylinder was 40 inches in diameter, 45 inches in length, and had a skin thickness of .08 inch. Both ends of the cylinders were covered. Figure 26 is typical of the results obtained and shows the resulting noise reduction of the outer cylinder versus 1/3 octave band center frequency. The squares and triangles represent the experiment noise reduction data of the two microphones that are located between the cylinders. As expected, in the low frequency range the sound field inside the cylinder will vary with position. At higher frequencies, the sound field will approach a uniform condition. The black circles are the predicted noise reduction values. For this calculation the internal structural loss factor for the cylinders used was .005. The acoustic absorption coefficients assumed were 10^{-3} for the cylinder walls and 0.5 for the ends. The overall external sound pressure level was 153 dB.

The results of this study were taken as evidence that with appropriate modeling of a space vehicle structure, the statistical energy method will provide useful response and noise reduction estimates. A noise reduction calculation was then made to establish the internal acoustic environment for an actual space vehicle equipment section. This prediction was required to support an acoustic test program for the equipment modules within this structure. Figure 27 compares the prediction made with measurements obtained at various locations within this equipment section during subsequent system level tests in a reverberant acoustic field. While the predicted level doesn't quite envelope the measured data, as one generally likes to see in a test specification, it did follow the general data trends and gave a reasonable estimate of the total internal acoustic energy level.

The direct modal superposition approach was used to predict the low frequency environment induced in an equipment section by random pressure fields. This prediction was required in support of a guidance error analysis that was being performed. The modes of the equipment section were generated using a finite element analysis and the required response obtained using classical linear random process theory. A finite element skeleton diagram of the equipment section under consideration is shown in Figure 28. The response required was that of the gyro mounting platform located at the inertia sensor node. Figures 29 and 30 compare the predictions made with measurements obtained during two subsequent system level reverberant acoustic tests of the equipment section. Again the predictions are following general data trends and provide reasonable estimates of the total energy level.

Most current random vibration prediction procedures, whether the procedures have been developed empirically or analytically, assume that the induced environment is directly proportional to the pressure level of the excitation. Figures 31 and 32 are presented in support of this assumption. Figure 31 presents in one-third octave frequency bands the function $10 \log <G^2>/<P^2>$ for two levels of acoustic excitation, one at 142.5 dB and the other at 150.5 dB. $<G^2>$ is the mean square spatial-temporal average of approximately 45 vibration measurements obtained within a typical spacecraft equipment section, and $<P^2>$ is the mean square spatial-temporal average of 4 acoustic measurements made of the reverberant excitation field. Figure 32 is a similar presentation, for the same equipment section, of the function $10 \log <Pe^2>/<Pi^2>$ where $<Pe^2>$ and $<Pi^2>$ are the mean square spatial-temporal averages of the external and internal acoustic fields respectively. The fact that these curves collapse reasonably well upon each other indicates that for this equipment section at least, the assumption of a linear relationship seems to be reasonable.

CONCLUSIONS

This paper has presented an approach and recent results related to the analysis and testing of spacecraft and spacecraft equipment.

Exact simulation of the service environment is not within the state-of-the-art. This paper has discussed the tests that are believed to best simulate the service environment.

The rather recent availability of large acoustic chambers makes it possible to expose large spacecraft systems to sound pressure levels similar to those generated by the inflight pressure fluctuations. However, criteria for establishing the appropriate test spectrum level, spatial distribution and directivity of the sound is still in early stages of development. Also, requirements for the spacecraft test specimen itself and its precise manner of installation in the chamber requires further work.

Acoustic test criteria, generally acceptable to all of the Aerospace industry, will gradually evolve as this industry becomes more familiar with the fluctuating pressure environment that the testing is to simulate. This familiarity will be obtained from a carefully planned integration of flight and ground measurements.

REFERENCES

1. Richard H. Lyon, Random Noise and Vibration in Space Vehicles, The Shock and Vibration Information Center, United States Department of Defense, 1967

DISCUSSION

Voice: How did you determine sweep rate?

Dr. Wrenn: We partially used the peak count technique. We know the total time that the background has to be on which is roughly the time that the environment is on and we usually set the sweep to cover that same amount of time. It is not all that precise. We are starting to use this peak count technique now to give us a little better guide in that area.

Mr. Galef (TRW Systems): You seem to be saying that the swept random was better than broad band random because it did not create as many failures and, of course, you have still fewer failures if they were not tested at all.

Dr. Wrenn: That is right. I wish we could do that and still fly it and have it work.

Mr. Galef: I have to admit that the only reason the swept random provides a more realistic representation of the flight environment is because the initial levels were simply too high. The swept random is certainly not a better simulation. It takes away some of the conservatism by providing a different type of, I would say, unrealistic test.

Mr. Wrenn: That is true. There are lots of arguments for this swept random as contrasted to the broadband and there are a number of camps that talk about this thing. We were forced to go that way because we were failing too many boxes and we could not afford to do that. It was too expensive. So we had to go through a different type of testing technique. Now that may have well been a lower broadband level. Perhaps that would have done the trick, but we found that the swept random was a useful tool. That is what we used and it works for us.

Mr. Smith (Bell Aerospace): Does not the need to change your test specification to reduce the number of failures really suggest that your simulation for the noise sources itself is wrong? You spoke of experiments in which you had more than 100 pressure transducers on a reasonably sizeable specimen. I suggest that the means that are used to produce the correct overall noise levels and spatial distribution do not reproduce more detailed characteristics of the aerodynamic sources. Those aerodynamic sources are probably less efficient in exciting structural response than your test sources.

Dr. Wrenn: Perfectly true. All that I am trying to go over today is what we feel is the best engineering simulation today for these environments. Perhaps in the future other techniques will evolve, and we grant that it is not the actual service environment. You just cannot simulate that now within the state of the art. We try to come up with the best test that gives us some engineering information so that we can fly these systems with high confidence that they are going to work.

Mr. Smith: I think I missed one point when you talked about your peak accumulation test approach. You had on a slide a narrow band filter which obviously gave a single degree-of-freedom type response, and then you went through the usual Rayleigh business. What determines the frequency of that filter or are you somehow using a number of these?

Dr. Wrenn: We do it for the entire frequency band. We treat each narrow band and then we go over the entire spectrum. We treat on a narrow band basis but we look at every narrow band.

Mr. Smith: So you are doing a number of summations both across distribution in some narrow band and then across narrow bands as well.

Dr. Wrenn: We are doing it for the entire spectrum, that is correct. The proven capability of a piece of equipment or its positive margin is not positive or negative overall but it is positive or negative in a given frequency band. Then, if it is positive in all frequency bands, it gives you the nice warm feeling that it is going to work.

Mr. Smith: Does not this mean again that you may be in effect counting a lot of that energy twice? You are putting a number of filters into the system and coming up with a whole number of peak distributions which you are then summing. If I had a broadband system and I put this through a number of narrow band filters into a whole stream of peak distributions and then add all of these up and say that this characterizes that broadband source, I would think I was overdoing things. This might be another reason why your test turned out rather worse than you had hoped.

Dr. Wrenn: The flight data corroborates it if you recall that one figure. We have measurements

...a lot of frequency bands for liftoff, transonic and ... We take a look at the peak distribution in the ... that ... back from signals on the vehicles and we actually count the peaks on these signals and they ... do come to a fairly close estimation of the Rayleigh distribution. It is a tool that we use.

Dr. Morrow (LRC Research Center): These high intensity noise tests are good tests and it will be a very useful technique to make use of them on the structure in the early parts of the program to help derive the best conditions for the units. This is something that has not been possible before. It will be possible to get much more data this way than is desirable in flight. Among the important characteristics of the pressure fluctuation field is one you did not mention. That is the cross power spectrum between one point and another. If you make a little more intensive study of this, it will be possible to obtain a somewhat more realistic effect in the high intensity noise field. It will also be possible to make corrections so as to get better estimates of the inputs to the several units.

Dr. Wrenn: That is a good comment, sir. That is something I had not mentioned because there is a lot of work to be done in this area of correlation and cross correlation. Once you pick a facility, a reverberant cell or a direct radiation reverberant type facility, you pretty well determine the correlation. I emphasize that these are just engineering tests that we built up to get additional confidence in the system. We have to have high reliability in these systems. The tests are expensive but they pay off.

Dr. Dreher, AFFDL: I would like to compliment you on a very thorough study. I was only concerned that you used the one-third octave analysis to present your data in. We have run a comparison between one-third octave analysis and narrow band analysis just recently. We plotted psd's on a one-third octave basis and also did it using a 10 Hz bandwidth filter. On that basis we found that on the average 28 percent of the actual vibration is larger than you would get using one-third octave. In addition to that we found that the peaks based on the narrow band analysis ranged as much as 4 1/2 to 9 db higher. How did you approach that particular problem?

Dr. Wrenn: First of all, I would like to thank you for your first comment. As far as the other comments are concerned, you are perfectly correct. It makes quite a difference as to whether you treat it as your filter bandwidth or your analysis bandwidth. We picked one-third octave quite frankly because acoustic data usually comes in one-third octaves. It does not come in narrow bands. We are not actually making a hard and fast computation on one side but what we are really doing is taking the cumulative random vibration capability, if you will, of qualification units. We are subtracting that from the cumulative random vibration capability or exposure of flight units; we are actually taking the difference of these things, and hope it will come out in the wash. It is just our first attempt. We may go to narrow bands later on as we get our acoustic data more refined.

Dr. Hou, Bellcomm: According to the slides, the peak distribution of the liftoff does not fit well to the Rayleigh distribution, but for the transonic test it fits well. Does the author have any explanation about this?

Dr. Wrenn: I think the basic assumptions are perfectly valid. It is indeed the g rms value of K at any particular measurement that is a function of time. During liftoff it goes up, then it decays and as we build up into the transonic flight region it builds up again. We go through max alpha q and it decays again. The g rms value is changing as a function of time. As a consequence we have a non-stationary process with which we could not operate. We broke the process up into small number of delta t's and each of these we treated as a stationary process. We feel that it is good enough to be used as a tool and it can help us in comparing distributions that have a wide differences in their spectral shapes and levels. In the past we did not have that capability. All we could do was to look at the levels and not the time. This is an effort to try to use this peak counting technique to help us in the selection of the system specifications for all the components, not just one box.

Mr. Zell (Picatinny Arsenal): Is it true that actually in the bandwidth that you chose to analyze the data, you were effectively determining the effect of q or the assumed q of the resonators of the structure? A bandpass filter effectively says that it ignores the contributions of the low frequencies to the peaks because it assumes that the all of the q is so high that all of the peaks are essentially due to the frequencies within a defined bandwidth. Perhaps the analog type of single degree of freedom analyzers used for shock analysis might be useful for this.

Dr. Wrenn: Yes that is a good comment. We have treated it in one-third octave bands just for convenience. We have taken a look at some limited results with the narrow bands but it is premature to report on them. There are lots of other problems. We will save that for future discussion.

Mr. Van Ert (Aerospace Corporation): It seems that some of the discussion regarding one-third octave band analysis might be a little bit misleading. It is my understanding that much of this data was analyzed in narrow band analysis, 10 or 20 Hz analysis bandwidth, and then just looked at in the one-third octave band.

Dr. Wrenn: That is true.

Mr. Van Ert: So some of these problems that are associated with clipping of peaks due to one-third octave band analysis would not be a problem in this case.

Dr. Wrenn: That is a good point.

Mr. Van Ert: The second thing I would mention is that the peak count analysis would permit comparison of a straight swept random with an all random. In other words, if I chose to run a test which was a 10 Hz random sweep, to simulate a broadband random environment, I could do so with a peak count

analysis. The one thing that I guess we would tend to overlook is the simultaneity of the two environments.

Dr. Wrenn: Right. Multiple random peaks that go above the background for example. There is a little gray area there now with regard to the multiple peaks. Right now we are closing our eyes and doing it hopefully as a tool to help us.
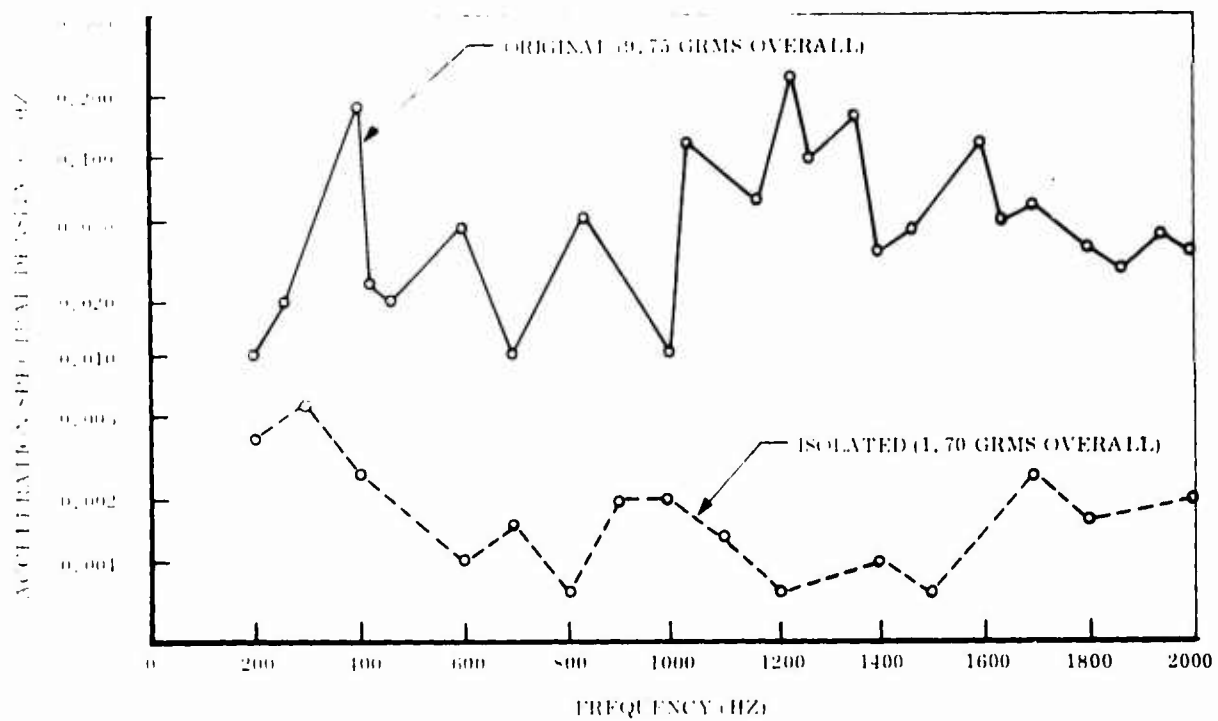
Fig. 1 Effect of Component Isolation
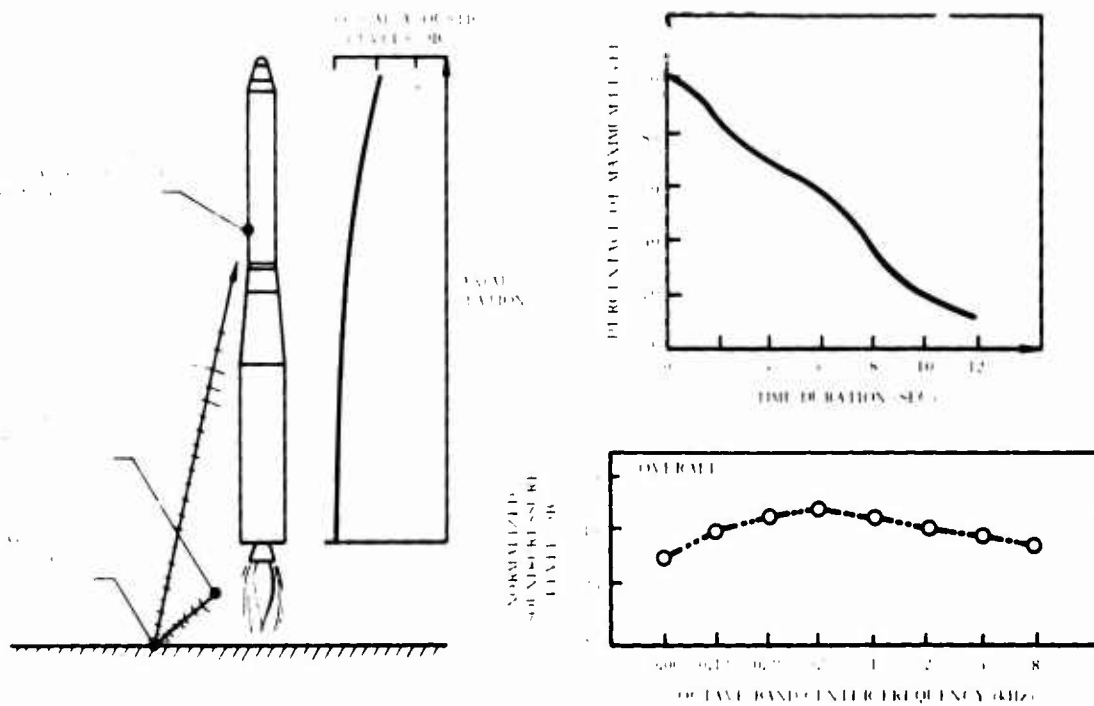
Fig. 2 Typical External Inflight Liftoff Fluctuating Pressure Environment

12
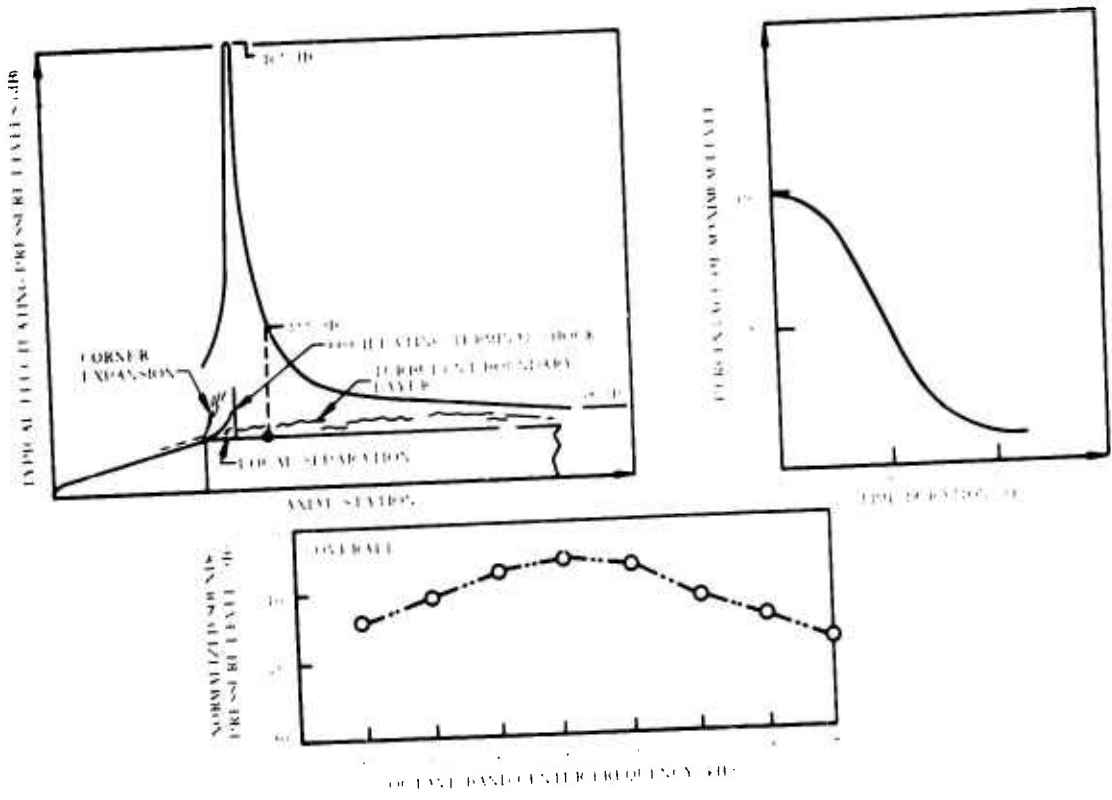
Fig. 3 Typical External Inflight Transonic Fluctuating Pressure Environment
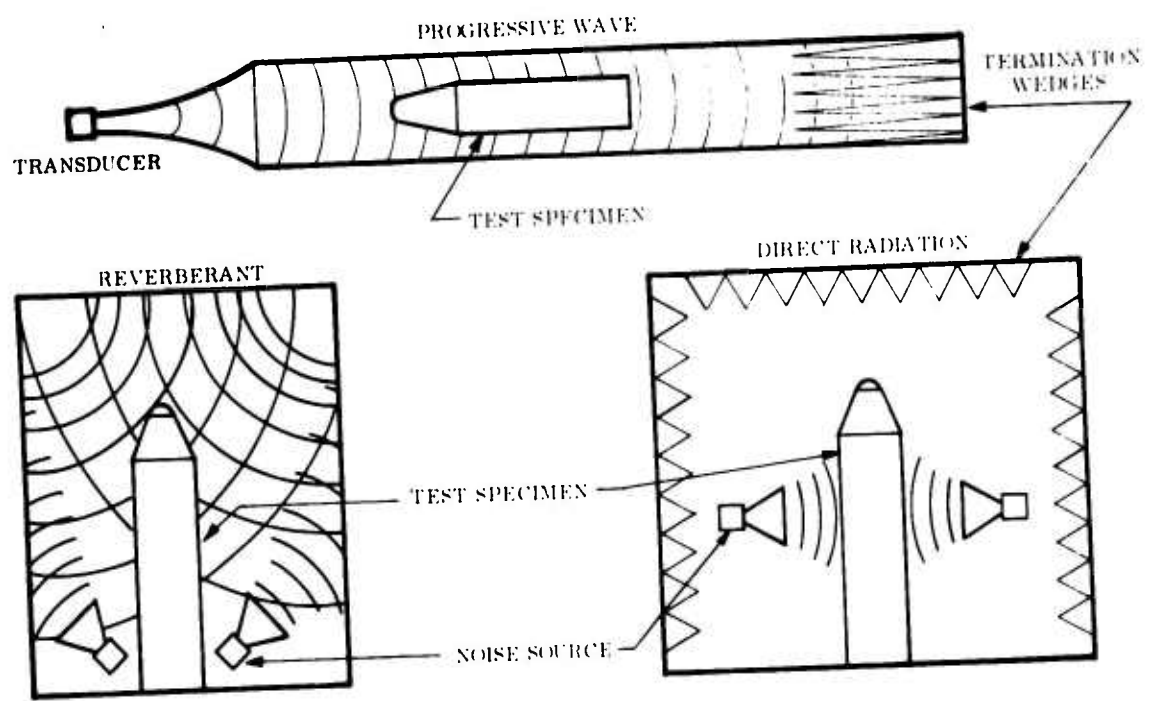
Fig. 4 Types of Acoustic Testing

13
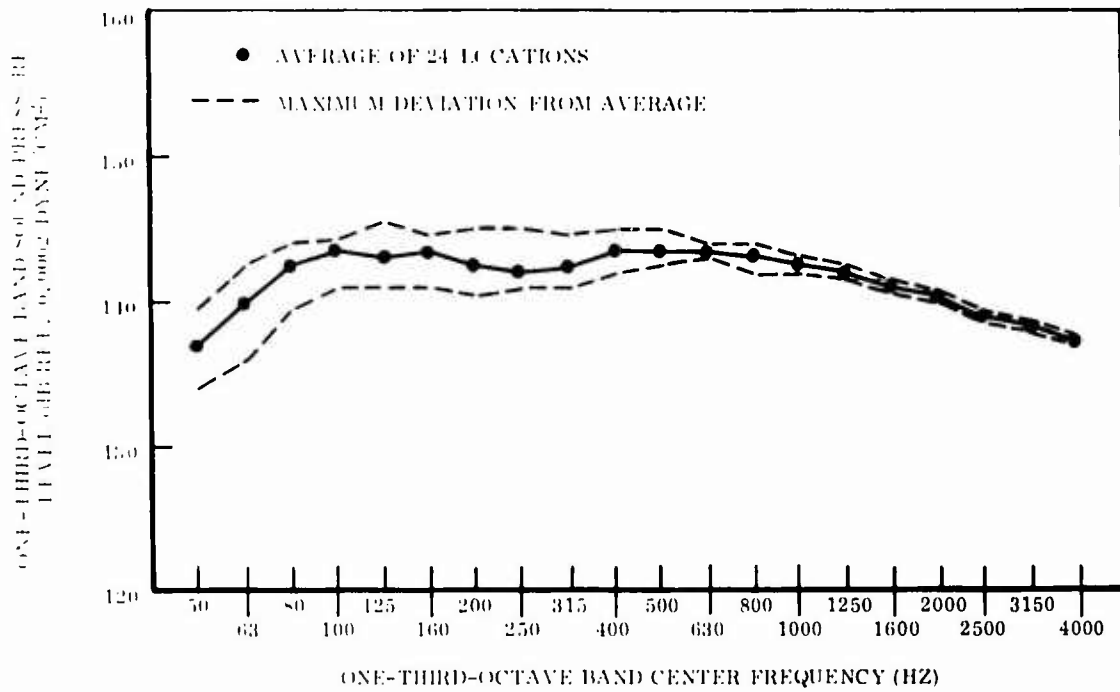
Fig. 5 Reverberant Field Spatial Uniformity

SPL_1 REVERBERANT LEVEL

SPL_2 SPL_1 3 dB

SPL_3 DIRECT FIELD 6 dB
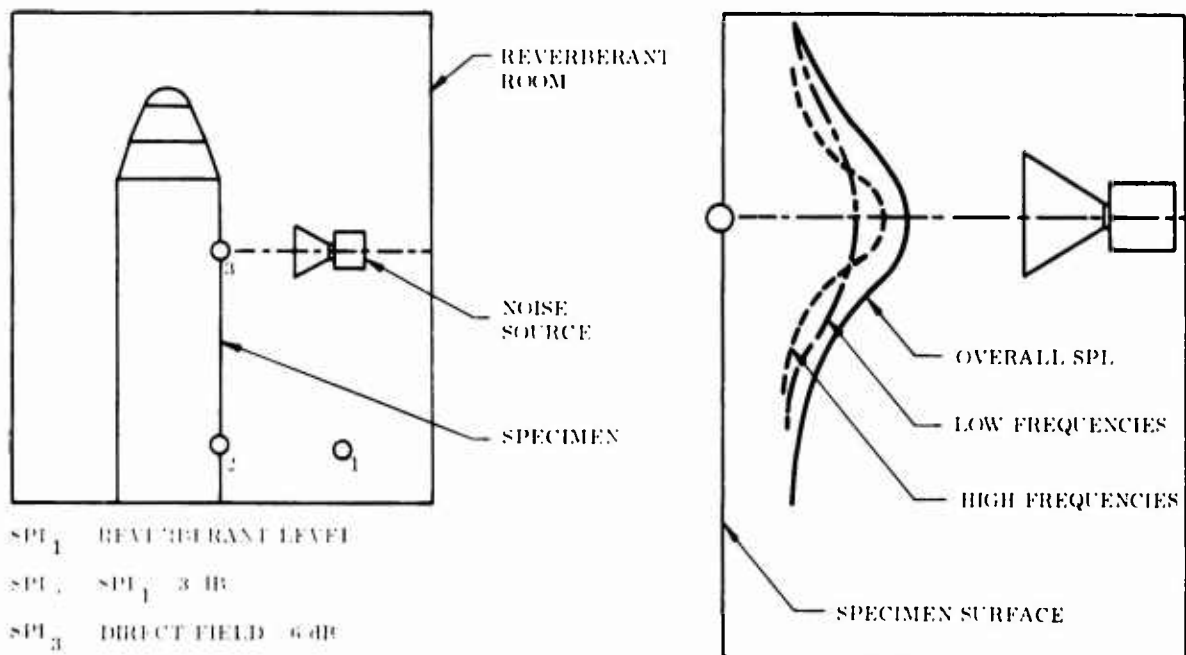
Fig. 6 Direct Radiation Test Setup

14
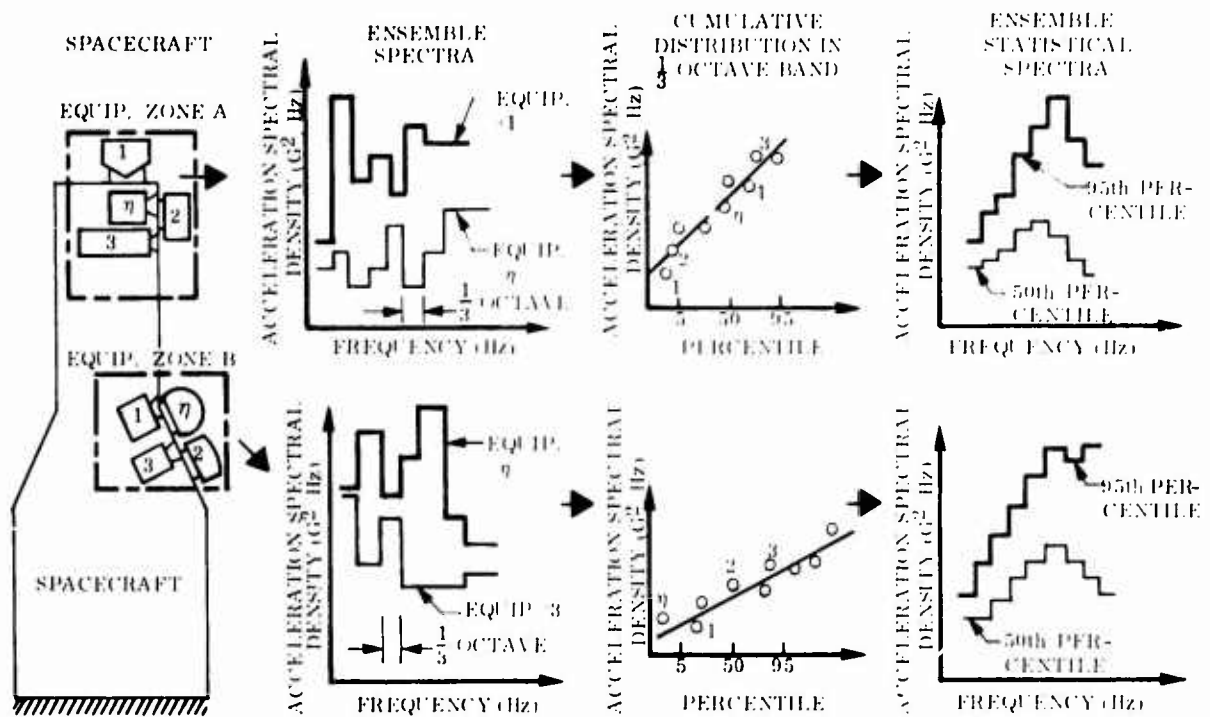
Fig. 7 Flow Diagram for the Derivation of Statistical Acceleration Spectra
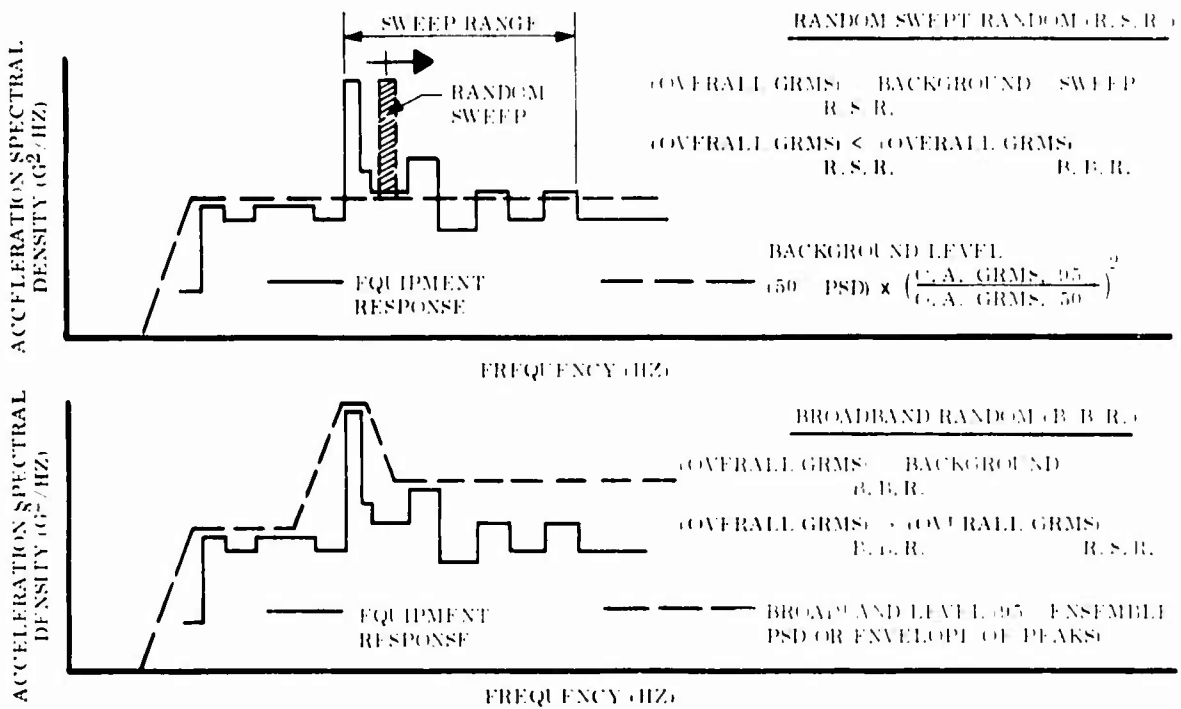
Fig. 8 Derivation of Random Vibration Equipment Test Specifications (Current Method)

15
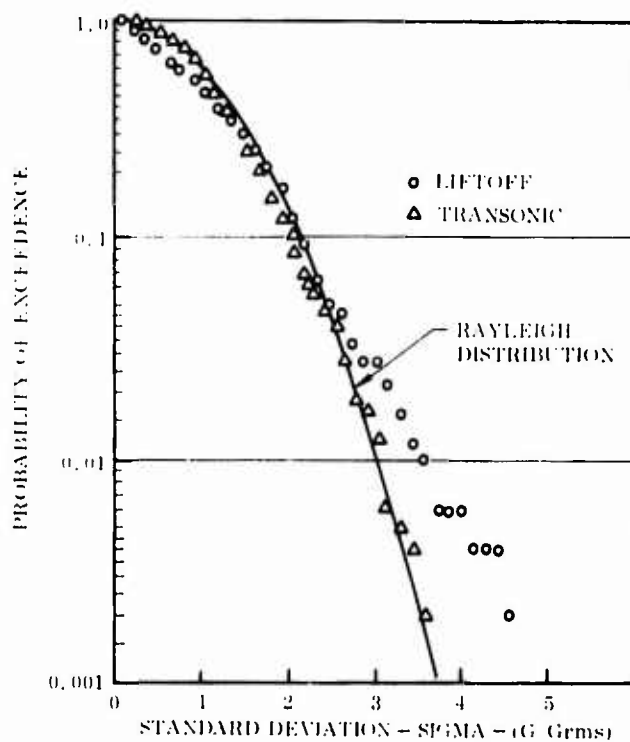
Fig. 9 Comparison of Rayleigh Distribution and Flight Data (In a Narrow Frequency Band)

$$N(G) = \Sigma f_c \Delta t \; EXP \left[-\frac{1}{2} (G \; GRMS)^2 \right]$$

FOR EACH NARROW BAND: N(G)

N(G) NUMBER OF PEAKS THAT EX-
CEED G (FOR RAYLEIGH DISTRIBUTION)
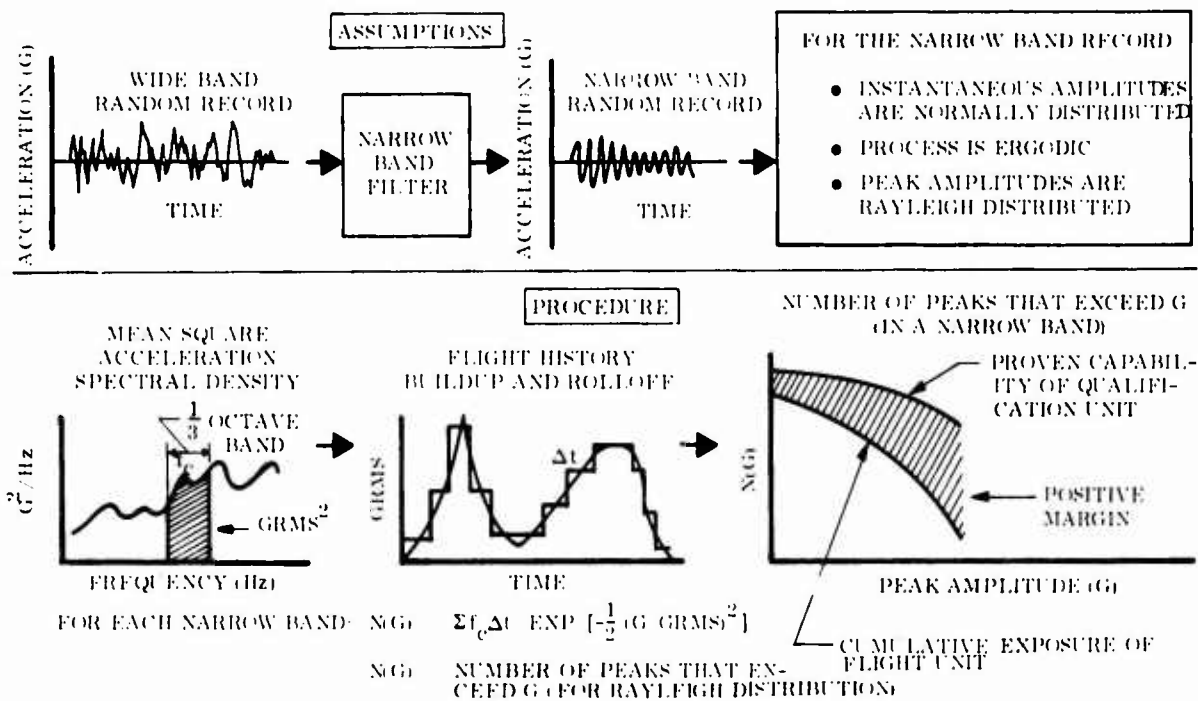
Fig. 10 Flow Diagram for the Peak Count Method

16

CELL	TYPE	CELL DIMENSIONS (ft)	DOOR SIZE (ft)	CRANE SIZE (tons)	HOOK HEIGHT (ft)	MAXIMUM SPECIMEN SIZE (ft)	RATED OVER-ALL SPL (dB)[a]	DATA CHAN-NELS
1	Reverberant	44 x 50 x 56 H	26 x 44 H	20	74.5	22 D x 70 H	156	140
2	Reverberant	20 x 26 x 31 H	15 x 31 H	5	28	13 D x 25 H	162	140
3	Reverberant	16 x 20 x 25 H	9 x 18 H	-	-	6 D x 20 H	170	28
4	Anechoic	31 x 31 x 31 H (less anechoic material)	8 x 9 H	-	-	4 D x 10 H	-	28

(a) Referenced to 0.0002 dynes/cm^2

Fig. 11 Test Cell Characteristics
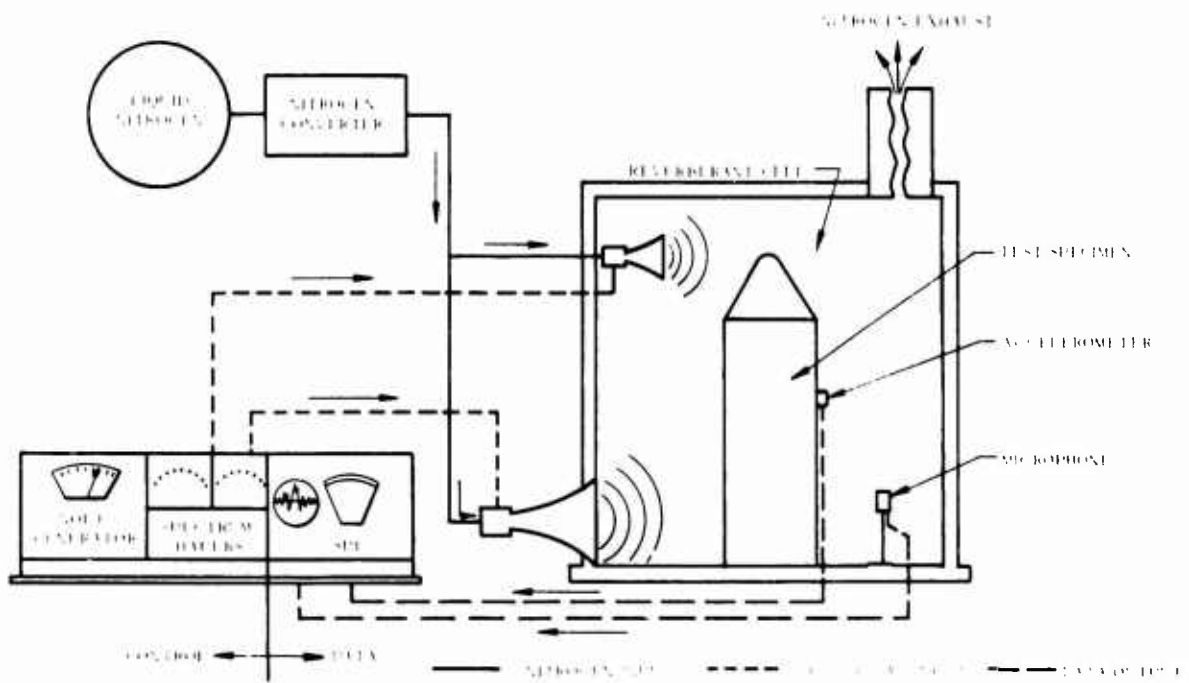
Fig. 12 Operational Diagram for Acoustic Test Cell

17
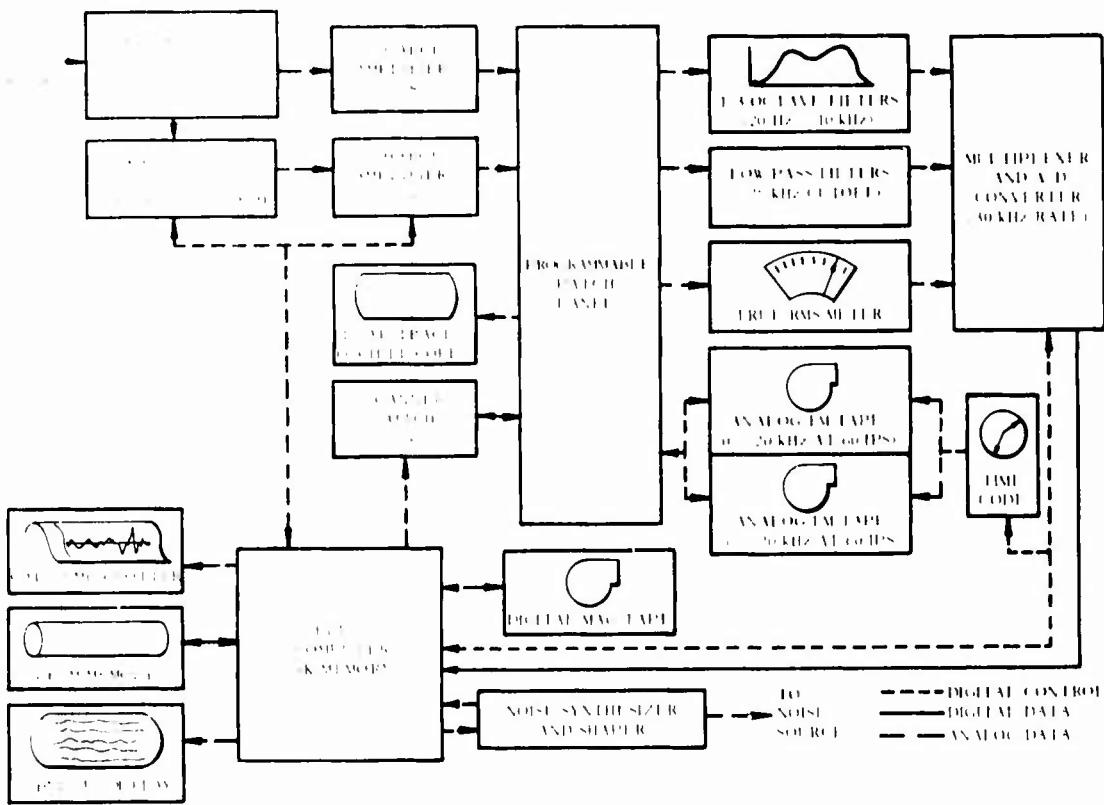
Fig. 13 Flow Diagram for Acoustic Data Acquisition System
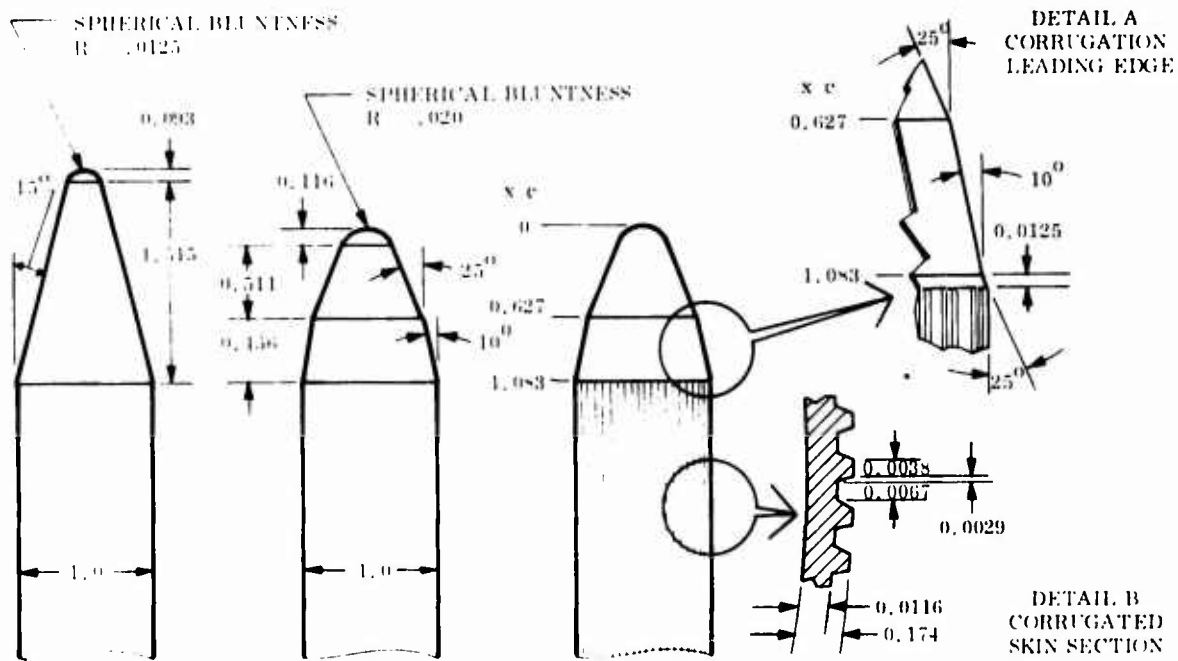
Fig. 14 Shroud Configurations

18
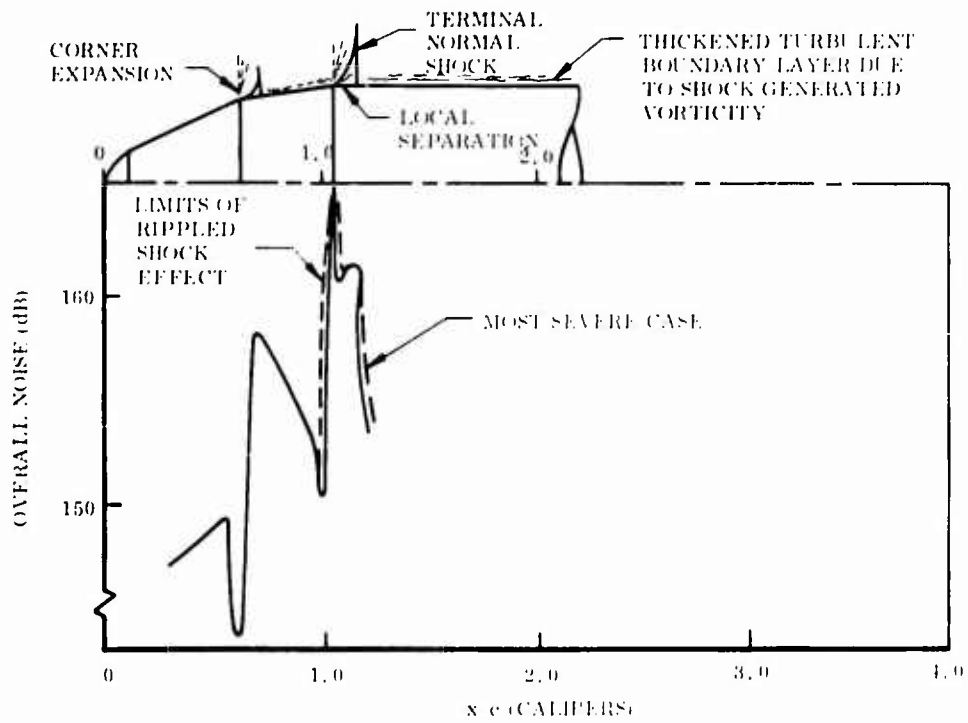
Fig. 15 Shock Induced Fluctuating Pressure Levels
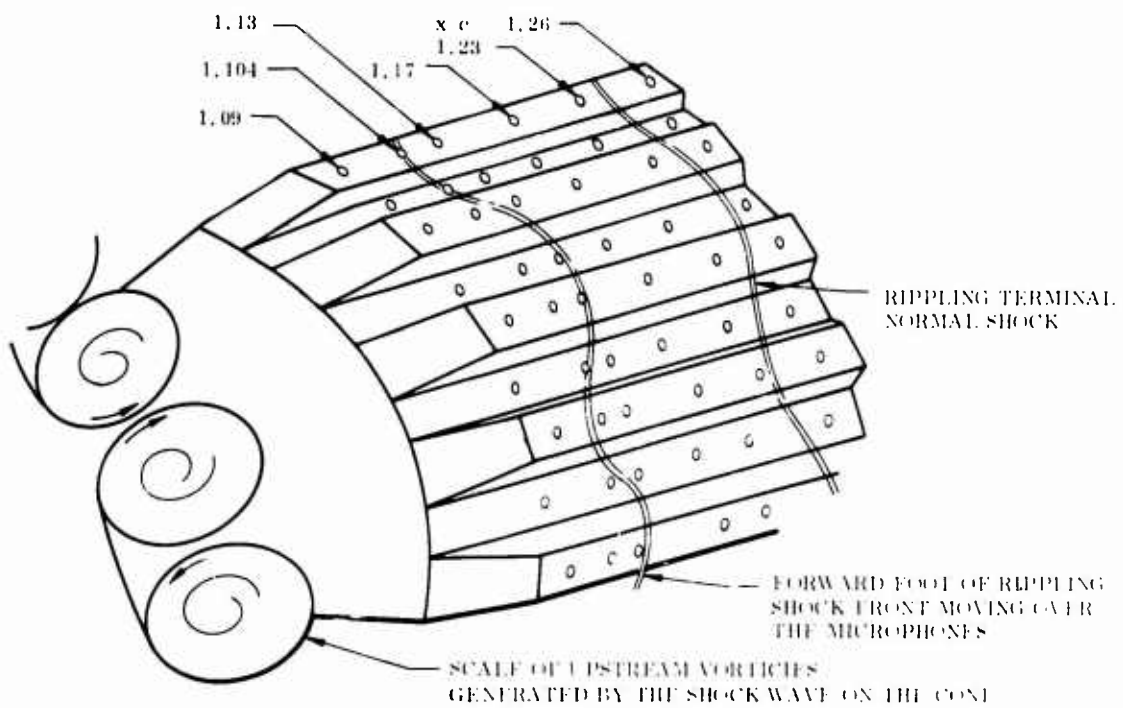
Fig. 16 Vortex Generated Rippling Shock Front

19
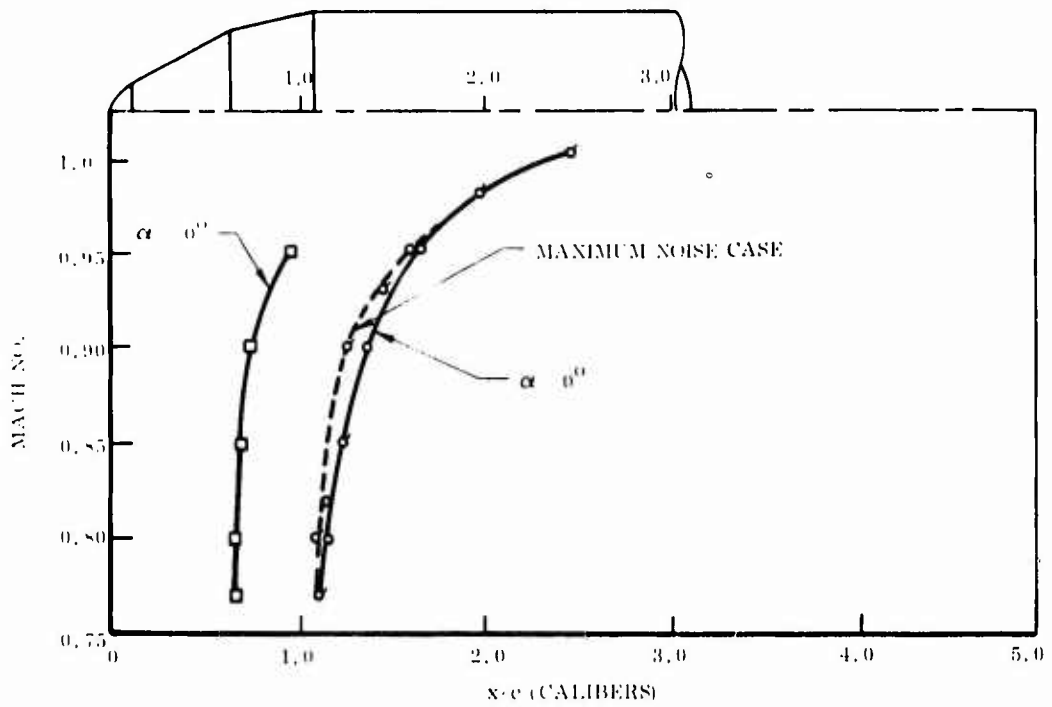
Fig. 17 Terminal Shock Movement
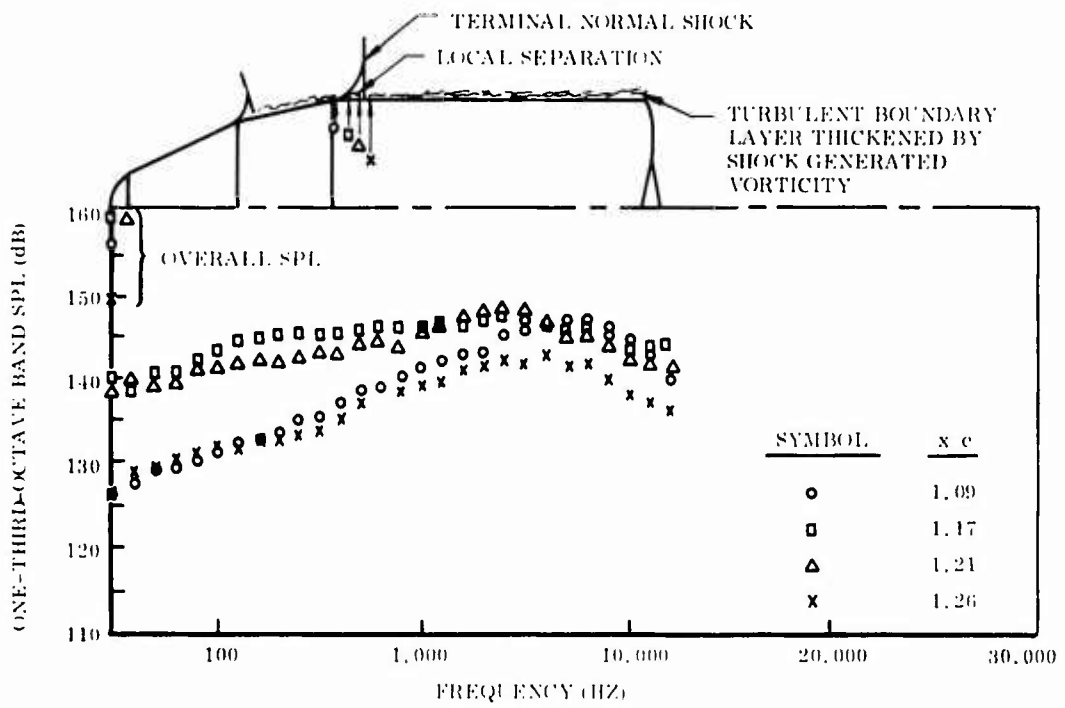
Fig. 18 Shock Induced Sound Pressure Levels

20
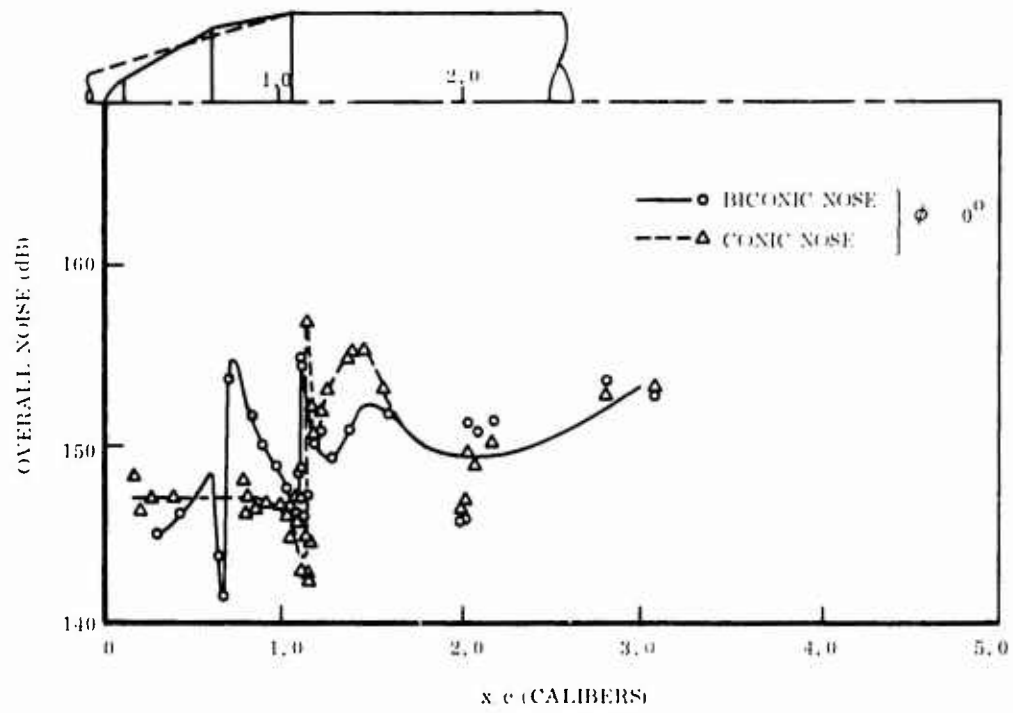
Fig. 19 Comparison of Nose Cone Configurations
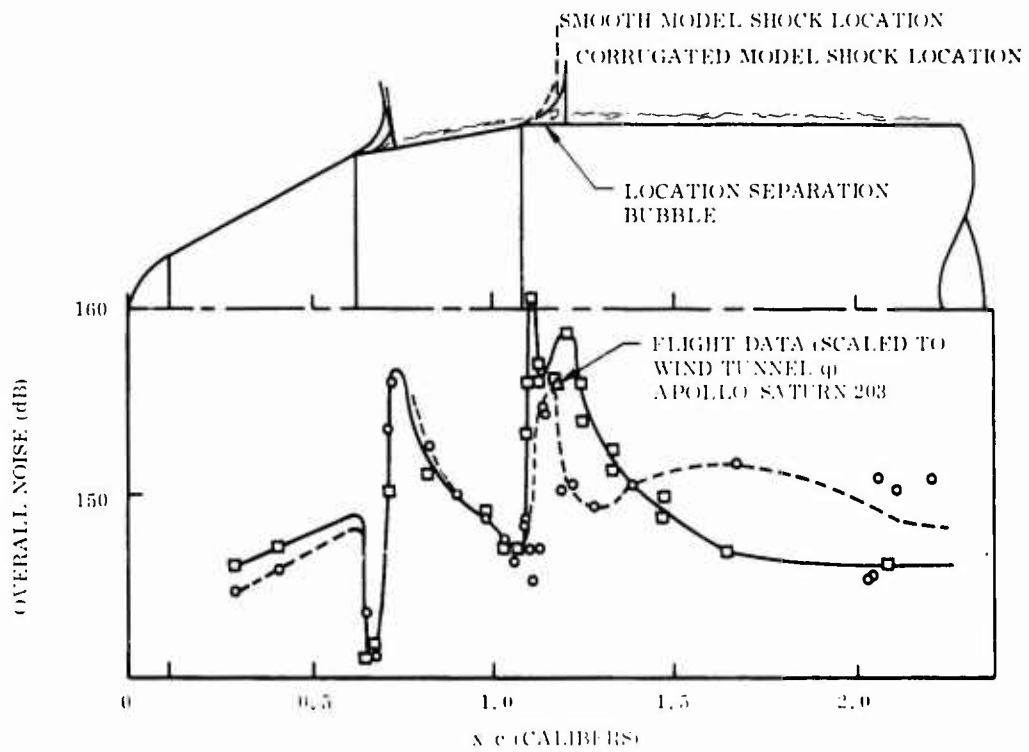
Fig. 20 Effect of Corrugations

21
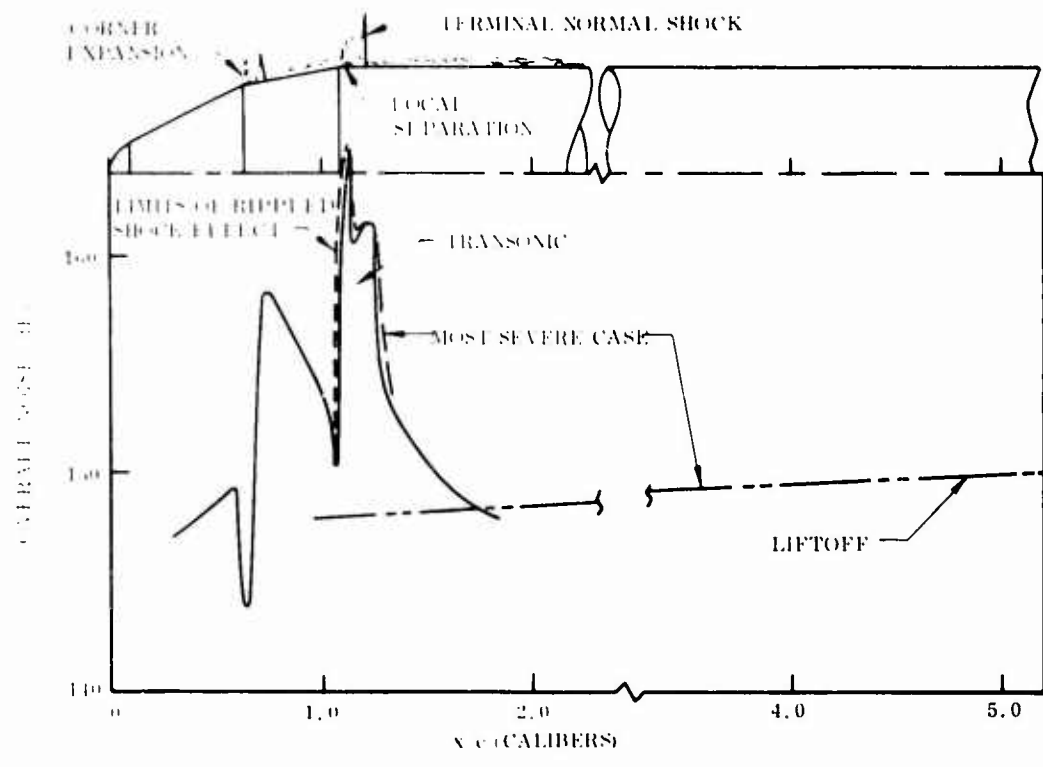
Fig. 21 Ascent Service Environment
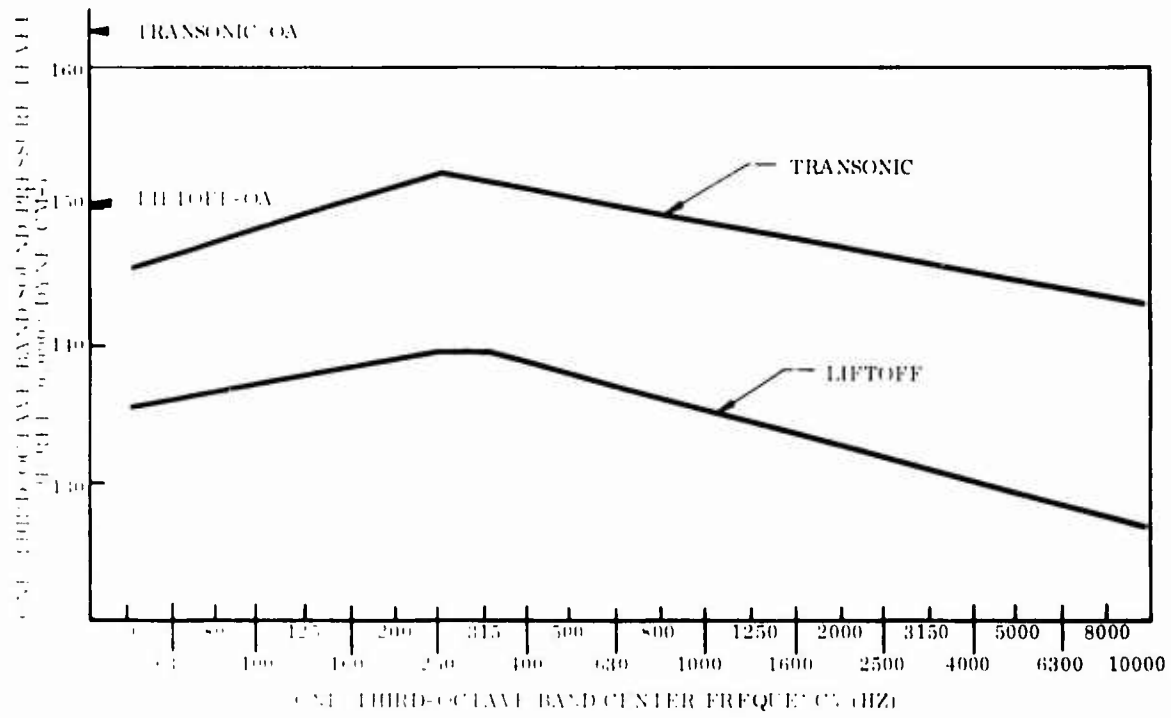
Fig. 22 Typical Spectra

22
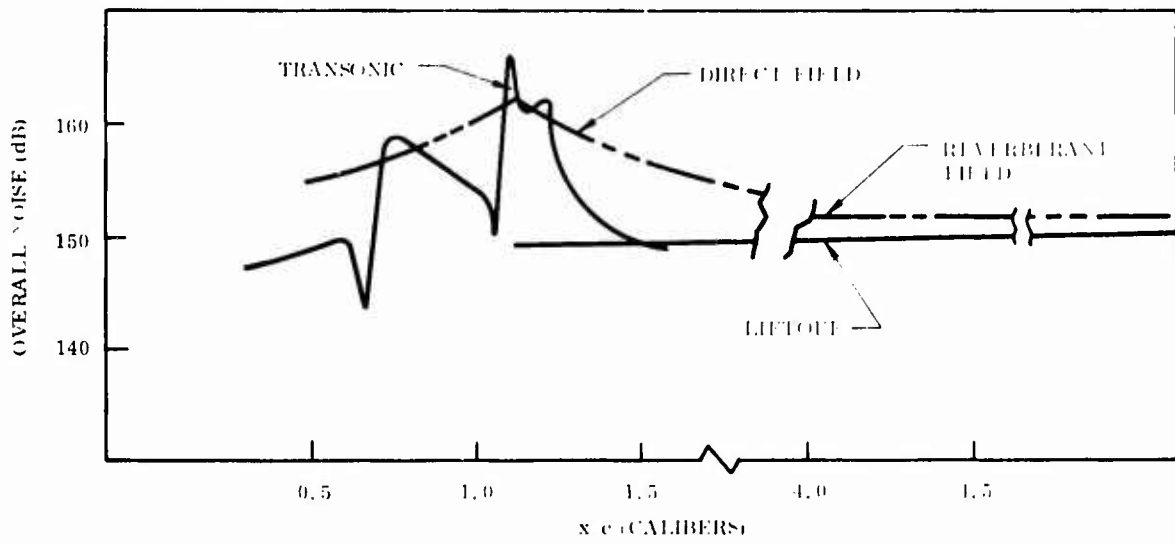
Fig. 23 Test Envelope for Service Environment
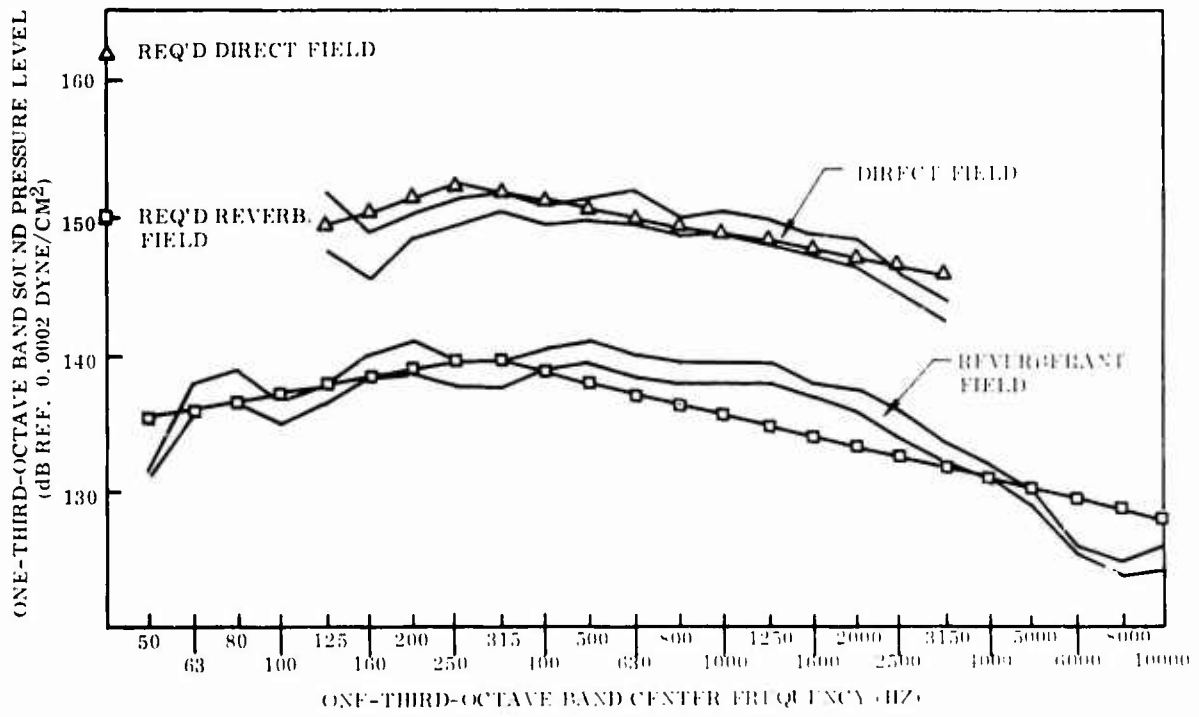
Fig. 24 Simulation of Service Spectrum

23

TYPICAL ENERGY BALANCE – INTERNAL ACOUSTIC FIELD

$$\omega \eta_{13} n_1 \left(\frac{E_1}{n_1} - \frac{E_3}{n_3} \right) + \omega \eta_{23} n_2 \left(\frac{E_2}{n_2} - \frac{E_3}{n_3} \right) = \omega \eta_{34} n_3 \left(\frac{E_3}{n_3} - \frac{E_4}{n_4} \right) + \omega \eta_{35} n_3 \left(\frac{E_3}{n_3} - \frac{E_5}{n_5} \right) + \omega \eta_3 E_3$$

E – TOTAL ENERGY
ω – ANGULAR FREQUENCY
n – MODAL DENSITY
η – COUPLING LOSS FACTOR

1 – EXTERNAL ACOUSTIC FIELD

2 – OUTER CYLINDER

3 – INTERNAL ACOUSTIC FIELD

4 – INNER CYLINDER

5 – INNER VOLUME ACOUSTIC FIELD
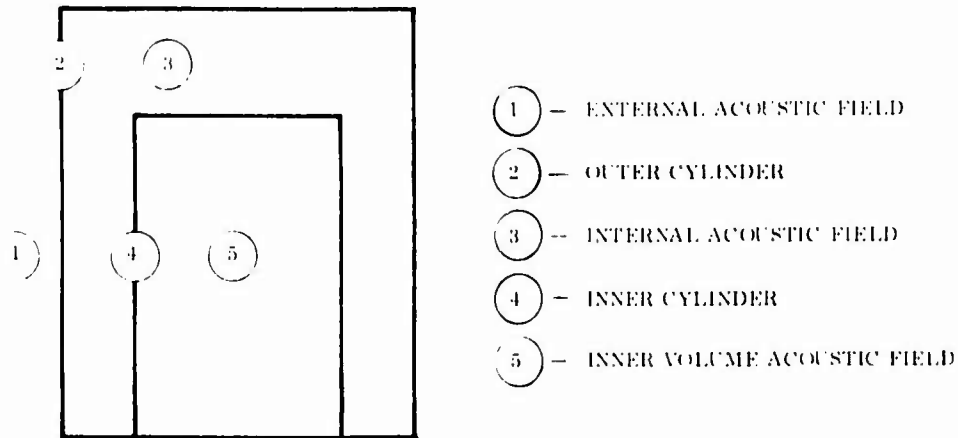
Fig. 25 Dynamic Model for Statistical Energy Analysis
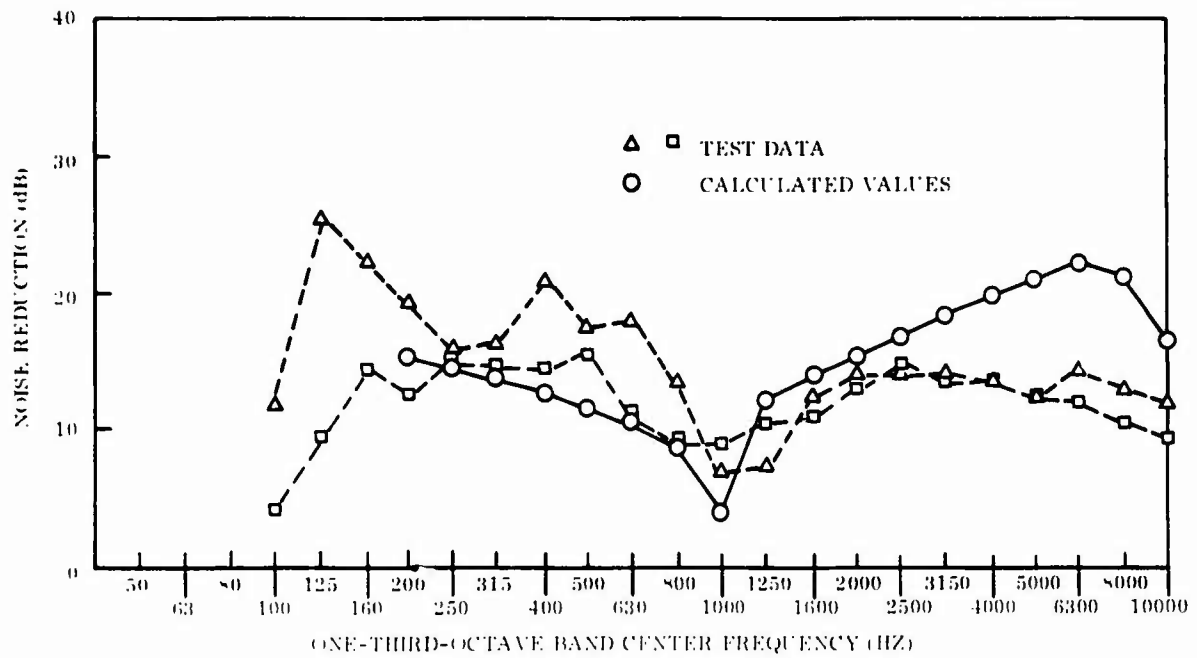
Fig. 26 Noise Reduction of Outer Cylinder

24
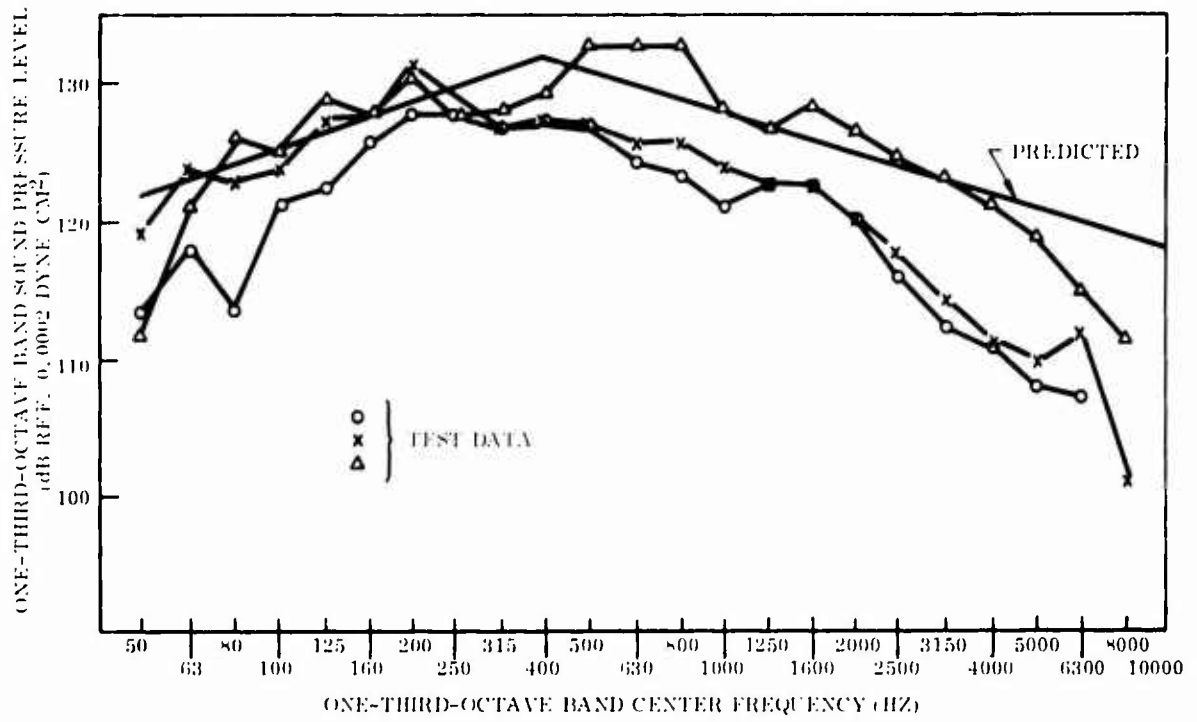
Fig. 27 Internal Measurements Compared to Statistical Energy Analysis Predictions
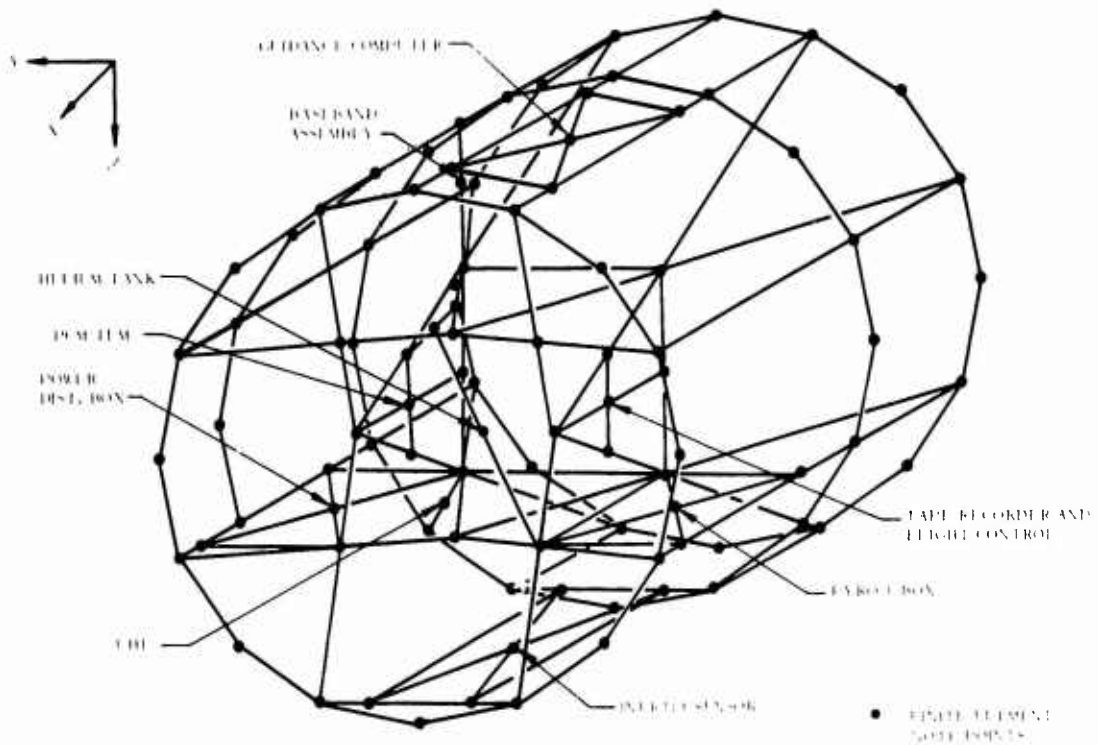
Fig. 28 Finite Element Model

25
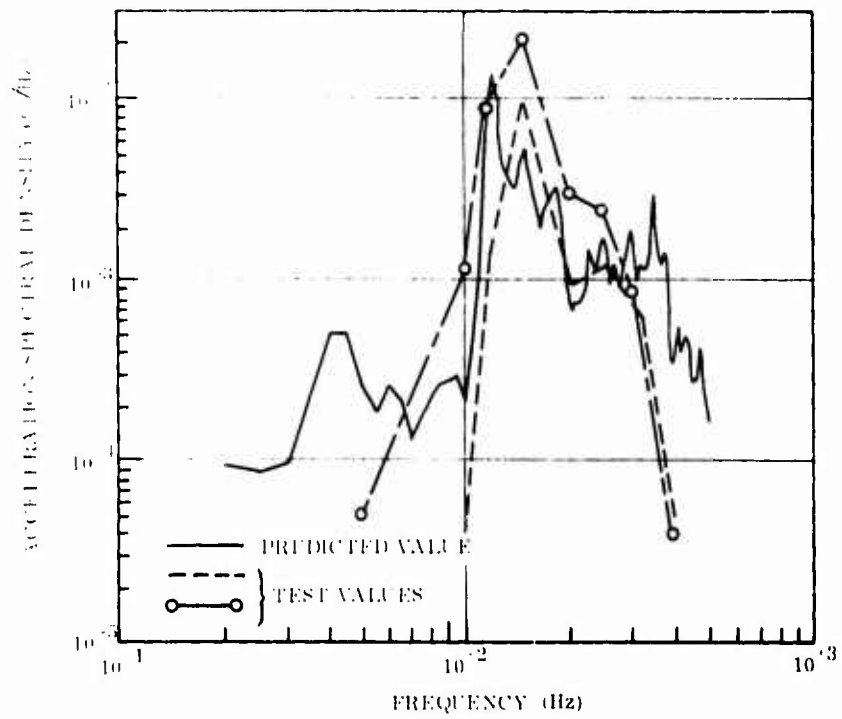
Fig. 29 Predicted Versus Actual Gyro Platform Response (Rectilinear Motion)
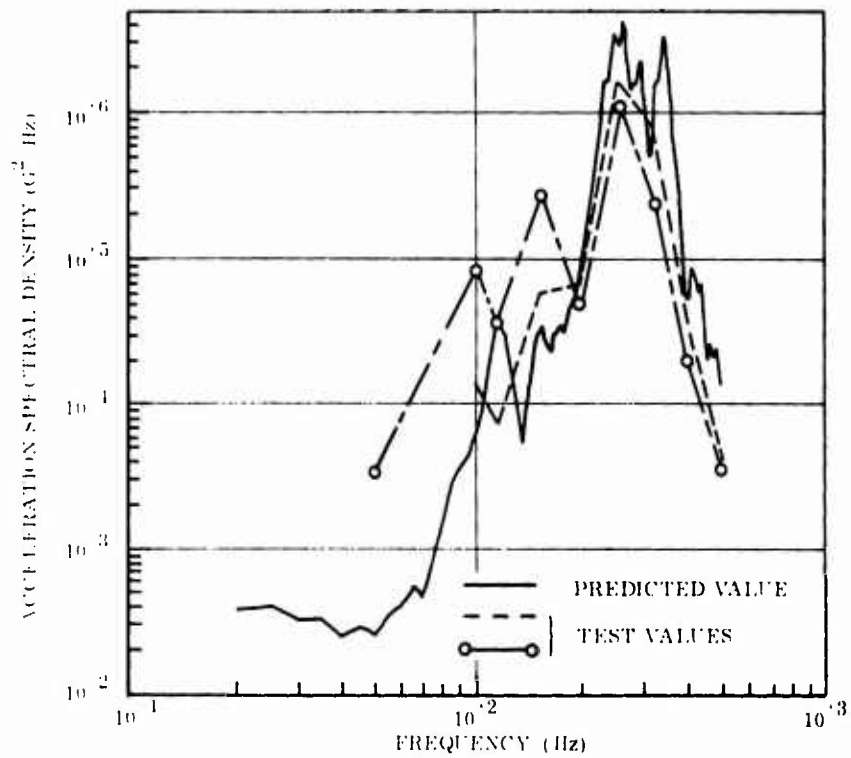
Fig. 30 Predicted Versus Actual Gyro Platform Response (Rotational Motion)

26
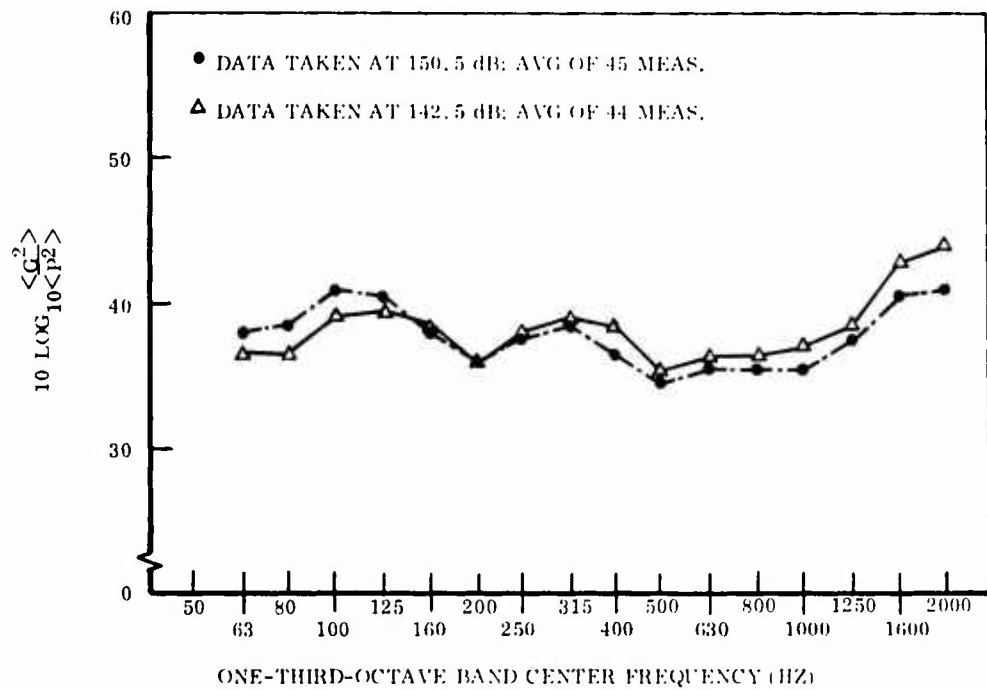
Fig. 31 Verification of Equipment Response Scaling
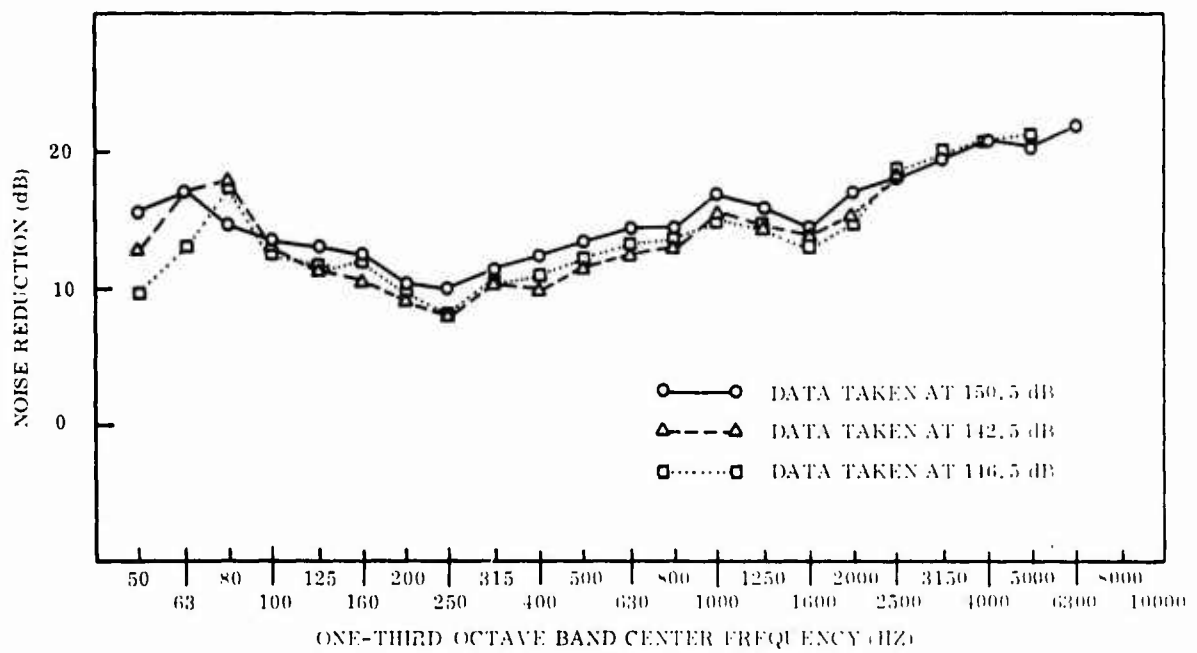
Fig. 32 Verification of Acoustic Field Scaling

27

METHODS USED TO REALISTICALLY
SIMULATE VIBRATION ENVIRONMENTS[*]

J. V. Otts
Centrifuge, Vibration, and Acoustics Division,
Sandia Laboratories, Albuquerque, New Mexico

Realistic laboratory simulation of a system's field vibration environment has been of major concern to the test engineers at Sandia Laboratories for the past 5 years. As a result, new test capabilities and test techniques, as well as procedures for deriving input test levels, have been developed and applied. This paper discusses the progress at Sandia by (1) summarizing and referencing past work which has been reported, and (2) detailing the more recent developments.

More specifically, several techniques used to derive force and/or acceleration input and limit levels are considered. These procedures are based upon field vibration data and the apparent weight[†] characteristics of the test unit. Both sinusoidal and random test specifications will be considered.

A large number of test techniques and capabilities are presented. These are outlined below.

(1) Force and/or acceleration limiting

(2) Force input control

(3) Electronic simulation of the test item's field foundation during force testing

(4) Reproduction of field response using field recordings

(5) Repetitive and single-shock pulse reproduction on shakers

(6) Input control of the product of force-acceleration

(7) Multipoint and multishaker input control

(8) Multiaxes (simultaneously) testing

INTRODUCTION

One phase of vibration testing is concerned with evaluating the structural and/or functional integrity of a system. The success of this type test is a function of realistic and accurate simulation of the field environment the system will experience during its service life. In addition, the test should be conservative, but not to the extent that unrealistic problems are encountered.

[†] Apparent Weight, W_A, is the complex ratio of force and acceleration and is related to mechanical impedance, Z, by $W_A = Z/j\omega$.

was presented as plots of peak and rms acceleration vs. frequency. This data resulted from a statistical enveloping technique. More recently, the VIBRAN system has been used. Foley [2] describes this system which presents the data in the form of acceleration level vs. 1/3 octave bands. In addition, the VIBRAN (1) displays the percentage of sample peaks which exceed various acceleration levels within each band. (2) gives the rms level within each band, and (3) gives the overall rms level between 0 and 1900 Hz.

Utilization of VIBRAN is demonstrated in reports by Murfin [4] and Otts. [5]

VIBRAN data is available for either an accumulation of similar systems or for specific systems. When data for a specific system is not available, the standard procedure is to pull data accumulated for systems similar in design and which have experienced similar environments. In this situation, the data provides a fairly conservative estimate of probable field responses.

Recorded Field Data

In addition to using recorded field data for the analyses described in B above, these recordings are also used to provide a direct input source for the shaker. This technique will be described in Section II below.

Unless otherwise specified, the EDB stores all field recordings for a period of 5 years.

Apparent Weight (W_a)

Apparent weight (W_a) is the ratio of vibratory input force to vibratory input acceleration as a function of frequency; i.e. $W_a(\omega) = [F(\omega)]/[\ddot{x}(\omega)]$, where F is the force in pounds, $\ddot{x}$ is the acceleration in g units, and ω is the circular frequency. Apparent weight, which has dimensions of pounds, is related to mechanical impedance by a factor of $j\omega$, where $j = \sqrt{-1}$. Measurement of apparent weight for sinusoidal and random inputs is considered by Otts [5] and Otts and Hunter [6] respectively.

The use of apparent weight in calculating vibration input specifications for the various test techniques will be considered in Section II. This system characteristic is measured on nearly all test items at Sandia. In fact, this data is being added to the Environmental Data Bank to be used in conjunction with field data as discussed by Murfin. [4]

Beam ... ... the ... of a function ... test parameters ... EDB ... appear ... This report describes the ... of Sandia Laboratories ... regards these ... Work ... it has been re ... provided as ... be ... in the refer ...

The ... used in deriving the test parameters will be considered first, followed by a discussion of the test technique developed to meet existing test requirements. Derivation of test parameters for specific test techniques will also be considered.

SOURCES USED IN DERIVING TEST PARAMETERS

Standard Specifications

Most standard specifications, such as MIL-STD-810, call out motion control of the input. The input amplitudes are essentially constant across the frequency test range, with the amplitude being derived from enveloped field measurements. The test levels described in the standards are not to be interpreted as an exact or conclusive representation of actual service operation. As stated in MIL-STD-810B, "the environmental levels specified should be modified when it is known that the test item will encounter conditions more severe or less severe." In other words, the standard specification is not realistic in most cases, but is designed to provide assurance that the test item could survive its service life.

It is indeed unfortunate that many test laboratories are restricted to following the standard specification even when accurate data sources, directly applicable to the system, are available.

Sandia Laboratories Environmental Data Bank

The primary source of vibration data for all Sandia test programs is the "Environmental Data Bank" (EDB). Foley [1, 2] and Gens [3] have previously described the EDB which is the result of 10 years of data collection, data analysis, and data storage.

The EDB contains computerized records of phases of vibration environments such as storage, transport, utilization, etc. Each phase is further divided into input and response information. Data from the EDB is available in two forms. Prior to 1963 the data

TEST TECHNIQUES

Motion Control

Motion controlled vibration tests where the input is maintained constant, can be classified as infinite apparent weight testing since the test item is not allowed to affect its environment as it does in the field. The disadvantages of this type test, as outlined by Otts, [5] include both overtesting and undertesting of the test item.

The problem of overtesting is further exaggerated by the specification of flat input levels derived from enveloped field response data such as described in I.A. and I.B above. The specification problem is considered by Vigness. [7]

Unfortunately, most vibration laboratories are compelled to run motion-controlled tests. This situation stems from (1) lack of more realistic sources of data, (2) reluctance to change test procedures, and (3) compulsory test specifications imposed by the contractor. Sandia Laboratories is minimizing use of this test technique and substituting more realistic techniques as described herein.

Motion Limiting the Response

Motion limiting is a technique which prevents the vibratory response at various points on the test item from exceeding specified levels. Basically, the input is reduced by switching the control to the response transducer whenever the motion exceeds the specified limit.

Motion limiting, applied to motion input control tests, causes the input motion to dip. This reduces the chances of overtest since the technique allows the test item to affect its own environment. This is further considered by Otts. [5]

Murfin [4] derives motion limits for sinusoidal tests. These limiting values are a function of field data. Witte and Rodeman [8] derive limits for random tests, which are again a function of field response data. For cases where there is no applicable field data, it has been a Sandia practice to limit the response at critical points to 20.0 g. This conservative level was derived from the fact that field data seldom reflects responses any higher than 14.0 g.

Sinusoidal tests can be limited using commercially available electronics. On the other hand, there is no established technique for automatic limiting during random testing. Manual adjustment of the random input spectrum, to prevent the rms level in each band from exceeding a specified level, is considered by Witte and Rodeman. [8] The amount of adjustment is derived from the transfer function between the input and response points on the test item.

Force Limiting the Input to the Test Item

Force limiting prevents the input force to the test item from exceeding specified levels. Should the specified force level be reached during motion-controlled testing, the input control switches to the force input.

Motion limiting is normally used in preference to force limiting due to the relative simplicity of mounting accelerometers. However, both techniques accomplish the same effect, that being to cause a dip in the foundation motion as described above.

Since the derivation of force limit values has not been considered previously, the necessary calculations are included below. Force limits can be derived as a function of field acceleration data and test item apparent weight data. For sinusoidal testing,

$$F(\omega) = W_a(\omega)\, G(\omega)$$

Where $F(\omega)$ = force limit amplitude at each frequency (lbs)

$W_a(\omega)$ = apparent weight

$G(\omega)$ - field acceleration (g)

It is customary to smooth the curves by taking an average apparent weight over as wide a frequency band as possible, and encompassing acceleration data over the same range.

For random testing,

$$F(\omega) = \left| W_a(\omega) \right|^2 G(\omega)$$

Where $F(\omega)$ = force spectral density within a frequency band (lbs^2/Hz)

$W_a(\omega)$ = band averaged apparent weight

$G(\omega)$ = field acceleration spectral density within a frequency band (g^2/Hz)

Another technique for deriving random
force limits would be to consider the rms force
at each acceleration within each band, and use
the equation for sinusoidal force limiting given
above.

Force Control of the Input

The arguments for force control versus
motion control have been presented by Otts, [5]
and therefore will not be reemphasized at this
time.

Force controlled vibration testing falls
into two basic categories: (1) control of force
input below the test item, and (2) control of
force input below the test system, where the
system includes the test item and its founda-
tion. Both techniques are considered below.

1. Force Input Below Test Item

Constant Force Input -- When the force
input below the test item is maintained at a
constant level, the apparent weight character-
istics of the foundation have no influence on
the force input or motion response of the test
item. Therefore, this is referred to as a
zero apparent weight test.

Although force control testing of this
type is not realistic, it is preferred to motion
control since the dynamic characteristics of
the test item are allowed to affect its own
motion response.

Derived Force Input (Sinusoidal) -- A
realistic approach to sinusoidal force control
is described by Murfin. [4] Basically, Murfin
derives the input force spectrum as a function
of field acceleration data and the apparent
weight characteristics of the test item.

$$F(\omega) = W_a(\omega)\, G(\omega)$$

Where the apparent weight, $W_a(\omega)$, is meas-
ured in the laboratory and the field accelera-
tion for the specific system, $G(\omega)$, is taken
from VIBRAN. The apparent weight used for
each data frequency band of VIBRAN is biased
towards the minimum value, thus providing a
conservative estimate within each band.
Murfin also considers the derivation of ac-
celeration response limits to be imposed dur-
ing this type test.

Derived Force Input (Random) - Witte
and Rodeman [8] describe the procedure used
in deriving random force specifications. The
technique utilizes enveloped field data from
the Environmental Data Bank and the driving

point apparent weight of the test specimen as
shown below.

$$F(\omega) = \left| W_a(\omega) \right|^2 G(\omega)$$

where $F(\omega)$ and $G(\omega)$ are the input force spec-
tral density and field enveloped acceleration
spectral density, respectively. The magnitude
of W_a is again biased towards the minimum in
each test band.

Random acceleration response limiting,
with the present equipment, requires that the
input spectrum be modified by calculated
amounts. The use of transfer functions be-
tween the input and response points, as de-
scribed by Witte and Rodeman, [8] was discus-
sed previously.

In summary, the control of a constant
force input is classified as zero apparent
weight testing. Although it is unrealistic, it
has the advantage over motion control in that
the dynamic characteristics of the test item
are allowed to affect its motion response.

Calculation of a force input spectrum,
where the amplitude is a function of field data
and the apparent weight of the test item, can
be classified as controlled apparent weight
testing since the input force and motion are a
function of field response, which in turn is a
function of the dynamic characteristics of the
test item and its foundation. Field measure-
ment of the vibratory force would be desirable,
but this presents extreme difficulty since force
transducers must be inserted directly in the
path of transmission.

2. Force Input Below Test System (Foundation and Test Item)

Force control of the input below both the
foundation and the test item is classified as
controlled apparent weight testing since the
dynamic characteristics of the foundation, as
seen by the test item, are taken into account.
As discussed in several articles, [4, 5, 9, 10]
the degree of reality in this test technique is
a function of one's ability to both accurately
determine and simulate the apparent weight of
the foundation, as seen by the test item, and
determine the force spectrum to be applied.
Nuckolls [9] and Otts and Hunter [6, 11] have
developed techniques whereby the dynamic
characteristics of the foundation can be elec-
tronically simulated for both sinusoidal and
random testing. Electronic simulation is re-
quired since it is not normally feasible to

32

insert the actual foundation in a laboratory test.

Application of this technique is described in several reports [10, 12, 13] where blocked force measurements were made to determine the vibratory force input from a rocket motor to the payload. The apparent weight of the rocket motor was measured and electronically simulated during a force-controlled vibration test on the payload.

Unfortunately, it is difficult for one to determine the apparent weight of most foundations. Therefore, this technique is seldom used although it is one of the more realistic approaches. Those force techniques previously described find more application in the laboratory.

Force-Motion Product Control

Witte [14] describes a technique which utilizes the product of the force below the system and the motion at the base of the system (above the force input) as the control signal. The method is a compromise between motion control and force control of the type classified as zero apparent weight testing.

Since the input motion and input force are both a function of the system's apparent weight, the test item is allowed to affect its vibration environment. Therefore, this force-motion product technique proves useful when nothing is known about the dynamic characteristics of the system's field foundation. As demonstrated by Witte, input force and input motion are both limited, and the effective source apparent weight is neither zero nor infinite.

The input force-motion control specifications are derived in a second paper by Witte. [15] Briefly, the input level is derived as a function of field acceleration data and the apparent weight characteristics of the test item. Acceleration limiting values are also derived in this paper. Application of this technique is intended only for sinusoidal testing since the control and derivation of force-motion products for random vibration have not been explored or developed.

Reproduction of Field Response

One of the greatest advancements towards realistic vibration tests was the development of a technique whereby field vibration could be reproduced in the laboratory. Otts and Hunter [16] describe an analog technique

while LeBrun and Favour [17] describe a digital technique which allows laboratory reproduction of field data. The computerized technique is more accurate and efficient.

Basically, both techniques equalize the transfer function between the signal source and the shaker output (or point on test item) to unity over the frequency test range. Phase preservation is also important. The field data, recorded on magnetic tape, is then used as the input to the shaker test system.

This procedure has been used to reproduce component and system field response to short burst vibration such as that experienced during rocket ignition, payload separation, and payload ejection from a bomb rack. To date, long duration responses have not been reproduced in the laboratory. However, there is no technical limitation to this type application.

Reproduction of Synthesized Signals

Obviously, the above reproduction technique can be used to produce system response in the form of short burst sinusoid, decaying sinusoid, single shock pulse and repetitive shock pulses, to name a few. This technique is sometimes used in an attempt to simulate field response such as resonant ringing. Otts and Hunter [18] consider application of the technique as well as the limitations imposed by the shaker system.

Multipoint Input Control

The multishaker test technique utilizes two or more shakers to supply the vibratory input to the system. Each shaker is individually controlled, usually to different input specifications. The technique is finding increased usage on test systems which utilize multipoint mounts in the field. Individual input specifications for each point are derived from field data recorded at the respective points. Normally, the VIBRAN analysis described in Section I.C is used to derive the input levels.

Cross-coupling between input points presents a control problem. Hunter and Helmuth [19] consider this problem, as well as propose a manual adjustment which solves the problem. However, there is not an automatic, electronic solution available to date.

A report in this technique, as applied to several test programs, is forthcoming.

2. J. T. Foley, "An Environmental Research Study," Institute of Environmental Sciences, April 1967 Proceedings.

3. M. B. Gens, "The Environmental Operations Analysis Function," Institute of Environmental Sciences, 1967 Proceedings.

4. W. B. Murfin, "Dual Specifications in Vibration Testing," Shock and Vibration Bulletin, 35, August 1968, Part I.

5. J. V. Otts, "Force Controlled Vibration Tests, A Step Toward Practical Application of Mechanical Impedance," Shock and Vibration Bulletin, 34, February 1965.

6. J. V. Otts and N. F. Hunter, "Random-Force Vibration Testing," Shock and Vibration Bulletin, 37, January 1968.

7. I. Vigness, "Measurement Equipment Vibrations in the Field as a Help for Determining Vibration Specifications," Shock, Vibration, and Associated Environments, 34, December 1963.

8. A. F. Witte and R. Rodeman, "Dual Specifications in Random Vibration Testing, An Application of Mechanical Impedance," Shock and Vibration Bulletin, 41, October 1970.

9. C. Nuckolls, "An Approximate Method of Simulating Mechanical Impedance in Vibration Testing," Institute of Environmental Sciences, 1965 Proceedings.

10. C. E. Nuckolls and J. V. Otts, "A Progress Report on Force Controlled Vibration Testing," Shock and Vibration Bulletin, 35, January 1968.

11. N. F. Hunter and J. V. Otts, "Electronic Simulation of Apparent Weight in Force Controlled Vibration Tests," 22nd ISA Conference, Preprint Number P15-1-PHYMMID-67, September 1967.

12. J. V. Otts, "A Study of the XW-25 Vibration Response to Structure-Borne Input from the Genie Rocket," Sandia Report SC-DR-66-186, May 1966.

13. M. W. Sterk, "A Comparison of the W-25 Field and Laboratory Data with Inputs from the Air-2A Rocket," Sandia Report SC-DR-69-312, June 1969.

CONCLUSIONS

Realistic vibration tests are a function of (1) the environmental data for reference, (2) the analysis used in deriving the test specifications, and (3) the test techniques used in the laboratory.

REFERENCES

1. J. T. Foley, "Preliminary Analysis of Data Obtained from the Army-MRC Sandia Corporation Transport Environment Measurement Project," Shock and Vibration Bulletin, 35, February 1966.

14. A. F. Witte, "A Force-Acceleration Control Technique for Vibration Testing," ISA Conference, Reprint Number 69-560, October 1969.

15. A. F. Witte, "Specification of Sine Vibration Test Levels Using a Force-Acceleration Product Technique," Shock and Vibration Bulletin, 41, October 1970.

16. J. V. Otts and N. F. Hunter, "Reproduction of Complex and Random Waveforms at Various Points on a Test Item," Shock and Vibration Bulletin, 36, January 1967.

17. J. M. LeBrun and J. Favour, "Feasibility and Conceptual Design Study--Vibration Generator Transient Waveform Control System," Contract NAS5-15171 Report.

18. J. V. Otts and N. F. Hunter, "Shock Reproduction on Shakers," ISA Conference, Reprint Number 69-561, October 1969.

19. N. F. Hunter and J. G. Helmuth, "Control Stabilization for Multiple Shaker Tests," Shock and Vibration Bulletin, 37, January 1968.

DISCUSSION

Mr. Trubert (Jet Propulsion Laboratory): You mentioned a multiple shaker at the end. Is this random excitation that you are talking about?

Mr. Otts: Is it random or sine? In this particular case we have done both. I might add we have run sinusoidal and we have run random type spectra. In this particular case on this test which was probably run a month ago it happened to be a random type input.

Mr. Trubert: You mentioned difficulty in the equalization of the three shakers. We at the Jet Propulsion Laboratory have done some work and it is possible to make an equalization using an analog computer. Are you aware of that?

Mr. Otts: Yes I am. We have considered this, however, unfortunately we do not for approximately the next one year have a shaker or a computer system available so we have to be old fashioned until that time.

Mr. Trubert: In what frequency range did you have your excitation?

Mr. Otts: Twenty to 2000 Hz.

Mr. Trubert: What kind of resonances did you have for your structure? Did you have a lot of resonances or just a few?

Mr. Otts: Quite a few. As a matter of fact, as it turns out, the first major resonance was probably around 100 Hz. It was quite typical of a large system. There were a good number of resonances encountered.

Mr. Trubert: That is a difficulty that we have found for the low frequencies. It is possible to equalize with another computer, but for the high frequency you need too many normal modes to be able to equalize.

Mr. Otts: Some sinusoidal surveys were made to determine approximately where the resonances would occur, and then each shaker, one at a time, was equalized and then turned off. They were then all brought up together, and of course we had to tweak the various bandwidths then to compensate for the peaks and valleys which occurred because of cross coupling. This is a problem. It is something we have not solved as yet.

35

SIMULATION OF COMPLEX-WAVE
PERIODIC VIBRATION

A. J. Curtis, H. T. Abstein, Jr., and N. G. Tinling
Hughes Aircraft Company
Culver City, California

A vibration test method that has general applicability for simulation of complex-wave periodic environments is described. The method, which was developed to simulate the effects of aircraft vibration induced by rapid fire (Gatling) guns, makes use of a repetitive pulse as an excitation signal for conventional electro-dynamic vibration systems. The method is a modification and extension of a similar method described in a paper by J. A. Hutchinson and R. N. Hancock at the 40th S and V Symposium.

The paper includes a description of the rather simple ancillary equipment which, in conjunction with conventional random vibration control equipment, is used to generate and control the desired complex waveform. The use of variable pulse repetition rate and multiple accelerometer signal control is described. In addition, a method for rapid analysis of the line spectrum of the resultant vibration using an existing comb-filter analog/digital vibration analysis system is included.

Results of the use of this test method during testing of an airborne weapon control system are described. The economy of test and superior simulation characteristics of the method, compared to alternative approaches such as Method 519 of MIL-STD-810, are discussed.

INTRODUCTION

The waveform of a complex-wave periodic vibration is a periodic deterministic waveform which can be described mathematically by a Fourier series. Such a waveform is common to any periodic vibration except perhaps a very excellent tuning fork. This waveform takes on particular significance when a number of the Fourier coefficients are of the same order of magnitude. Measurements of vibration due to rapid fire cannon have shown that many harmonics must be employed to adequately describe the waveform.

At the 40th Shock and Vibration Symposium, Hutchinson and Hancock [1] described a method of simulating this type of vibration using a pulsed excitation. This paper describes a modification and extension of that method together with a description of equipment for general test implementation and data analysis.

DESCRIPTION OF ENVIRONMENT

Of all the sources for complex-wave periodic vibration, the one of most interest recently, is high speed "Gatling" guns in aircraft. These guns typically fire at rates of 20 to 100 rounds per second and create periodic high blast pressures around the gun muzzle in addition to periodic reaction forces at the gun mount. The reaction forces can be isolated from the aircraft structure [1] but no method has been found to effectively reduce the blast pressures impinging on the exterior fuselage panels. An idealized waveform of the pressure acting on the exterior skin is shown in

Fig. 1 [2]. The pressure pulse has a short
duration with respect to the period of the pulse
repetion frequency (PRF). Expansion of this
waveform in a Fourier series of the form

$$F(t) = a_0 + \sum a_n \sin(w_n t + \phi_n)$$

results in the coefficients shown in Fig. 2.
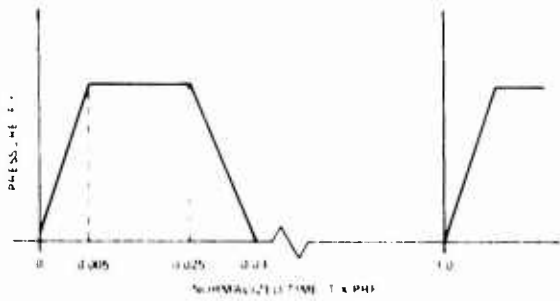
Fig. 1 - Idealized pressure waveform of
Gatling gun, time normalized by firing
frequency (PRF).

Note that the amplitude of the coefficients
remains at a fairly constant value over a
broad frequency range. For example, at a
PRF of 100 Hz the blast pressure acting on
the exterior of the aircraft would have signif-
icant levels covering a frequency range from
100 Hz to well over 2000 Hz. The structural
vibration of the fuselage resulting from this
excitation will possess the same characteris-
tics as the excitation. It will consist of line
spectra at the harmonic frequencies with
amplitudes and phase angles dependent on the
dynamic transfer characteristics of the
structure.

In a report on the measurement and analy-
sis of gunfire vibration on the F-5A aircraft
[3] it was noted that the high frequency portion
of the structural vibration appeared to have
random characteristics and required random
vibration analysis techniques. This random
characteristic can be attributed to the vari-
ability of firing rate and pressure waveform.
During any one burst, i.e., a series of rounds,
the pressure and PRF will vary because of
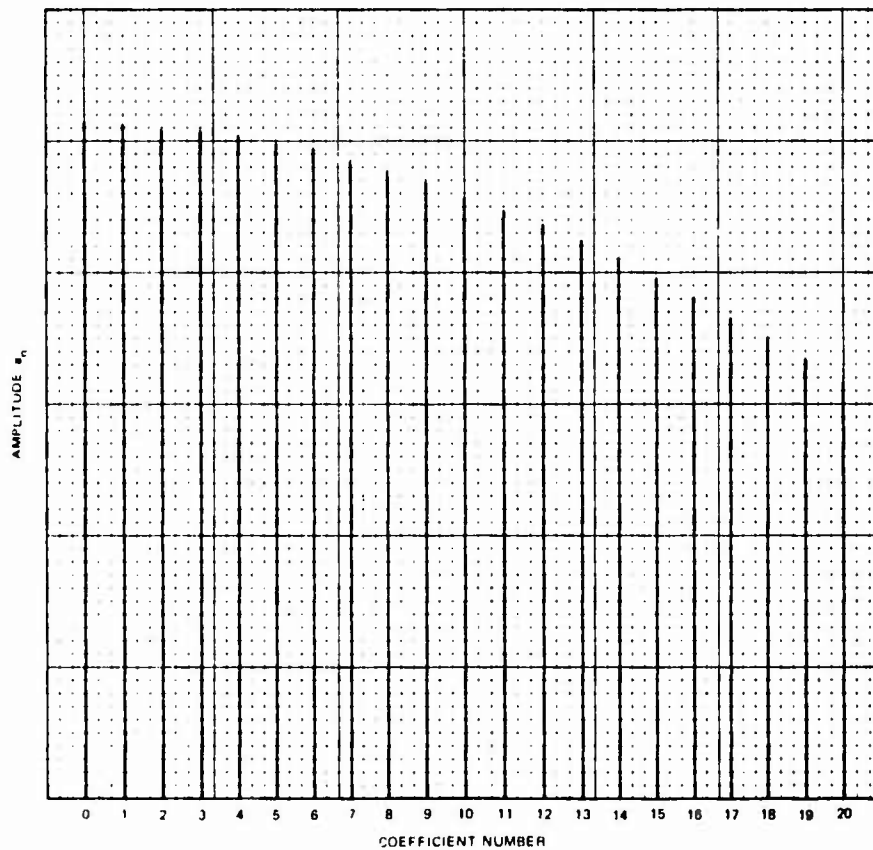
Fig. 2 - Fourier series coefficients of waveform shown in Fig. 1.

38

differences in ammunition charge, variations in hydraulic pressure which regulates speed, mechanical tolerances, etc. Even though the pressure amplitude varies from one round to another its variation is not considered significant because of the large amount of variation required to produce a substantial appearance of randomness. In addition, the variation in pressure amplitude would have the same effect on all harmonics; an occurrence which is not observed in measured data. On the other hand, variations in pressure waveform, even if slight, may result in significant variation in the amplitudes of the higher ordered harmonics.

Small variations in the PRF can also have significant effects on the amplitude of the filtered high frequency harmonics. The absolute value of the variation in frequency of any harmonic is proportional to the harmonic number and, therefore, will be greater in the higher frequency region. When the data is analyzed with constant bandwidth filters the variation in frequency with respect to the filter bandwidth will increase with frequency and thus the amplitude will appear to become more random. If the data is analyzed with constant percentage bandwidth filters, i.e., bandwidths proportional to center frequency, the randomness in signal output will also increase in frequency because of the increasing density of the harmonics within the bandwidth of the filter. The harmonics are separated by a constant value of frequency equal to the PRF and, therefore, have a density proportional to the analysis bandwidth.

In addition to the variation of PRF within a burst of data, there is a greater variation of PRF from one burst to another. A ±5 percent

variation from the fundamental PRF is typical. Considering this variation, the possible excitation frequencies, normalized by the PRF, are shown in Fig. 3. In the low frequency region there are several bands of zero amplitude. Above the ninth harmonic the spectrum is continuous and all frequencies can occur.

Complex periodic waveform vibration also exists in tracked vehicles such as tanks and armored personnel carriers or in equipment with rotating or impacting machinery. It is likely that the PRF is also variable for these situations and the techniques for simulation of gunfire vibration as discussed here are generally applicable.

SIMULATION GOALS

The goal of any laboratory simulation of vibration is to simulate the damaging effects of vibration on the test item. To this end the closer the excitation waveform represents the actual service waveform, the better the chance for success. Any method of simulation gunfire vibration should attempt to achieve this goal and also be economical to perform, use existing vibration test equipment to the greatest extent, and require minimum development of unique ancillary equipment. A listing of feasible excitation waveform types is not long:-

1. Sinusoidal

2. Broadband Random Noise

3. Narrowband Random Noise

4. Pulsed

5. Pulsed and Broadband Random
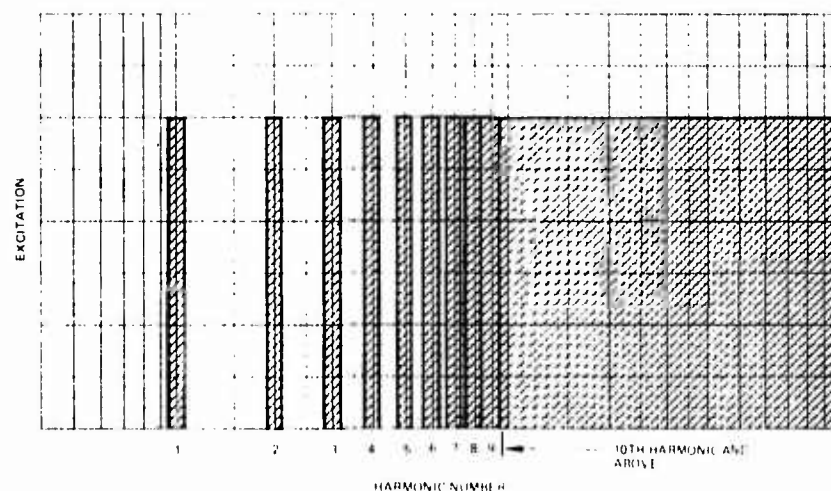
Fig. 3 - Excitation frequencies of complex periodic waveform with ±5% variation of PRF.

39

For each type, a number of options exist in defining the procedural details. However, selection of the waveform can be pursued generally independent of these details.

1. Use of sinusoidal excitation has some appeal since a periodic, or at least, almost periodic waveform is to be simulated and thus each harmonic of the waveform can be simulated in turn. The weakness of this approach is that the relationship between the effects of applying each harmonic individually and all harmonics simultaneously is difficult, if not impossible to assess, particularly with respect to functional performance of the equipment. The rather obvious possibility of using the sum of the outputs of a number of oscillators, one for each harmonic, can be quickly discarded when the problems of amplitude and frequency control are considered.

2. Use of broadband random excitation immediately permits simultaneous excitation of all harmonics of the environment. However, it is clear, as discussed later, that a broadband level which, in some undefined way, is equivalent to the level of the harmonics, must be very conservative in the frequency bands between the harmonics. Further, having for some time resisted opportunities to simulate random vibration environments by sinusoids, it seemed a little inconsistent for the authors to argue strongly for the simulation of a periodic environment by a random excitation.

3. Narrowband random excitation is, of course, no more deterministic than broadband random excitation. Compared to broadband random excitation, narrowband excitation does offer the advantage of avoiding the previously mentioned conservatism and, with appropriate selection of bandwidth and center frequency, providing excitation which covers the known variation in repetition rates. Reference [4] describes an existing, programmable narrowband random vibration excitation system which can generate and control three simultaneous, tuneable narrowband excitations. Use of this system would permit the simultaneous simulation of up to three harmonics. With incorporation of additional servo loops, as many harmonics as desired could be generated, but with obvious increase in procedural complexity and facility cost.

Regarding the use of random excitation to simulate a complex-wave periodic, i.e., deterministic, excitation, two points are of interest. First, the phase relationships between the harmonics are undefined in any existing data and will certainly vary from point to point in the structure. Thus random excitation, with its statistically varying phase, will in an indirect manner, simulate all the possible phase relationships of an actual environment. Secondly, as part of the development of the test method, the response of a single degree-of-freedom system to recorded gunfire vibration was examined, using an analog shock spectrum computer. It was interesting to note that the pseudo shock-spectra obtained for several damping factors (Q's) indicated that the spectra varied more as $\sqrt{Q}$ than Q itself, which is typical of the response to random excitation. This indicated that random excitation would perhaps provide a better simulation of effects or responses than could be obtained from a single sine wave.

4. At some point during consideration of the first three types of excitations, the following situation was realized, either consciously or not. The environment was created from a pulsed excitation and had been broken down into its constituent parts, i.e., harmonics, for understanding and quantitative description. The simulation methods being considered essentially attempted to synthesize the constituent parts and then mix them back together. With this realization, the possibility of starting with a pulsed excitation and then modifying it appropriately to achieve the proper mix became the obvious choice of excitation waveform. Several simulation requirements are immediately fulfilled. First, all harmonics are generated at once. Second, the deterministic nature of the waveform is achieved. Third, the phase relationships, even if incorrect, are at least not artificially controlled and would be repeatable for a given test set-up. Fourth, variation of the pulse-repetition rate would tune all harmonics correctly. Fifth, the test duration is immediately determined since "realtime" testing is achieved. In addition, it became apparent that the use of a variable-PRF pulse generator together with otherwise standard vibration test equipment would permit the generation of an appropriate excitation. It is assumed that Hutchinson and Hancock [1] must have gone through a similar thought process when developing their very similar method at approximately the same time as the authors of this paper.

5. During the investigation of gunfire data to define the environment and develop a test method, it appeared that even during ground firing, vibration excitation at a reduced level, which appeared to be essentially random in nature, was present between the peaks in the spectrum at the multiples of firing rate. Although reduced in level, the level exceeded

the noise floor of the analysis equipment. In addition, it is evident that during inflight gunfiring, the gunfire excitation will be superimposed on the normal inflight random vibration. It is thus desirable to be able to simulate the combination of pulsed and broadband random excitation. This is achieved by the test method described below.

DESCRIPTION OF SIMULATION METHOD

A functional block diagram of a vibration system which can be used to generate and control the pulsed and broadband random excitation is shown in Fig. 4. It will be clear that the broadband random excitation is completely independent of the pulsed excitation and can be deleted at will. However the shape of the spectrum cannot be chosen completely independently of the pulsed excitation.

The pulsed waveform is obtained from a pulse generator which permits control of both the repetition rate (PRF) and pulse duration. Selection of the pulse duration and, more importantly, the ratio of pulse duration to repetition period (duty cycle) is determined by the number of harmonics to be generated. For ease of equalization it is desired that the amplitudes of the harmonics of interest be reasonably equal: since the rate of decrease in harmonic amplitudes is a function of the duty cycle, the greater the number of harmonics to be generated, the smaller the duty cycle should be. For example: for a duty cycle of 0.1, the Fourier coefficient is zero for the tenth harmonic with relative amplitudes dropping rapidly beyond the first few harmonics; however, for a duty cycle of 0.05, the first Fourier null occurs at the twentieth harmonic with relative amplitudes not dropping nearly so rapidly. In practice, a lower limit on the duty cycle is imposed by the equalizing equipment which is used. This stems from the fact that, as the duty cycle is decreased, the pulse amplitude must be increased to maintain the minimum

harmonic amplitudes required for adequate excitation; for a given equalizer, there will be a maximum input pulse amplitude which cannot be exceeded without causing saturation or clipping.

The pulse is fed to the input of a standard random vibration equalizer, switched to the manual mode, in order to adjust the relative amplitudes of the individual harmonic components to the desired values. Since the relative amplitudes of the harmonics of the pulse are known, either theoretically or by measurement of the pulse generator output, the relative amplitudes of the desired test spectrum can be obtained by adjusting the gain of each equalizer filter which contains a harmonic to the appropriate value. For example, if the desired harmonics are all equal, the transfer function through the equalizer should be the inverse of the envelope of the line spectrum of the pulse generator. For frequencies above the highest harmonics to be generated, the equalizer filters are set to maximum attenuation. The output of the equalizer which contains all the desired harmonics adjusted to the desired relative amplitudes is then fed to the power amplifier through the normal control console.

As shown in Fig. 4, control of the test level requires only control of the overall rms acceleration. However, it is advisable to use a low pass filter between the control accelerometer(s) and the rms meter so that the test level is not reduced below that desired, by the presence of unwanted higher frequency output from the control accelerometer.

Superposition of random excitation on the pulsed excitation is quite straightforward as shown in Fig. 4. In order to easily adjust gains, and to enable both combined and separate random and pulsed excitation during test set-up, it is necessary to use a random noise generator external to the equalizer system. The signal from the noise generator is fed to the equalizer through a gain setting potentiometer.
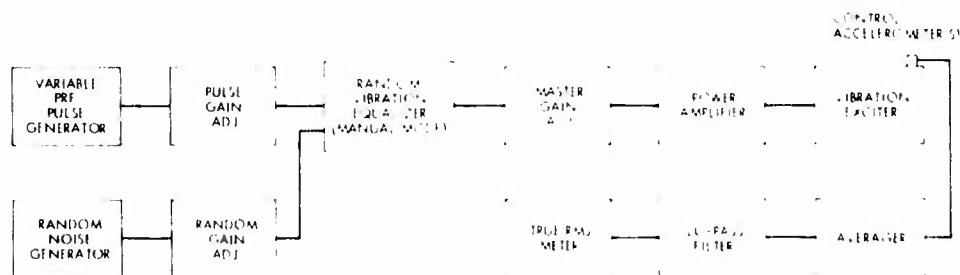
Fig. 4 - Functional block diagram of pulsed vibration excitation system.

41

The shape of the spectrum over most of the frequency range is determined by the previously discussed requirements for adjusting the relative harmonic amplitudes. However, with proper selection of duty cycle, an essentially white noise spectrum shape can be achieved.

The equalizer shown in Fig. 4 serves two purposes. The first, adjustment of the relative harmonic amplitudes, has been discussed. The second is for equalizing the radiation exciter-fixture-test article dynamic system. Equalization of the system to fulfill these purposes is accomplished by using random noise excitation in the usual fashion for manual equalization using the spectrum calculated to provide the desired relative harmonic amplitudes. The equalization can be performed at a low acceleration level with the test article in place. Alternatively, the authors believe preferably for typical "black boxes", the equalization can be performed at a level consistent with the test level and with an empty fixture. The loading of the fixture by the unit as the PRF is changed will then occur naturally and analogously to the situation in the aircraft installation. This also avoids excess vibration exposure of the test article since equalization in the manual mode may be lengthy.

After equalization, it is necessary to separately set the gains for the random and pulsed excitations. With the master gain (see Fig. 4) set to a desired operating point, and the random gain at zero, and using the initial test PRF, the pulsed gain is increased and the gain setting noted. Next, with the master gain at the same setting and the pulsed gain set to zero, the random gain is increased until the desired rms acceleration is achieved and the gain setting noted. The test can then be commenced with these gains set for the individual excitations and by increasing the master gain until the overall rms acceleration is achieved. As the PRF changes, either continuously or preferably stepwise, the overall rms acceleration is maintained by either manual or servo control of the master gain setting.

Fig. 4 shows an accelerometer signal averager, sometimes known as a time division multiplexer in the control system. It is desirable to use the average of several accelerometer signals for test level control for the same reasons as for any other type of excitation. Some of the problems associated with the use of averagers are discussed in a companion paper and will not be repeated here since they are not peculiar to the use of pulsed excitation.

The need to generate pulsed excitation over a range of PRF's has been mentioned previously. To obtain the most comprehensive test, it would be desirable to vary the PRF continuously over the appropriate range. However, the range involved is usually a small percent of the nominal PRF and is of the same order as typical resonant bandwidths. Thus a practical compromise is to step the PRF through the range in a suitable number of steps with small enough increments to excite any resonances within the range to essentially maximum response. This rather small compromise permits a significant reduction in test complexity and data reduction costs. In addition, test repeatability is improved from almost non-existent to very good. These benefits accrue from the following practical considerations:

1. If the PRF is to be varied continuously, the sweep parameter (whether it be voltage, resistance or capacitance) must be capable of being programmed in a repeatable manner. On the other hand, it is a relatively simple task to achieve precise repeatability of an incremental series of PRF's.

2. The excitation is a combination of pulsed and random excitation. If the PRF is constant, the excitation can be described by the harmonics of the pulsed excitation and the spectral density of the random excitation. If the PRF is continuously varying, the waveform is non-stationary. The excitation can then only be described by an approximation based on an assumed constant PRF during selected data samples. The difficulty of achieving a complete and accurate description of the excitation is clear.

3. The ability of the test technician to adjust the test level as the PRF steps from one value to the next is considered to be better and more consistent than his ability to continuously adjust the level as the PRF sweeps across the range.

Fig. 5 illustrates an example determination of the minimum number of PRF steps required. The total PRF range is divided into a number of equal increments and test PRF's placed at the center of each increment. The transfer function for a resonance with an assumed damping factor is drawn with the maximum value midway between adjacent PRF's. The maximum amount by which full resonant response is not achieved can be measured. In Fig. 5 using the PRF variation for

42
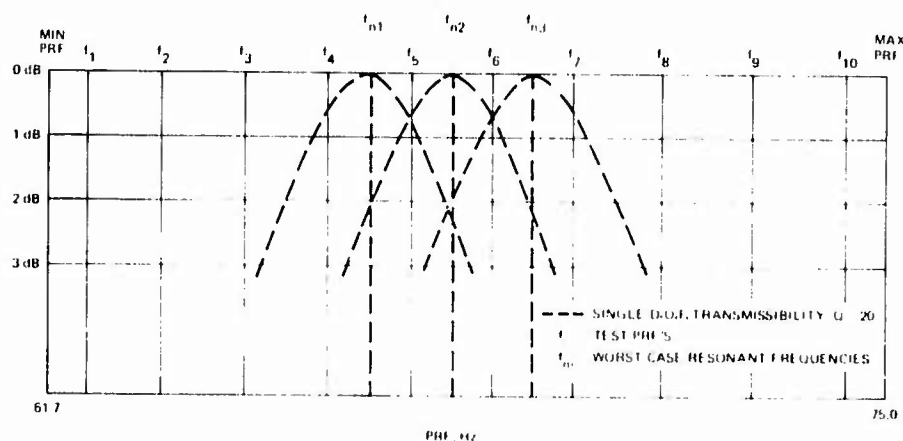
Fig. 5 - Minimum response to stepped PRF

an M-61 gun and a Q of 20, it is seen that ten steps provide response within 1 db of maximum.

USE OF METHOD

The following describes an application of the recommended method in the authors' laboratory. Sufficient detail is included to illustrate practical limitations and problems which can be encountered.

Test Requirements

It was necessary to simulate the effects of two different gunfiring rates. The range of uncertainty (due to temperature and hydraulic pressure variations) for the lower firing rate was from 61.7 to 75.0 Hz and, for the higher firing rate, was from 95.0 to 108.3 Hz. Test exposure time in each axis for each firing rate was 10 minutes at harmonic amplitudes specified in Fig. 6. Random base excitation was also required at a nominal level of 3g rms.

FREQUENCY (FUNDAMENTAL AND HARMONICS)
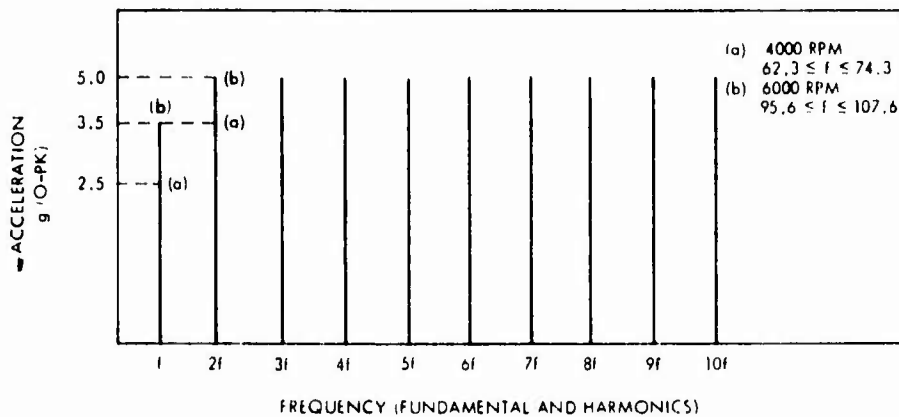
Peak Acceleration, g Peak			
Part	Fundamental	2nd Harmonic	3rd-10th Harmonic
1	2.5	3.5	5.0
2	2.5	5.0	5.0

Fig. 6 - Gunfire vibration test spectrum

43

... ... PRF's was
... ... factory
... ... within
... ... nd Table I.

... ... Variation

...	H. ? Firing Rate
...	6.6
...	96.9
...	98.2
...	99.5
...	100.6
...	102.1
...	103.4
...	104.8
...	106.2
...	107.6

As ... noted earlier, the ratio of pulse
... (the percent ... per ... duty cycle)
... gn... determines the rate of decrease in
amplitude of successive harmonics. For ease
... equalization requirements and,
... importantly, to permit use of a rapid
set ... technique soon to be described,
the ... was made to use a constant duty
cycle. The duty cycle chosen was 0.04 (first
... null at the twenty-fifth harmonic)
which yields a first reduction in amplitude of the
fundamental ... relative to the fundamental of
less than 3 db. Pulse generation was achieved
by the use of simple conjunction circuitry with
... and using trimpots to
adjust both PRF's and pulse widths. To sim-
plify the test operator's task and to assure test
repeatability, it was decided to provide for

automatic sequencing of PRF dwell times. This
was achieved by the use of a simple ring
counter for switching PRF's. Two pulse train
outputs were provided: one, with variable
amplitude, is used for test excitation; the other,
with constant amplitude, is recorded on the
test data tape for later use in analysis. A PRF
code signal consisting of ten incremental DC
voltages (positive for high firing rate PRF's
and negative for low firing rate PRF's) is also
provided and recorded during test for later
analysis use.

The derivation of the equalization settings
for the line spectra of Fig. 6 is shown in Fig. 7.
Since a constant duty cycle is maintained, the
equalization setting for a particular harmonic
is constant as the PRF is varied, assuming the
desired amplitude of the harmonic is constant.
The ideal equalization then becomes a stair-
case function. In Fig. 7, a pair of continuous
curves within which the staircase function must
lie, is shown for both the high and low PRF's.
It should be noted that a reference value of
$0.1 \ g^2$ Hz was chosen arbitrarily as a matter
of convenience. To avoid the necessity for re-
equalization between high and low PRF tests,
compromise equalization settings are shown by
the single curve between the pairs of ideal
curves. The maximum difference between the
ideal and compromise settings is less than
1 db. During test the high firing rate PRF's
were run first and only a brief test shutdown
was required to re-set to minimum those
equalizer channels applicable only to the high
PRF's, before proceeding with the low firing
rate tests.

Test Control

As has been described in a preceding
section, it was necessary to pre-adjust the
relative amplitudes of the pulsed excitation and
the random excitation. To avoid the necessity
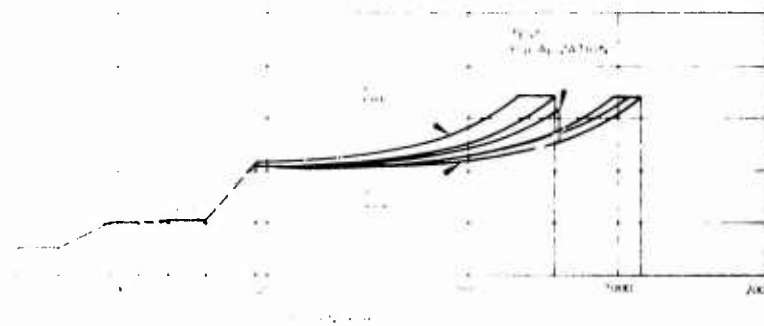
Fig. 7 - Equalization settings

for logging and re-setting of each gain adjustment (see Fig. 4), a "noise only" spring-loaded switch was provided. This permitted setting the pulsed excitation amplitude (with noise gain set to zero) and then setting the noise excitation amplitude without disturbing the pulse gain setting. The control signal was passed thru a 1500 Hz low-pass filter and monitored on a true-rms VTVM.

The control signal was derived from the output of a multiplexing averager (TDM) with the number of input accelerometer signals varying from two to six, depending on the test article. There are several potentially serious problems inherent in the use of a TDM which are beyond the scope of this paper. It should be noted, however, that significant errors in both test control and data reduction can occur at low frequencies if alternate TDM inputs are out of phase. This can occur in the neighbor-hood of a low frequency resonance or, more importantly, if the physical orientation of control accelerometers differ by 180°.

Data Reduction

As has been noted, the maximum time duration at each PRF was 60 seconds. If the taped test data were looped, it would have been possible to determine the harmonic amplitudes by using a swept wave analyzer. However; since each test would have required looping and analysis of 60 data sequences (10 high firing rate PRF's and 10 low firing rate PRF's, for each of three axes), and since the resulting mass of data would have required further processing for easy correlation with test phenomena, the above analysis approach was deemed impractical.

In seeking alternatives, a digital analysis technique was particularly attractive because of an already existing system [5] using a comb-filter array of 52, 10-percent bandwidth channels in conjunction with a multiplexer and analog-to-digital converter under the control of a small general purpose computer. Only minor modifications of the gunfire simulation generator and test method were required to permit implementation of the following analysis technique.

For each PRF an array of ten filter channels was selected based upon the joint criteria of maximizing the desired harmonic response and minimizing the effect of adjacent harmonic response in each filter chosen. A self-calibration mode was devised, taking advantage of the fact that, since the duty cycle of the excitation pulse train was controlled carefully, the ratios between harmonic amplitudes and pulse train amplitude were measurable constants. Thus, a single pass of any given data sequence (10 successive PRF's) permitted the calculation of the gain factors for each channel for all ten filter arrays, by the simple expedient of adjusting the rms input amplitude of the recorded pulse train to a pre-determined constant, measuring each channel output and dividing it by the product of the corresponding harmonic amplitude ratio and the pulse amplitude. The time-saving factor of this approach is obvious but an additional advantage accrued in the elimination of potential errors due to minor variations in tape recorder speed control during data recording and playback which are, of course, reflected in apparent data frequency variations. The gain factors so derived are stored in arrays of core for later addressing during successive analysis runs.

A sampling rate of 10 K samples/sec is used during an analysis time of 11 seconds while multiplexing each array of 10 filter channels plus a broadband channel (the latter is used for measuring the broadband rms amplitude of the signal being analyzed). Thus, 10 K samples are accumulated for each channel and the number of samples per cycle at the highest harmonic frequency is nearly 10. The decoding of the PRF signal is made independent of possible amplitude variations due to imprecision in record/reproduce alignment; this is achieved by computer measurement of the maximum code voltage (first PRF) and minimum code voltage (10th PRF) and calculation of the ten incremental steps between actual maximum and minimum. The actual code voltages thus derived are stored in the computer in a comparison table which is used for PRF identification.

During analysis runs, successive samples from the multiplexed filter channels are digitized, squared and stored using a simple algorithm of Simpson's Rule for estimating the mean square for each harmonic. The peak values are then calculated, scaled to engineering units (taking account of variable system gains and transducer sensitivity) and digital magnetic tape records written for subsequent output via teletypewriter. A typical end result is shown in Fig. 8. Presentation of both the measured broadband and calculated (for the 10 harmonics only) rms values is doubly useful. Since the calculated value should be only slightly less than the test level, it serves as a rough check of the adequacy of test performance. At the same time, since the unfiltered measured value should be somewhat greater

45

HIGH G.F. RATE   REC. NO. 0007   YEAR 1970

HARMONICS: PEAK G'S   BROADBAND: RMS G'S

PRF'S

	107.6	106.2	104.8	103.4	102.1
FUND	.37409E+01	.33393E+01	.32485E+01	.31805E+01	.31162E+01
2ND	.46883E+01	.41317E+01	.45838E+01	.43282E+01	.43132E+01
3RD	.53177E+01	.58210E+01	.51759E+01	.46422E+01	.67101E+01
4TH	.51652E+01	.47319E+01	.51665E+01	.54863E+01	.49821E+01
5TH	.64872E+01	.50767E+01	.41519E+01	.54051E+01	.67704E+01
6TH	.44421E+01	.63102E+01	.57013E+01	.50672E+01	.55145E+01
7TH	.57074E+01	.44790E+01	.65728E+01	.61666E+01	.65275E+01
8TH	.47014E+01	.52297E+01	.39603E+01	.53894E+01	.40807E+01
9TH	.45231E+01	.51582E+01	.46977E+01	.47744E+01	.57823E+01
10TH	.22116E+01	.48735E+01	.50869E+01	.41717E+01	.53556E+01
BB-M	.11754E+02	.11964E+02	.11898E+02	.11639E+02	.12010E+02
BB-C	.10790E+02	.11134E+02	.10993E+02	.11016E+02	.12163E+02

PRF'S

	100.8	99.5	98.2	96.9	95.6
FUND	.31295E+01	.33707E+01	.49369E+01	.33736E+01	.36633E+01
2ND	.45751E+01	.52720E+01	.62474E+01	.60705E+01	.75473E+01
3RD	.46374E+01	.49595E+01	.56385E+01	.51689E+01	.49195E+01
4TH	.44018E+01	.47284E+01	.53575E+01	.47494E+01	.46126E+01
5TH	.39756E+01	.32007E+01	.22187E+01	.27295E+01	.39060E+01
6TH	.53231E+01	.45995E+01	.54202E+01	.52404E+01	.43574E+01
7TH	.63548E+01	.53397E+01	.50061E+01	.56443E+01	.44980E+01
8TH	.61143E+01	.59815E+01	.51427E+01	.45023E+01	.41045E+01
9TH	.55936E+01	.60247E+01	.36982E+01	.41561E+01	.39283E+01
10TH	.48659E+01	.59647E+01	.51751E+01	.51351E+01	.52159E+01
BB-M	.11641E+02	.11653E+02	.11501E+02	.11769E+02	.11638E+02
BB-C	.11148E+02	.11264E+02	.11185E+02	.10684E+02	.10721E+02

BB-M: MEASURED BROADBAND (ALL HARMONICS PLUS BASE NOISE)
BB-C: RMS OF LINE SPECTRUM (10 HARMONICS ONLY)

Fig. 8 - Typical teletype print-out of gunfire vibration test data analysis

than the calculated value, potential analysis errors due to occasional malperformance of the digital system or the analog tape record/ reproduce system often can be detected by comparison of the two values.

Since the analysis of one data track from one test sequence must take nearly 10 minutes (with the same true for a self-calibration run), the speed usually associated with digital sys- tems cannot be realized. However, the aver- age time required from receipt of raw data to generation of an output (typified by Fig. 8) varies from about 0.7 to 0.9 hours. This includes analog tape editing and self- calibration runs; the maximum time occurs where only one data track per sequence is analyzed and the minimum time applies where five or more data tracks per sequence are analysed. The results of several early analog

analyses of similar data indicate that the time per output for an equivalent data format would be about sixteen hours.

COMPARISON OF METHOD TO MIL-STD-810B. METHOD 519

In late 1969, a gunfire vibration test was added to the vibration tests included in MIL-STD 810B. It is known as Method 519, Gunfire Vibration, Aircraft. As this is the only military specification (known to the authors) applicable to gunfire vibration, it is appropriate to compare some of the features of the method described here to Method 519.

Method 519 is a random vibration test with the test spectrum shown in Fig. 9. If facility limitations dictate, an alternate spectrum, shown in Fig. 10, which employs swept narrowband on broadband random is permitted. The maximum spectral density, G_{max}, is determined by consideration of the muzzle energy of the particular gun, the number of guns and their firing rate, the weight of the test article and the vector distance between gun muzzle and installed equipment. Thus the test level is tailored to the particular installation, which is commendable. However, the frequency range of the test spectrum is fixed rather than being keyed to the permissible firing rates of the gun. For several typical
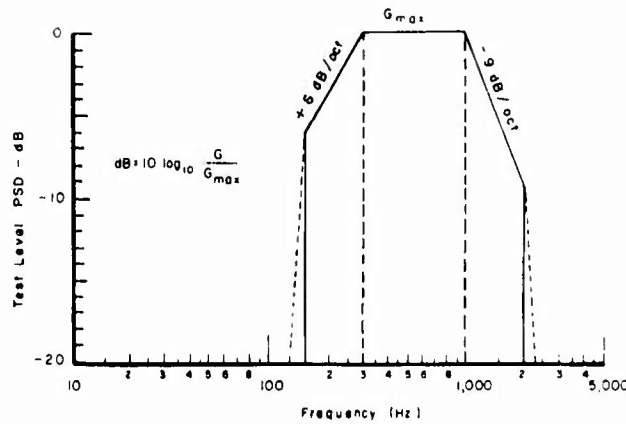
Fig. 9 - Random vibration test curve.
Fig. 519-5 of MIL-STD-810B.
29 September 1969
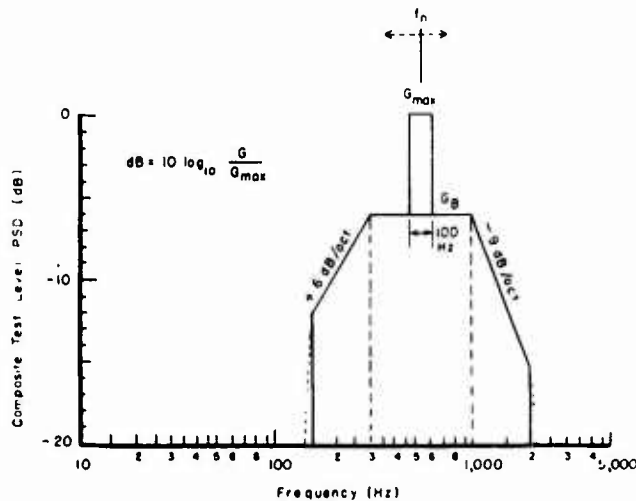
Fig. 10 - Swept random vibration test curve.
Fig. 519-7 of MIL-STD-810B.
29 September 1969

47

gunfire rates, e.g., 25 Hz, 67 Hz and 100 Hz, the lower harmonics are outside the test range. It is suggested that Method 519 should be modified to ensure that the appropriate frequency range of excitation is covered. It is believed that the pulsed excitation method has the advantage of automatically exciting the appropriate frequency ranges.

It is not the purpose of this paper to discuss gunfire vibration levels. However it is appropriate to illustrate the previously mentioned conservatism of broadband random excitation due to "filling in" the valleys of the spectrum between harmonics. Method 519 was applied to a typical installation of avionics and the test levels shown in Table II obtained. It is anticipated that some difficulty would be experienced in testing even some of the lighter weight units to the required rms accelerations.

Even the alternative narrowband sweep, which employs a 100 Hz bandwidth would be difficult to achieve at the tabulated spectral density values. Further, published gunfire vibration data from an installation not dissimilar to that used for Table II does not indicate rms accelerations approaching those listed.

Thus it is concluded that, compared to use of a pulsed excitation, the use of broadband random excitation as in Method 519 leads to conservative vibration test levels which are also difficult and expensive to create in the laboratory.

CONCLUSION

The foregoing paragraphs have described the requirements for adequate simulation of complex wave periodic vibration. It has also been shown that these requirements can be fulfilled by addition of an inexpensive variable-PRF pulse-generator to any existing random vibration system. Experience gained during design-development and qualification testing of an avionics system comprised of approximately

TABLE II
Method 519 Gunfire Vibration Levels for Typical Aircraft Installation

Weight (lbs.)	Zone	D (in.)	G_{max} (g^2/Hz)	G'_{max} (g^2/Hz)	Grms
135.0	.	36.3	3.6	1.33	39.3
142.0	.	35.1	3.8	1.29	38.7
39.0	.	35.6	3.7	NA	65.6
39.0	.	31.3	4.9	NA	75.5
34.0	-	27.7	4.3	NA	70.7
28.0	.	31.7	4.9	NA	75.5
25.7	.	28.2	5.8	NA	82.1
71.0	.	25.9	6.4	NA	86.3
65.0	.	14.6	9.2	NA	103.4
63.0	-	95.1	0.095	NA	10.5
41.8	-	107.5	0.076	NA	9.4
17.4	-	91.7	0.105	NA	11.0
39.5	.	43.5	2.0	NA	48.2
158.5*	-	131.4	0.055	0.015	4.2
171.0*	-	170.8	0.041	0.011	3.5
179.0*	-	174.6	0.040	0.011	3.5

* No test required since G'_{max} less than 0.04

30 black boxes has shown the test method to be extremely cost-effective. Barring failures in the unit, three axes of gunfire excitation described earlier can be accomplished in approximately four hours. Final proof of the adequacy of the simulation must await exposure of this equipment to actual gunfire excitation.

The inadequacy of sinusoidal excitation and the conservatism of broadband random excitation have been indicated. It is recommended that a pulsed excitation be included in Method 519, Gunfire Vibration, Aircraft, of MIL-STD-810B.

REFERENCES

1. J. A. Hutchinson and R. N. Hancock, "A Method to Simulate Gunfire Induced Vibration Environment", Shock and Vibration Bulletin, No. 40 Part 6, pp 27-35, Dec. 1969.

2. J. E. Gross and R. Pittman, "Gun Firing Environment and its Relation to Structural and Equipment Integrity", Shock and Vibration Bulletin No. 34, Part 2, pp 261-269, Dec. 1964.

3. R. F. Carmichael and D. Pelke, "Measurement, Analysis and Interpretation of F-5A 20-mm Gunfire Dynamic Environment", Shock and Vibration Bulletin No. 34, part 4, pp 191-204, Feb. 1965.

4. A. J. Curtis, J. G. Herrera and R. F. Witters, "Combined Broadband and Stepped Narrowband Random Vibration", Shock and Vibration Bulletin No. 35, Part 2, pp 33-47, January 1966.

5. A. J. Curtis and J. G. Herrera, "Random Vibration Test Level Control Using Input and Test Item Response Spectra", Shock and Vibration Bulletin No. 37, Part 3, pp 47-60, January 1968.

RATIONALES APPLYING TO

VIBRATION FOR MAINTENANCE

A.H. Grundy
Canadian Forces Headquarters
Ottawa, Canada

The parameters associated with the measure-
ment of vibration as an indicator of wear
and the need for maintenance are discussed.
It is concluded that velocity is the most
appropriate parameter. Examples are given.

INTRODUCTION

In practice there are no perfect bearings,
perfect shafts, perfect gears, or perfect blades
in machines, and as a consequence, even new
machinery vibrates. During use, all moving
parts wear, or deflect slightly in time so that
clearances increase, and rotating parts become
out of balance. All this increases vibration
above its original level, which can therefore
be a measure of wear. It is found that the in-
crease in wear produces increase in vibration,
which in turn increases wear. Consequently, a
smoothly running item will run satisfactorily
for a long time, and as wear becomes "notice-
able", it increases cumulatively.

This speeding up of the increase in vibra-
tion can be detected by recording vibration
levels regularly. From experience, therefore,
vibration levels can be used to predict the
wearing out of parts, that is, mechanical fail-
ure, before it happens.

We can, by this means, keep smoothly running
equipment in service for a long time without
disruption or introduction of foreign matter,
or replacement misalignment, in contrast to
planned maintenance schemes, based on the
earliest failure time of similar machines. It
also means that we can keep equipment, known to
be worn, in service until it is convenient to
overhaul it avoiding breakdowns, which enforce
inconvenient idleness, because of the warning
vibration can give.

It is possible to select displacement,
velocity, acceleration, linear scales, log-
arithmic scales, peak to peak, average, or
root mean square values, as parameters for
measuring vibration. Whilst it is possible

mathematically to convert from one parameter
to another if sufficient information is known,
there are some parameters which reduce work,
effort, and thought, and yet tell all the
answers required.

Traditionally, it is the engineers hand and
ear which plans maintenance before failures
occur. Though the ruler, micrometer, and dis-
placement vibration gauge are the earliest
forms of measurement they are far from being the
best. It is a known fact that frequency of
vibration must be taken into account in the
measurement of movement (vibration) in order to
assess its importance.

For instance if you move a little boy's
shoulders backwards and forwards six inches
taking two or three seconds in each direction
he will probably not object too much, if, how-
ever, the frequency is raised to 10 times per
second, he will object violently (if you have
not already broken his neck). Similarly with
a machine or equipment, a movement of 1 foot
per second may not have any deleterious effect,
but a displacement of one hundredth of this at
1000 cycles per second would disintegrate it
because of the high "g" forces involved.
Frequency is vital.

Figure 1 shows the logarithmic com-
parisons of the three vibration parameters,
acceleration, velocity, and displacement
against frequency; at any selected frequency, an
acceleration or displacement can be obtained
from a velocity measurement, or vice versa. Thus,
in a sense, measurement in one parameter fixes
the results in the other two parameters. How-
ever, there are several considerable advantages
in choosing velocity, which will be shown later.

51
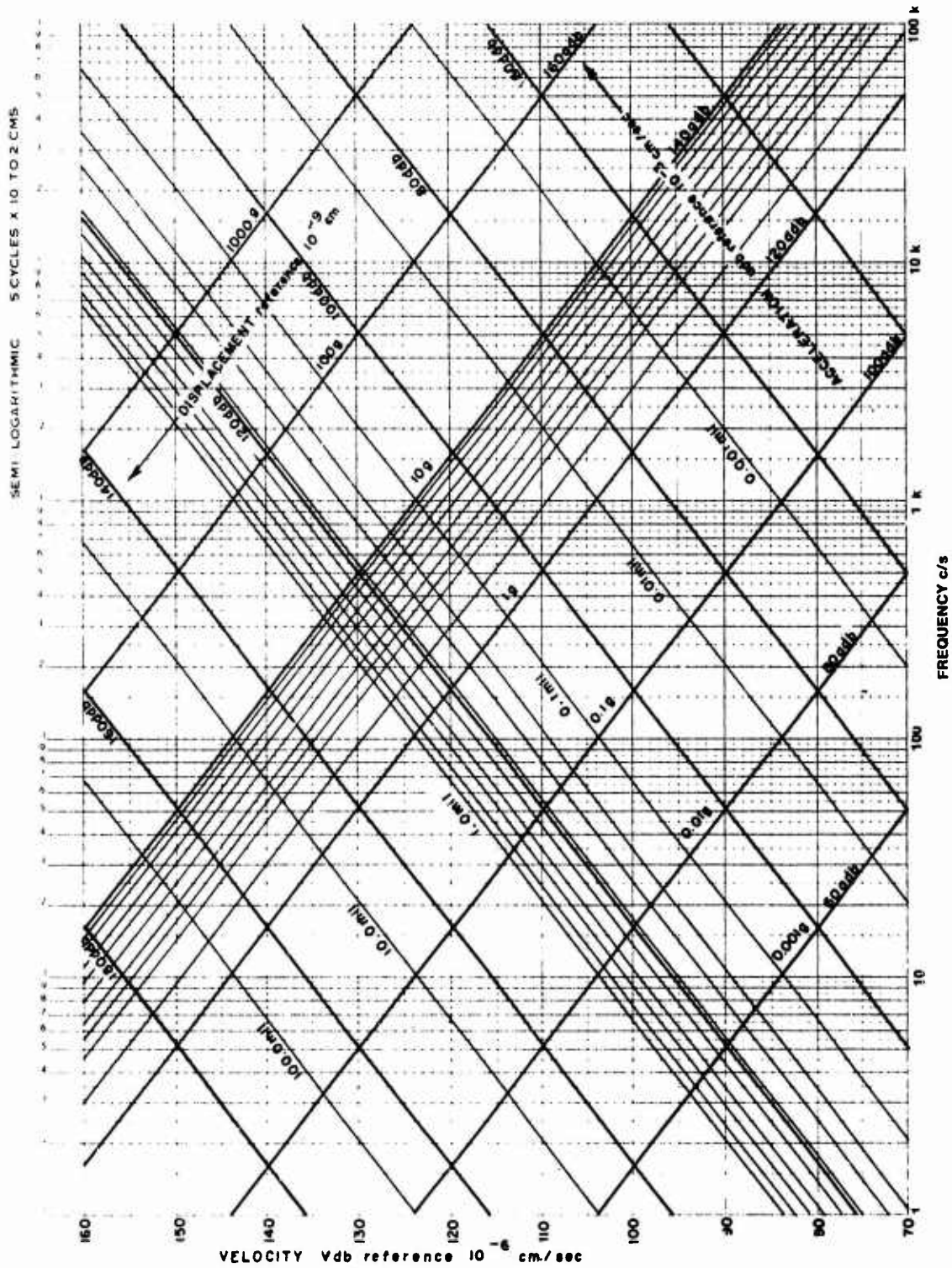
Fig. 1 Velocity, Frequency, Displacement Relations

RATIONALE

Movement, i.e. displacement, obviously is important as a factor in wear. (no movement, no wear). Frequency is also important (see above). Therefore a parameter combining both, could be an advantage i.e. velocity (displ. X freq.) or acceleration(displ. X freq. X freq.) if they contain the right proportions.

Force per unit area of relatively moving surface is also important in wear. However, when we are considering a particular equipment we are considering a fixed design, and therefore this element of the parameter is proportional to force. Force is a mass acceleration, and as we are considering a particular item, the mass is a "constant", and therefore acceleration is the variable. However vibration acceleration is oscillatory and not constant in one direction. Wear is proportional to friction which is therefore constant under a constant force (acceleration). Oscillatory acceleration is different, in that frequency has an effect, in fact at several kilo cycles per second and above, a shaft feels slippery not rough, and has very little friction at very high frequency. That is, the friction with oscillatory acceleration in inversely proportional to frequency. Dividing acceleration by frequency gives VELOCITY as the correct parameter.

This is in line with another consideration which is that the above formula, "force = mass acceleration", is true at very low frequencies, but as frequency increases the impedance of a structure alters. This impedance alteration is somewhat dependent on wavelength, and therefore the coupled mass, (whose reduction reduces the force as the frequency increases) (with constant acceleration). For this reason, force is less than proportional to acceleration, and is nearer to velocity.

A mathematical type of proof that velocity is an important gauge for wear in machinery is as follows:

At any given time the wear is proportional to the energy being dissipated at the relatively moving part.

Energy = work = force X distance, i.e. acceleration X distance =
= distance X acceleration = cms x cms/
(sec X sec) =
= $(cms/sec)^2$ = $(velocity^2)$, i.e. 2 log velocity
= 2 x bels of velocity or decibels for convenience.

Thus, wear is somewhat proportional to velocity decibels (vdb).

We therefore see that from the movement (displacement) considerations we should in some way multiply by frequency to get a parameter for wear, which indicates velocity.

Also from force (acceleration) considerations we should divide by frequency to get a parameter for wear, which, again indicates velocity.

It now appears that we have a single parameter, velocity, which is crudely proportional to wear, (or condition of the equipment).

The above is borne out firstly by vibration tests on a helicopter. The problems were (a) shaking of the instrument panel (and pilot's seating, etc.) and (b) failure of a centrifugal clutch. The former was caused by the rotor imbalance, and the latter by a high frequency chatter (2000 cps) from epicyclic gearing. Logarithmic scaled graphs of the following shapes were plotted. Fig. 2
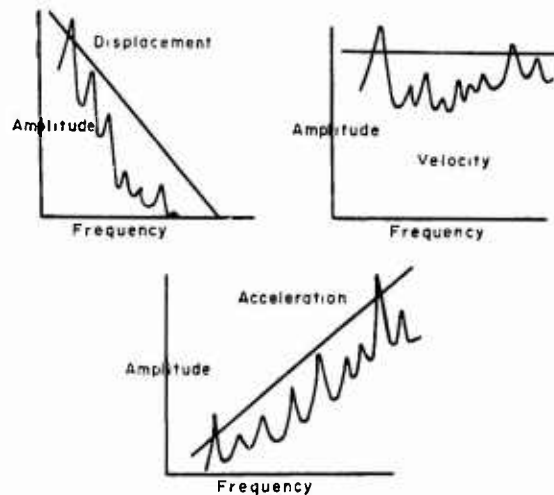
Fig. 2

(Actual Ship gearbox vibration measurements (at the end of this paper) and also helicopter transmission vibrations are plotted in the three different parameters for comparison in Appendix A).

If the straight lines are the equivalent limits then it is theoretically possible to diagnose problems with each type of vibration, but, in fact Displacement is too insensitive to discriminate high frequency and Acceleration is poor at low frequency. Also for D and A, a frequency graph must be plotted to compare results. Not so, with velocity, and the above criteria simplify approximately to; Fig. 3

53
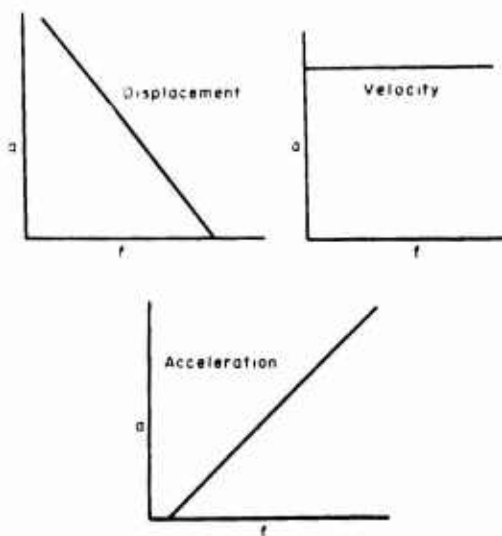
Fig. 3

which again simplifies to
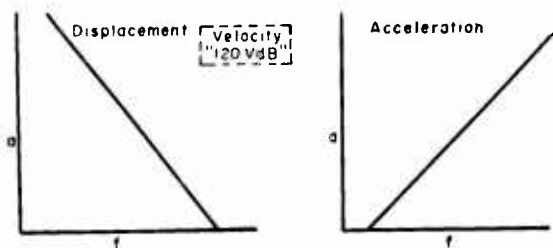
Fig. 4

By using velocity we have a single number which can be set for different types of machine, obviating the need for discrete analysis <u>every</u> time for every component, as frequency is automatically taken into account.

A further confirmation of this parameter is found, not just from an engineer's hand, but from average human feeling. Researchers have found that up to about 10 to 20 cycles per second human feeling is proportional to acceleration, and that above 20 cps, it is directly proportional to velocity including the thousands of cycles per second range. Further, when the whole range of feeling vibration is split into just perceptible, perceptible, very noticeable, unpleasant and very unpleasant, (5 limits), it is found that they are evenly spaced on a logarithmic scale, and <u>very</u> unevenly spaced on a linear scale. (Fig. 5) Thus human feelings over almost the whole of the vibration range is proportional to velocity, and logarithmic amplitude.

Fig. 5 shows the linear spacing of vibration subjective effects and Fig. 6 shows the logarithmic spacing. It is obvious from the even spacing of the logarithmic curves that subjective feeling is logarithmically proportional.

For all the above reasons, vibration velocity in decibels (vdb) has been chosen for the parameter of machinery condition.

It is known that some machines when new are inherently smooth when well made, and may vibrate, as low as 80 vdb. This machine when worn, may give 110 to 120 vdb which represents a change of 40 vdb. On the other hand, a new diesel or free piston compressor may vibrate at 115 to 120 vdb when new, yet is worn at 125 to 135 vdb, which is only 10 vdb increase.

The possible .ariation from 10 to 40 vdb change between new and worn machines precludes us from measuring an original level and saying a 20 vdb increase means an item is worn out.

This also brings us to an important reason for having new, and refurbished equipment to as low a level as possible. There are figures to indicate that an item which starts out at a vibration level of say 115 vdb may last only a few hundred hours before overhaul, whereas a machine starting at a level of say 80 to 90 vdb can last for 10,000 hours. Vibration can therefore, not only tell us when a machine is ready to fail, but may be used to lengthen its life many times.

Balancing in situ, is also a big factor in long life and is set by vibration measurements.

It is also known that machinery covers, panels, etc. vibrate at high levels without failure, extremely high shock impulses (from underwater explosions) permanently damage or break, even ruggedised machinery. These vibration levels are in the range of 150 to 175 vdb. It is therefore recommended that a machine be prohibited from operating, if any <u>bearing</u> level reaches 140 vdb, and the machine may only be operated in a real emergency (if it <u>will</u> operate).

<u>Further limitations on the Parameter of</u>
<u>Vibration Velocity for expressing wear</u>
(or transfer to air or water noise)

Vibration means movement. Movement implies a displacement, and it is assumed that the higher the level measured, the more vibration there is.

Even compressing the scale into decibels instead of linear comparisons shows in Fig. 7 that displacement vibration of a ship's gearbox has important peaks in it. In Fig. 7 the right hand half is real and the left hand half is fictitious for illustration. As stated above, higher levels give the impression of "more" vibration so that diagnosis of a problem

54
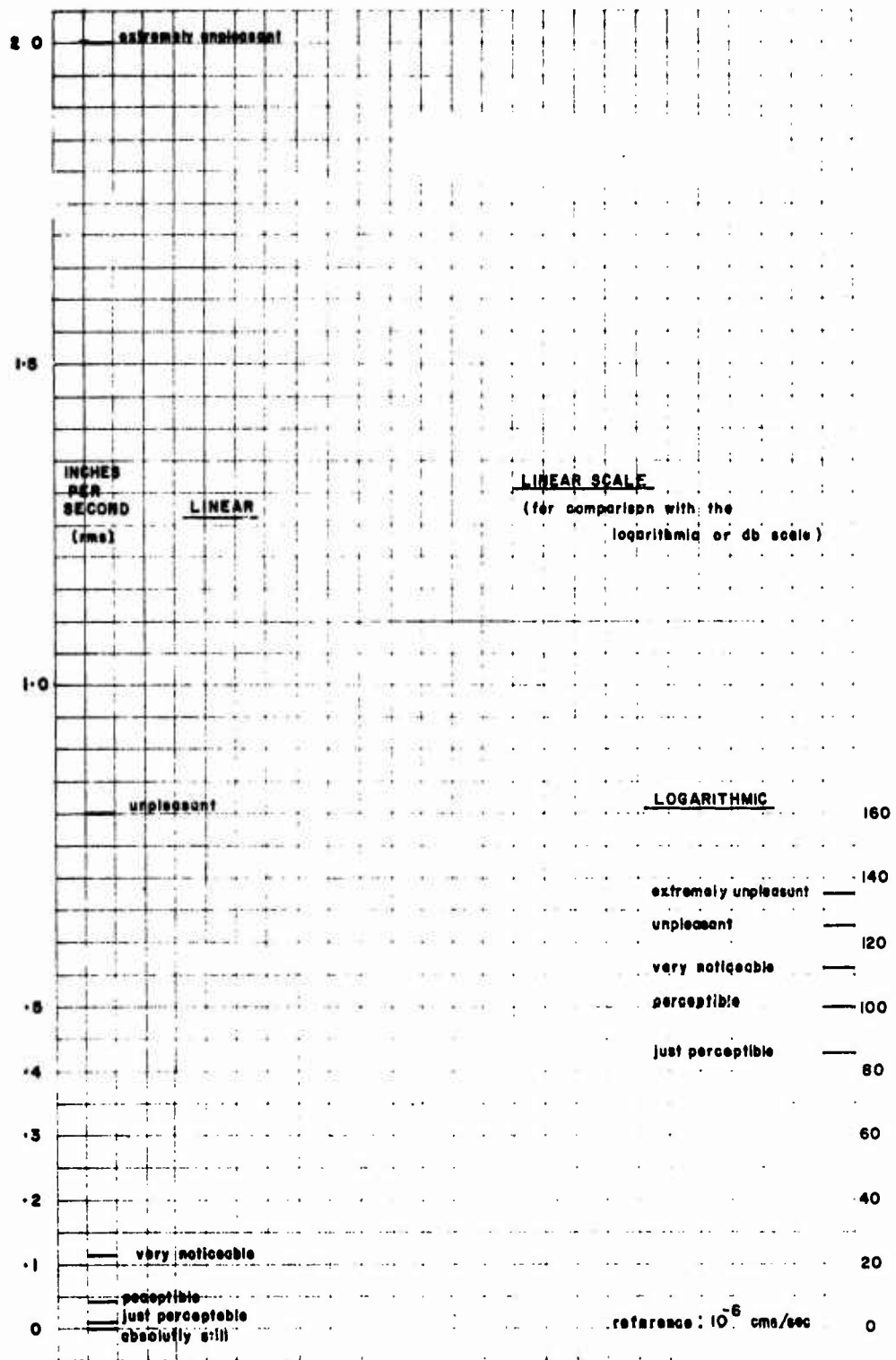
Fig. 5 Human Perception of Vibration
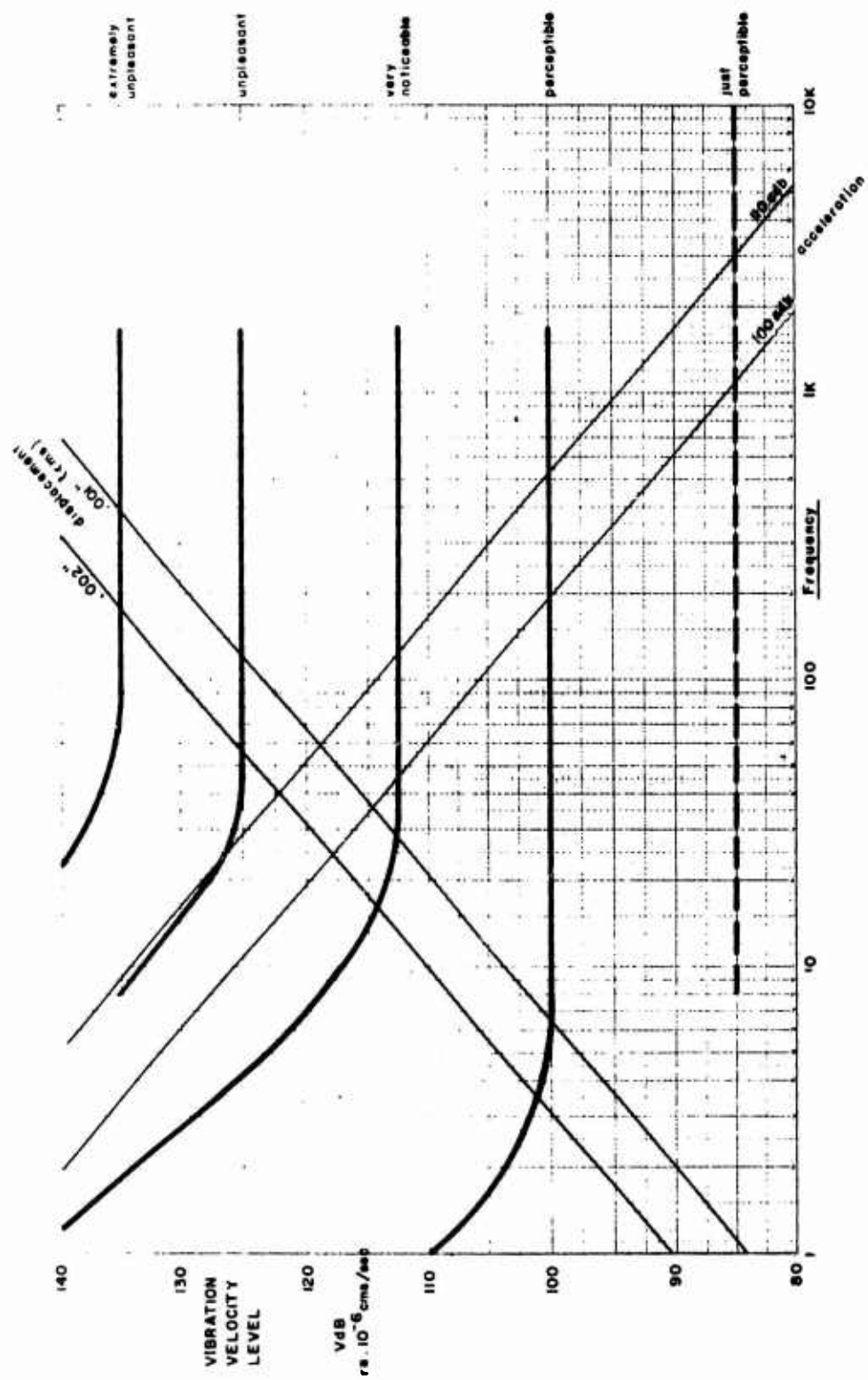
HUMAN PERCEPTION OF VIBRATION
FIG. 6
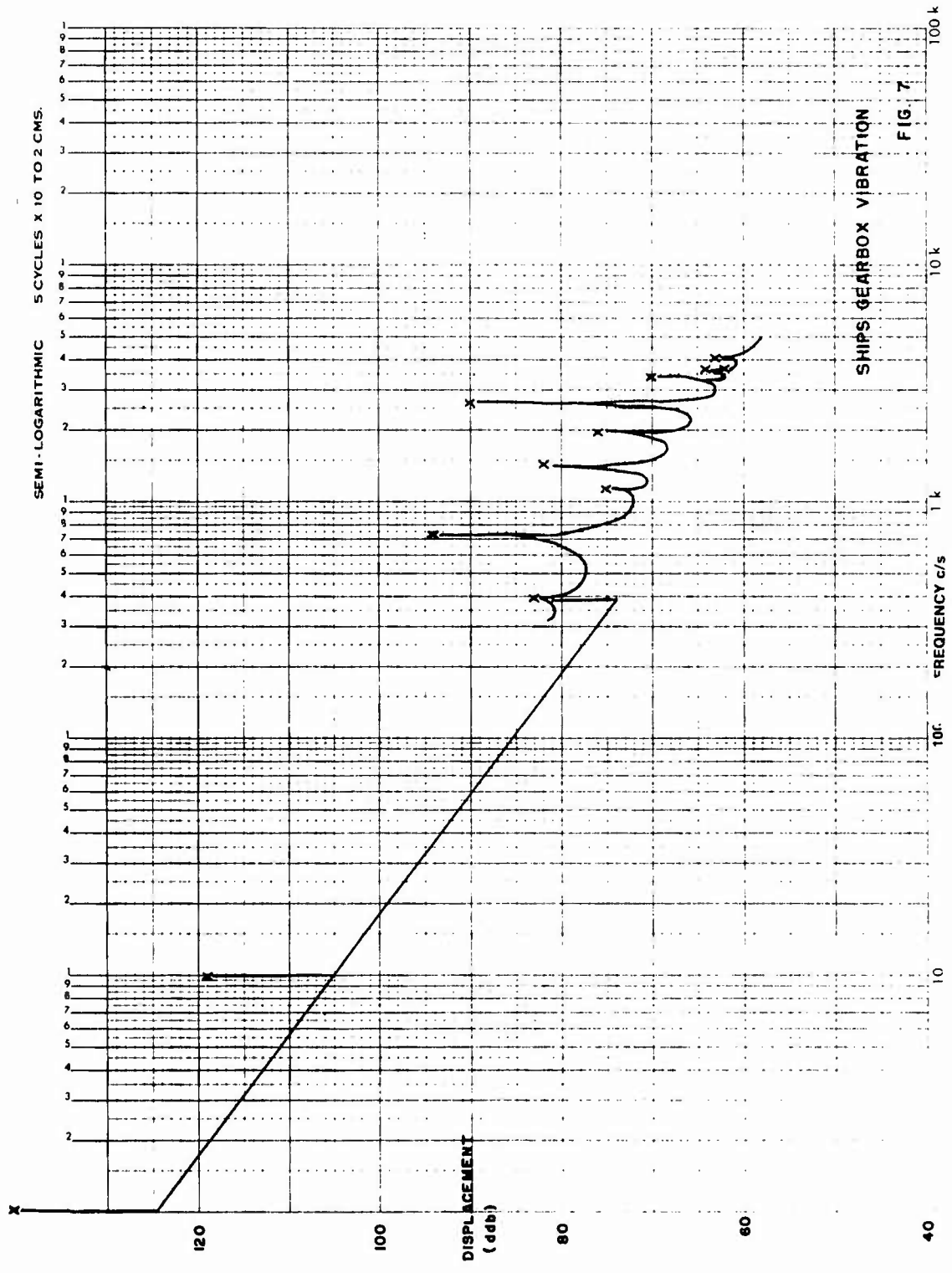
Fig. 7 Ships Gearbox Vibration

in the gearbox from reading Fig. 7 says that we should concentrate on the 1 cycle frequency, take note of the 10 cycle frequency, and ignore the rest as not significant.

We could plot the same gearbox measurements using acceleration, thinking that acceleration is a complete measure of force. This is plotted for us in Fig. 8. It can be seen that the high levels of vibration are now at $2\frac{1}{2}$ kilohertz with a secondary interest at 700 hertz. The one and ten cycle results are quite insignificant.

The third alternative is to plot velocity measurements, and this is shown in Fig. 9. This shows the highest vibration levels, and therefore the problem areas to be at $2\frac{1}{2}$ kilohertz, with 700 cycles another important item. The one and ten cycle effects are secondary, but not insignificant.

The above theorising is borne out in practice, indicating that velocity measurements are the important ones, with acceleration a secondary importance, to be interpreted with caution. Displacement is definitely a tertiary consideration.

It is well known to anyone making measurements in vibration (or noise) that frequency is an essential parameter no matter what others are selected. This means that measuring instruments must respond to virtually all vibratory frequencies, and a second well known point is that a single overall vibration measurement is completely inadequate to describe any vibratory effect, except very crudely.

In order to bring frequency into the analysis we must filter the signal and split the results up into bands of frequency whether octave band widths, half, third, double or single cycle bands. The more splits there are the more defined is the signal, however, it also follows that two analysis are more difficult to compare and more work to obtain, record, and analyse, the more frequency bands used.

Overall levels can be compared immediately, the higher number indicating the most vibration but they are useless as described above. Octave bands require eight or ten measurements to cover the frequency range, give a definite picture of frequency characteristics, can be compared one machine against another, and can be compared with any standards of effects such as annoyance or tolerance, wear or damage, and even speech interference as vibration is its source.

The same advantages can be claimed for one half, third or tenth, but comparison with standards becomes more difficult with more splits. There is twice, three times, or ten times the work, to measure, record and analyse, with no better, in fact less definite results. For comparison or standards compliance, the octave band measurements have all the advantages.

When there is a problem, we need to diagnose the fault, and the frequency emitted by the faulty part can indicate precisely whether it is a shaft, bearing, gearbox or blade and even which it is.

Diagnosis of vibration sources or faulty parts can occasionally be done by crude analysis on such as a buckled wheel or even an out of balance wheel. However, when we come to gearboxes with shafts, bearings, gearteeth etc. all revolving at different speeds at the same time life becomes more complicated. Frequency definition is paramount, and in fact to suit all normal circumstances a frequency bandwidth of a few cycles, or a few percent bandwidth at the most, is required.

The above can be illustrated by the ship's gearbox measurements in Fig. 9 where we see results mainly from gear teeth. In this double reduction gearbox, the secondary meshing frequency is 700 hertz and its vibration fundamental together with harmonics 2-2, 2-3, and 2-4, are indicated at the bottom of the graph.

Simularly the primary meshing frequency with its harmonics 1-2, and 1-3 are indicated. If these results are transferred to full octave band and one third octave band, the results are shown in Fig. 10. Diagnosis on the basis of Fig. 10 shows that the secondary gear train is the important problem with the primary gear train less important.

This diagnosis is wrong. If we rely on the third octave as being more "accurate" than the full octave, we go further and state that the fourth harmonic of the secondary meshing frequency is the important fault. This also is wrong.

In fact, as can be seen from the analysis in Fig. 9, the peak at 2.6KHz is definitely away from the 2.5KHz fourth harmonic of the secondary gearing. It did in fact turn out to be a ghost frequency on the primary pinion impressed as a continuous error by the original gear cutting.

It can therefore be seen that despite automatic analysis of part octave bands or percentage bands, discrete analysis in bands of a few cycles or one or two percent (6 at the outside) are required for DIAGNOSIS. Faulty diagnosis can easily occur using anything but discrete frequency analysis.

If crude guesswork is required, a one third octave analysis is better than octave analysis. However, a one third octave analysis is not a compromise between octave and discrete analysis. It is very hard to compare with standards where the octave is not. It is three times the work to measure, record and analyse. It leads to faulty diagnosis in anything but the most obvious of cases and is no substitute for discrete analysis.
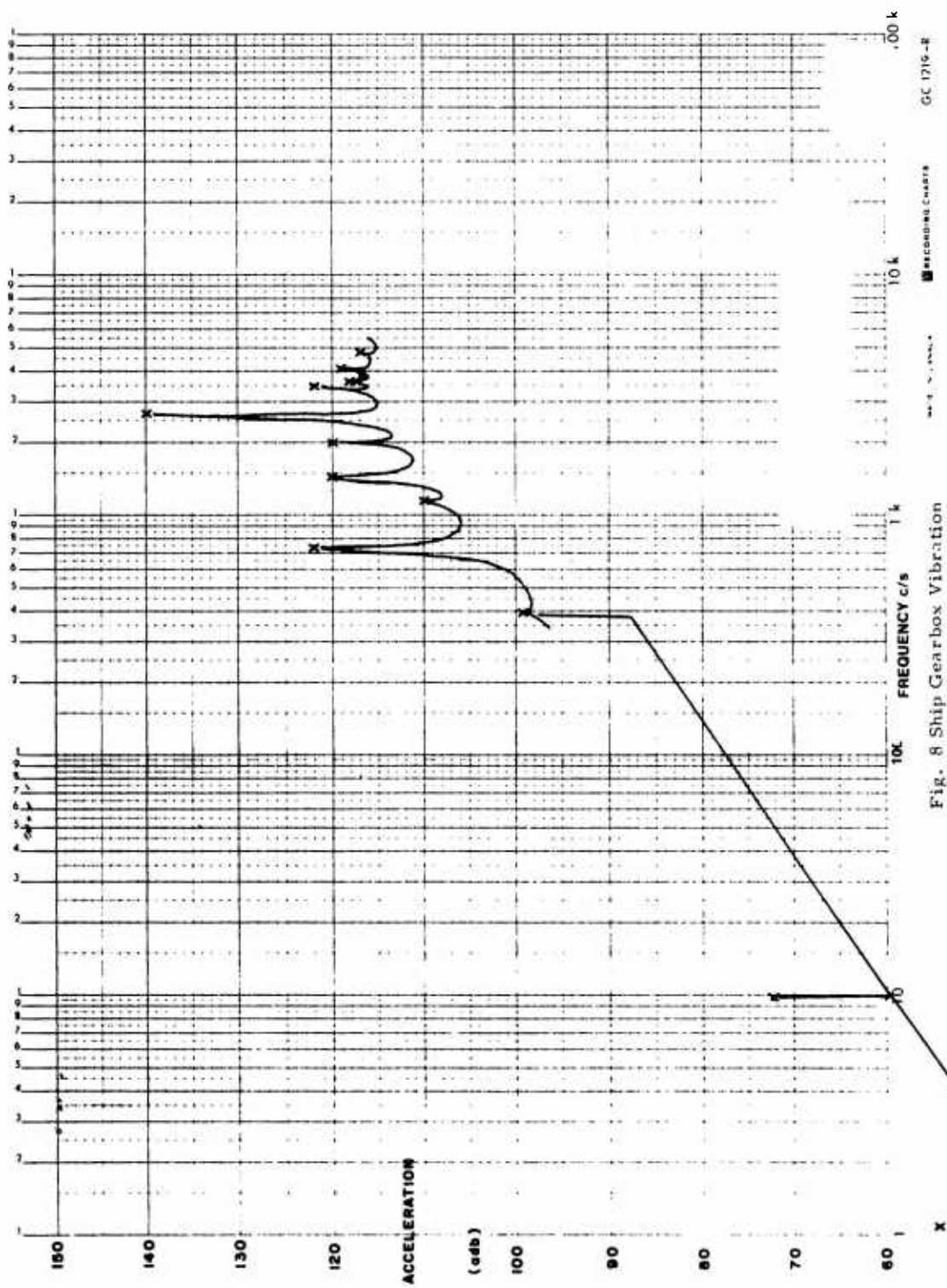
Fig. 8 Ship Gearbox Vibration
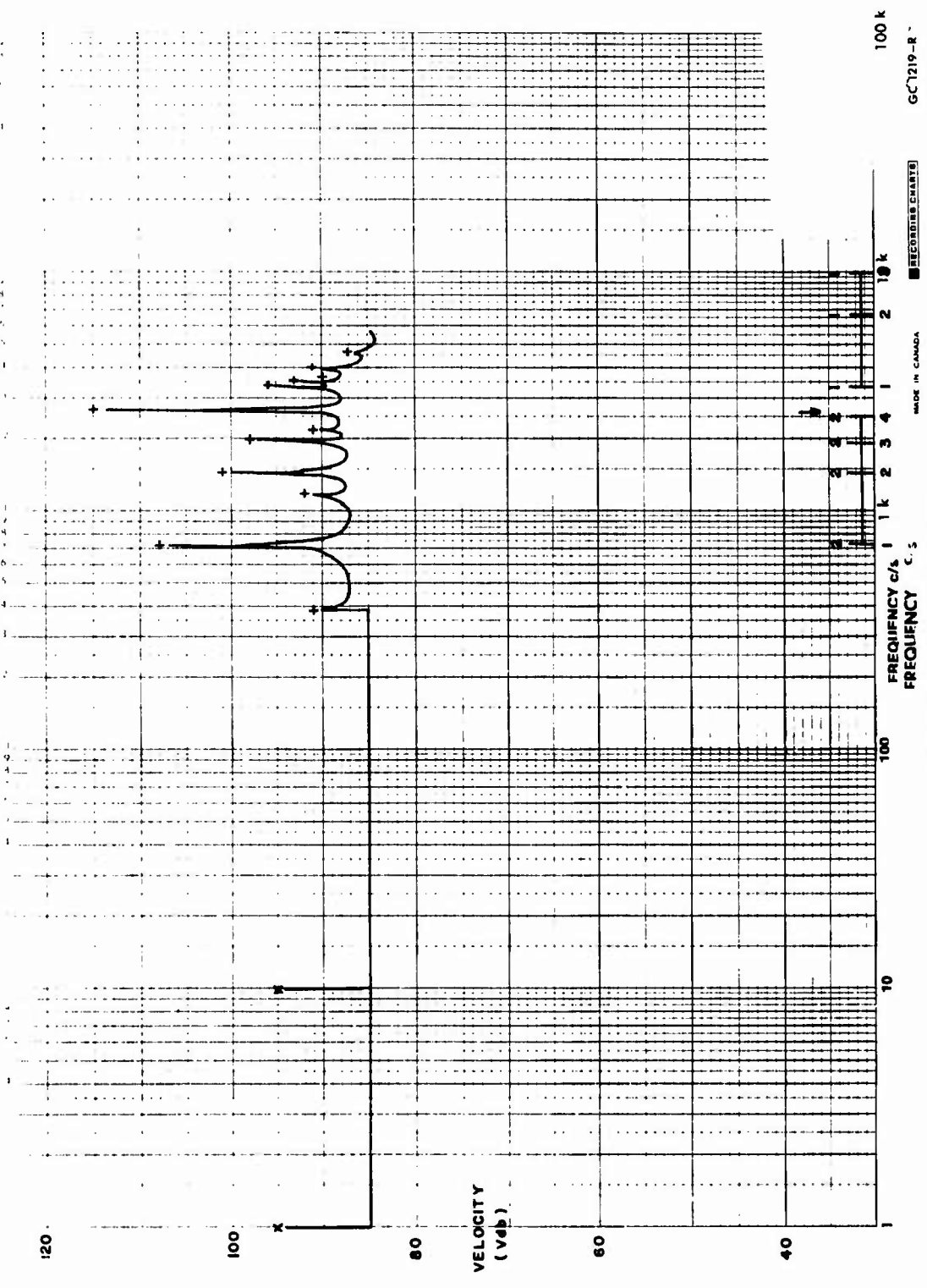
Fig. 9 Ships Gearbox Vibration

60
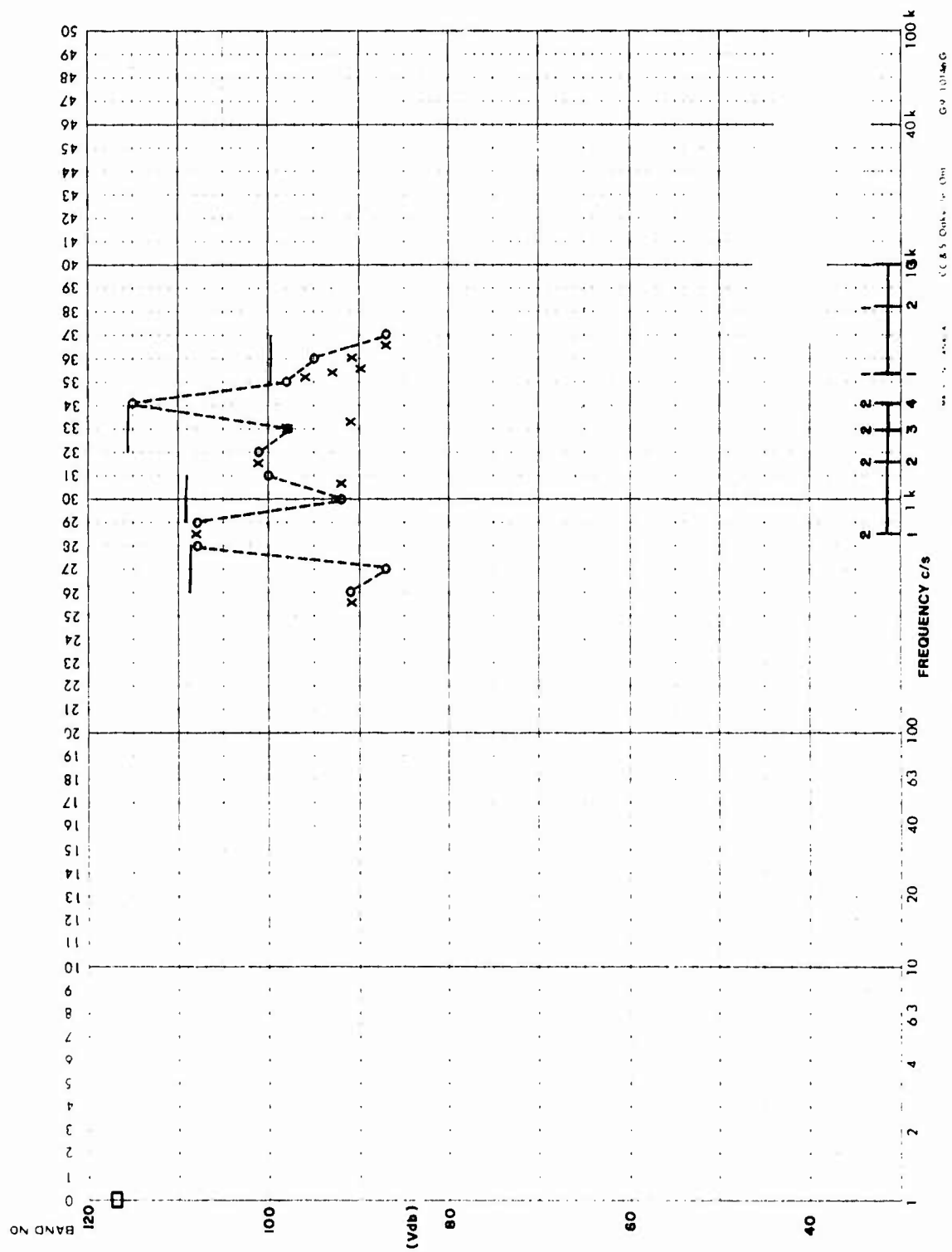
Fig. 10 Ships Gearbox Vibration

Helicopter Transmission Vibration

Measurements of the vibration of the transmission
of a Hiller Helicopter which were recorded in displacement,
velocity and acceleration are shown for comparison purposes
in Figure 11, 12 and 13.
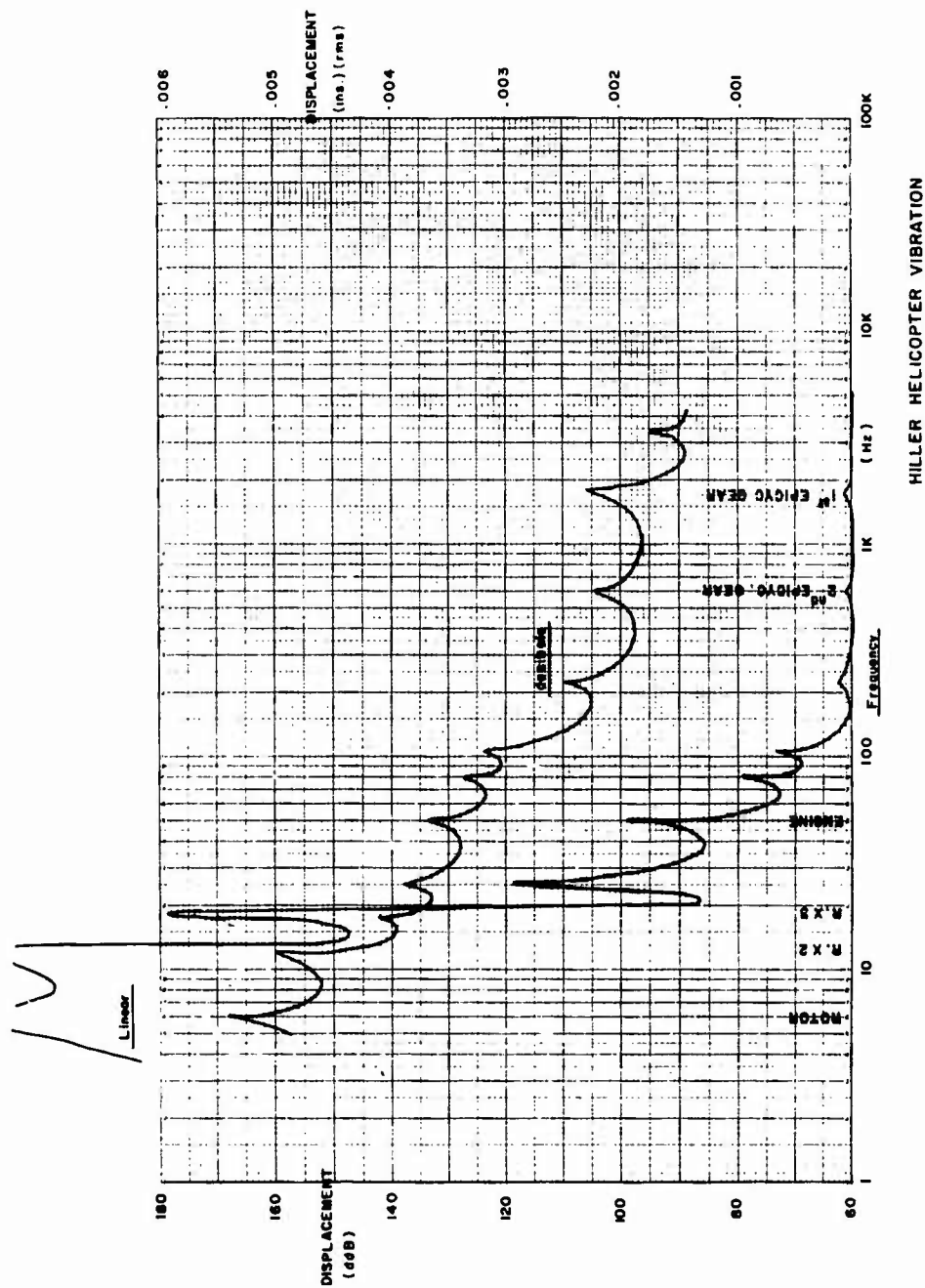
Fig. 11 Hiller Helicopter Vibration in Displacement Decibels
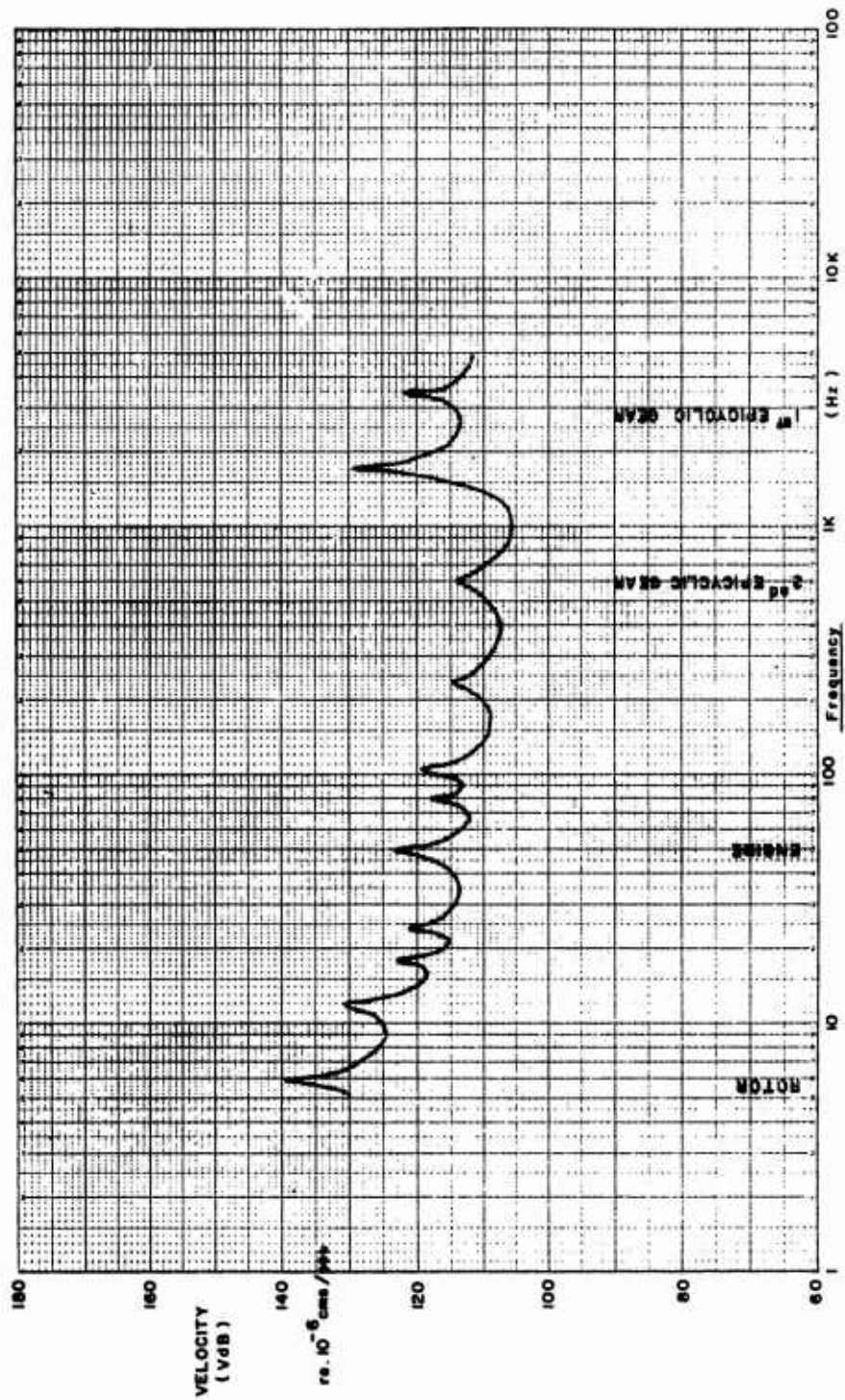
Fig. 12 Hiller Helicopter Vibration in Velocity Decibels

63
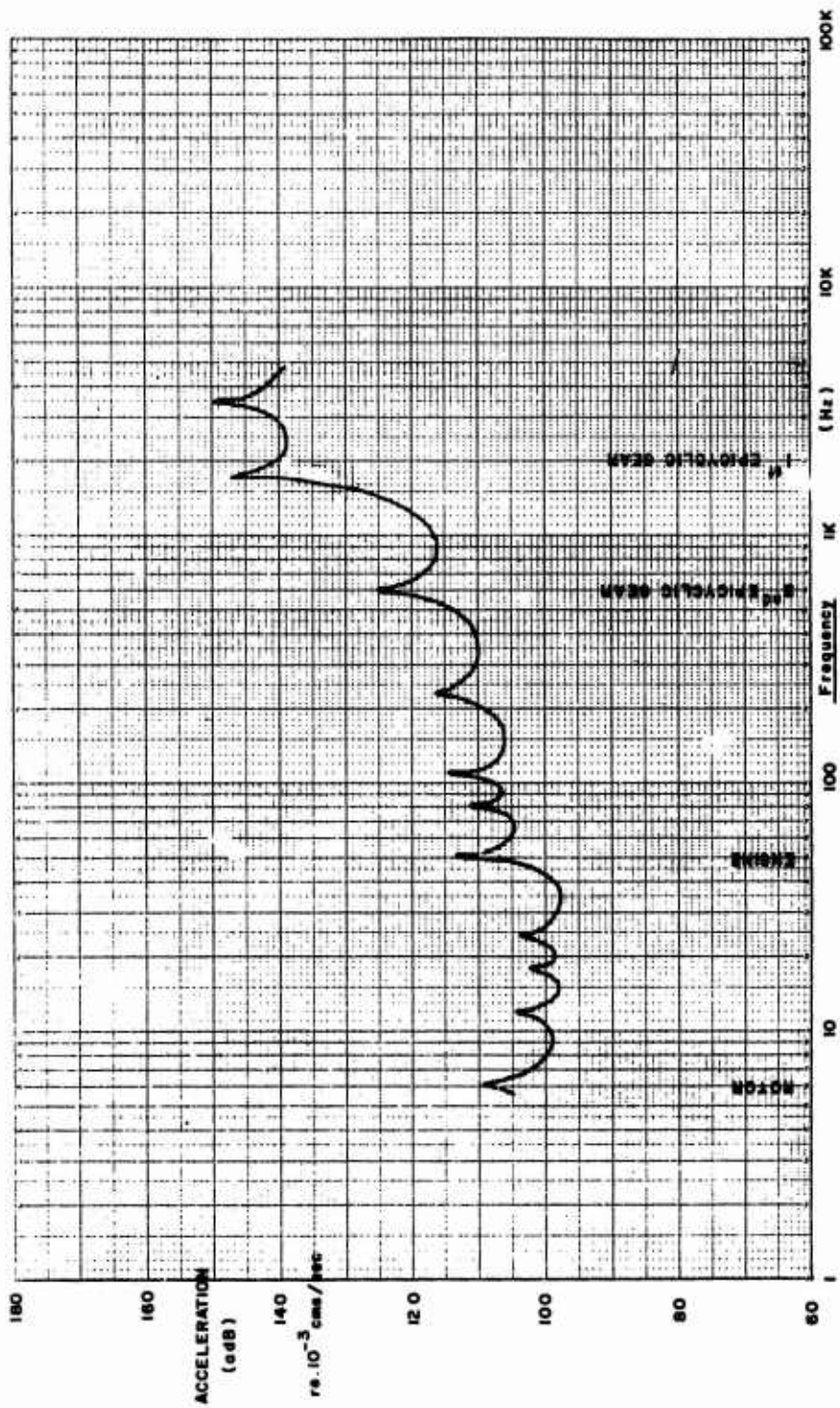
Fig. 13 Hiller Helicopter Vibration in Acceleration Decibels   .LER HELICOPTER VIBRATION

64

Practical Application of Vibration Analysis

JUSTIFICATION FOR SELECTING VERTICAL DIRECTION
OF MEASUREMENT ONLY

80 sets of meaningful readings were selected.

(definition of meaningful: - solid positions located close to main bearings of major components with so many readings tak . that graphs of Average vertical, average athwart, average longitudinal, and highest V, A, C, L, & lowest C, A, C, L, readings were all plotted).

(Definition of "sensitivity": A greater change in vibration levels for the same amount of wear.)

Out of the 80 positions, the criteria, compared with 3 sets of graphs for each position.

56% - no change whether V, A, or L selected, and similar sensitivity between new, average, and worn;

28% - no change of decision, whether V, A or L selected, but different sensitivity between directions of measurement;

16% - no difference whether V, A or L selected, but different character of curves.

In the 28% figure above, 75% of the most sensitive direction possible, were vertical. Only 12% each most sensitive were Athwart and Longitudinal. This was true whether main shafts were vertical or horizontal and irrespective of whether "vertical" was along the shaft or radial to it. 70% of the sensitive ones were radial 30% longitudinal.

In the 16% figure above, 57% of the most sensitive direction possible were vertical, the others longitudinal when it was radial to the shaft. 85% if the sensitive one were radial 15% longitudinal.

56% - (75% of 28%) - (57% of 16%) = 86%. Therefore vertical measurements five 86% most sensitive results, with no change of decision in the other 14% of cases.

Therefore, vertical measurements are almost always specified, and only one direction is measured.

The only case where radial direction of measurements (athwart or longitudinal) takes preference over the vertical is where most of the main shafts in the machine are vertical, and most of the machine is above the feet or securing lungs. (e.g. Sharples Purifier)

When the vertical overall measurements indicate that close attention (i.e. octave analysis) is required, then octave analysis should be performed in all three directions at the point in question. If time of measurement is still to be saved the direction of maximum readings may be chosen to be exclusion of the other two.

Recording and Measuring Details

It is proposed that the machinery sketches be labelled in the following manner:

a. Show rectangular blocks in the positions required on the machine for testing.

b. Select the major bearing positions to indicate the condition of the machine. Label them numerically.

c. Select the minor bearing or other positions to indicate local conditions and label them alphabetically.

d. Divide the sketches with a wavy line to separate parts of a composite machine (so that slightly different limits may apply e.g. electric motor and refrig. compressor on same base).

Mark on the sketches, the criteria for wear (there may be more than one, for composite machines) in the form Worn 120/125 VdB. This means at 120 VdB Overall Level, start taking octave analysis, and also check all the lettered points as well as the numbered points. When any octave level reaches 125 VdB the unit is worn sufficiently to be replaced immediately.

Compare the readings obtained on an equipment with the criteria on the machinery sketch, and mark on a new record sheet the date of the next set of measurements to be taken. For instance, if the limits are 120/125 VdB and overall vibration levels are at 110 VdB then readings are due in a month's time. If the maximum overall reading is 122 VdB, measurements are due next week. It also helps to enter this latter machine on a "Caution" list.

Figure 14 shows a convenient vibration data analysis form.

Fig. 14   Typical Vibration Analysis Data Sheet

SPECIFICATION OF SINE VIBRATION TEST LEVELS
USING A FORCE-ACCELERATION PRODUCT TECHNIQUE*

A. F. Witte
Vibration and Acoustics Test Division,
Sandia Laboratories, Albuquerque, New Mexico

A technique has been proposed where the laboratory test levels are defined by the product of input force and input acceleration. This technique offers several advantages over both motion and force control when little is known about the field environment. It can be classified as a force technique since it allows the test item to affect the laboratory vibration environment. The technique is a compromise between constant acceleration control and constant force control and requires no knowledge of dynamic characteristics of the vibration source or the phase relationship between input force and input acceleration. Input force and acceleration are related to the test specimen's apparent weight by a constant which is the control level.

This paper proposes a method of specifying the control level by using an envelope of the relative minimum values of the test specimen apparent weight characteristics and the envelope of accumulated peak field accelerations experienced by similar units subjected to similar field environments. It includes a description of all mathematics used to develop the technique, includes results obtained from a mathematical model, and also briefly describes laboratory equipment necessary for the use of the technique.

INTRODUCTION

Because of contributions by Otts, Nuckolls, Hunter and Murfin [1-6] several force techniques have been developed for use in laboratory vibration testing. These have often replaced the motion techniques which previous to 1963 were used exclusively. The most sophisticated of these techniques requires considerable knowledge of the dynamic characteristics of the field vibration source.

However, quite often it is necessary for the test engineer to subject a specimen to a laboratory vibration test when little is known about the field vibration source and/or field vibration levels. As a result of this lack of knowledge, the test engineer is usually forced to obtain, from a central "data bank," enveloped field data obtained from a group of dynamically similar specimens subjected to similar environments. The resulting environment is generally the envelope of all peak accelerations experienced by the group of field specimens. The test engineer often then subjects the test unit to sinusoidal acceleration inputs whose peak values are those specified by the enveloped field environment. The drawbacks of this method are obvious; the engineer has resorted to motion control techniques, the dynamic characteristics of the test specimen are not allowed to affect the input vibration

environment, and the possibility of a serious overtest exists. The engineer can use acceleration or force limiting techniques to reduce the drawbacks of motion control but the limits set are often arbitrary and have little basis for their use.

A control technique has been developed which allows the dynamics of the test specimen to affect the vibration environment, and knowledge of the dynamic characteristics of the field vibration source is not required for its use. [7] The technique allows the test engineer to control the product of the laboratory input acceleration and input force at specified levels It is a compromise between acceleration and force control. Both input force and input acceleration levels vary but are limited to finite values by the dynamic characteristics of the test specimen. This results in a laboratory source impedance being neither infinite nor zero.

The purpose of this paper is to expand on this technique and to discuss a method of specifying vibration control levels which results in a "logical simulation" of field vibration environments in the laboratory. The discussion will be confined to sinusoidal vibration test methods. Mathematically, the technique can be extended to random; however present test equipment limitations prevent its use.

NOMENCLATURE

$A_i(\omega)$ = Peak amplitude of laboratory sinusoidal input acceleration, (g)

$A_i(\omega)$ = Laboratory input spectral density, (g^2/Hz)

$A_f(\omega)$ = Enveloped maximum field acceleration levels (g)

$A_r(\omega)$ = Peak amplitude of component sinusoidal response acceleration, (g)

$F_i(\omega)$ = Peak amplitude of laboratory sinusoidal input force, (lb)

$S(\omega)$ = Enveloped field acceleration spectral density, (g^2/Hz)

$H(\omega)$ = Frequency response function, A_r/A_i, (dimensionless)

$K(\omega)$ = Control level of input vibratory excitation, $F_i A_i$, (lb-g)

$W_a(\omega)$ = Test specimen apparent weight, F_i/A_i (lb/g)

$\overline{W}_a(\omega)$ = Envelope of minimum values of W_a characteristics, (lb/g)

ϕ = Phase angle, (rad)

ψ = Phase angle, (rad)

ω = Circular frequency, (rad/sec)

BASIC THEORY

The input laboratory acceleration and force to a test specimen (which has linear dynamic characteristics) will be defined as $A_i \sin \omega t$ and $F_i \sin(\omega t + \phi)$, respectively, where A_i and F_i are peak values of force and acceleration.

Consider the situation where the level of the frequency dependent product of peak input force, $F_i(\omega)$, and peak input acceleration, $A_i(\omega)$, will be controlled at some specified value $K(\omega)$. One can write the following equation:

$$F_i(\omega)A_i(\omega) = K(\omega) \quad . \tag{1}$$

The test specimen's apparent weight, $W_a(\omega)$, is defined as the complex ratio

$$W_a(\omega) = F_i(\omega)\big/A_i(\omega)^* \quad . \tag{2}$$

Note that for this discussion, the phase angle of apparent weight will not be used.

Using Eqs. (1) and (2), one can obtain relationships for peak acceleration and force as functions of the test specimen apparent weight:

$$\left[F_i(\omega)\big/A_i(\omega)\right]\left[F_i(\omega)A_i(\omega)\right] = K(\omega)\left|W_a(\omega)\right| \quad ;$$

$$F_i^2(\omega) = K(\omega)\left|W_a(\omega)\right| \quad ;$$

therefore

$$F_i(\omega) = K^{1/2}(\omega)\left|W_a(\omega)\right|^{1/2} \quad ; \tag{3}$$

---

*Apparent Weight, $W_a(\omega)$, the complex ratio of force and acceleration and is related to mechanical impedance, $Z(\omega)$, by $W_a(\omega) = Z(\omega)/j\omega$ where $j = \sqrt{-1}$.

and

$$\left[A_i(\omega)/F_i(\omega)\right]\left[F_i(\omega)A_i(\omega)\right] = K(\omega)\frac{1}{|W_a(\omega)|} ;$$

$$A_i^2(\omega) = K(\omega)\frac{1}{|W_a(\omega)|} ;$$

therefore

$$A_i(\omega) = K^{1/2}(\omega)\frac{1}{|W_a(\omega)|^{1/2}} . \qquad (4)$$

One can see that peak input force, $F_i(\omega)$, is a function of the square root of the specimen apparent weight, $|W_a(\omega)|$. It attains a relative maximum value whenever the apparent weight exhibits a relative maximum and becomes minimum whenever the apparent weight becomes minimum. However, the peak acceleration, $A_i(\omega)$, is a function of $1/|W_a(\omega)|^{1/2}$. It exhibits a relative minimum value whenever the apparent weight reaches a relative maximum and a relative maximum at relative minimum apparent weight values.

These characteristics appeal to one's intuition since greater force should be required to drive the test specimen at frequencies where its apparent weight is maximum, and acceleration should tend to notch at these same frequencies. The reader should note that this is a compromise between acceleration control and force control techniques. [7]

SPECIFYING A CONTROL LEVEL

The problem becomes one of specifying the frequency dependent control level, $K(\omega)$. For many test situations only two pieces of information are available to the test or specifications engineer for determining laboratory test specifications:

(1) Maximum acceleration levels experienced by dynamically similar test specimens subjected to similar environments. This data can sometimes be obtained from a central "data bank." [8]

(2) The dynamic characteristics of the test specimen which includes apparent weight and frequency response characteristics. This information can usually be obtained from a preliminary low level sinusoidal survey.

These two pieces of information will be used to define the control level $K(\omega)$. In defining the control level several conditions will be fulfilled.

1. Specified input acceleration levels are frequency dependent curves that envelope expected maximum field acceleration levels; therefore laboratory input acceleration levels should not exceed enveloped field levels.

2. Maximum field acceleration levels occur at frequencies where the test specimen apparent weight characteristics exhibit relative minimum values, and laboratory input acceleration levels should tend to peak at these same frequencies.

3. Minimum field acceleration levels occur at frequencies at which the test specimen apparent weight characteristics exhibit relative maximum values, and laboratory input acceleration levels should tend to notch at these same frequencies. *

Consider defining the control level, $K(\omega)$, by the following relationship:

$$K(\omega) = \overline{W}_a(\omega) A_f^2(\omega), \qquad (5)$$

where

$\overline{W}_a(\omega)$ is the frequency dependent envelope of the minimum values of the test specimen apparent weight, $|W_a(\omega)|$,

and

$A_f(\omega)$ is the frequency dependent envelope of expected maximum field acceleration levels.

---

* The validity of conditions 2 and 3 can be questioned since the effect of the dynamic characteristics of field vibration source on input acceleration levels have been neglected. However, these peak-notch relationships appeal to one's intuition.

From the relationships found in Eqs. (3), (4), and (5), one can write the following equations:

$$A_i(\omega) = \left[\overline{W}_a(\omega) \, V_f^2(\omega)\right]^{1/2} \left|W_a(\omega)\right|^{1/2}$$

or

$$F_i(\omega) = \left[\overline{W}_a(\omega) \left|W_a(\omega)\right|\right]^{1/2} A_i(\omega) , \qquad (6)$$

and

$$A_i(\omega) = \left[\overline{W}_a(\omega) \, V_f^2(\omega)\right]^{1/2} \frac{1}{\left|W_a(\omega)\right|^{1/2}}$$

or

$$A_i(\omega) = \left[\overline{W}_a(\omega) / \left|W_a(\omega)\right|\right]^{1/2} A_f(\omega) . \qquad (7)$$

Note from Eq. (7) and $A_i < A_f$ whenever $\overline{W}_a < W_a$. Since $\overline{W}_a(\omega)$ is the envelope of the minimum absolute values of the test specimen apparent weight the relationship $A_i < A_f$ will always hold. Thus, one can effectively limit input acceleration levels to maximum values specified by the field envelope, $A_f(\omega)$. The relative maximum values of A_i occur at frequencies where $|W_a|$ exhibits a relative minimum. Relative minimum values of A_i occur at frequencies where $|W_a|$ exhibits a relative maximum. The three initially specified conditions have been satisfied.

EXAMPLE CASE

Consider for the purpose of this discussion, the test specimen shown in Figure 1. The specimen is complex and can be thought of as a combined "lumped" mass and distributed system. The apparent weight characteristics of of the test specimen (shown in Figure 2) reflect its complexity. The input vibratory motion and force at the specimen base are $A_i \sin \omega t$ and $F_i \sin (\omega t + \phi)$ respectively. The response acceleration of an integral component within the specimen is $A_r \sin (\omega t + \psi)$. The frequency response function $H(\omega)$ for this location is defined by the complex ratio

$$H(\omega) = \frac{A_r(\omega)}{A_i(\omega)} \qquad (8)$$

and the magnitude of its characteristics is shown in Figure 3.

The envelope $\overline{W}_a(\omega)$ of the minimum absolute values of $W_a(\omega)$ is shown in Figure 2.

Note that the envelope consists of straight lines and does not have gross "discontinuities." In making these envelopes, one should avoid "discontinuities" in order not to have them in the control curve. Figure 4 shows the envelope of anticipated field acceleration levels. Again, "discontinuities" were avoided. The control level (the product of A_i and F_i) can be calculated using Eq. (5) and plotted as shown in Figure 5. It is a series of straight lines with no gross "discontinuities" and its level can easily be programmed and controlled in the laboratory.

At this point one can mathematically determine the effects of the input specification on the test specimen. Recall from Eq. (7) that the laboratory input acceleration level A_i can be obtained using

$$A_i(\omega) = \left[\overline{W}_a(\omega) / \left|W_a(\omega)\right|\right]^{1/2} A_f(\omega) .$$

One can calculate the frequency dependent apparent weight ratio,

$$\left[\overline{W}_a(\omega) / \left|W_a(\omega)\right|\right]^{1/2} ,$$

and plot it as shown in Figure 6. This ratio is always less than or equal to unity. The resulting laboratory input acceleration level is shown in Figure 4. Notice that $A_i(\omega) \leq A_f(\omega)$, and that $A_i(\omega)$ does in fact notch when $|W_a(\omega)|$ exhibits a relative maximum and peaks when $|W_a(\omega)|$ exhibits a relative minimum.

Using Eqs. (7) and (8), one can obtain a relationship for response acceleration as a function of the enveloped field acceleration.

$$A_r(\omega) = \left|H(\omega)\right| \left[\overline{W}_a(\omega) / \left|W_a(\omega)\right|\right]^{1/2} A_f(\omega) . \qquad (9)$$

A plot of response acceleration is shown in Figure 7. Notice that the response acceleration $A_r(\omega)$ has a tendency to be "limited" to some value since the apparent weight ratio tends to notch at frequencies where $H(\omega)$ peaks and peaks where $H(\omega)$ notches. However this limit level is a function of the systems dynamic characteristics and the engineer has no real control over it. One can see from this example that response accelerations of resonant components which make the apparent weight characteristics peak are considerably lower than those which would be obtained if the input acceleration was controlled at enveloped field levels.

72
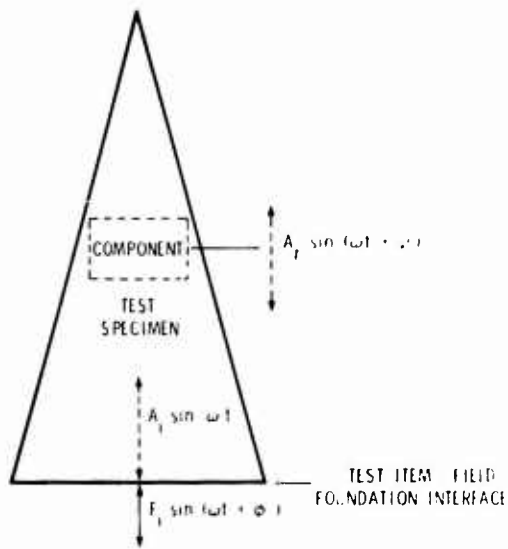
Figure 1. Test specimen.

Figure 2. Apparent weight characteristics.
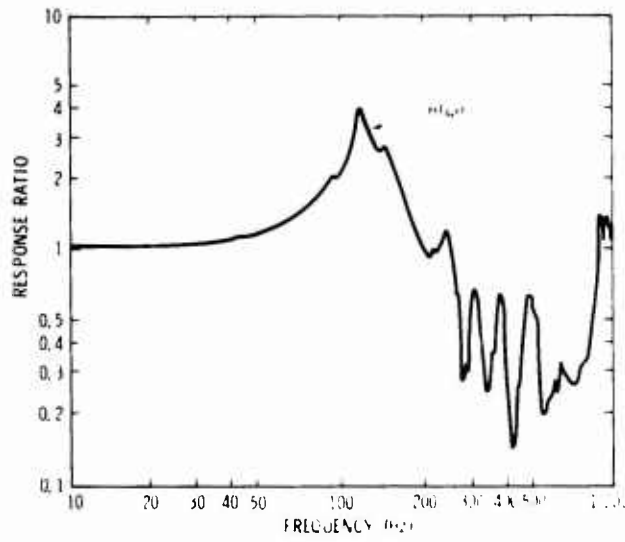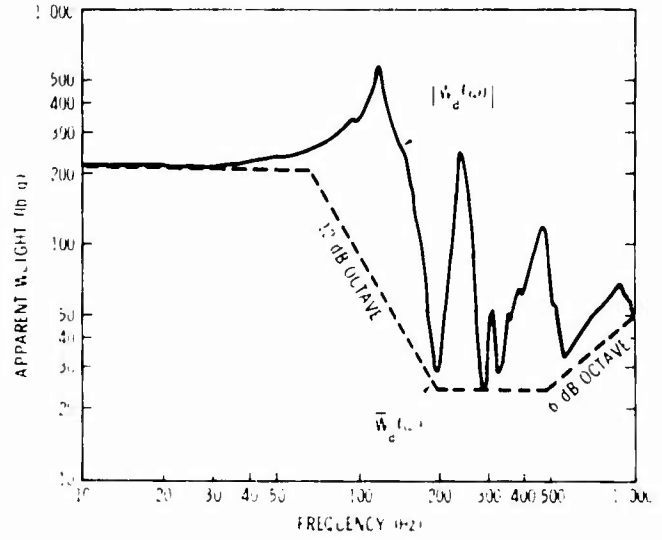
Figure 3. Frequency response function for antenna component.

73
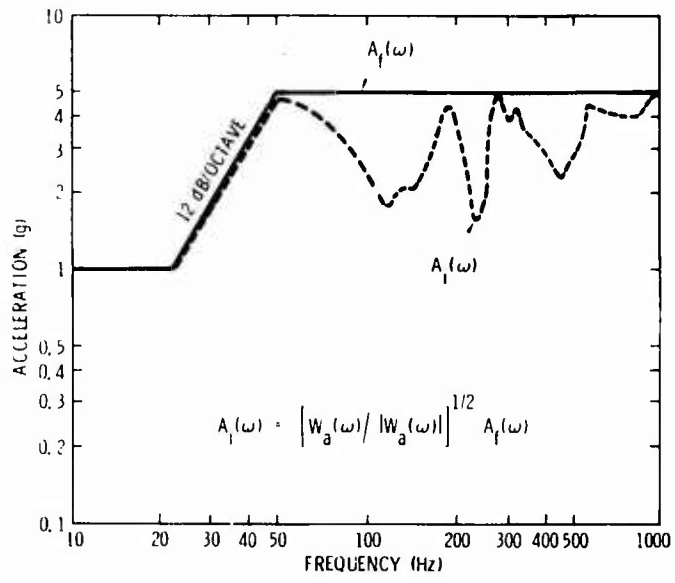
Figure 4. Field and laboratory input acceleration levels

$$A_i(\omega) = \left[W_a(\omega) / |W_a(\omega)| \right]^{1/2} A_f(\omega)$$
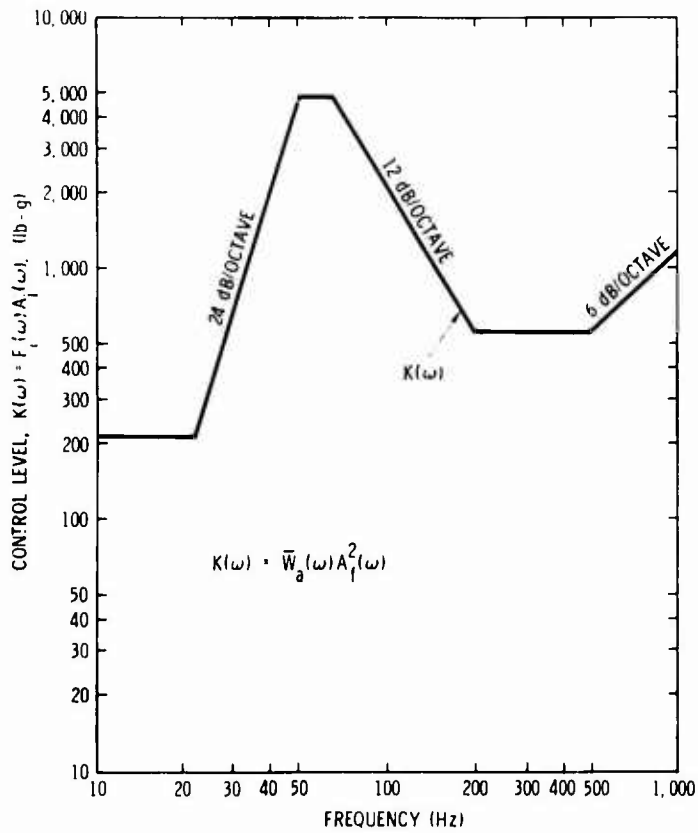
Figure 5. Control level

$$K(\omega) = \bar{W}_a(\omega) A_f^2(\omega)$$

74
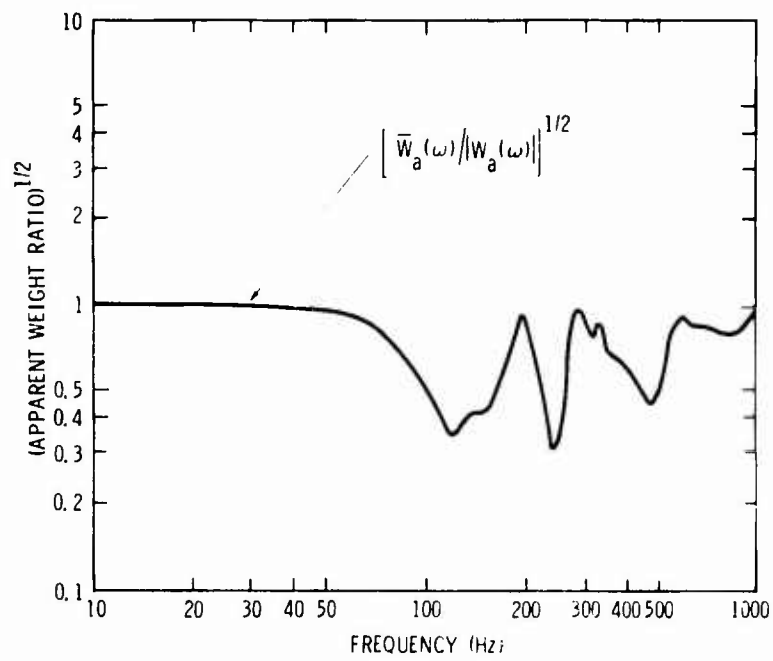
Figure 6. Apparent weight ratio

$$A_r(\omega) = |H(\omega)| \left[\bar{W}_a(\omega) / |W_a(\omega)| \right]^{1/2} \quad A_1(\omega)$$
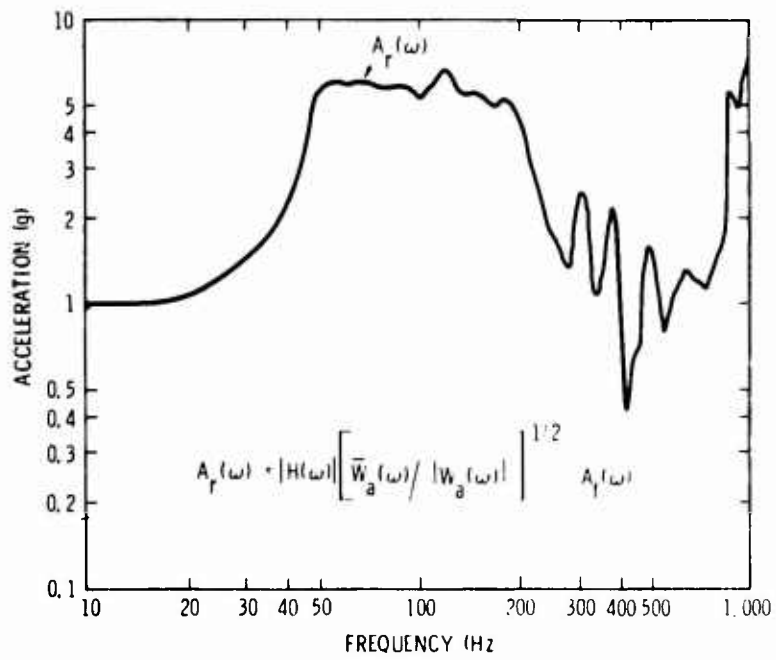
Figure 7. Component response characteristics

75

$$F_i(\omega) = \left[\overline{W}_a(\omega)\,|W_a(\omega)|\right]^{1/2} A_f(\omega)$$
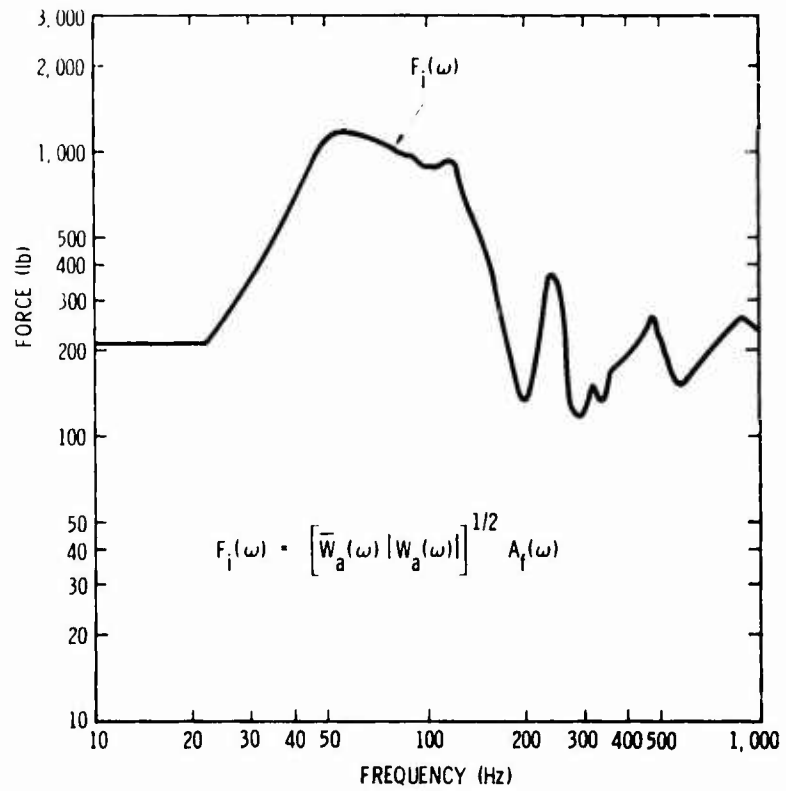
Figure 8. Input laboratory force
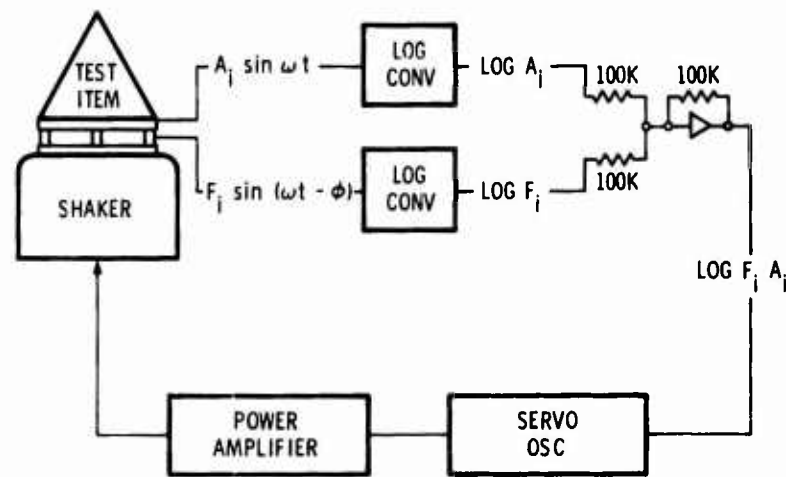
Figure 9. Test equipment

76

The force required to drive the system can be obtained using Eq. (6) and is shown in Figure 8. The force is not constant but has a tendency to peak with peaks in $\left|W_a\right|$ and notch with notches in $\left|W_a\right|$.

TEST EQUIPMENT

The equipment necessary to implement this technique is not excessive. Most testing laboratories would have all equipment; Figure 9 shows a block diagram of necessary equipment. Notice the only additional equipment required over the normal oscillator, power amplifier, shaker system are two log converters and an operational amplifier, which are used for the multiplying operation. Signal distortion may require the use of tracking filters preceding the log converters.

The output of each log converter is a d. c. signal proportional to the log of $A_i(\omega)$ or $F_i(\omega)$. The resulting output of the operational amplifier is a d. c. signal proportional to the log of the product, $F_i(\omega)A_i(\omega)$. This signal can be fed directly to the servocontroller variable gain stage by bypassing the rectifying circuits. Level programming must be done by operating on the d. c. signal proportional to log $F_i(\omega)A_i(\omega)$ before it enters the servocontroller. Programming may be done manually by having the operator follow a plotted curve of log $F_i(\omega)A_i(\omega)$ while changing gain of the signal.

PROCEDURE FOR SPECIFYING LABORATORY TEST LEVELS

A summary of procedures necessary to implement the technique follows:

1. An initial low-level resonance survey must be made to obtain test specimen $W_a(\omega)$ characteristics. Additional information, such as frequency response functions $H(\omega)$, can also be obtained but are not necessary for the performance of the test.

2. Draw the envelope, $\overline{W}_a(\omega)$, of the minimum values of $\left|W_a(\omega)\right|$.

3. Obtain an envelope, $A_f(\omega)$, of expected field acceleration levels

4. Calculate the control level $K(\omega)$ using Eq. (5),

$$F_i(\omega)A_i(\omega) = K(\omega) = \overline{W}_a(\omega) \, A_f^2(\omega)$$

and plot the value of $K(\omega)$.

5. Use this value of $K(\omega)$ as the laboratory input control level.

RANDOM CONSIDERATIONS

Theoretically the technique can be extended to control random vibration tests. This can be done if one controls the product of rms input force and rms input acceleration for narrow frequency bands. The random control level $K(\omega)$ can be defined by

$$K(\omega) = \overline{W}_a(\omega) \, S(\omega) \tag{10}$$

where $S(\omega)$ is the envelope of expected maximum field input acceleration spectral density levels. Mathematically the results are similar to those experienced in the sinusoidal case, and the laboratory input acceleration spectral density, A_i, is related to the enveloped field acceleration spectral density by

$$A_i(\omega) = \left[\overline{W}_a(\omega) \Big/ \left|W_a(\omega)\right|\right] S(\omega) . \tag{11}$$

Practically speaking, a technique has not yet been devised to shape a narrow band rms force-acceleration product using presently available equipment.

CONCLUSIONS AND COMMENTS

The force-acceleration product technique has several advantages over existing control techniques when little is known about the dynamic characteristics of the field vibration source.

1. The dynamic characteristics of the test specimen are allowed to logically affect the vibration environment and both $F_i(\omega)$ and $A_i(\omega)$ are dependent on the test specimen apparent weight characteristics.

2. Input acceleration levels are limited to maximum values specified by enveloped field data.

3. Response acceleration levels tend to be limited since notches in input acceleration levels occur at frequences where frequency response peaks also occur.

4. The control level is phase insensitive since it is a product of peak values of the sinusoidal input force and acceleration. This advantage may make the technique attractive when testing with multiple shakers.

The assumptions made are:

1. The apparent weight characteristics of the field vibration source and their effect on the vibration environment have been ignored.

2. One must also assume linear test specimen apparent weight characteristics. Non linear characteristics may cause laboratory input acceleration levels to exceed enveloped field levels. Any change in apparent weight characteristics over those used to obtain the envelope of minimum values will result in a change in the laboratory input acceleration levels with respect to the enveloped field levels. (Limiting circuits may be used in conjunction with the technique in order to insure that specified maximum input and/or response levels are not exceeded.)

3. All of the field input is assumed to be transmitted by the field foundation through the test item-field foundation interface. It is doubtful that aerodynamic loading could be simulated using the technique.

LIST OF REFERENCES

1. Otts, John V., "Force Controlled Vibration Tests: A Step Toward Practical Application of Mechanical Impedance," The Shock and Vibration Bulletin, February 1965, Bulletin 34, Part 5.

2. Nuckolls, C. E., "An Approximate Method of Simulating Mechanical Impedance in Vibration Testing," Institute of Environmental Sciences, 1965 Annual Technical Meeting Proceedings, p. 577.

3. Otts, J. V., and Nuckolls, C. E., "A Progress Report on Force Controlled Vibration Testing," The Shock and Vibration Bulletin, January 1966, Bulletin 35, Part 2.

4. Hunter, N. F., and Otts, J. V., "Electronic Simulation of Apparent Weight in Force Controlled Vibration Tests," Instrument Society of America, 22nd ISA Conference Proceedings, 1967.

5. Otts, J. V., and Hunter, N. F., "Random-Force Vibration Testing," The Shock and Vibration Bulletin, January 1968, Bulletin 37, Part 3.

6. Murfin, W. B., "Dual Specifications in Vibration Testing," The Shock and Vibration Bulletin, August 1968, Bulletin 38, Part 1.

7. Witte, A. F., "A Force-Acceleration Control Technique for Vibration Testing," Instrument Society of America, 1969 Annual Conference Proceedings, Paper 69-560.

8. Gens, M. B., "The Environmental Operations Analysis Function," Institute of Environmental Sciences, 1967 Annual Technical Meeting Proceedings, p. 29.

DISCUSSION

Voice: I would first of all like to congratulate Mr. Witte on a most interesting paper which goes some way towards solving one of the problems of overtesting. Instead of using the product of force and acceleration as control, which has not got a physical significance, you should look at the product of force and velocity at the input point which has got a physical significance in terms of power. I wonder how your results would have come out if you had used that concept instead.

Mr. Witte: In my original paper, I did consider this. One of the reasons that we have gone to acceleration is the fact that it is measured in the field easily and most of our field data comes back in terms of acceleration.

78

SOME EFFECTS OF EQUALIZATION WITH A DEAD MASS V

AN ELASTIC SYSTEM ON ACCELERATION AND STRESS

R. E. Kuba
Washington University

In order to provide some data on the question of where equalization
should be done in a random vibration test, an exciter, fixture, test
article system has been analyzed as a tens-mass system. Two conditions
have been considered: first with the test article represented as a
5-mass elastic system, and second with the test article represented as
a single mass. Comparisons have been made of the acceleration
responses of the masses in the full system, and of the force responses
of the springs in the full system, for various equalization points,
under the two conditions. RMS responses to random vibration inputs
have also been compared, both rms accelerations of masses and rms
forces in springs. The differences in both mass motions and spring
stresses are as much as a factor of 20 at any specific frequency. The
differences in RMS response to random vibration are factors of 4. It
would seem prudent to reconsider the desirability of using a dead mass
to equalize a random vibration setup.

INTRODUCTION

In a recent tour of a test facility, the author was impressed by the size and number of vibration exciters, and by the automatic equipment for sweep testing and for random vibration testing. The fixtures were stiff and strong and the team tables were impressively massive. Bags of lead shot were stacked near a shaker, and a question disclosed that the shot was used as a "dead mass" for equalizing random vibration setups. In order to get some facts about the difference between equalizing with a dead mass and with an elastic system the calculations reported herein were made.

THE SYSTEM AND ITS ANALYSIS

In order to have a system for analysis that was not so small as to be trivial, and yet was not so large as to be too costly to analyze, the 10-mass system shown in Fig. 1 was devised. The masses and springs were arranged as in an exciter-fixture-test article system. The natural frequencies were then determined and found to be distinct and fairly well spaced in the range from 46 to 318 cps.

In a system such as this, the phenomena of interest are the motions of the masses and the stresses in the springs. The motions (accelerations) are associated with malfunction problems, short circuiting, gyro precession, relay chatter, and the like. The spring stresses are associated with fatigue damage accumulation and eventual fracture. In random vibration, the best tool

for comparing motions and stresses is the set of transmissibilities as a function of frequency.

To calculate transmissibilities, the complex impedance matrix was formed and inverted to get the mobility matrix for each of 40 frequencies. The range between successive natural frequencies was divided so that there were three additional frequencies between each pair to give more detailed data than just 10 frequencies would give. In addition, each eigenvalue was reduced to insure that the impedance matrix would be non-singular; thus:

$$\omega_r^2 = \omega_o^2(1-\zeta^2) \tag{1}$$

in which

ω_o^2 = eigenvalue from undamped system

ζ = damping coefficient, taken as 0.03

ω_r = reduced frequency

The set of frequencies used for calculation are listed in Table 1.

The stiffness, k, and the mass, M, matrices were formed in the usual way, and the damping matrix, C, was calculated as:

$$C = 2\zeta \ [M^{\frac{1}{2}} \ k \ M^{\frac{1}{2}}]^{\frac{1}{2}} \tag{2}$$

where the square roots are term-by-term. Next the complex impedance, $Z(i\omega)$, was defined as

...in the lower frequency range. ... single to elastic transmissibility ... in Fig. ..., and it ranges from 0.24 ... equalization at mass 1, from 0.05 ... equalization at mass 5, and from ... for equalization at mass ... From ... conclude that, at any specific frequency, the difference between equalizing with a dead mass and with an elastic system can well be a factor of 20 or more.

Similarly if Figs. 4 and 5 are compared, the same kinds of differences appear in the height and location of peaks as before. The ratios of each frequency are the same for spring forces as for mass motions, as they should be.

Table 4 shows the RMS g's at mass 9 for a spectral density excitation of $1g^2$/cps for the different cases. The difference between equalization with an elastic system and a single mass is a factor from 2 to 6.

Table 5 shows the RMS pounds in spring 8-9 for a spectral density excitation of $1g^2$/cps for the different cases. Again the difference between the two kinds of equalization is a factor from 2 to 6.

CONCLUSIONS

Since the masses and springs used in the calculation system are within the range of real test systems, it would seem prudent to reconsider the desirability of using a dead mass to equalize a random vibration setup. The penalty for the dead mass equalization could well be a factor of 20 at any specific frequency, or a factor of 5 on RMS of random responses. These factors are too large to risk.

TABLE 1. FREQUENCIES USED FOR COMPUTATION			
FREQ. NO.	CPS	FREQ. NO.	CPS
1	0.4035	.1	1~2.~1
2	0.4659	..	1~...1
3	2..9~~	.~	...~.
4	32.459	.4	....~3
5	3..757	.~	...~.~
6	45.~00.	..	...~.~
7	55.~~~	..	..2.4.
8	64.293	..	...7..
9	71.742	.~	2~7..~
10	7~.4~~	3~	.47.47
11	91.50~	31	2.2.~7
12	102.~9	32	~75.~1
13	113.14	33	.~~..~
14	1.2.5~	34	~~1.~1
15	126.30	35	~05.~~
16	1.~..~	36	~~~.80
17	133.~1	37	313.86
18	1~~.~7	~~	317.~~
19	1~4.57	39	~~1.~4
20	170.~~	40	~.~.7~

TABLE 2. POUNDS AT MASS 1 FOR 1G AT MASSES 1,5,6

FREC.   POUNDS AT MASS 1 FCR 1G AT

NO.	MASS 1 *		MASS 5		MASS 6	
	ELASTIC	SINGLE	ELASTIC	SINGLE	ELASTIC	SINGLE
1	27CC	15543	2699	15539	2699	15538
2	2335	13461	2334	13456	2334	13455
3	1823	922	420	471	328	372
4	176	199	398	406	213	235
5	48	77	363	406	105	150
6	3	46	421	714	10	119
7	43	53	252	704	216	181
8	71	68	193	399	713	263
9	114	80	122	302	530	320
10	18	92	15	241	15	353
11	103	120	293	149	170	349
12	224	126	113	86	170	277
13	162	63	45	45	106	184
14	10	37	7	32	23	162
15	20	39	15	35	61	191
16	33	43	27	41	130	234
17	44	48	37	46	207	281
18	49	54	42	51	156	329
19	86	87	57	61	290	520
20	224	141	49	49	327	517
21	70	53	27	27	226	335
22	14	13	11	11	105	159
23	14	14	11	12	114	173
24	15	15	13	13	133	202
25	17	17	15	15	159	239
26	19	19	17	18	187	270
27	30	21	28	27	344	445
28	41	15	32	28	428	553
29	47	86	28	19	411	403
30	30	7	25	4	412	96
31	29	26	54	43	995	1112
32	35	34	95	80	1955	2304
33	39	43	123	80	2780	2536
34	37	10	162	8	4007	270
35	36	24	200	56	5096	1991
36	36	29	260	129	6819	4700
37	36	31	345	223	9299	9329
38	36	34	457	340	12642	13037
39	37	35	598	483	16966	19009
40	37	36	771	656	22407	26440

* ELASTIC   10-MASS SOLUTICN

SINGLE   MASSES 6-10 AS A SINGLE MASS
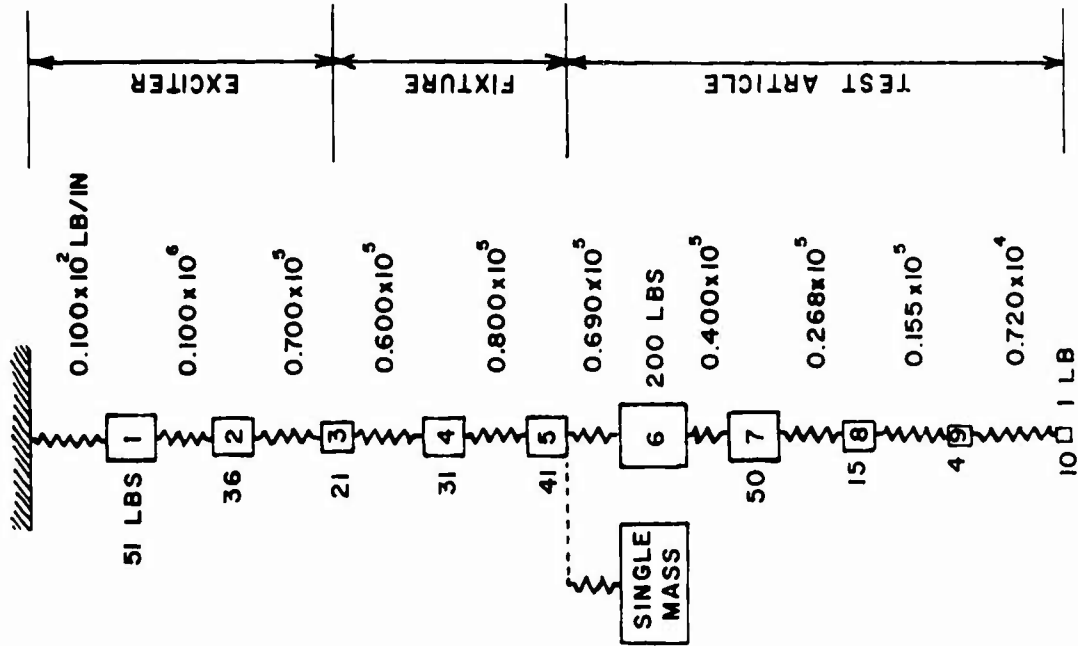
FIGURE 2
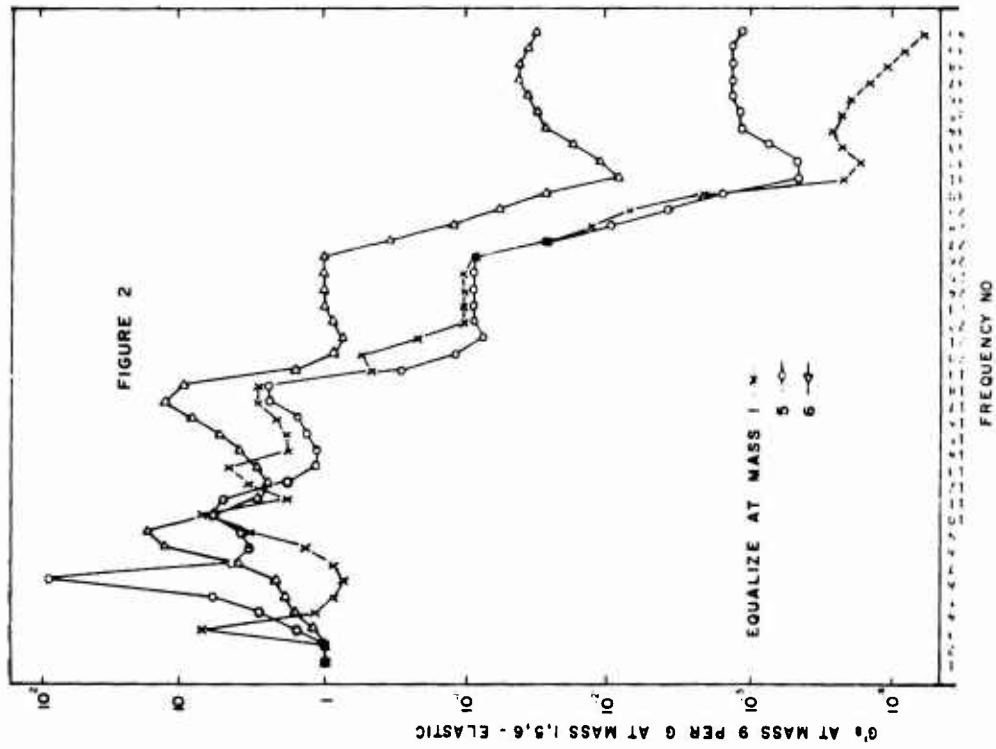
EQUALIZE AT MASS 1 ...

5
6

FREQUENCY NO

g's AT MASS 9 PER G AT MASS 1,5,6 - ELASTIC

EXCITER

FIXTURE

TEST ARTICLE

0.100x10² LB/IN

0.100x10⁶

0.700x10⁵

0.600x10⁵

0.800x10⁵

0.690x10⁵

200 LBS

0.400x10⁵

0.268x10⁵

0.155x10⁵

0.720x10⁴

I LB

51 LBS   1

36   2

21   3

31   4

41   5

6

50   7

15   8

4   9

10
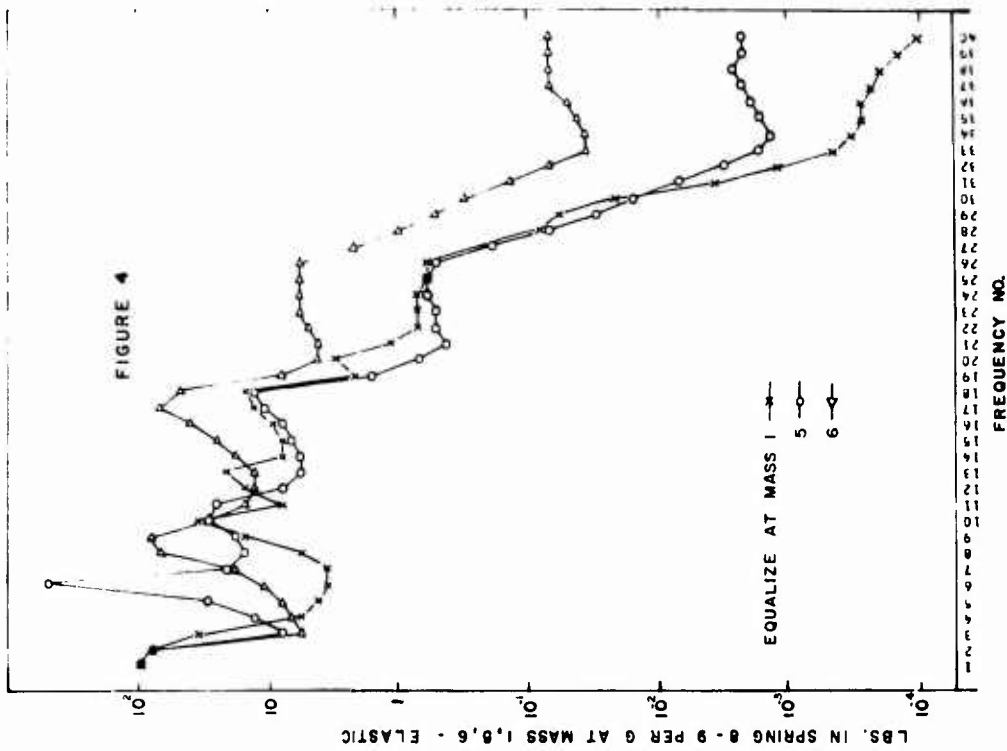
SINGLE MASS

FIGURE 4. TRANSMISSIBILITIES
- ELASTIC SYSTEM -
LBS. IN SPRING 8-9 PER G AT MASS 1,5,6
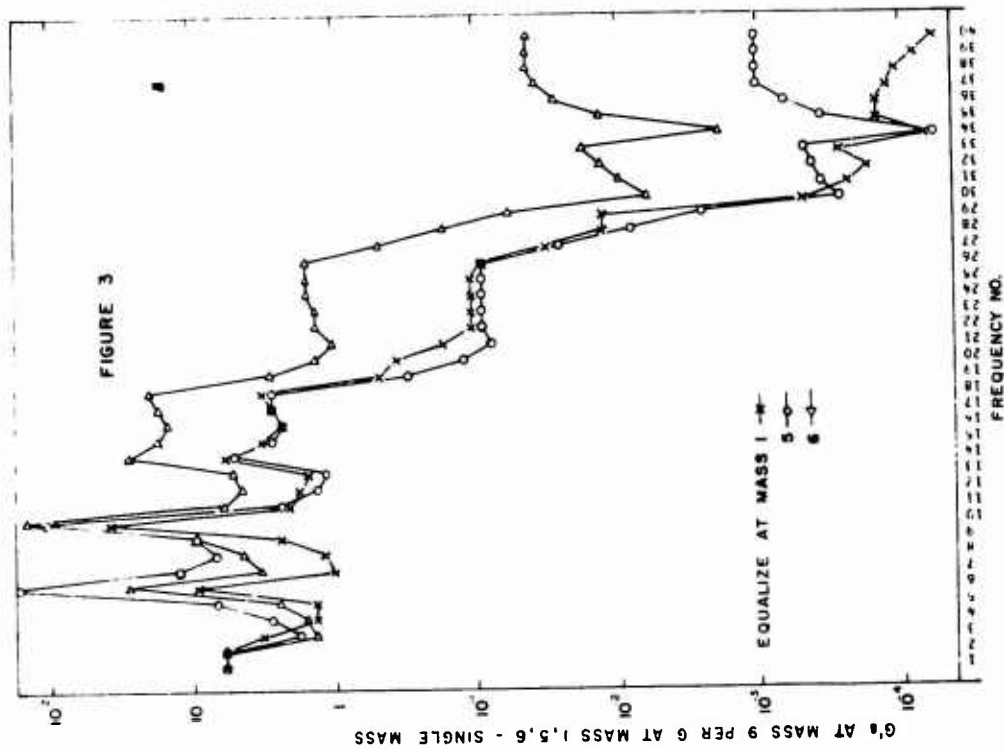
FIGURE 3. TRANSMISSIBILITIES
- SINGLE MASS -
G'S AT MASS 9 PER G AT MASS 1,5,6

FIGURE 6

EQUALIZE AT MASS 1 — ✳
5 – ○
6 –△–

FREQUENCY NO.

FORCE AND G RATIOS, SINGLE / ELASTIC
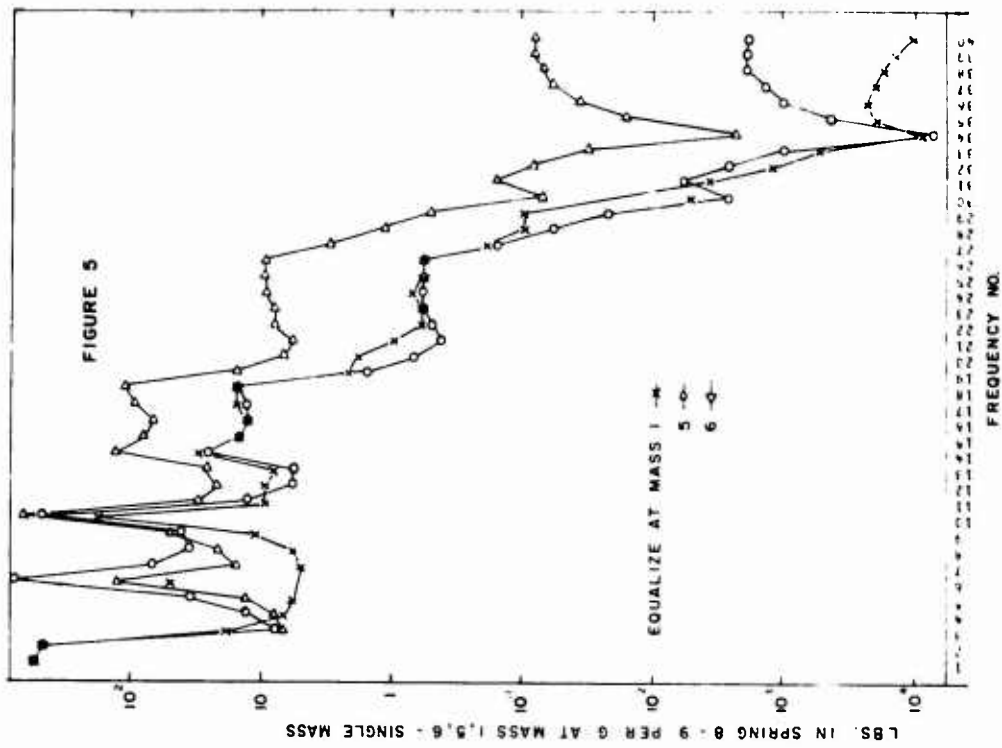
FIGURE 6. RATIOS OF TRANSMISSIBILITIES
SINGLE MASS/ELASTIC SYSTEM
(SAME FOR FORCE AND MOTION)

FIGURE 5

EQUALIZE AT MASS 1 — ✳
5 – ○
6 –△

FREQUENCY NO.

LBS. IN SPRING 8 - 9 PER G AT MASS 1,5,6 - SINGLE MASS

A METHOD FOR PREDICTING STRUCTURAL RESPONSES
FROM LOWER LEVEL ACOUSTIC TESTS[*]

D. O. Smallwood
Centrifuge, Vibration, Acoustics Division
Sandia Laboratories, Albuquerque, New Mexico

Many times it is desired to know the responses of a structure at acoustic levels above the capabilities of the laboratory. A technique which does not assume system linearity has been developed for extrapolating lower level test data to higher sound pressure levels. The technique consists of plotting the RMS structure acceleration response as a function of the input RMS sound pressure level in a frequency band (usually 1/3 octaves). Experimental results have shown that many structures exhibit response characteristics which plot as straight lines on a log-log plot indicating response characteristics of the form $g = ap^n$ where g is the response, p is the input pressure, and a and n are constants. Frequently n is some number other than one indicating a particular form on nonlinear response. Experimental results from several test programs are presented. A theoretical one degree-of-freedom system with nonlinear damping is also discussed to illustrate the results. The usefulness of the technique lies not only in the increased accuracy of the predicted responses but in an increased understanding of the nonlinearities of the system.

NOMENCLATURE

A = A constant

a = A constant

B = The rate of increase of an exponential function (dB/sec)

C = Capacitance

d = Displacement

ε = Error

g = Acceleration structural response

$H(\omega)$ = The system frequency domain transfer function

i = Current

K = A constant

ln = Logarithm to the base e

P = Sound pressure auto spectral density

p = Sound pressure

R = Resistance

SPL = Sound pressure level

t = Time

V = Voltage

ω = Frequency

ω_n = The undamped natural frequency of a one-degree-of-freedom system

x = Structural response

ζ = Linear viscous damping coefficient, the fraction of critical damping

INTRODUCTION

Many times it is desired to know the response of a structure at acoustic levels above the capabilities of the laboratory. The results of these tests can then be used to justify a high level test (which can be considerably more expensive) or to use as a basis for a vibration test to simulate the acoustic environment.

Several authors [1, 2, 3] have suggested the use of a vibration test as a substitute for an acoustic test assuming a linear system. It is well known, however, that many real systems are not linear. For example, it is acknowledged that structural damping is usually a function of the amplitude [4, 5, 6].

In an effort to study the linearity of structural systems and to use this information to predict the structural response at higher acoustic levels, a procedure was developed which does not assume a linear structure.

TEST METHOD

The test method is in reality a very simple procedure as shown in Figure 1. The test item is subjected to a broad-band random acoustic excitation whose amplitude varies monotonically with time. It has been found that an exponential rate of change in the amplitude works well. The spectrum shape should ideally be the same shape as the high level spectrum to which the results will be extrapolated. The input SPL (Sound Pressure Level) and the structural responses are recorded on a magnetic tape. The recorded SPL and structural responses are then filtered using identical filters, averaged, converted into a log amplitude, and plotted on an X-Y plotter. The result is log-log plot of structural response as a function of the SPL in a given bandwidth. This procedure is then repeated for each bandwidth of interest. Third octave filters are not the only filter which

could be used. They are typically used for the following reasons. They are: 1) commonly available in an acoustic facility, 2) of a reasonable narrow bandwidth while 3) the total number of curves which must be plotted for each response is kept to a manageable number.

It is acknowledged that an RC averaging circuit when used to measure a monotonically changing level will give a biased result. For example, if the level is increasing the RC average will always give a result which is below the true value. However it is shown in Appendix A that for an exponentially varying level the error is constant, predictable, and can be controlled to an acceptable level. Also if the same RC time constant is used for both the response and the input channel the errors for each channel will be nearly the same and will cancel.

TEST RESULTS

This method has been used on a number of test programs and selected results from three programs are shown in Figures 2-6. All three test items were similar (re-entry bodies) but from different programs. Figure 2 shows the overall response (40 - 10,000 Hz) of 5 accelerometers on the first test item mounted on the structure and at internal locations. It is seen that the responses generally follow straight lines on the log-log plot but not necessarily with a linear slope. Figure 3 shows the set of curves obtained for one of the accelerometers for each 1/3 octave bandwidth. Again notice that the curves are in general straight lines on the log-log plot. This experimental observation makes extrapolation to higher levels a relatively easy procedure. The observation that the responses will plot as straight lines on a log-log plot has been found to be generally true for the types of structures tested. Figure 4 shows the response of one accelerometer on a different structure. Again
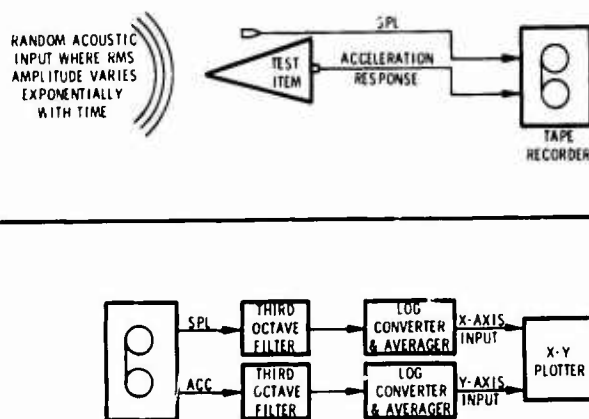
Fig. 1 - Test setup
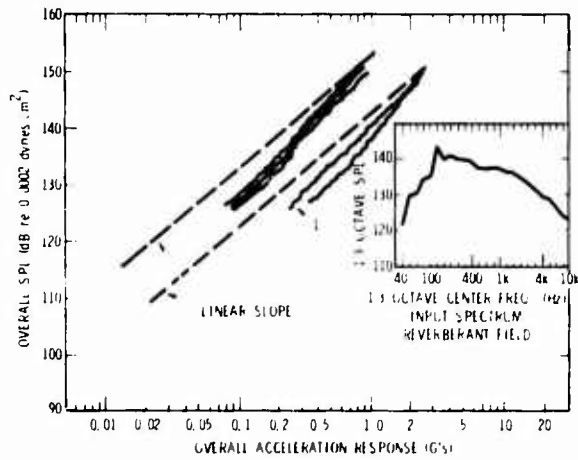
Fig. 2 - Overall linearity response
of 5 accelerometers
Test item A
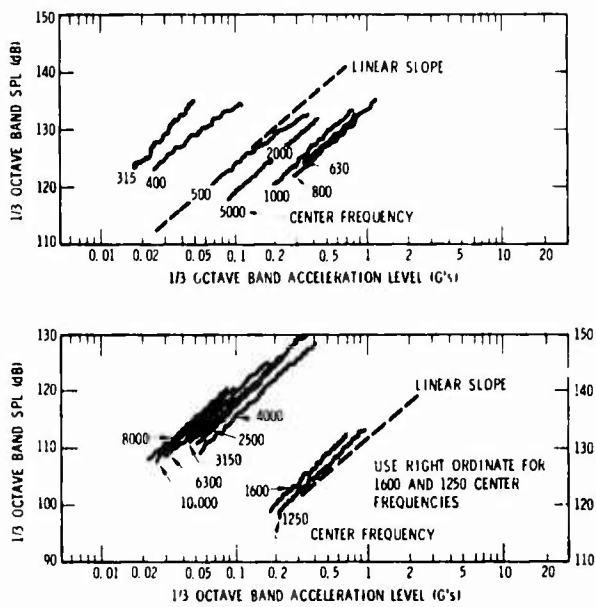
Fig. 3 - Linearity response
of accelerometer 1
Test item A
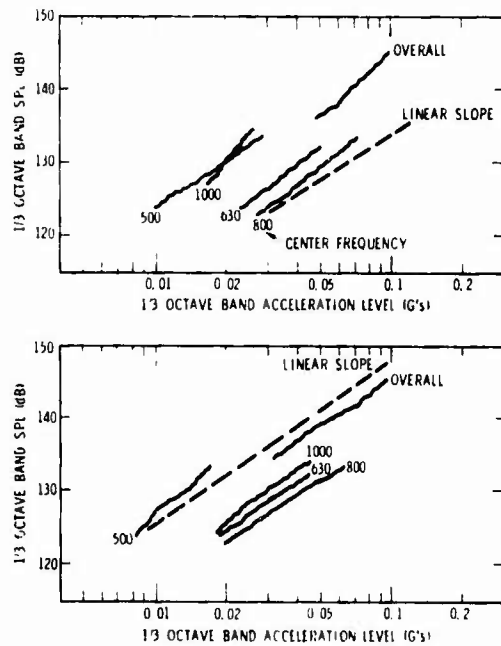
Fig. 4 - Linearity response
of two accelerometers
Test item B

89

the behavior is similar. Figures 5 and 6 show the response of yet a third structure to both a progressive and reverberant sound field. Note the responses still tend to follow straight lines on the log-log plot even though both the levels and slopes are field dependent. This emphasizes that not only must the spectrum shape be duplicated in the laboratory, but the type of acoustic field must also be considered.
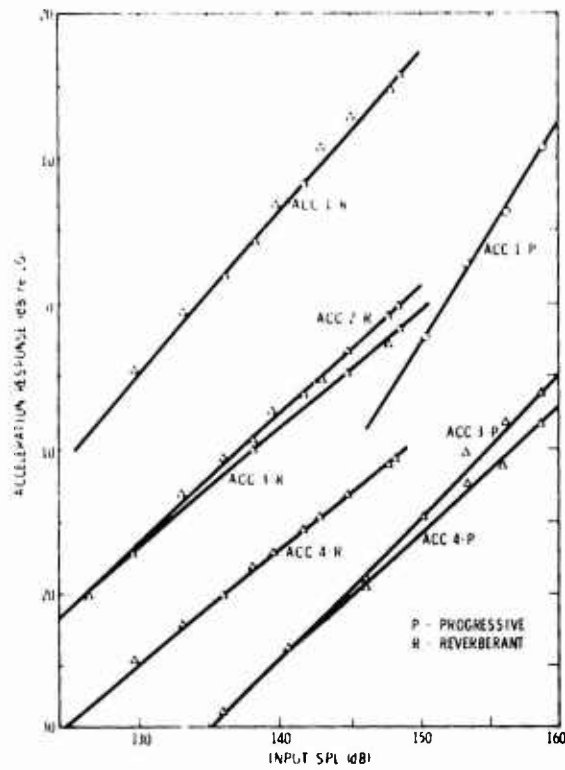
Fig. 5 - Linearity response
Test item C

Exceptions to the above behavior have been found but they are easily recognized and extrapolation can still frequently be done. Also the experimental results have not been extended beyond 160 dB (re .0002 dynes/cm^2).

The above results suggest that nonlinearities of the form $g = ap^n$ are common.

AN EXPERIMENTAL EXAMPLE

An experimental example will illustrate the type of nonlinearities which can give results similar to those shown. A voice coil from an electrodynamic speaker was excited with a progressive acoustic wave and the resulting coil displacements were measured. The results are shown in Figure 7. Notice that as
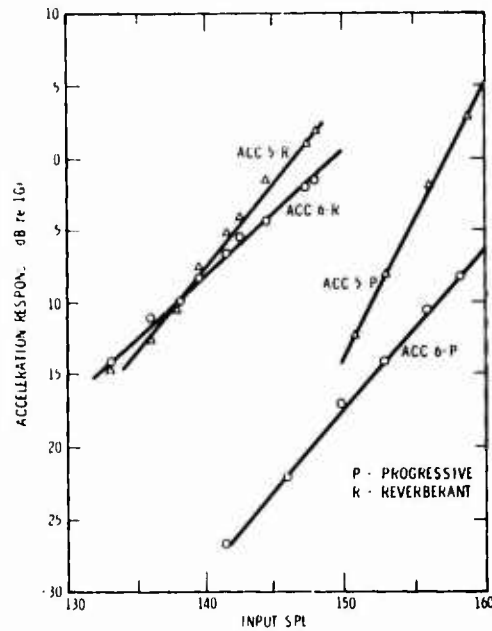
Fig. 6 - Linearity response
Test item C

the amplitude is increased the peaks and notches become less severe and the peaks shift down in frequency. This is characteristic of a system which becomes more highly damped for increased amplitudes. However if the damping was the only factor affecting the response, one would expect the amplitudes of the peaks to rise at a rate less than linear as the increased damping would tend to decrease the rate of increase in amplitude. However, the peaks rise proportional to $d = p^{1.5}$ (at 400 Hz). This indicates a nonlinear spring as well.

If displacement is plotted as a function of sound pressure (Figure 8) for a number of frequencies the characteristic straight lines again appear. From the preceding figure we can see that the nonlinear slopes are a result of increased damping, and a nonlinear spring characteristic. This causes a smoothing of the curves, shifts in the resonant peaks, and a nonlinear rate of increase in amplitude.

ONE-DEGREE OF FREEDOM SYSTEM WITH NONLINEAR DAMPING

To further explore the type of system which will give responses similar to the preceding results consider a one-degree of freedom system with the following characteristics.

Assume that the damping ratio (ζ) is a function of the input pressure, but that at any

90
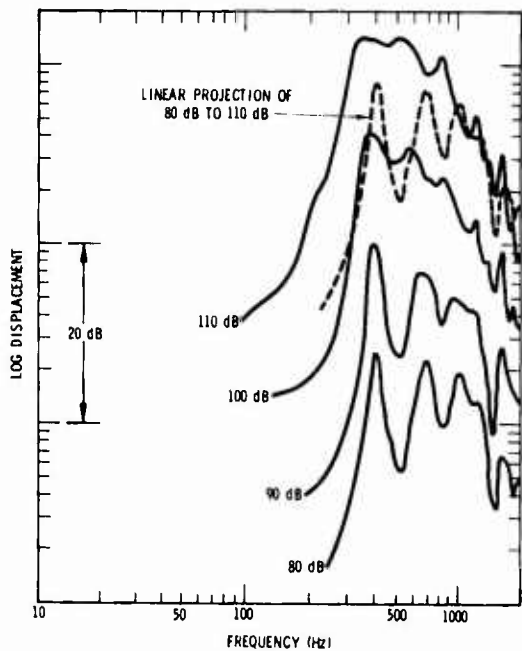
Fig. 7 - Displacement of a voice coil
as a function of frequency
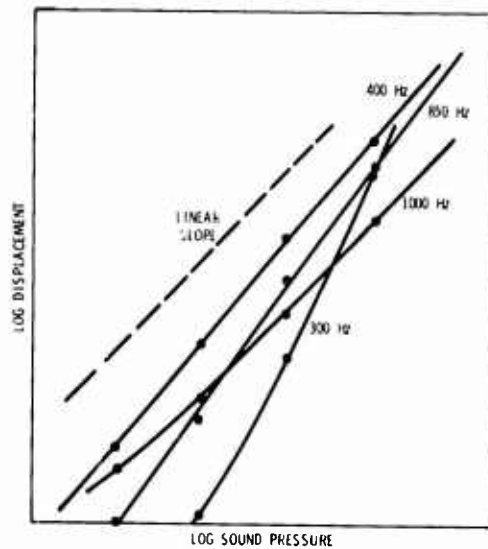
Fig. 8 - Displacement of a voice coil
as a function of the input SPL

pressure the system transfer function can be
represented by an equivalent linear function

$$x = \frac{p}{\sqrt{\left[1 - \left(\frac{\omega}{\omega_n}\right)^2\right]^2 + \left[2\zeta \frac{\omega}{\omega_n}\right]^2}}$$ (1)

where $\zeta = f(p)$.

If $2\zeta \frac{\omega}{\omega_n} \ll \left[1 - \left(\frac{\omega}{\omega_n}\right)^2\right]$ (i. e. small damping,
not near the reso-
nant frequency)

or if ζ = constant, then x will be a linear
function of p.

If $2\zeta \frac{\omega}{\omega_n} \gg \left[1 - \left(\frac{\omega}{\omega_n}\right)^2\right]$ (i. e. ω is near ω_n
such that
$1 - \left(\frac{\omega}{\omega_n}\right)^2 \approx 0$)

then

$$x \propto \frac{p}{\zeta(p)}$$ (2)

at any frequency near ω_n.

This response will plot as a straight line
on a log-log plot if ζ is of the form

$$\zeta \propto p^n$$ (3)

Eq. (2) then becomes

$$x \propto p^{1-n}$$ (4)

Several authors [4, 6] indicate that this form of
damping is not unreasonable.

91

We have calculated the expected value of the response of a linear system in the frequency band due to a broad band random input is given by

$$E\left[x^2\right] = \int_{\omega_1}^{\omega_2} P |H(\omega)|^2 \, d\omega \qquad (\ )$$

For the transfer function given in Eq. (1) and for P constant, the solution of Eq. ( ) is given by Crandall & Mark [7].

For example, if we let ω_n = 400 Hz and plot the response of the 400 to 630 Hz third octave Figure 9 results. From Figure 9 it is seen that an increasing damping coefficient (ζ) with pressure will result in a response with a slope of less than unity. If the damping decreases with an increase in pressure the slope of the response will be greater than unity. Curves plotted for other third octaves will show similar results except that the deviations from a linear response will become less sensitive to changes in the damping.
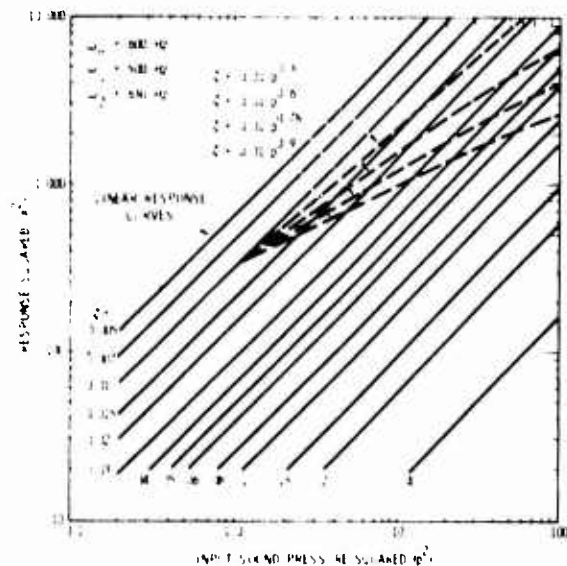
Fig. 9 - Response of a one-degree
of freedom system

If we assume the damping is of the form in Eq. (3) the response can be plotted for various values of n. (See Figure 9.) Again we can see that the straight line relationship on a log-log plot holds reasonably well. This result could be expected as the most significant contribution to the response is from frequencies

near ω_n and at these frequencies Eq. (4) is valid.

CONCLUSIONS

A simple test procedure has been presented for conducting a linearity study of a complex structure. It is seen that in a large number of cases the resulting responses will be of the form g = a p^n where n is not necessarily equal to one (1). When this condition is true the resulting responses will plot as straight lines on a log-log plot facilitating extrapolation. It has been shown with one example that a number of nonlinear characteristics can result in the above behavior. It was also shown that for the case of a single degree of freedom system damping of the form $\zeta \propto p^n$ will result in the above behavior.

The usefulness of the technique lies not only in the increased accuracy of the predicted responses but in the increased understanding of the nonlinearities of the system.

REFERENCES

1. D. U. Noiseux, "Simulation of Reverberant Acoustic Testing by a Vibration Shaker," Shock, Vibration, and Associated Environments, Bulletin No. 33, Part III (1963), pp. 125-136.

2. J. H. Putukian, "Simulating Missile-Firing Acoustical Environment by Equivalent Mechanical Vibration," Shock, Vibration, and Associated Environments, Bulletin No. 34, Part IV (1964), pp. 83-91.

3. T. D. Scharton and T. M. Yang, "Substitute Acoustic Tests," Shock, Vibration, and Associated Environments Bulletin No. 38, Part I (1968), pp. 115-124.

4. T. L. Parrott and J. A. Drischler "Strain Response of Simply Supported Beams to Point and Acoustic Loading," Shock, Vibration and Associated Environments Bulletin No. 36, Part V (1967), pp. 77-84.

5. C. M. Harris and C. E. Crede, editors, Shock and Vibration Handbook, Volume 3, Part 48, pp. 32-36, McGraw-Hill, New York, 1961.

6. J. E. Ruzicka, editor, Structural Damping, The American Society of Mechanical Engineers, New York, 1959, passim.

7. S. H. Crandall and W. D. Mark, Random Vibration in Mechanical Systems, p. 72, Academic Press, New York, 1963.

RC AVERAGING ERROR

When an RC averaging circuit is used to measure the level of a signal whose RMS level changes monotonically with time a biased estimate of the level will result.

An RC averaging circuit can be represented by the following circuit (Figure A-1).
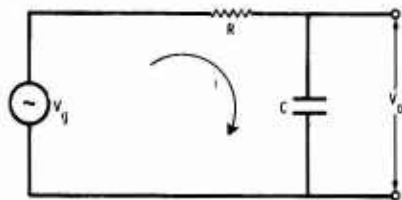
Fig. Al - RC Averaging circuit

The differential equation governing this circuit is

$$Ri + \frac{1}{C} \int_0^t i\,dt = V_g . \qquad (A-1)$$

The general solution of Eq. (A-1) is

$$i = \frac{1}{R} e^{-t/RC} \int e^{t/RC} \frac{dV_g}{dt} dt$$

$$+ K e^{-t/RC} \qquad (A-2)$$

Since

$$V_g - V_o = iR \qquad (A-3)$$

The solution becomes

$$V_g - V_o = e^{-t/RC} \int e^{t/RC} \frac{dV_g}{dt} dt$$

$$+ K e^{-t/RC} \qquad (A-4)$$

Let

$$V_g = A e^{at} \qquad (A-5)$$

then

$$\frac{dV_g}{dt} = aA e^{at}$$

and from Eq. (A-4)

$$V_g - V_o = \frac{aA}{a + 1/RC} e^{at} + K e^{-t/RC}$$

If at $t = o$ $V_g - V_o = 0$,

$$K = - \frac{aA}{a + 1/RC}$$

and

$$V_g - V_o = \frac{aA}{a + 1/RC} \left[e^{at} - e^{-t/RC} \right] . \qquad (A-6)$$

For large t, $e^{-t/RC} = 0$. Using Eqs. (A-5) and (A-6) for large t

$$\frac{V_g - V_o}{V_g} = \frac{a}{a + 1/RC} = \frac{RCa}{RCa + 1} .$$

If we let B be the increase in level in dB/sec then $a = B \frac{\ln 10}{20}$, and the error for large values of t will be

$$\epsilon = \frac{V_g - V_o}{V_g} = \frac{RCa}{RCa + 1} \qquad (A-7)$$

where $V_g = A e^{at}$.

Therefore, for an exponential change in the input, the error is constant for a given RC averaging time and a given rate of increase (a) and can be calculated from Eq. (A-7). For example let

$$B = 1/3 \text{ dB/sec and } RC = 2 \text{ sec}$$

then

$$\epsilon = \frac{2(.0385)}{1 + 2(.0385)} = 7\% .$$

93

SWEEP SPEED EFFECTS IN RESONANT SYSTEMS

RONALD V. GULL
1Lt   USAF
1750th Test Squadron
Tyndall AFB, Florida

The performance characteristics of all systems and system components are functions of frequency. The determination of frequency response curves usually assumes steady-state conditions. When the characteristics are determined under sweep excitation, they will, in general, differ from the steady-state characteristics. This difference is known as the SWEEP SPEED EFFECT. The solution presented here assumes a linear increase or decrease in frequency. This solution has been checked experimentally and does accurately predict the response of a resonant system to a linearly swept excitation.

INTRODUCTION

The performance characteristics for all systems and system components are functions of frequency. The characteristics determined from swept excitation will, in general, differ from steady state characteristics. This difference is known as the SWEEP SPEED EFFECT, which like all other effects may be advantageous or detrimental. The effect occurs in systems of all kinds; electrical, mechanical, acoustical, or any other system which exhibits an underdamped resonance and an excitation for which the frequency is time dependent.

The solution to the response equation for a second order single-degree-of-freedom to a sinusoidal forcing function is widely known and the response at any frequency can be found. If this response is plotted versus frequency, a curve, similar to curve (a) in Figure one, will be produced. This is the steady state response curve. The determination of such frequency response curve, experimentally, can only be done by dwelling at each test frequency an indefinite length of time until all transient responses have decayed to negligible levels. In practice, such a procedure is often either impossible or undesirable, and the test frequency is varied with time.

The rate of change of signal frequency with time is known as the sweep speed, angular acceleration, or frequency velocity, and represents the general case of a system under frequency modulated excitation. A curve, such as curve (a) in figure one, can be reproduced using a sweep frequency test if the frequency velocity is very low. As the frequency velocity increases the first deviation from the steady state is a decrease in the amplitude at resonance and an apparent shift at the resonant frequency in the direction of the sweep. The system requires a certain amount of time for the response to reach its steady state level. If the time spent at each frequency during the sweep is too short, a lower peak is to be expected. On further increase in frequency velocity, a second phenomenon occurs. Additional amplitude peaks appear where there are no resonances. In Figure one three curves are shown; (a) is the extremely slow sweep curve, (b) shows the decrease of amplitude and the change of resonance with a low frequency velocity, and (c) shows the additional peaks at a higher frequency velocity.

If system properties are determined at sweep speeds other than those which will excite the system in use, erroneous "properties" or calibration
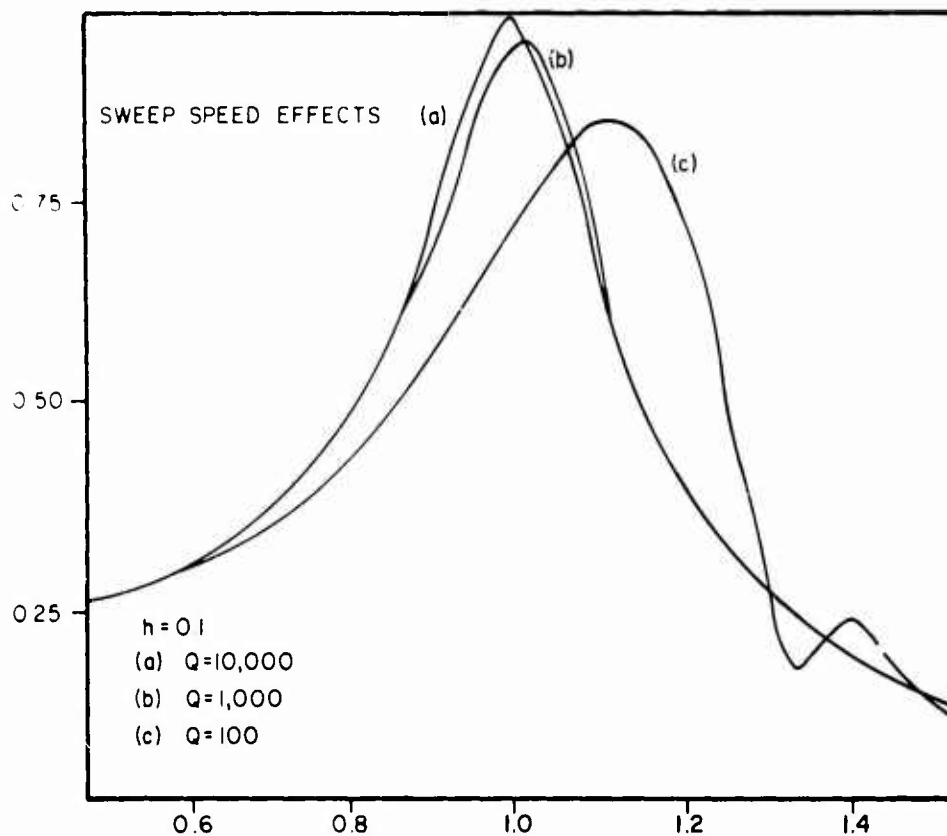
Fig. 1 - Sweep Speed Effects

curves" will result from the frequency response test. Thus "quick" vibration tests may reveal resonances much higher than intended operating frequency with peaks which appear acceptably low. Steady state operation can then result in system destruction. However, sweep speed of high value can be used to avoid the effects of serious resonances through which one must pass to reach operational conditions. This procedure is common practice in rotation machinery such as turbines, where the effects of several critical speeds can be minimized by accelerating through them fast enough. The severity of the sweep speed effect depends on system undamped natural frequency, the damping ratio at that frequency, and the frequency velocity of the excitation.

Past theoretical studies attempting closed form mathematical solutions include Lewis (4), Dimentberg (3), and Cronin (2). Lewis presents a graphical and nomographical solution to the problem; furthermore, the input data required for use of the solution are not readily available from the normal formulation of any real, physical problem. Dimentberg formed his solution with the use of Fresnel Integrals for which tables with complex arguments are not readily available. This fact, added to the complexity of the solution, makes it very difficult to use. Cronin's solution uses Error Functions and, though complicated, is usable. The solution proposed in this study is based on the Auxiliary Function of the Error Function and has many advantages over past solutions. It is simple, it fits the standard vibration solution format, and the functions involved are readily accessible in tabulated form. The solution is in the form of a steady state FM response for which digital computer program was written, and a transient FM response which in most cases has died out by the time the system passes through its first resonance.

96

The response of a linear single-degree-of-freedom system to a forcing function is given by the following equation:

$$\frac{d^2x}{dt^2} + 2h\omega_n\frac{dx}{dt} + \omega_n^2 x = F(t) \qquad (1)$$

where x is the response, F(t) is the forcing function, t is time, h is the damping ratio, and wn is the undamped resonant frequency in radians per second. The forcing function for a linearly changing frequency is:

$$F(t) = P \sin(\omega_c t \pm v t^2) \qquad (2)$$

where P is an amplitude constant, w_0 is the starting frequency and v is the frequency velocity in radians/second/second. The response of a system to a linearly increasing frequency is given by the equation:

$$\frac{d^2x}{dt^2} + 2h\omega_n\frac{dx}{dt} + \omega_n^2 x =$$

$$P \sin(\omega_c t + v t^2) \qquad (3)$$

The particular solution to this equation is shown in equation (4)

$$\frac{x}{x_0} = T_1 \sin(v t^2 + \omega_c t + \theta_1) + TFM_1 \qquad (4)$$

$$T_1 = \frac{1}{2}\sqrt{\frac{\pi Q}{2(1-h^2)}(A^2 + B^2)} \qquad (5)$$

$$\theta_1 = \frac{\pi}{4} + ARC TAN\left(\frac{A}{B}\right) \qquad (6)$$

$$A = \mathcal{R}e\left[W(z_1) + W(z_2)\right] \qquad (7)$$

$$B = \mathcal{I}m\left[W(z_1) + W(z_2)\right] \qquad (8)$$

$$Z_1 = e^{-i\frac{\pi}{4}}\sqrt{\frac{Q}{2}}\left(r + \sqrt{1-h^2} - i h\right) \qquad (9)$$

$$Z_2 = e^{-i\frac{\pi}{4}}\sqrt{\frac{Q}{2}}\left(r - \sqrt{1-h^2} + i h\right) \qquad (10)$$

Where X_0 is the static response, r is the instantaneous Frequency divided by the resonant frequency, and W(z) is

the auxiliary function of the error function. In the equations above, the symbol Q is the non-dimensionalized sweep parameter given by:

$$Q = \frac{\omega_n^2}{2v} \qquad (11)$$

The transient FM response contains only three time dependent functions which are the sine and cosine of the damped resonant frequency and the exponental decay function. The transient FM response (TFM) is given by:

$$TFM_1 = \frac{1}{2}\sqrt{\frac{\pi Q}{2(1-h^2)}} e^{-h\omega_n t}\left(e^{\frac{h\omega_r}{2}}\sin\omega_0 \sin\phi_1 + \right.$$

$$\left. + e^{\frac{1}{2}hQ\sqrt{1-h^2}} \cos\omega_0 \cos\phi_2\right) \qquad (12)$$

$$\omega_0 = \omega_n\sqrt{1-h^2} \qquad (13)$$

$$\phi_1 = \frac{\pi}{4} + \frac{1}{2}Q\left[(r_0 + \sqrt{1-h^2})^2 + h^2\right] \qquad (14)$$

$$\phi_2 = \frac{\pi}{4} + \frac{1}{2}Q\left[(r_0 + \sqrt{1-h^2})^2 - h^2\right] \qquad (15)$$

and ro is the ratio of the starting frequency to the resonant frequency. Since the decay factor multiplies the entire function, this part of the response will die out soon after the application of the forcing function. The transient FM response can usually be neglected. However, there could be cases where frequency velocity is high enough for this portion of the response to become important. Sweep rates of this magnitude are generally only possible in electrical systems. The response of a system to a linear sweep down in frequency is given by:

$$\frac{d^2x}{dt^2} + 2h\omega_n\frac{dx}{dt} + \omega_n^2 x = P\sin(\omega_c t - v t^2) \qquad (16)$$

The particular solution to this equation is:

$$\frac{x}{x_0} = T_2 \sin(\omega_c t - v t^2 + \theta_2) + TFM_2 \qquad (17)$$

where

$$T_2 = \frac{1}{2}\sqrt{\frac{\pi Q(C^2 + D^2)}{2(1-h^2)}} \qquad (18)$$

$$\phi_2 = \frac{\pi}{4} + \arctan\left(\frac{c}{D}\right) \tag{19}$$

$$c = A_i\left[W(z_3) + W(z_4)\right] \tag{20}$$

$$D = \omega_n\left[W(z_3) + W(z_4)\right] \tag{21}$$

$$z_3 = -e^{-i\frac{\pi}{4}}\sqrt{\frac{Q}{2}}\left(r - \sqrt{1-h^2} + ih\right) \tag{22}$$

$$z_4 = -e^{-i\frac{\pi}{4}}\sqrt{\frac{Q}{2}}\left(r + \sqrt{1-h^2} - ih\right) \tag{23}$$

and the transient FM response is:

$$TFM_2 = \frac{1}{2}\frac{\pi Q}{2(1-h^2)}e^{-\omega_n h t}\left[e^{+\omega h(r+\sqrt{1-h^2})}\cos(\omega_D + \phi_i) - e^{+\omega h(r-\sqrt{1-h^2})}\cos(\omega_D - \phi_i)\right] \tag{24}$$

The steady state FM response was programmed into a digital computer to predict the amplitude of a system given the values of the damping ratio, the sweep factor, and the ratio of the instantaneous frequency divided by the undamped resonant frequency. The values given by the computer were then verified by comparing them with the values obtained experimentally. Two experimental systems were used to check the theoretical values. One was an electrical resonant circuit and the other was a galvanometer. Both systems can be modeled by the response equation and both have easily adjustable damping. Values were checked in the damping range of 0.007 to 0.3 at sweep factors of 100 to 10,000. Good agreement was found in all points compared. This solution, not only fits a standard vibration solution format, but is also simple enough to use. The transient FM response was neglected when the computer program was written and did not cause the data taken to deviate more than the tolerances on the experimental apparatus. It was found that the first additional peak began to appear when

both theoretically and experimentally. To reproduce the steady state curve with a swept excitation requires that one specifies the tolerance expected. With a swept excitation there will be some depression of the amplitude at the damped resonance.

Bibliography

1. Abramowitz and Stegun, I.A.: "Handbook of Mathematical Functions," Dover Publications, Inc., New York (1965).

2. Cronin, Donald L.: "Response of Linear, Viscous Damped Systems to Excitation Having Time-varying Frequency," Report for NASA and NSF in partial fulfillment of requirements for the degree of Doctor of Philosophy.

3. Dimentberg, F.M.: "Flexural Vibrations of Rotating Shafts," Butterworth, London (1961), Chapter 3.

4. Lewis, F.M.: "Vibrations during Acceleration Through a Critical Speed," Transactions of the ASME, Vol 54 (1932), pp 253-261.

5. Stein, P.K. "Measurement Engineering," 5th Edition (1969), Imperial Lithl., Phoenix, Ariz.

THE DYNAMIC RESPONSE OF A STEEL EYEBAR CHAIN SUSPENSION BRIDGE

OVER THE OHIO RIVER TO VARIOUS APPLIED EXCITATIONS

E. F. Turner, J. L. Viner
Federal Highway Administration
Department of Transportation
Washington, D.C.

The eyebar chain suspension bridge over the Ohio river at St. Marys, West Virginia is almost identical to the bridge at Point Pleasant, West Virginia which collapsed suddenly in December, 1967 with a tragic loss of 46 lives. Following this failure, it was deemed advisable to make a study of the dynamic stress amplifications and vibration responses of the St. Marys bridge to provide further insight into the possible causes of the Point Pleasant bridge failure if any unusual behavior were observed. A cooperative field study of the dynamic behavior of the St. Marys bridge was immediately undertaken by the Federal Highway Administration and the West Virginia State Road Commission.

Dynamic responses of the bridge were induced in two ways. The bridge was first excited by the use of an improvised harmonic vibration generator (located on the riverbank beneath the structure) which exerted a direct vertical cyclic pull on the underside of the midspan point of one of the end spans through a steel wire rope. Resonant vibrations were induced in the structure in the first four normal modes. The measured frequencies and the corresponding mode shapes compared favorably with predicted values.

A second type of bridge excitation was provided by the passage of a three-axle truck weighing 44,300 pounds crossing the bridge at low speeds. Strain, displacement and acceleration transducers were installed on the bridge at critical points suggested by local failures noted in the Point Pleasant bridge wreckage. Mean live load stress levels determined at various points throughout the bridge during the vehicle passage were not excessive. Vibrations induced by the vehicle passage were generally of much higher frequency than induced by the vibration generators and represented various modes of individual structural member vibrations

INTRODUCTION

Following the failure of the eyebar chain suspension bridge over the Ohio River at Point Pleasant, West Virginia in December, 1967, with a loss of 46 lives, it was deemed advisable to make a study of the dynamic stress amplifications and vibration responses of a similar eyebar chain suspension bridge which carries Alternate U. S. Route 50 over the Ohio River at St. Marys, West Virginia (Fig. 1).

The St. Marys bridge is located 90 miles upstream from the site of the Point Pleasant bridge and is part of the West Virginia State Highway System. A full-scale model is thus available for a variety of tests which may shed additional light on the cause of the Point Pleasant bridge failure if any unusual behavior is observed.

With the concurrence of the West Virginia State Road Commission, the Federal Highway Administration's Structures and Applied Mechanics Division promptly initiated a research program to instrument the bridge and conduct a study of the static and dynamic responses to various live loadings. This group and the West Virginia State Road Commission cooperated in the endeavor with the latter organization providing on-site logistic support for the conduct of the experimental study by the Federal Highway Administration.

The dual objectives of the test program

It was proposed to verify the calculated natural frequencies and mode shapes by exciting the structure with a harmonic force while the bridge was entirely free of vehicular traffic. Calculations of the theoretical natural mode shapes and frequencies (Appendix A) indicated that the first four vertical modes would be within the range of frequencies available from the vibration generators. Low-frequency resonant vibrations in a suspension bridge may indicate susceptibility to undesirable aerodynamic excitation.

The Federal Highway Administration bridge research test vehicle (Fig. 2) was used to provide a 44,000-pound, 3-axle moving load for obtaining the live load response of the bridge under a typical heavy truck.

THE BRIDGE

The description and history of the Point Pleasant bridge have already been well documented as a result of its disastrous failure.[1] The St. Marys bridge superstructure was designed and built concurrently with the Point Pleasant bridge about 40 years ago and is essentially identical except for minor differences in the approaches dictated by the difference in the sites. The St. Marys bridge consists of a two-lane 27-foot truss-stiffened roadway suspended from two parallel steel eyebar chains spaced at 30'-0" centers. The eyebar chains are anchored at each bank of the Ohio River and pass over two intermediate pier towers. The center span is 700 feet long and the two anchor spans are each 380 feet long. Short approach spans connect to the bridge at each end. Each eyebar chain consists of closely spaced parallel pairs of eyebars linked together and to adjacent pairs in the chain by a common connecting pin joining four eyebars at each joint. The eyebars vary in length from 25 feet to 55 feet and vary in thickness in proportion to design loading, averaging about 2 inches. The shank between eyes is 12 inches wide. The bridge design live loading consists of a uniform load of 1400 pounds per linear foot of roadway and 42,000 pound concentrated load.

The suspension chains form the upper chords of the stiffening trusses in those panels where the chain and the truss upper chord are contiguous in the end spans and center span. The stiffening truss members otherwise consist of steel built up sections. Where the stiffening truss and the eyebar chain are not contiguous, vertical steel hangers connect the trusses to the eyebar chains at each panel point. Each chain passes over vertical end posts at each end of the structure which deflect the chains downward to the anchorages. The existing bridge roadway is a replacement of the original floor system and is composed of a network of stringers and floor beams supporting a 3-inch deep concrete-filled steel grid deck.

INSTRUMENTATION

The dynamic responses were monitored through the use of strain gages, deflectometers, and vertical and horizontal accelerometers. Strain gages on the vertical faces of upper chord members in the center span were oriented along the longitudinal axis of each member. These gages were located midway between truss panel points at approximately the 1/4-, 3/8-, 1/2-, 5/8-, and 3/4-points of the center span and served as the primary indicators of mode shape in the center span. Gages at the 3/8-, 1/2-, and 5/8-points were located on eyebars and the remaining two on truss channel webs.

The responses measured through other strain gages located on bridge members for the purpose of determining live load strain responses and higher frequency localized vibrations are the subject of a separate report.

The deflectometers used for this study each consist of a metal cantilever beam with gages mounted near one end which is rigidly attached to the structure. The free end is then deflected an amount greater than the expected live load deflection and held in this position by a fine steel cable anchored in the ground beneath the bridge. The live load deflection of the structure decreases the initial deflection and the resultant change in strain registered at the fixed end of the gage can be translated to displacement through a factor established by previous laboratory calibrations. Vertical deflectometers were located near midspan of each of the end spans.

Only four accelerometers were available for the field study. Two ± 0.25 g horizontal accelerometers were attached to lower chord members of the downstream truss near midspan of the center span and of the Ohio end span. Two ± 1.0g vertical accelerometers were moved from point to point in the center span and the Ohio end span during various phases of the testing to determine mode shapes of the response.

All the transducers described above were of the variable resistance type and were wired as Wheatstone Bridge circuits with external bridge completion resistors provided when necessary. Four-conductor grounded-shield cable in lengths up to 120 feet was used to connect the transducers to the signal conditioning equipment in the Federal Highway Administration research instrument van which had been located beneath the Ohio end span. Signal conditioning, amplification, bridge balancing, calibration and attenuation for the transducer circuits were provided by instrumentation in the van. A direct-read oscillograph utilizing light-beam galvanometers was used to monitor resonances and to record the amplified transducer response signals.

BRIDGE EXCITATION AND LOADING METHODS

The first objective of the test program called for a harmonic forced vibration input. Inertial force generators were not feasible for this purpose due to the low natural frequencies required. A method of providing an adequate low frequency harmonic energy input to the bridge with precise frequency control had to be devised. The calculations made in the process of devising such a vibration generator are included in appendix B. It was decided to utilize a direct cyclic pull on the underside of the Ohio end span of the bridge which was over dry ground. Two alternative devices were provided for exerting the cyclic low-frequency pull on the underside of the bridge. In one, the drive axle torque of the bridge research test vehicle was exploited to obtain a pulsating cyclic force at frequencies as low as 20 cycles per minute. The vehicle was positioned beneath the mid-span section of the endspan, the left side of the drive axle jacked up and the wheels removed. A steel fixture designed to translate the rotating motion of the truck drive axle into a variable 6-inch to 14-inch double amplitude vertical stroke through a link and pin assembly was then attached to the hub of the drive axle (Fig. 7).

The reciprocating vertical force thus generated by the rotation of the drive axle was then transmitted to the bridge in the following connection sequence: first through a 22-turn loop of 5/8-inch diameter shock cord to provide elasticity in the connection; then through a 3/4-inch manila triple tackle to permit releasing the connection; finally through a 5/8-inch wire rope connected to an eye bolt bracket clamped to the bottom flange of the bridge floor beam at the load point. This system was capable of applying over 6000 pounds of static pull on the bridge through the reaction of the vehicle. The resultant amplitude of bridge motion is calculated to be a small fraction of the available vertical stroke for this level of input force even assuming the stretch in the wire rope and in the triple tackle assembly to be small. The shock cord loop was designed

for approximately 70 percent elongation. The number of turns in the loop necessary to transmit the maximum force was calculated from the known elasticity of the shock cord.

An alternate method of forced vibration generation consisted of a power take-off from a portable pump with a driven double-amplitude reciprocating plunger. The pump was substituted for the trailer axle (Fig. 8) of the test vehicle and was driven by a 7½ horsepower gasoline engine. The frequency available from this device at a lower range from 6 to a cycles per second. The pump offered better frequency control but less force output than the vehicle drive axle take-off. The connection from the pump reciprocating arm to the bridge was the same as for the vehicle drive axle take-off except that the loop of shock cord was eliminated.

Both methods of forced vibration were also employed in attempts to generate torsional modes of vibration in the bridge by moving the connection on the underside of the bridge to the lower chord of the truss on the downstream side of the roadway. Pure torsional modes could not be excited since the normal modes predominated even with eccentric loading. In both vibration generators, a strain gage was installed on the reciprocating link to help to identify the resonant frequencies.

The second objective of the test program called for heavy vehicle passages across the bridge in the absence of other traffic. The Federal Highway Administration bridge research test vehicle was also utilized for this part of the program and was loaded with aggregate to provide a 17,000-pound load on both the driver and the trailer axles. The load on the front axle was 4,700 pounds making a total vehicle weight of 44,000 pounds. The vehicle traversed the bridge in each direction along each normal traffic lane at speeds of 5 mph and 15 mph. Due to the steep ascending grades on the bridge (5.5 percent) and the sharp turns and intersections near both ends of the bridge, the sustained maximum speed attainable with the loaded vehicle were only slightly over 15 mph. A two-way radio permitted communication between the instrument van and the test vehicle.

NATURAL MODE ANALYSIS

Natural mode shapes, natural frequencies, and mode shapes together could be determined from the free vibration of the bridge immediately after release of the vibration generator and also from the motion of the bridge. The resilient pickup position in the attached cable after stopping the generator was analytically transformed but not perfectly true. Small irregularities in direction were also measured with the vibration generator in situ.

was found to be about 0.5 that of the center span displacement.

In runs 2, 3, 4 and 5 there appeared to be a tendency for the natural frequency to decrease and the logarithmic decrement to increase in the afternoon runs as compared with the morning runs. This could be a temperature effect.

A second symmetric mode with natural frequencies between 73.0 and 74.2 cycles per minute was obtained in runs 7, 8, 9 and 10. logarithmic decrements of around 0.04 were observed in the three runs in which the pump motor provided the excitation. Run 8 in which the drive axle of the truck provided the excitation indicated a logarithmic decrement of 0.06.

A series of records was made during forced vibration at a frequency of 72.5 cycles per minute while a vertical accelerometer was placed successively at each center span panel point between midspan and the Ohio tower. The resulting responses have been normalized to the relative response of the deflection gage in the end span and are shown in Fig. 5.

When an attempt was made to excite torsional modes in the bridge with the truck drive takeoff, a single amplitude motion of about 0.06 inch in the end span was observed at frequencies of 47.7 and 49.0 cycles per minute on the two deflection gages on opposite sides of the bridge. In addition, the data indicated the presence of a beat frequency of around 4 cycles per minute. An attempt to excite torsional vibration with the pump drive resulted in a 46.7 cycle per minute response of the bridge with heavy beating. Vertical accelerometers at the 1/4-point in the center span indicated the torsional response at that point to be out of phase with the torsional response of the mid-point of the Ohio end span. Other than these responses, no significant torsional bridge motions were noted.

TEST VEHICLE CROSSINGS

Crossings of the bridge with a heavy vehicle in the absence of other traffic were made in order to obtain the responses of selected critical elements of the structure under such loading. These responses are the subject of a separate report.

DISCUSSION OF RESULTS

The mode shapes and frequencies of the vertical vibrations observed during the vibration generator tests have been presented in Table 1. The calculated natural frequencies and mode shapes of the first four vertical modes are given in Appendix A.

The calculated value of the first symmetrical natural frequency of 30.5 cycles per minute is in reasonably good agreement

$$M = \frac{\pi^2}{L^2} E I \, y_c \, \sin \frac{\pi x}{L}$$

where: y_c = maximum deflection
    L = span length

with the experimentally determined value of 33.5 cycles per minute. Similarly, good agreement between the calculated and observed mode shape was obtained. The ratio of the calculated value of the natural frequency of the first asymmetric mode of 4x.x cycles per minute to the natural frequencies determined in runs 2, 3, 4, 5 and 6 (Table I) is about the same as the ratio of calculated to experimentally determined values of the fundamental symmetric natural frequency. The calculated first asymmetric mode shape differed significantly from that observed, however. The mode shape obtained from run 6 was rather like that of the second calculated asymmetric mode. Inasmuch as no other asymmetric modes were obtained from the test program, it is conceivable that the mode of run 6 and that of runs 2, 3, 4 and 5 may be two separate natural modes of the structure.

The ratio of the calculated second symmetric natural frequency of 69.0 cycles per minute to the measured values obtained in runs 7, 8, 9 and 10 fits into the pattern of the similar ratios in the fundamental symmetric and asymmetric modes. The calculated and measured mode shapes are in good agreement.

If the combined effects of (1) the difference between the resonant frequency of the bridge and the frequency of excitation, (2) the drift in the excitation frequency, and (3) the non-harmonic components of the forcing function are assumed to make the bridge behave as an equivalent viscous damped ideal single degree of freedom system with a sinusoidal forcing function operating at 95 percent of the fundamental resonant frequency, then the measured 6300-pound input force corresponds to a 0.155 horsepower input. Using the theoretical value of the deflection of the end span (assumed as simply supported) under a concentrated load at mid-span of 1000 lb. = 0.022 inch (from appendix B) and the theoretical fundamental natural frequency = 30.5 cycles per minute (from Appendix A) and assuming $\delta = 0.15$, the maximum end span displacement would be:

$$y = (0.4)(1.1) \sqrt{\frac{0.155}{1.0}} = 0.173 \text{ inch single}$$

amplitude. Using the experimentally determined values of natural frequency = 33.5 cycles per minute, deflection of end span under a concentrated load of 1000 lb. at mid-span (extrapolated from truck crawl run data) = 0.155 inch, $\delta = 0.15$, then $y = 0.173 \sqrt{\frac{.155}{.022}} \left(\frac{30.5}{33.5}\right)^2 \sqrt{\frac{.15}{.1}} = .1xx$

inch, single amplitude.

In this particular case the differences between the assumed values and experimentally determined values tend to somewhat offset one another.

The measured end-span displacement at 33.5 cycles per minute was .1x inch single amplitude indicating very good agreement

between predicted and measured displacement for the fundamental mode.

While the static and dynamic responses of the bridge to the moving test vehicle are the subject of a separate report, it may be pointed out here that the maximum live load stress levels determined at various points throughout the bridge during the vehicle passages were not excessive. Vibrations induced by the vehicle passage were generally of higher frequency than induced by the vibration generators and represented localized structural member vibrations in certain axial and flexural modes.

SUMMARY OF RESULTS

The first two symmetric normal modes of vibration were identified in the test program. The mode shapes and frequencies were in good agreement with calculated values.

There was some indication of the possible existence of two separate asymmetric vertical modes, very close to one another in frequency, at around 5x cycles per minute. This observed frequency is in reasonable agreement with the calculated frequency of the first asymmetric mode. Neither experimentally determined vibration pattern was in good agreement with the calculated first asymmetric mode shape; however, the second experimentally determined asymmetric mode shape was in reasonable agreement with the calculated second asymmetric mode shape.

Quantitative measurements of damping obtained for each experimentally determined mode of vibration indicated that the bridge was a lightly damped structure.

The calculations of dynamic response for given levels of input force from the vibration generators were more than adequate for the purpose of choosing appropriate vibration generation equipment and motion sensing instrumentation.

REFERENCES

1. Eyebar Bridges and the Silver Bridge Disaster, ENGINEER, Publication of the Engineers Joint Council, January - February, 19xx.

Bridge Research Test Vehicle

Fig. 5 - Relative Displacement Amplitudes for Vertical
Harmonic Load on Tower of Span Midpoint
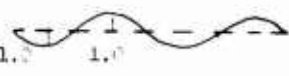
Table 1 - Natural Modes, Frequencies, and Participation Factors of
Structure from Vibration Analysis Program

105

$$KE = \frac{W}{2g} \omega^2 \left[\int_0^{L_1} \eta_1^2 \sin^2 \frac{\pi x}{L_1} dx + \int_{L_1}^{L_2} \eta_2^2 \sin^2 \frac{\pi x}{L_2} dx + \int_{L_2}^{L_3} \eta_3^2 \sin^2 \frac{\pi x}{L_3} dx + \int_{L_3}^{L_4} \eta_4^2 \sin^2 \frac{\pi x}{L_4} dx \right]$$

η

η

Δ

...ding viscous damping,

$$\Delta = \delta (...) \quad [1]$$

where: δ = logarithmic decrement of damping.

If $\delta = .1 ...$,

Mode	Δ (ft.-lb.)
	,
	1 ,
	.,
	40,...
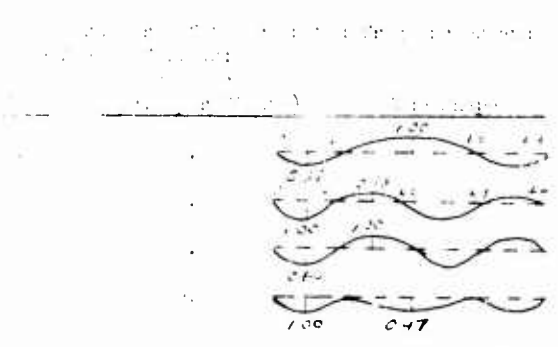
Mode	1. h.p. Input Equivalent
1	1, 0 ft.-lb./cycle
	. . ft.-lb./cycle
	. . ft.-lb./cycle
	4. ft.-lb./cycle

Since $\propto (\omega \eta_0)^2$, for ω constant, and a change in kinetic energy from KE_1 to KE_2, the amplitude at any particular point will change as follows:

$$\frac{\eta_{0_1}}{\eta_{0_2}} = -\sqrt{\frac{KE_2}{KE_1}}$$

Substituting (1) and (2) into (3) the resonant single amplitudes that can be maintained by a 1. h.p. input in these modes with $\delta = .15$ can be obtained. The results are given in Table 51 in the columns labeled Perfect Frequency Control.

In order to utilize the results in the table, it is necessary to estimate the sinusoidal force, F_0, required to deliver 1.0 h.p. to the bridge.

$$F = F_0 \sin \omega t$$

$\Delta = \Delta_0 \sin \omega t$ = Deflection of mid-point of side span

$\Delta = (D.F.) (\Delta \text{ static})$

where:

D.F. = dynamic amplification factor, that is, the ratio of the dynamic response to the static deflection of the system under the maximum load applied.

Assuming the end span to be simply supported and taking the average moment of inertia of the stiffening trusses from Appendix A as representative of end span stiffness, then:

Δ static $= \frac{...}{...} = ... 1$ foot, for $F = 1,000$ lb.

$$\Delta = \frac{...1 ... F_0}{1} \quad (D.F.) \sin \omega t$$

Work performed in one cycle $= W$

106

APPENDIX REFERENCE

1. "Aerodynamic Stability of Suspension
   Bridges," Part V, Appendix I, Bearne J.
   Vincent, U. of Washington, Engineering
   Experiment Station Bulletin 116, June 1954.

$$W = \int_0^{2\pi/\omega} F\Delta\, dt$$
$$= 1.9 \times 10^6 F_o^2 (A.F.) \left[2 \int_0^{\pi/\omega} \sin^2 \omega t\, dt \right]$$
$$= 1.9 \times 10^{-6} F_o^2 (A.F.) \left(\frac{\pi}{\omega} \right) \tag{4}$$

For 1.0 h.p. input, $W = \dfrac{33,000}{\frac{\omega}{2\pi}}$ (5)

$$F_o = \frac{24,000}{\sqrt{A.F.}}$$

Since the frequency control of the some-
what crude vibration generation equipment was
unknown prior to the actual trials, an allowance
for such effects was made. If these effects
are taken to be equivalent to the excitation of
a viscous damped single degree of freedom
system with a sinusoidal forcing function
operating near the system resonant frequency,
then

$$A.F. = \frac{1}{\sqrt{\left(1 - \left(\frac{\omega}{\omega_n}\right)^2\right)^2 + \left(2 \frac{c}{c_c} \frac{\omega}{\omega_n}\right)^2}}$$

where:

ω = Forcing frequency

ω_n = Natural frequency

$$\frac{c}{c_c} = \frac{\delta}{2\pi}$$

Again with $\delta = 0.15$

ω/ω_n	Amplification Factor
1.00	20.7
0.95	5.9
1.05	5.1
0.90	4.6
1.10	5.1

From (4) it can be seen that the work performed
in one cycle is proportional to A.F. Therefore
the resonant response this would maintain
would then be proportional to $\sqrt{A.F.}$

This effect is indicated in Table P1
under the columns labeled $\pm 5\%$ frequency
control and $\pm 10\%$ frequency control.

For perfect control (A.F. = 20.7):
$F_o = 5300$ lb. to deliver 1.0 h.p. to
    bridge

For $\pm 5\%$ frequency control (A.F. = 4.6):
$F_o = 9,200$ lb. to deliver 1.0 h.p. to
    bridge.

107

... ... for the ... amplitude
... ... for 1 ... ... Input

					±? Frequency Control Maximum Displacement	±15 Frequency Control
					1.1 in.	... in.
					.? in.	0.4 in.
					.4 in.	0.3 in.
					.3 in.	0.2 in.

DUAL SPECIFICATIONS IN RANDOM VIBRATION TESTING, AN APPLICATION OF MECHANICAL IMPEDANCE*

By

A. F. Witte
Vibration and Acoustics Test Division,
Sandia Laboratories, Albuquerque, New Mexico

and

R. Rodeman
Applied Mechanics Division,
Sandia Laboratories, Albuquerque, New Mexico

Effective methods of specifying "realistic" test levels for both sine and random vibration have been developed for situations where considerable information about the dynamic characteristics of the field vibration source is available. Methods have also been devised for sinusoidal testing where little is known about the dynamic characteristics of the field source. However, little has been done in the area of random testing for situations where the characteristics of the vibration source are not well known. This paper presents a technique which modifies one which has been previously proposed for sinusoidal testing. The technique utilizes enveloped field data and the impedance characteristics of the test specimen to generate a laboratory random input force spectrum. It also utilizes transfer impedance characteristics to modify the input force spectrum in order to impose response motion limiting in the laboratory situation.

INTRODUCTION

In general, there are presently two accepted methods of specifying vibration test levels: motion control and force control. Specification of input motion is used more often than force since field measurements are made in terms of motion. However, Otts [1] has shown that motion-controlled tests can be extremely conservative, and has proposed the use of force control for the laboratory situation. On the other hand, for effective use of most force techniques one must have knowledge of the dynamic characteristics of the field foundation to which the specimen is normally attached. [2] Typically, this information is not available for newly designed systems which must be qualified for field use.

Murfin [3] proposed the use of a force technique for sinusoidal vibration testing which utilized a "band average" of the test specimen's apparent weight characteristics and the envelope of peak field acceleration levels to calculate an "average" input force spectrum. This "average" force in conjunction with a limit on input acceleration levels was used to specify laboratory test levels. The technique has several advantages:

109

(1) the dynamic characteristics of the fixed foundation are not required,

(2) acceleration levels experienced in the laboratories peak and notch at frequencies where the apparent weight characteristics notch and peak, respectively, and

(3) laboratory acceleration and force levels are limited to reasonable values.

This paper extends the technique proposed by Murfin [3] to the random mode. The random method has the same advantages as those found in the sinusoidal situation, however, the implementation of the technique for the random situation is more difficult. The use of the technique for random testing requires considerably more pretest calculation, and limiting input and response acceleration levels cannot be performed using automatic equipment.

The mathematical as well as the laboratory procedures required to effect this technique are described along with the results of a laboratory test which are compared with data obtained in the field situation.

NOMENCLATURE

$A_i(\omega)$ Peak amplitude of sinusoidal input acceleration, (g);

$A_r(\omega)$ Peak amplitude of sinusoidal response acceleration, (g);

$\mathscr{A}_i(\omega)$ Laboratory input acceleration spectral density, (g²/Hz);

$\mathscr{A}_r(\omega)$ Laboratory response acceleration spectral density, (g²/Hz);

$F_i(\omega)$ Peak amplitude of sinusoidal input force, (lb);

$\mathscr{F}_i(\omega)$ Laboratory input force spectral density, (lb²/Hz);

$\mathscr{G}(\omega)$ Envelope field acceleration spectral density, (g²/Hz);

$H(\omega)$ Frequency response function, $A_r(\omega)/A_i(\omega)$ complex, (dimensionless);

$W_a(\omega)$ Apparent weight, $F_i(\omega)/A_i(\omega)$ complex, (lb/g);

$W'_a(\omega)$ Transfer apparent weight, $F_i(\omega)/A_r(\omega)$ complex, (lb/g);

$\overline{W}_a(\omega)$ "Band averaged" apparent weight (lb/g);

ω Circular frequency, (Radians/sec).

THEORY

Consider a test specimen (shown in Figure 1) which exhibits linear dynamic characteristics and has its driving point apparent weight* characteristics defined by the frequency dependent complex ratio

$$W_a(\omega) = \frac{F_i(\omega)}{A_i(\omega)} \qquad (1)$$

The specimen is to be subjected to a laboratory environment where $\mathscr{A}_i(\omega)$ and $\mathscr{F}_i(\omega)$ are the input acceleration and force spectral densities for a Gaussian process. The apparent weight characteristics of the test specimen can also be defined by

$$\left| W_a(\omega) \right|^2 = \frac{\mathscr{F}_i(\omega)}{\mathscr{A}_i(\omega)} \qquad (2)$$

One can write the dimensionally consistent relationship that defines an average laboratory input force spectrum, $\mathscr{F}_i(\omega)$, by

$$\mathscr{F}_i(\omega) = \left| \overline{W}_a(\omega) \right|^2 \mathscr{G}(\omega) \qquad (3)$$

where $\overline{W}_a(\omega)$ is a "band average" of the test specimen's apparent weight characteristics, and $\mathscr{G}(\omega)$ is the envelope of expected maximum field input acceleration spectral density levels.†

---

*Apparent Weight, $W_a(\omega)$, the complex ratio of force and acceleration, is related to mechanical impedance, $Z(\omega)$, by $W_a(\omega) = Z(\omega)/j\omega$ where $j = \sqrt{-1}$.

†The frequency dependent envelope $\mathscr{G}(\omega)$ can be obtained by enveloping maximum input acceleration spectral density levels experienced in the field by similar test specimens subjected to similar field environments.

110

By using the relationship found in Eqs. (2) and (3) one can mathematically determine the relationship between the laboratory input acceleration spectral density, $\mathscr{A}_i(\omega)$, and the enveloped field acceleration spectral density, $\mathscr{G}(\omega)$:

$$\mathscr{A}_i(\omega) = \left\{ \frac{\left|\bar{W}_a(\omega)\right|}{\left|\bar{W}_a(\omega)\right|} \right\}^2 \mathscr{G}(\omega) \quad . \tag{4}$$

Note that whenever

$$\frac{\left|\bar{W}_a(\omega)\right|}{\left|W_a(\omega)\right|} \leq 1; \text{ then } \mathscr{A}_i(\omega) \leq \mathscr{G}(\omega) \tag{5}$$

and whenever

$$\frac{\left|\bar{W}_a(\omega)\right|}{\left|W_a(\omega)\right|} > 1; \text{ then } \mathscr{A}_i(\omega) > \mathscr{G}(\omega) \quad . \tag{6}$$

One can see from the relationships (5) and (6) that the laboratory acceleration spectral density, $\mathscr{A}_i(\omega)$, has a tendency to notch whenever the test specimen's apparent weight characteristics, $W_a(\omega)$, peak; and $\mathscr{A}_i(\omega)$ peaks whenever $W_a(\omega)$ has a tendency to notch. These peak notch characteristics agree with logic.

The relationship of the magnitudes of the acceleration peaks and notches with respect to the enveloped field spectrum is a function of how one band averages the test specimen's apparent weight characteristics. Since $\mathscr{G}(\omega)$ is the envelope of peak acceleration spectral densities experienced in the field, one would logically like to limit the maximum laboratory accelerations to levels "in the area" of the field spectral density, $\mathscr{G}(\omega)$. This can be done by using a band average of $W_a(\omega)$ which is heavily biased toward a minimum value within a given frequency band (ω_1 to ω_2). Therefore, an "averaging" method proposed by Murtin [5] will be used:

$$\bar{W}_a(\omega) = W_a \min$$

$$+ .1 \, (W_a \max - W_a \min) \left|_{\omega_1}^{\omega_2} \right. \quad . \tag{7}$$

Using this method still results in laboratory acceleration levels which may exceed $\mathscr{G}(\omega)$. One may require that maximum values of the laboratory input spectrum, $\mathscr{A}_i(\omega)$, be limited to a certain percentage of the enveloped field spectrum $\mathscr{G}(\omega)$. Limiting for the sinusoidal case can be done quite easily with the proper equipment; however, for the random situation limiting cannot be as easily accomplished. With present random testing equipment, one must resort to modifying the input spectrum to accomplish the required limiting. Calculations must be made in order to modify the input spectrum.

The frequency response function, $H(\omega)$, for a linear mechanical system is defined by the frequency dependent complex ratio

$$H(\omega) = \frac{A_r(\omega)}{A_i(\omega)} \tag{8}$$

where $A_i(\omega)$ and $A_r(\omega)$ are sinusoidal input and response functions respectively. The magnitude of the frequency response function can also be defined by the random relationship

$$\left|H(\omega)\right|^2 = \frac{\mathscr{A}_r(\omega)}{\mathscr{A}_i(\omega)} \tag{9}$$

where $\mathscr{A}_i(\omega)$ and $\mathscr{A}_r(\omega)$ are the random input and response spectral densities respectively.

A relationship between a response acceleration spectrum and the input force spectrum can be obtained by using Eqs. (2) and (9):

$$\mathscr{F}_i(\omega) = \frac{\left|W_a(\omega)\right|^2}{\left|H(\omega)\right|^2} \mathscr{A}_r(\omega) \quad . \tag{10}$$

If a limit value were set on $\mathscr{A}_r(\omega)$; then a new input force spectrum would have to be calculated

$$\mathscr{F}_i'(\omega) = \left\{ \frac{\left|W_a(\omega)\right|}{\left|H(\omega)\right|} \right\}^2 \mathscr{A}_r(\omega)^{\text{limit}} \quad . \tag{11}$$

We now have two laboratory input force spectra specified, i.e., Eq. (3)

$$\mathscr{F}_i'(\omega) = \left|W_a(\omega)\right|^2 \mathscr{G}(\omega)$$

and Eq. (11)

111

$$\hat{\mathscr{F}}_i'(\omega) = \left\{ \frac{|W_a(\omega)|}{|H(\omega)|} \right\}^2 \mathscr{F}_p(\omega)^{\text{limit}} \quad .$$

The actual laboratory input force spectrum must be the combination of both $\hat{\mathscr{F}}_i(\omega)$ and $\hat{\mathscr{F}}_i'(\omega)$. In order to impose the required limit on $\mathscr{F}_p(\omega)$, the test must be performed using $\hat{\mathscr{F}}_i'(\omega)$ whenever $\hat{\mathscr{F}}_i'(\omega) > \hat{\mathscr{F}}_i(\omega)$ and $\hat{\mathscr{F}}_i(\omega)$ whenever $\hat{\mathscr{F}}_i(\omega) > \hat{\mathscr{F}}_i'(\omega)$.

Note that when it is required to limit the input acceleration spectral density, Eq. (11) may be used. For this situation, one can make $\mathscr{A}_i(\omega) = \mathscr{A}_p(\omega)$ and $H(\omega) = 1$. Eq. (11) can therefore be simplified to:

$$\hat{\mathscr{F}}_i'(\omega) = |W_a(\omega)|^2 \mathscr{A}_i(\omega)^{\text{limit}} \quad . \tag{12}$$

Again a new force spectrum has been defined.

In order to impose the required motion limiting, one must then define the laboratory input force spectrum as the envelope of the minimum values of the composite spectrum formed by overlaying all calculated force spectra.

The reader should note that the following relationship also holds:

$$\left| \frac{W_a(\omega)}{H(\omega)} \right| = \left| \frac{F_i(\omega)/A_i(\omega)}{A_r(\omega)/A_i(\omega)} \right| = \left| \frac{F_i(\omega)}{A_r(\omega)} \right| \quad . \tag{13}$$

The term

$$\left| \frac{F_i(\omega)}{A_r(\omega)} \right|$$

is nothing but the magnitude of the transfer apparent weight characteristics of the test specimen, $W_a'(\omega)$. Eq. (11) may therefore be written as

$$\hat{\mathscr{F}}_i'(\omega) = \left| W_a'(\omega) \right|^2 \mathscr{A}_r(\omega)^{\text{limit}} \quad . \tag{14}$$

Note if it is required to limit input acceleration spectral density that Eq. (14) can be used.

For this situation $\mathscr{A}_i(\omega) = \mathscr{A}_r(\omega)$ and $|W_a(\omega)| = |W_a'(\omega)|$, and Eq. (14) is transformed to Eq. (12).

$$\hat{\mathscr{F}}_i''(\omega) = \left| W_a(\omega) \right|^2 \mathscr{A}_i(\omega)^{\text{limit}} \quad .$$

STEPS FOR SPECIFYING INPUT SPECTRUM

In many test situations there are only two pieces of information available to the test engineer or specifications engineer for defining input control levels: (1) field data from similar test specimens subjected to similar environments, and (2) the dynamic characteristics of the test specimen. These pieces of information are used to generate the laboratory input force spectrum.

The steps necessary to implement the methods previously described for an actual test are briefly described below:

1. Obtain from a central "data bank" all possible random input field spectra (and their associated probability densities) experienced by dynamically similar test specimens and form a "composite" acceleration spectral density plot.

2. Envelope the maximum values of the composite spectrum to obtain the spectrum $\mathscr{G}(\omega)$.

3. Perform sinusoidal surveys at several input levels[*] to obtain the following characteristics of the test specimen:

   a. Driving point apparent weight, $W_a(\omega)$

   b. Frequency response functions for limit locations, $H(\omega)$, or

   c. Transfer apparent weight characteristics for limit locations, $W_a'(\omega)$.

4. Obtain "band averaged" apparent weight characteristics using Eq. (7),

   $$W_a(\omega) = W_a \text{ min}$$

   $$+ .1 (W_a \text{ max} - W_a \text{ min}) \quad .$$

[*] Tests are performed at several levels to determine the linearity of the test specimen.

5. Using the enveloped spectral density $\mathcal{S}(\omega)$ and the "band averaged" apparent weight $\overline{W}_a(\omega)$, calculate the input force spectrum using Eq. (3).

$$\mathcal{F}_i(\omega) = \left| W_a(\omega) \right|^2 \mathcal{S}(\omega) \quad .$$

6. Determine necessary acceleration limit locations and limit levels.

7. Calculate modified force spectra using Eq. (11)

$$\mathcal{F}_i'(\omega) = \left\{ \left| \frac{W_a(\omega)}{H(\omega)} \right| \right\}^2 \mathcal{A}_r(\omega)^{limit} \quad ,$$

or Eq. (14)

$$\mathcal{F}_i'(\omega) = \left| W_a'(\omega) \right|^2 \mathcal{A}_r(\omega)^{limit},$$

for limiting response accelerations. Use Eq. (12)

$$\mathcal{F}_i''(\omega) = \left| W_a(\omega) \right|^2 \mathcal{A}_i(\omega)^{limit}$$

for limiting input accelerations.

8. **Overlay all calculated force spectra and envelop the minimum force requirements to obtain the laboratory input force spectrum.**

The reader should note that several of the previously outlined steps require the use of the test engineer's judgment. These are the steps which require enveloping or averaging of data. Several trials may be required before an input spectrum which can meet random test equipment capabilities is obtained. Even after the final input spectrum is obtained, it may have to be modified slightly during random equalization. Test specimen linearity characteristics may also affect the input and response spectra such that the input force spectrum would have to modified.

EXAMPLE CASE

A specific example will be used to illustrate the techniques previously described.

The intent of the test was to subject the test specimen to a conservative laboratory vibration environment which would logically "simulate" the vibration environments experienced in the field.

FIELD DATA

Normally field data would be obtained from a central "data bank" for similar vibration environments on a dynamically similar test specimen. However, for this particular situation, field data was available for several environmental events to which the test specimen had been previously subjected. The analog accelerometer signals from a flight test, with eight separate events, were displayed in the time domain. It was determined from this data that the analog signals were relatively noise free and that the data was stationary. These analog signals for each of the eight events were analyzed by a band pass system called VIBRAN [4]. VIBRAN gives the distribution of the peaks over a frequency interval and computes the RMS value for this frequency band. The three most active of the eight events, as seen from the VIBRAN analysis, were selected for processing in the PSD and probability density format. The probability density plots were compared to a Gaussian probability density with the same mean and variance as the field data. This comparison indicated that a Gaussian test with the same mean and variance as the flight data would be conservative. The data also indicated that a pure 190 Hz sinusoid was present. The PSD plot for the separate events were overlaid to form a composite spectrum and an envelope of the composite spectrum was made. Figure 2 shows the composite PSD and the envelope. The 190 Hz sinusoid is shown as a line spectrum.

TEST SPECIMEN AND LABORATORY SETUP

Consider the test specimen shown in Figure 1 which contained many components that caused the system to be dynamically complex. Input laboratory force and acceleration were measured at the test specimen/field foundation interface using force gages and accelerometers. Response accelerations of specific components within the test specimen were also measured.

APPARENT WEIGHT AND INPUT FORCE SPECTRUM

The specimen apparent weight characteristics, shown in Figure 3, and frequency
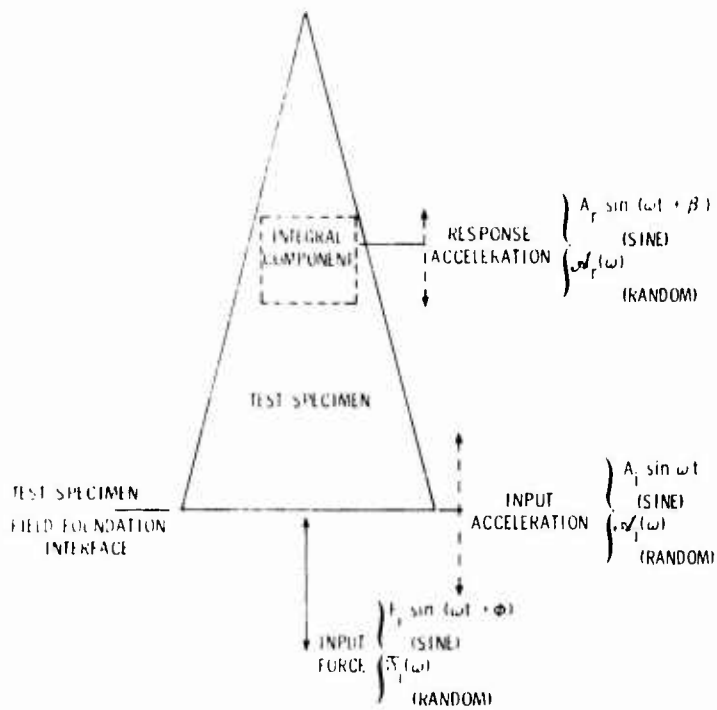
113

Figure 1. Test specimen
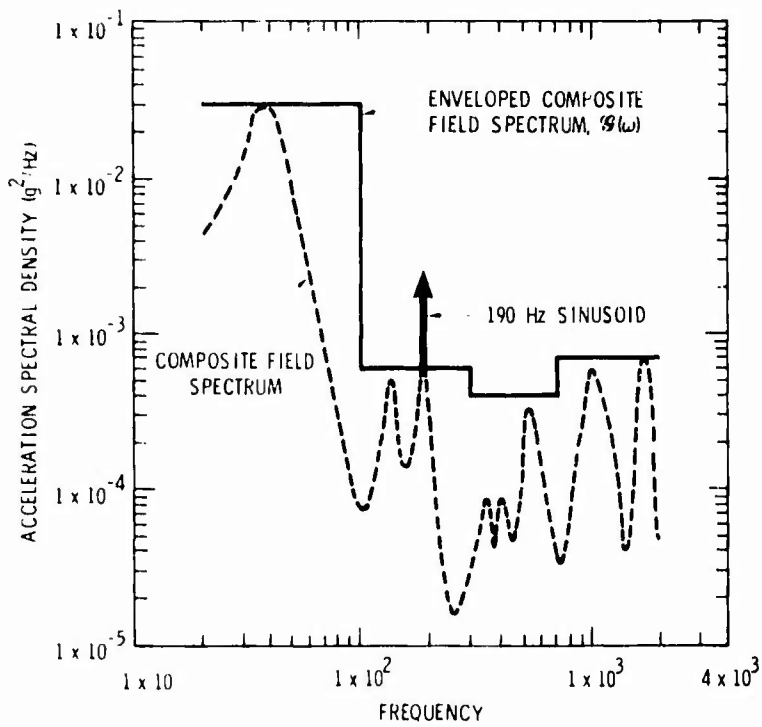
Figure 2. Field acceleration spectral

114
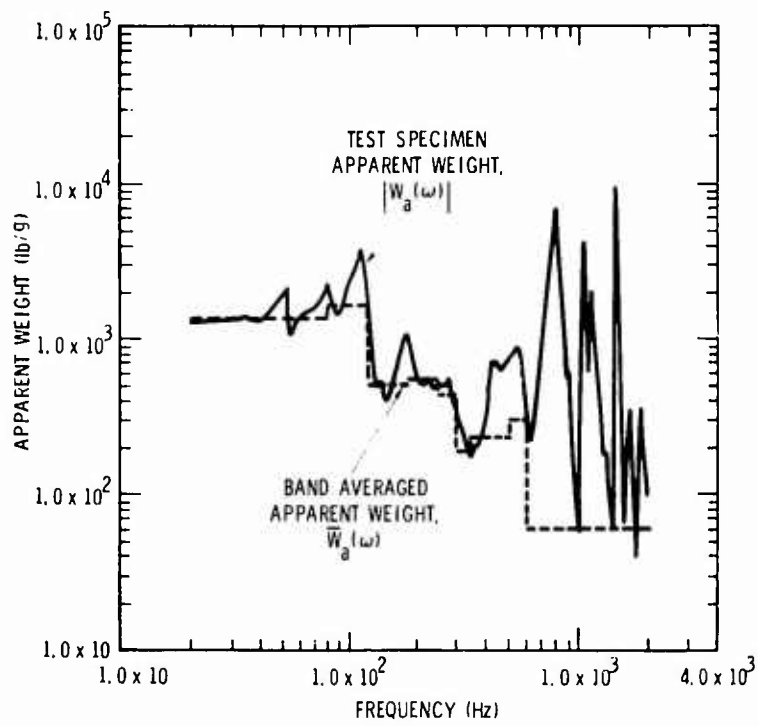
Figure 3. Test specimen apparent weight characteristics
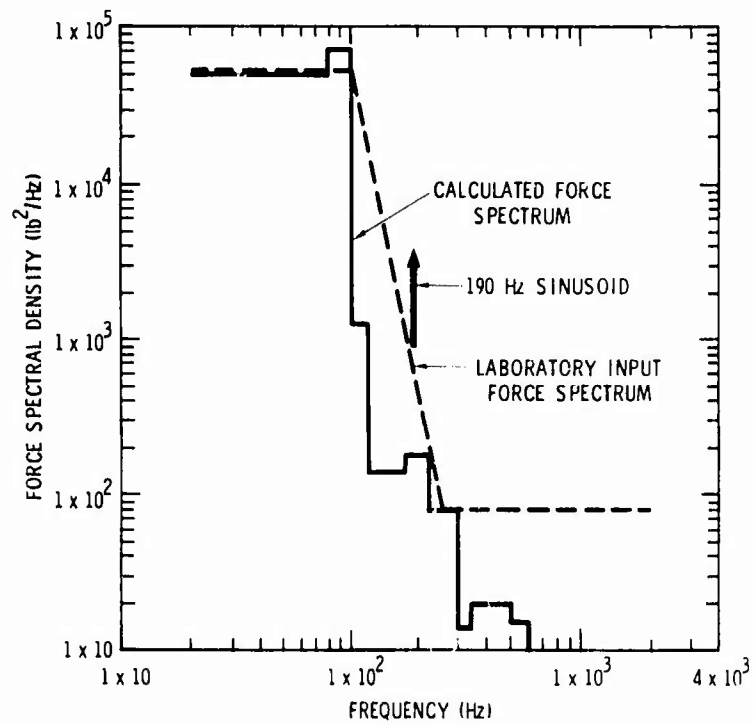
Figure 4. Calculated laboratory force spectral density

115
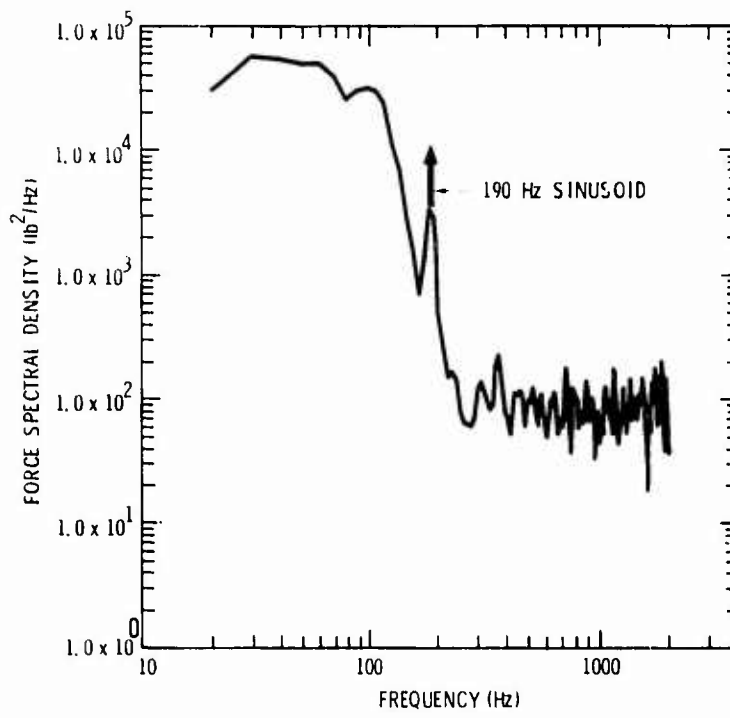
Figure 5. Laboratory input force spectral density
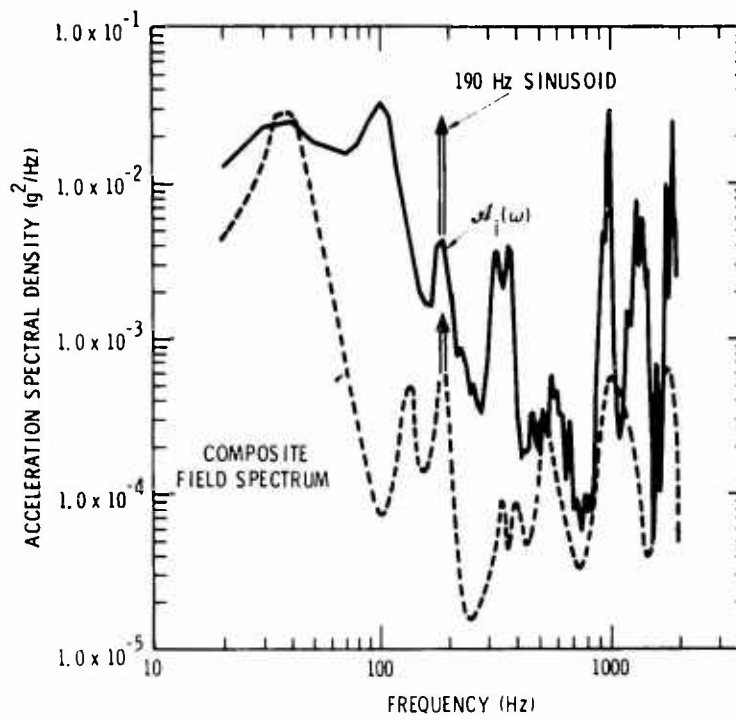
Figure 6. Laboratory input acceleration spectral density

116

response functions were measured in the laboratory. This data was obtained from two sinusoidal surveys having relatively low but different input acceleration levels. Tests were performed at two levels to determine the linearity of the specimen's dynamic characteristics. Note that by examining the composite field PSD and the specimen's apparent weight characteristics, one can observe that the field spectrum has a tendency to notch at frequencies where the apparent weight characteristics peak and a tendency to peak at frequencies where the apparent weight characteristics notch. These peak-notch relationships agree with the basic philosophy used to develop the technique.

The band average of the apparent weight characteristics is also shown in Figure 3. One can see that, if the force is uniform over a given frequency band, almost all the vibration will take place at that frequency within the band where the apparent weight is a minimum, thus the band averaging is strongly biased towards the minimum within the frequency band as is shown by Eq. (7). The bands for averaging the apparent weight were in octaves or half octaves from 20 to 2000 Hz. The random force input spectrum was then calculated by using Eq. (3). The calculated force spectrum is shown in Figure 4. The dynamic range of this calculated spectrum was approximately 40 dB. However the spectrum was modified to allow sufficient dynamic working range for the random equalizer servocontrols at the high and low spectrum levels. The spectrum, shown in Figure 4, was also modified for a rolloff rate (20 dB/octave) which was compatible with the equalizer characteristics. These modifications resulted in a laboratory input force spectrum which was in general higher than that required to test the specimen to field levels.

ACCELERATION LIMITING

An integral component with a known failure level was selected for acceleration limiting. The frequency response function for this component had been measured during the two low level sine surveys. The random response of this component was calculated using Eq. (10) with the calculated force spectrum, this response was then compared with the known failure level of the component. In this particular instance the failure level was not approached and limiting was not required. The resulting laboratory input force spectrum is shown in Figure 4. One should note that lowering the spectrum level at the higher

frequencies due to limiting requirements would have created control problems.

SUPERIMPOSING THE SINUSOID

A pure sinusoid was superimposed on the random signal at 199 Hz to simulate the field spectrum. The level of the sinusoid was acceleration controlled. The method of superimposing this signal on the random laboratory spectrum is not within the scope of this paper and will not be discussed.

RESULTS OF THE LABORATORY TEST

The laboratory input force spectrum and resulting input acceleration spectrum are shown in Figures 5 and 6. One can see that above 120 Hz, the frequencies at which peaks and notches occur in the laboratory acceleration spectrum agree quite well with those seen in the composite field spectrum. However, because much of the laboratory force spectrum was necessarily raised, the input acceleration levels were in general higher than those experienced in the field situation. Below 120 Hz better agreement between laboratory and field accelerations may have been obtained by using a different envelope of the composite spectrum. A similar comparison was also obtained for response data from integral components.

CONCLUSIONS AND COMMENTS

For this particular situation field data supported the philosophy that field accelerations peak at frequencies where the apparent weight characteristics of the test specimen notch and that accelerations tend to notch at frequencies where apparent weight characteristics peak. The technique provides a means of obtaining these peak-notch relationships in the laboratory. In doing this, the technique provides a more logical "simulation" of field random vibrations than either force or acceleration control techniques when little is actually known about the field environment. The method requires considerable calculation for its use, and results are highly dependent on enveloping and averaging methods used. One can also see from the example case that the dynamic range of the input force spectrum may be much greater than the enveloped field acceleration spectrum. This is true because the input force spectrum is related to the field acceleration spectrum by the square of the band averaged apparent weight characteristics. This relationship tends to amplify the dynamic range of the input control spectrum. This is

a disadvantage since the extended range may be beyond the capabilities of the random equalizer.

LIST OF REFERENCES

1. Otts, John V., "Force controlled Vibration Tests: A Step Toward Practical Application of Mechanical Impedance," The Shock and Vibration Bulletin, February 1965, Bulletin 34, Part 5.

2. Otts, J. V., and Nuckolls, C. E., "A Progress Report on Force Controlled Vibration Testing," The Shock and Vibration Bulletin, January 1966, Bulletin 35, Part 2.

3. Murfin, W. B., "Dual Specifications in Vibration Testing," The Shock and Vibration Bulletin, August 1968, Bulletin 38, Part 1.

4. Sandia Corporation Vibration Analysis Committee, Vibration Analysis for Weapon Development Test Programs, Sandia Corporation, SCDR-321-61, 1962.

118

VIBRATION

A DIAGNOSTIC TOOL FOR SHOCK DESIGN

Culver J. Floyd

Raytheon Company
Submarine Signal Division
Portsmouth, Rhode Island

Vibration testing can result in successful shock testing the first time. Analysis of failures and results during parts qualifications, engineering exploratory testing, formal vibration and reliability testing, and comparison with shock test results indicates that higher level, higher frequency vibration tests will indicate failures probable in shock tests.

INTRODUCTION

Exploratory vibration testing can provide the engineering information required for an adequate shock design. Successful shock tests can result the first time. This in turn can produce lower testing costs, shorter test times and the product will not be marginal.

Over the past several years Raytheon's Submarine Signal Division has done a great deal of testing to MIL-STD-167 and MIL-S-901. During these tests, acceleration data has been gathered at anvil, deck, cabinet, chassis and part levels.

Related to these tests other exploratory and qualification tests were done. These tests include:

1) Non-standard parts qualification tests per MIL-STD-202, MIL-STD-242, MIL-STD-750 and MIL-STD-883

2) Engineering exploratory shock and vibration at the chassis level (up to 50 pounds)

3) Cabinet level vibration, soft and hard mounts

4) Cabinet level shock, soft and hard mounts

5) Cabinet level reliability tests per MIL-R-22732, soft and hard mounted.

Examination of stress levels, frequency spectra, material characteristics and failure indicates that successful completion of a shock test can be accomplished if exploratory vibration tests are run at chassis and cabinet levels without the electronics being energized. These

vibration tests in the cabinet vertical plane should be at the level of 10 g and should cover the frequency range from 5 to 100 Hz.

Vibration levels in the front-to-back and side-to-side direction should be 4 g. Machine operating time to scan the spectra in each of the three orthogonal axes need be no more than two minutes. This technique will identify mechanical problems before the formal vibration and shock tests begin. Savings will accrue from eliminating multiple set ups, electrical checks in the environmental lab and down time for technicians during repair.

PARTS QUALIFICATION PROGRAM

First let us consider the parts qualification program. These are parts such as transformers, transistors, filters, chokes, test jacks, switches, plugs, etc.

These parts are used in most of the military equipment which is procured to one

of the following equipment specifications:

MIL-E-16400	Electronic Equipment, Naval Ship and Shore, General Specification For
MIL-E-21200	Test Equipment for Use with Electronic and Fire Control Systems, General Specification For
MIL-E-5400	Electronic Equipment, Airborne, General Specification For
MIL-E-8189	Electronic Equipment, Guided Missiles, General Specification For

Each of these leads back to one or more of parts qualification specifications. Typical of these are:

ANA 400	Electronic Equipment: Aircraft and Guided Missiles Applicable Documents
MIL-STD-242	Military Standard Electronic Equipment Parts, Selected Standards

These in turn either specify their own shock and vibration environment or lead to these test specifications:

MIL-STD-167	Military Standard: Mechanical Vibration of Shipboard Equipment
MIL-STD-202	Military Standard: Test Methods for Electronic and Electrical Component Parts
MIL-STD-331	Fuse and Fuse Components, Environmental and Performance Tests For
MIL-STD-810	Military Standard: Environmental Test Methods
MIL-STD-883	Test Methods and Procedures for Microelectronics
MIL-S-901	Military Specification, Shock Tests H. 1. (High Impact) Shipboard Machinery Equipment and Systems, Requirements For

The requirements of these various test specifications are listed in Tables 1 and 2.

A plot of several of these vibration specifications is shown in Figure 1.

Table I
Comparison of Test Specifications

Spec. No.	Methods	
	Vibration	Shock
MIL-STD-167B	5-15 Hz .060 DA 16-25 Hz .040 DA 26-33 Hz .020 DA 24-40 Hz .010 DA 41-50 Hz .006 DA	
MIL-STD-202D	201A - 10-55 Hz .060" DA 3 dir.	207A (Lt. Wt. Hi. Impact S T MIL-S-901) 213 NOTE 1
MIL-STD-331	104. Proc. II. Para. 4.2.1 3 axes 10-60 Hz 0.1" DA or 2 G	101 102 114 Para. 5.1
MIL-STD-750	2046 60 - 20 Hz - 20G 3 axes 3 axes	2016 1500G 0.5 ms. 2021 3000G 0.2 ms.
MIL-STD-781	40 - 20 Hz 2.2G	
MIL-STD-810B	514 Proc. IX & XI. Part 1 10-55 Hz .030" Exc. 514 Proc. IX, Part 2. 514 Proc. XI. Part 2.	516 Proc. I, III, IV 2 Proc. II is a drop test

MIL-STD-883	2005 60 - 20 Hz A - 20G,
	B - 50G, C - 70G
		2002 A. 500G E. 10,000G
		        B. 1500G F. 20,000G
		        C. 3000G G. 30,000G
		        D. 5000G 0.1 to 1.0 ms.

* See summary of Method 213 - MIL-STD-202 and Method 516 - MIL-STD-810 on Table 2.

120

Table 2
Comparison of MIL-STD-810

Condition	Package	Duration, MS	Wavelength
A	50	11	1 2 sine
B	75	·	1 2 sine
C	100	·	1 2 sine
D	200	·	1 2 sine
E	100	3 ·	1 2 sine
F	·	·	1 2 sine
G	·	3	saw 11
H	·	·	saw 11
I	·	·	1 ·
J	·	11	1 ·
K	·	11	saw 11

Shock of MIL-STD-8

Procedure		Procedure X			M
	Type				
I	Bare Drop	·	·	I·	·
III	Crash Safety	·	·	II	·
IV	Bounce Loose	I·	I·	·	·

NOTE: Shock Parameters · · · Recommended Peak Parameters · M · Average · · Mil Pounds · M

Procedure		Peak Value, Feet		Net Pounds · M	
	Type				
I	Bare Drop	·	·	II	·
III	Crash Safety	·	·	·	·
IV	Bounce Loose	I·	I·	·	11

NOTE: · · Parameters a apt · Recommended Peak Parameters · M · · Average Pounds · M ·
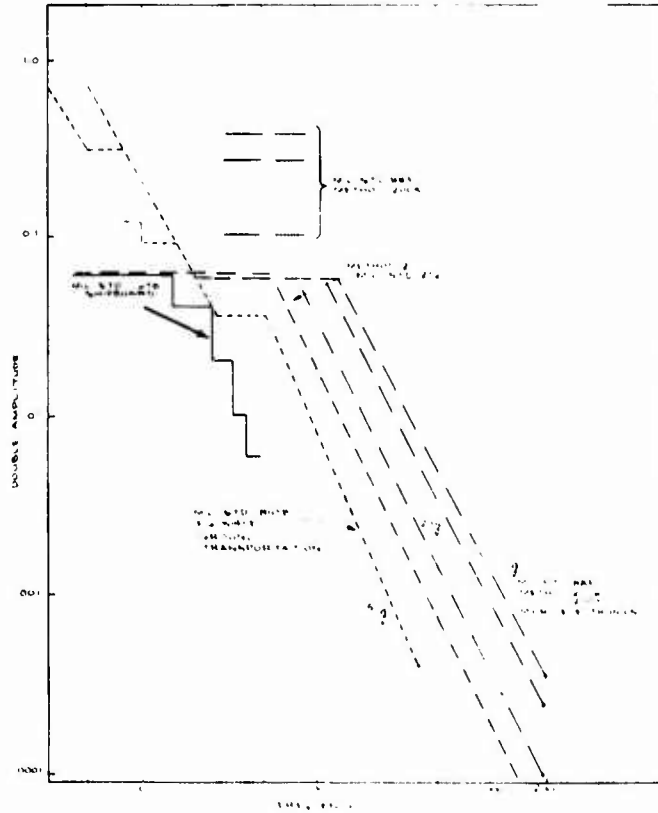

Fig. 1. Parts Qualification - Typical Vibration Test Requirements

121

All are not shown since many have slight variations in amplitude and frequency. However, all of the vibration specifications used for qualifying parts have amplitude equal to or

larger than MIL-STD-167. Similarly, the test frequencies are much higher, extending often to 2000 Hz.

The reason for selection of these test frequencies for shipboard parts is not a part of this paper. These tests have been specified by various Government agencies. The parts are meeting these specifications during qualification tests. The parts often are originally qualified for use in ground vehicles, aircraft and missiles which may have more severe high frequency vibration environment than shipboard.

The significant point here is that transistors, coils, transformers, capacitors, switches, etc., withstand a much more severe environment than MIL-STD-167 during parts qualification.

Similarly in the shock tests, the pulses applied directly to the part during qualification have a much higher g level and much shorter duration than in cabinet level tests (See Figure 2).
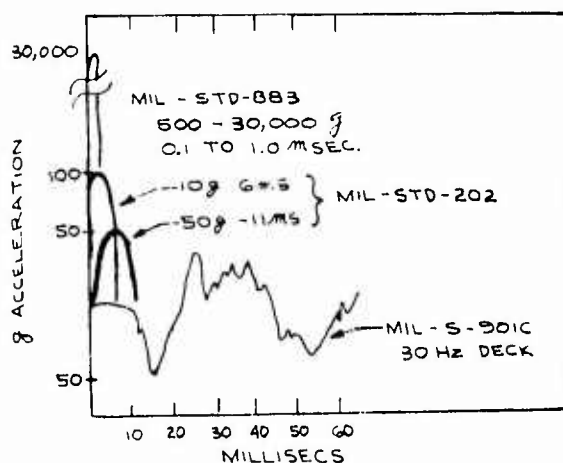
Fig. 2. Typical Shock Test Pulses

Transmissibilities within the part is thus greater than 1 at much higher frequencies (>100 Hz) than the transmissibility within the part during MIL-S-901 tests. To state if another way the shock environment during parts qualification is more severe than during cabinet level MIL-S-901 testing.

CHASSIS LEVEL EXPLORATORY TESTS

Recently on the AN/BQS-13 Program

exploratory shock and vibration tests were run on 185 typical chassis or other subassemblies. The procedure for these tests was simple.

The chassis was assembled and wired but not electrically tested. Just prior to the electrical test it was taken from the production line for one day. At the environmental lab it was vibrated at .020DA along each of three orthogonal axes sufficiently long to identify resonances. If resonances appeared below 40 Hz, they were reparied. Resonances between 40 Hz and 100 Hz were noted for future reference.

The chassis was then shock tested along three orthogonal axes. A Barry drop tester was used to produce 50 g at the specimen. High speed motion pictures were taken for future reference.

Chassis parts and cabling which passed these tests gave no trouble in MIL-S-901 shock tests.

CABINET LEVEL VIBRATION TESTS

Monitoring of electronic performance during vibration tests usually consume more time and money than the vibration tests. Cabinet level vibration testing to MIL-STD-167 requires only about fifteen hours of machine running time. However, the elapsed time even for a perfect test may be a week or more. Most of this time is concerned with the electronic test gear required to exercise the cabinet electronics and to monitor the cabinet electronics performance. Even after everything is working, several hours may be required to electrically check out the more complex cabinets, sometimes involving three or four test electrical engineers.

Should a failure occur in the cabinet during vibration test, it usually is returned to the factory for repairs. These repairs may take several days or several weeks. During this repair time, the electronic exercise and monitoring equipment is often cannibalized for other work. When the repaired cabinet returns to the environmental test facility, much time is lost trying to get the exercise gear operating again. Eliminating this duplication in setting up the exercise gear and in electrical checks will more than pay for the exploratory test described.

If the chassis have been through exploratory vibration, the structural failure sometimes occurs at the chassis slide - cabinet interface which was not necessarily duplicated during chassis exploratory tests.

Wiring failures are common. Nearly all wiring failures are attributable to insufficient clamping. Troubleshooting for broken wires proved to be very time consuming.

Parts which have been qualified previously almost never fail. Occasional failures in non-standard parts occur if the vendor is still trying to qualify his part.

CABINET LEVEL SHOCK TESTS

Cabinet level shock tests were conducted on various cabinets of the AN/BQS-13. These results are reported in Reference (1).

These were done on the medium weight MIL-S-901 machine. The machine operating time is a matter of a few minutes. Perhaps 10 minutes is required to raise the hammer, drop, and reset the hammer. The elapsed time, however, could run a week due to cabinet exercise equipment and test equipment set up and check out, as well as troubleshooting broken wires.

Cabinet failures in shock were again primarily either structural or wiring plus a few non-standard non-qualified parts.

From the behavior of cabinets under vibration up to 33 Hz, we could predict probable failure areas. If the cabinet level test has included exploratory vibration at 10 g to 100 Hz, the failure would have occurred and been repaired even before starting formal vibration tests.

If shock tests were successful the first time, duplication of the exercise equipment set up and test could be avoided. Money and time loss would not occur.

CABINET LEVEL RELIABILITY TESTS

A reliability provision appears in many contracts. MIL-R-22732 defines these tests. Vibration in the vertical direction of 1 or 2 g at some discrete frequency (typically 28 Hz) is performed for 10 minutes of each hour during a several thousand hour life test. Vibration time thus can accumulate to more than 100 hours. Typically the several systems of the AN/BQS-13 were vibrated at 1 g at 28 Hz for an accumulated time of 430 hours without failure. Each system consists typically of twenty large equipment cabinets and ten small boxes. The large equipment cabinets are shown in Figure 3.
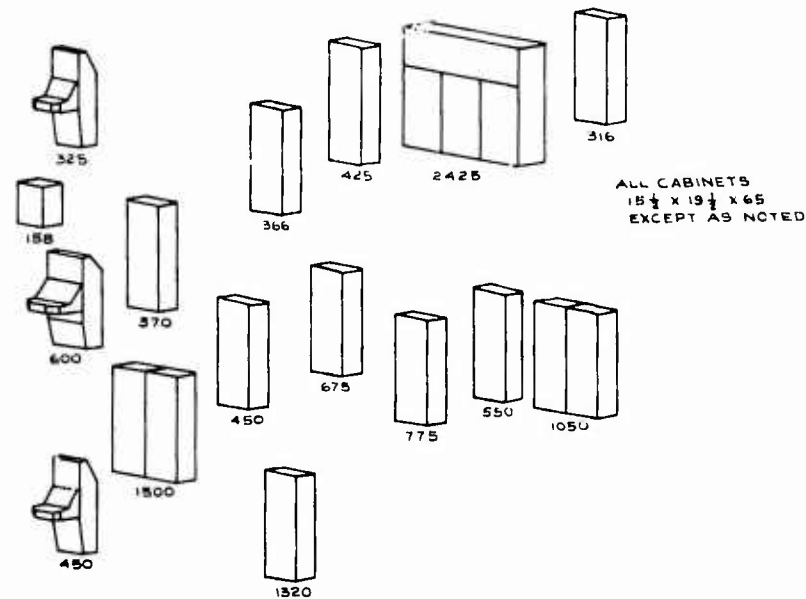
Fig. 3. Types and Weights of Cabinets (1968 Tests)

123

The number of cycles of vibration for these reliability tests is much longer than any endurance test specified for any parts qualification or cabinet environmental test.

Figure 4 shows a typical S-N curve for many materials. This curve is a plot of the number of cycles to fracture versus the stress level per cycle. The curve varies for different materials but always has the steep slope dropping rapidly away from 100% as the number of cycles increases and becomes asymtotic in the millions of cycles ranges.
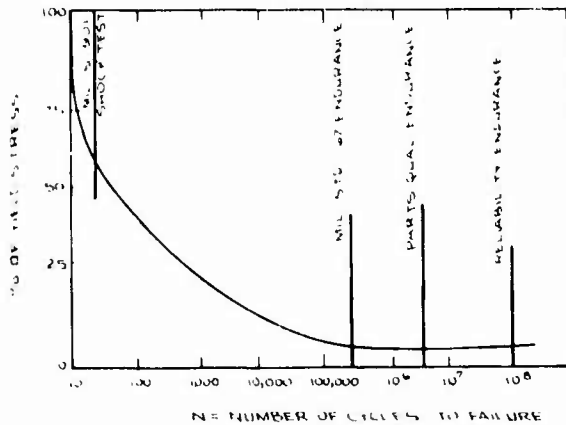
Fig. 4. Typical S, N Curve

Hence to meet the reliability endurance requirements one must design for low stress during 1 or 2 g vibration at perhaps 28 Hz. This is completely compatible with allowing high stress for a few cycles during shock tests.

SHOCK AND VIBRATION EQUIVALENCE

Several people have reported on the equivalence between shock and vibration. Gennaci and Foster have computed what vibration would cause displacement equivalent to certain shock inputs. (Reference (2)). The results of this technique have been combined with a shock spectrum of a typical pulse which we measured during AN/BQS-13 shock tests (Figure 5).

Figure 6 shows the vibration amplitude necessary to produce the equivalent response of the shock spectra if the structure is vibrating at its natural frequency. Note MIL-STD-167 and the Reference 1 g curve. Also note the 10 g curve lying nearly along the equivalence line.

SUMMARY

In summary, are these results and conclusions:

1) Parts which qualified with high amplitude high frequency vibration tests gave no trouble during MIL-STD-167 or MIL-S-901 cabinet level tests.

2) Chassis which had resonances above 47 Hz gave no trouble during the 167 or 901 tests.

3) Cabinet level structure and cable did have a few failures in vibration.

4) Cabinet level structure and cable behavior during vibration did give warning of failure in shock when tested only as high as 1 g and 33 Hz.

5) Equipment passing 167 and 901 gave perfect performance during reliability tests with no failures at all.

6) Consideration of the equivalence of shock and vibration bear out the above.

These conclusions then lead to this proposal. As a part of engineering development at the chassis level or cabinet level or just prior to formal 167 and 901 testing, perform the following exploratory tests:

1) Vibrate at 10 g from 5 to 100 Hz in the cabinet vertical direction.

2) Vibrate at 4 g from 5 to 100 Hz in the cabinet side-to-side and front-to-back direction.

3) Sweep and range once upwards and once downwards taking one minute in each direction.

4) Perform this exploratory test without the electronics being energized.

5) Visually observe during and after test to assess needed changes, if any.

Savings in dollars and time will result, if this procedure is followed. Repetitive electrical set ups and check outs will be eliminated, down time for electrical test personnel will be eliminated, and successful vibration and shock tests will result. This technique was demonstrated during the AN/BQS-13 tests when all parts not exploratory tested experience failure, while those parts that did undergo exploratory testing proved successful.

124

[1] C. J. Floyd, "Normal Mode Structural Analysis – Calculations and Results", Bulletin No. 39, Part III, Naval Research Laboratory Washington, D. C., Jan. 1969.

[2] I. Gennaci, J. Earl Foster, "The Equivalence Between Shock and Vibration Excitation", University of Wyoming, Laramie, Wyoming, Electronic Packaging and Production, Oct. 1963

Fig. 5. Design Shock Spectrum

Fig. 6. Shock Equivalence

125

Mr. Henderson (Hughes Aircraft Company): Your shock tests were all conducted with the 30 Hz so-called soft deck. That would change the intensities, would it not?

Mr. Floyd: Well, not really, because we also used the so-called hard deck.

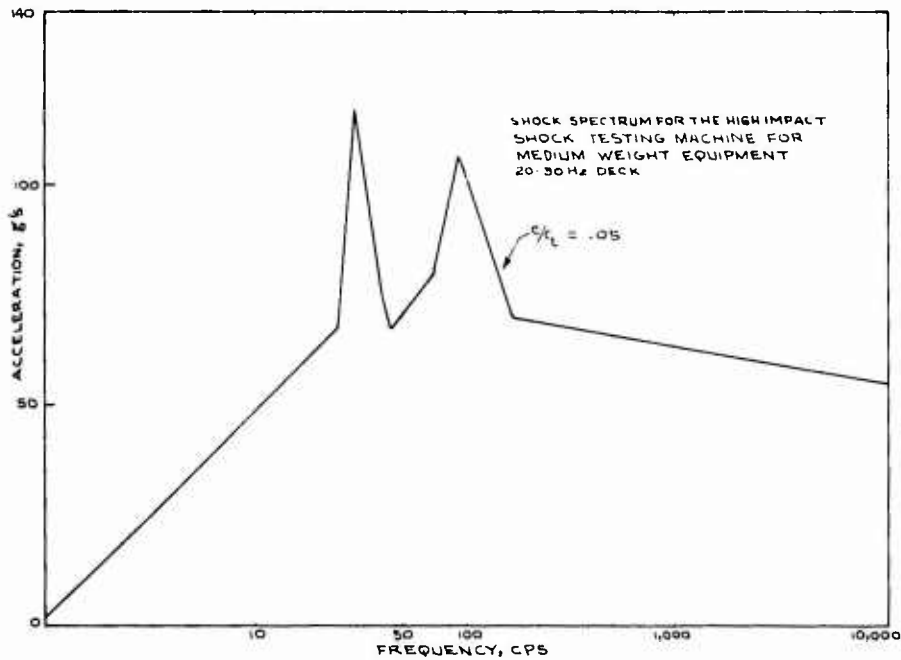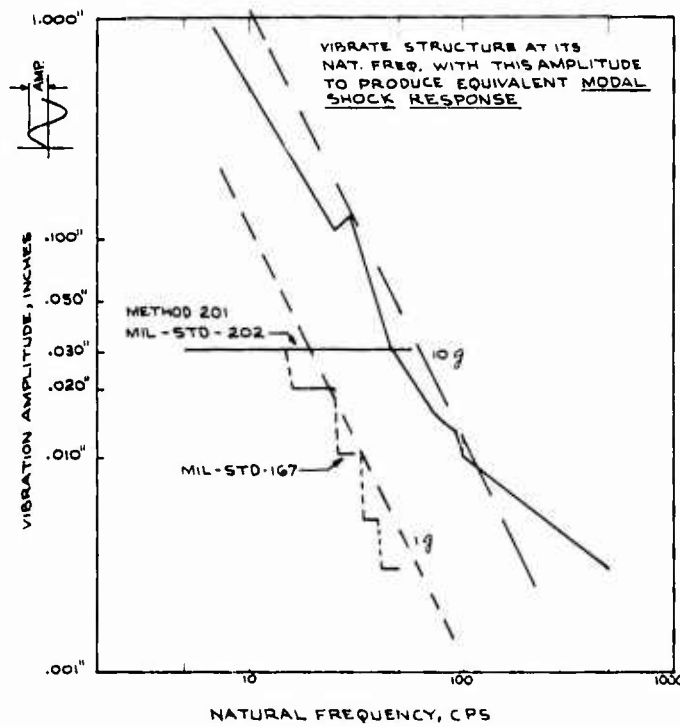Mr. Henderson: If a piece of equipment was hard mounted to the 901C hammer, would you not get much more intense shocks on loads out of this?

Mr. Floyd: We had one group of cabinets that was done on the so-called hard deck. Here we followed the 901 guide-line as far as the angles and channels are concerned. We did get a spreading out of the pulse even in that, after it got into the cabinet. Now it is true that the pulse at the anvil was very short and very high. It was reduced a little bit in height and increased in width as it got under the deck. It was perhaps 70 or 80 Hz, in that order. After it got into the cabinet it dropped quite markedly into perhaps a 40 Hz range. The point I am making is that, if we vibrate at these higher levels, the equipment inside of the cabinet will respond in much the same manner as it might in the shock test. We do not know whether it will or not.

Mr. Forkois (NRL): We found that, if your natural frequencies are above the frequency of the vibration test, you do not have too much trouble in the shock test. A 10-g input for a free-standing cabinet is a very severe test. The old aircraft specification specified 60 mils up to 55 Hz, which was 10 g's. I have tested some antennas at this level and the inputs were too severe and never agreed actually with the aircraft itself. I think you are going to run into a lot of trouble trying to put 10 g's into a lot of this equipment. They had specified the 10 g input in three mutually perpendicular directions. I think you are going to find that you are going to have more problems in vibration than you do in shock. In vibration we do our testing in three mutual perpendicular directions. When you go to the shock machine we have an inclined bulkhead which produces shock components simultaneously in three directions. I think the effect is a little different. You may have some trouble correlating it.

Mr. Floyd: I suspect you are right in everything you say. I perhaps forgot to mention that we did have trouble with some cabinets on the Mil-S-901C shock test. Those cabinets really warned us that they were going to give us trouble during the Mil-Std-167 test which went as high as 33 cycles. Mil-Std-167 now of course goes to 50 cycles, and I am looking forward to seeing whether or not we are going to have more trouble.

Mr. Paladino (Naval Ship Systems Command): We are responsible for 167. We raised 167 to go to 50 Hz for one reason. We now have hydrofoils which have a higher blade passing frequency. We do not intend that all equipment be tested to 50 Hz. It is only tested to the frequency range for a particular vehicle, if it is a destroyer, carrier, submarine, or whatever it is, we do not want to imply that everyone must meet 167 to 50 Hz. It is clearly spelled out in the standard but I think people have misinterpreted this. 167 is a standard that does ferret out a bad resonant condition. It is about a 1.2 g maximum input. If you have a bad resonance due to amplification you can come up with maybe 7 g's. This is a bad piece of equipment and it will not survive the two-hour test. As Mr. Forkois said, if you are free of resonances up through the test range of 167 your changes of surviving 901C are very good. So if there are resonances and you apply 10 g's in a vibration test you are going to tear it apart in a matter of minutes.

Mr. Floyd: Thank you. I was not aware that Mil-Std-167 could be reduced for submarines. I have learned something this afternoon.

Mr. Paladino: I am not saying that you reduce it for submarines. Submarines are the ones that usually test up to 33 Hz. There are some surface ships, like carriers, you cannot test up to 33 Hz. You have to take the number of blades that you have on your propeller times the top rpm. That is the bracket that you test at in 167. Right underneath the table it tells you how to use it and many people have been misinterpreting this and going up to 50 Hz. We do not want them to do that.

126

THE RESONANT RESPONSE OF A MECHANICAL SYSTEM SUBJECTED TO LOGARITHMICALLY SWEPT

AND NOTCHED BASE EXCITATION, USING ASYMPTOTIC EXPANSION

B. N. Agrawal
COMSAT Laboratories
Clarksburg, Maryland

The objective of this paper is to present the method of determining spacecraft structure response, subjected to logarithmically swept and notched base excitation, in sinusoidal-vibration testing. The asymptotic method is used to obtain the response of a viscously damped single-degree-of-freedom mechanical system subjected to logarithmically swept and notched base excitation. The unnotched responses and perfect notches are obtained for various notching factors, damping coefficients, sweep rates, and natural frequencies.

INTRODUCTION

It is common practice to subject spacecraft in environmental qualification testing to a sinusoidal-vibration excitation, swept at a constant octave sweep rate through some frequency range. To simulate flight dynamic loads more accurately (i.e., to avoid overtest), test specifications have been modified in some cases to permit notching of the vibration input at the fundamental spacecraft resonant frequency. The environmental engineer faces not only the problem of developing a satisfactory notch, but also of interpreting the response data. Although the concept of the notched vibration test has been approved and carried out for a number of years, the literature regarding the analytical response to such an excitation is quite limited. Lewis [1] has presented a solution for the response of a single-degree-of-freedom system subjected to linear swept vibration excitation. However, most current vibration testing specifies a constant octave sweep rate. Morse [2] has given a mathematical solution for the acceleration response to the logarithmically swept sinusoidal-vibration excitation for a viscously damped single-degree-of-freedom mechanical system. However, his mathematical solution is in a form not readily applicable for engineering use; he has used analog simulation to obtain the response.

In this paper the asymptotic method developed by Kryloff, Bogoliubov [3], and Mitropolskii [4] is discussed briefly with modifications [5]. The asymptotic method is used to obtain the response of the viscously damped single-degree-of-freedom mechanical system subjected to logarithmically swept and notched base excitation. The solution can also be applied to obtain the response of the nonlinear mechanical system with time-dependent natural frequency [6].

The responses are calculated by varying sweep rates, damping coefficients, and natural frequencies. In this paper the concept of the perfect notch is discussed. A notch is assumed to be perfect when the allowable response is maintained across the entire notch. In actual practice, the allowable response may correspond to spacecraft acceleration response or strain at some critical structural element due to a worst-case flight loading. For the perfect notches calculated in this paper, the deviation of the response from the allowable response is arbitrally kept within a ±1-percent limit across the entire notch. This limit can be modified according to the test equipment used. The perfect notches are obtained for various notching factors, damping coefficients, sweep rates, and natural frequencies.

127

The following terminology is used in this paper:

(a) peak-amplitude ratio = the ratio of the peak-response amplitude to the maximum steady-state amplitude;

(b) peak-frequency ratio = the frequency ratio at which the response amplitude is maximum;

(c) notching factor = the ratio of the allowable response to the maximum steady-state response without notching;

(d) bandwidth of the notch = $f_2 - f_1$ (Fig. 1);

(e) central frequency of the notch = $1/2(f_1 + f_2)$ (Fig. 1);

(f) initial frequency of the notch = f_1 (Fig. 1); and

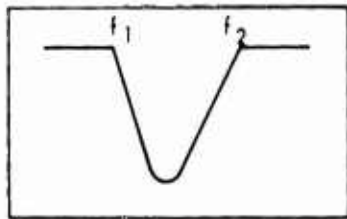(g) final frequency of the notch = f_2 (Fig. 1).

Fig. 1 - Notch

ASYMPTOTIC METHOD

The generalized D.Eq. of motion of a single-degree-of-freedom mechanical system may be written as follows:

$$\ddot{X} + \omega^2(\tau)X = \varepsilon f(\tau, \theta, X, \dot{X}) \qquad (1)$$

By setting $\varepsilon = 0$ in Eq. (1), the following solution is obtained:

$$X = a \cos \psi$$
$$\dot{a} = 0$$
$$\dot{\psi} = \omega \qquad (2)$$

For the condition when $\varepsilon \neq 0$, the solution in Eq. (2) will be modified so that when $\varepsilon \to 0$, the solution should be represented by Eq. (2). The solution is sought in the following form:

$$X = a \cos \psi + \varepsilon U_1(\tau, a, \theta, \psi) \qquad (3)$$

The functions a and ψ are determined from the following D.Eqs.:

$$\dot{a} = \varepsilon A_1(\tau, a, \theta, \psi)$$
$$\dot{\psi} = \omega + \varepsilon B_1(\tau, a, \theta, \psi) \qquad (4)$$

After replacing a and ψ in Eq. (3) by the functions defined in Eq. (4), U_1, A_1, and B_1 are selected to satisfy Eq. (1) up to the order of ε. This implies that the coefficients of ε in Eq. (1) should be equated to zero. To obtain a unique solution, another condition is imposed--that U_1 should not contain first harmonics of ψ.

By using Eqs. (3) and (4), the left side of Eq. (1) can be written as follows:

$$\ddot{X} + \omega^2 X = \varepsilon[\cos \psi(DA_1 - 2aB_1\omega)$$
$$- \sin \psi(a\partial\omega/\partial\tau + 2A_1\omega$$
$$+ aDB_1) + D^2U_1 + \omega^2U_1]$$
$$+ \varepsilon^2[\quad] + \ldots \qquad (5)$$

where

$$D \equiv \nu(\tau) \frac{\partial}{\partial\theta} + \omega \frac{\partial}{\partial\psi}$$

By expanding the right side of Eq. (1) into Taylor's series,

$$\varepsilon f(\tau, \theta, X, \dot{X}) = \varepsilon f(\tau, \theta, X_0, \dot{X}_0)$$
$$+ \varepsilon^2[\quad] + \ldots \qquad (6)$$

where

$$X_0 = a \cos \psi$$
$$\dot{X}_0 = -a\omega \sin \psi$$

By expanding $f(\tau, \theta, X_0, \dot{X}_0)$ into Fourier series,

$$f(\tau, \theta, X_0, \dot{X}_0) = F(\tau, \theta, a, \psi)$$
$$= \sum_{K_0} \sum_{K_1} [F_{s,K_0,K_1}$$
$$\cdot \sin (K_0\theta + K_1\psi)$$
$$+ F_{c,K_0,K_1}$$
$$\cdot \cos (K_0\theta + K_1\psi)] \qquad (7)$$

The subscripts s and c correspond to the coefficients of the sine and cosine functions, respectively. The subscripts K_0 and K_1 correspond to the coefficients of θ and ψ, respectively, in the argument of the sine and cosine functions.

Equating the coefficients of ϵ in Eqs. (5) and (6) and using Eq. (7) results in the following:

$$D^2 U_1 + \omega^2 U_1 = \sin \psi (a\partial\omega/\partial\tau$$

$$+ 2A_1\omega + aDB_1)$$

$$- \cos \psi (DA_1 - 2aB_1\omega)$$

$$+ \sum_{K_0} \sum_{K_1} [F_{s,K_0,K_1}$$

$$\cdot \sin (K_0 \psi + K_1 \tau)$$

$$+ F_{c,K_0,K_1}$$

$$\cdot \cos (K_0 \psi + K_1 \tau)] \qquad (8)$$

Consider the resonance condition:

$$\nu(\tau) = \omega \qquad (9)$$

To get a unique solution, the terms of the first harmonics of ψ and those with frequencies close to ω in the right side of Eq. (8) are equated to zero. Hence,

$$\sin \psi (a\partial\omega/\partial\tau + 2A_1\omega + aDB_1)$$

$$- \cos \psi (DA_1 - 2a_1B_1\omega)$$

$$+ F_{s,0,1} \sin \psi + F_{c,0,1} \cos \psi$$

$$+ F_{s,1,0} \sin \theta + F_{c,1,0} \cos \theta = 0 (10)$$

By solving Eq. (10) for A_1 and B_1 and substituting into Eq. (4), the following is obtained:

$$\dot{a} = -\frac{1}{2} \epsilon F_{s,0,1}/\omega - \frac{1}{2} \epsilon a(\partial\omega/\partial\tau)/\omega$$

$$- \epsilon F_{s,1,0} \frac{\cos (\theta - \psi)}{\nu + \omega}$$

$$+ \epsilon F_{c,1,0} \frac{\sin (\theta - \psi)}{\nu + \omega}$$

$$\dot{\psi} = \omega - \frac{1}{2} \epsilon F_{c,0,1}/(a\omega)$$

$$- \epsilon F_{s,1,0} \frac{\sin (\theta - \psi)}{a(\nu + \omega)}$$

$$- \epsilon F_{c,1,0} \frac{\cos (\theta - \psi)}{a(\nu + \omega)} \qquad (11)$$

By integrating Eq. (11) numerically, the response amplitude a and phase angle ψ can be obtained.

SINGLE-DEGREE-OF-FREEDOM MECHANICAL SYSTEM
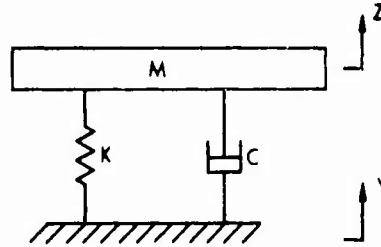
Fig. 2 - Single-degree-of-freedom mechanical system

Consider a single-degree-of-freedom mechanical system as shown in Fig. 2. The D.Eq. of motion for the system is as follows:

$$M\ddot{Z} + C(\dot{Z} - \dot{Y}) + K(Z - Y) = 0 \qquad (12)$$

Let

$$X = Z - Y$$

$$\ddot{Y} = -A(\tau) \cos \tau \qquad (13)$$

Substituting X into Eq. (12) and rearranging the terms results in the following:

$$\ddot{X} + \omega_n^2 X = A(\tau) \cos \tau - 2\xi\omega_n\dot{X} \qquad (14)$$

Hence,

$$\epsilon f(\tau, \psi, X_0, \dot{X}_0) = A(\tau) \cos \psi$$

$$+ 2\xi\omega_n^2 a \sin \psi \qquad (15)$$

So, by comparing Eq. (15) with Eq. (7),

$$\epsilon F_{s,0,1} = 2\xi\omega_n^2 a$$

$$\epsilon F_{c,0,1} = 0$$

$$\epsilon F_{s,1,0} = 0$$

$$\epsilon F_{c,1,0} = A(\tau) \qquad (16)$$

129

Using Eq. (11), the following solution for Eq. (14) can be obtained:

$$X = a \cos (\psi - \tau)$$

$$\dot{a} = -\zeta \omega_n a + A(t) \frac{\sin (\psi)}{\tau + \omega_n}$$

$$\dot{\psi} = \omega - \omega_n + A(t) \frac{\cos (\psi)}{a(\tau + \omega_n)} \qquad (17)$$

where $\psi = \omega \tau - \phi$.

By integrating Eq. (17) numerically, the amplitude a and phase angle ψ can be obtained. The amplitude $\bar{a}$ of the absolute acceleration, $\ddot{Z}$, can be obtained by the following relation:

$$\bar{a} = [(a\omega^2 + A \cos \psi)^2$$

$$+ A^2 \sin^2 \psi]^{1/2} \qquad (18)$$

RESULTS

Response amplitude is obtained by integrating Eq. (17) by the Rounga Kutta method for a and ψ and using Eq. (18). The responses are calculated for unnotched excitation by varying the damping coefficient, the sweep rate, and the natural frequency. Typical responses are given in Figs. 3 and 4. Perfect notches and the responses are calculated by varying the notching factor, the damping coefficient, the sweep rate, and the natural frequency. Typical perfect notches and responses are presented in Figs. 5, 6, and 7. The peak-amplitude and the peak-frequency ratios are plotted vs damping coefficients for sweep rates (2 octave/min, 4 octave/min) and for natural frequencies of 8 and 25 Hz in Figs. 8 and 9, respectively. The initial- and final-frequency ratios of the notch are plotted vs the notching factor for the natural frequencies of 8 and 25 Hz in Figs. 10 and 11, respectively.
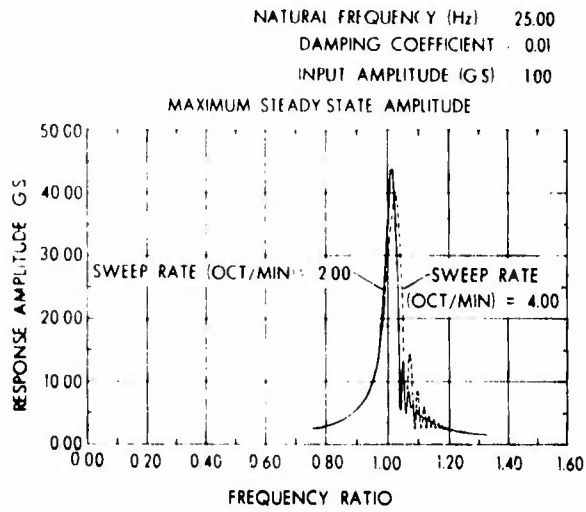
Fig. 4 - Response for swept excitation
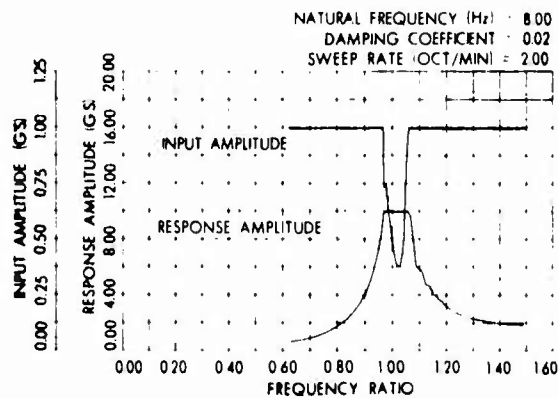
Fig. 5 - Response for swept notched excitation
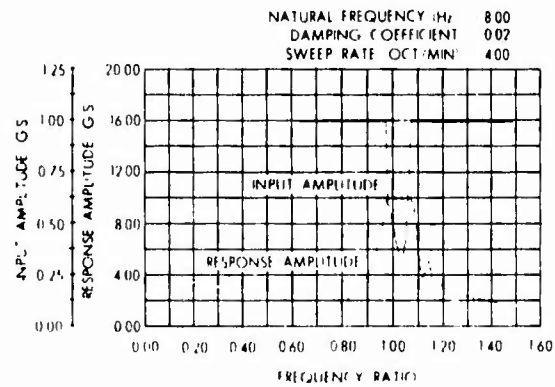
Fig. 3 - Response for swept excitation

Fig. 6 - Response for swept notched excitation

130

NATURAL FREQUENCY (Hz) = 25.00
DAMPING COEFFICIENT = 0.02
SWEEP RATE OCT/MIN: = 2.00

Fig. 7 - Response for swept
notched excitation

NATURAL FREQUENCY (Hz) = 8.00
SWEEP RATE (OCT/MIN. = 2.00
- - - - DAMPING COEFFICIENT = 02
——— DAMPING COEFFICIENT = 05
FFR FINAL FREQUENCY RATIO
IFR INITIAL FREQUENCY RATIO
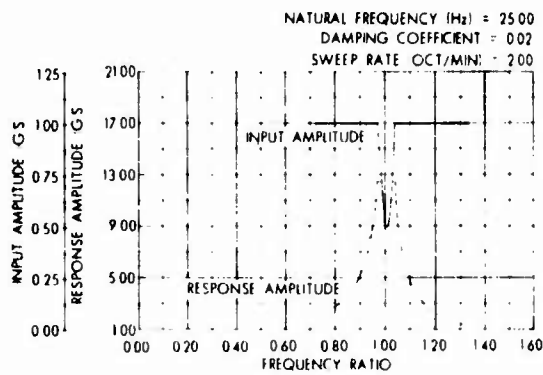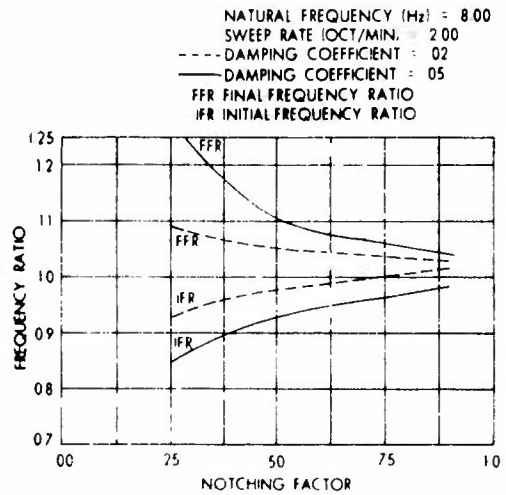
Fig. 10 - Initial- and final-frequency
ratio for a perfect notch

Fig. 8 - Peak-amplitude ratio
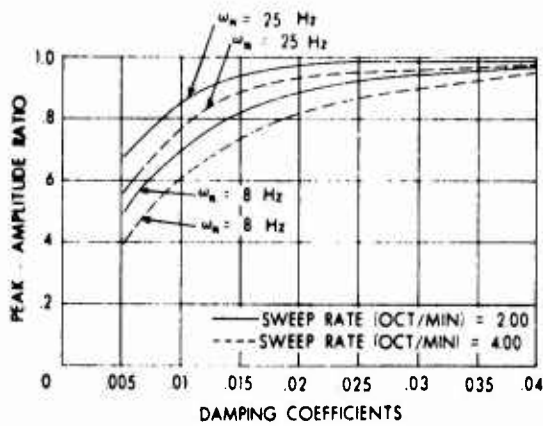
NATURAL FREQUENCY Hz : 25.00
SWEEP RATE OCT. MIN 2.00
- - - - DAMPING COEFFICIENT 02
——— DAMPING COEFFICIENT 05
FFR FINAL FREQUENCY RATIO
IFR INITIAL FREQUENCY RATIO
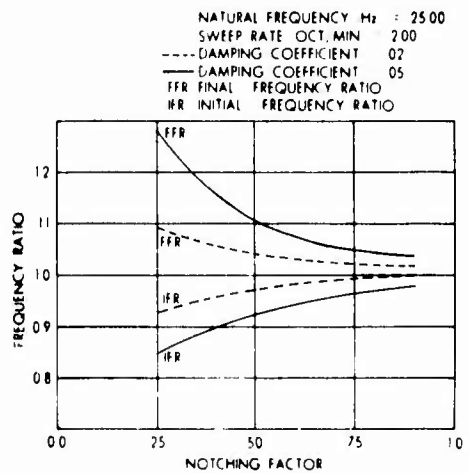
Fig. 11 - Initial- and final-frequency
ratio for a perfect notch
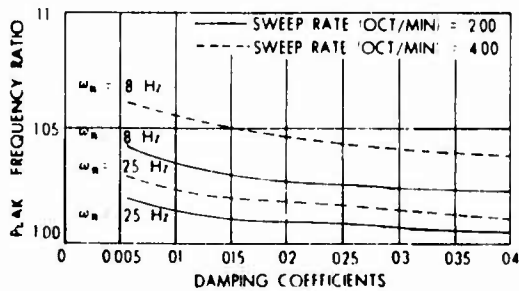
CONCLUSIONS

On the basis of these results, the
following general conclusions can be
drawn.

(a) The peak amplitude of the response
occurs at the excitation frequency
higher than the natural frequency.
The peak-frequency ratio increases
for higher sweep rates and for
lower damping coefficients and
natural frequencies.

Fig. 9 - Peak-frequency ratio

131

(b) The peak amplitude of the response is less than the maximum steady-state amplitude. The peak-amplitude ratio increases for higher natural frequencies and damping coefficients and for lower sweep rates.

(c) The oscillatory behavior of the response amplitude after reaching peak amplitude increases for lower damping coefficients and natural frequencies and for higher sweep rates.

(d) The bandwidth of the notch increases for higher damping coefficients and for lower notching factors.

(e) The central-frequency ratio of the notch is higher than unity. It increases for higher damping coefficients and sweep rates and for lower notching factors.

(f) Knowing the notching factor, the damping coefficient, the natural frequency, and the sweep rates, one can determine the bandwidth and the central frequency of the notch from graphs similar to Figs. 10 and 11.

Study on the shape of the notch is being conducted by the author. From the preliminary data it appears that the perfect notch is closer to the rectangular notch for lower natural frequency and closer to the triangular notch for higher natural frequency.

ACKNOWLEDGMENTS

NOMENCLATURE

X	normalized coordinates
a	amplitude of the response
	natural frequency
f	external excitation
$\epsilon > 0$	small parameter
$\iota = \epsilon t$	slow time
$\dot{\theta} = \nu$	frequency of excitation
γ	phase angle
M	mass of the system
c	damping coefficient
K	stiffness constant
ζ	critical damping factor
Y	base displacement
Z	mass displacement
A	amplitude of base acceleration
D.Eq.	differential equations

REFERENCES

[1] F. M. Lewis, "Vibrations During Acceleration Through A Critical Speed," Trans. of ASME, Vol. 54, No. 23, pp. 253-260, 1932.

[2] R. E. Morse, "The Relationship Between A Logarithmically Swept Excitation and the Build Up of Steady State Resonant Response," The Shock and Vibration Bulletin, Bulletin 35, Part 2, January 1966.

[3] N. Kryloff and N. Boboliubov, Introduction to Nonlinear Mechanics. Princeton University Press, New Jersey, 1947.

[4] Yu A. Mitropolskii, Problems of the Asymptotic Theory of Non-stationary Vibrations. Izd. Nauka, Moscow, 1964; English translation: D. Davey & Co., Inc., New York, 1965.

[5] B. N. Agrawal, "Resonances in Non-stationary Nonlinear Mechanical Systems," Ph. D. Dissertation, Syracuse University, May 1969.

[6] R. M. Evan-Iwanowski, "Nonstationary Vibrations of Mechanical Systems," Journal of Applied Mechanics Review, March 1969.

EFFECTS OF FLIGHT CONDITIONS UPON GUNFIRE
INDUCED VIBRATION ENVIRONMENT

J. A. Hutchinson and B. G. Musson
LTV Aerospace Corporation
Vought Aeronautics Division
Dallas, Texas

This paper discusses the statistical characteristics of the structural response measured on the A-7 airplane while firing the M61 rapid-fire gun. The amplitude versus frequency plots from narrowband analysis and amplitude histogram plots which are presented provide a graphic presentation of the gunfire signal characteristics. A discussion of the relationship between the flight conditions and the measured gunfire vibration levels along with the significance of these relationships in terms of qualification requirements is also presented.

INTRODUCTION

Rapid fire-rate, large caliber guns are being used to aid in the fulfillment of the ever increasing requirement for more "fire power" on modern military aircraft. At the Vought Aeronautics Division (VAD) of the LTV Aerospace Corporation, the General Electric M-61 20 mm multi-barrel gun is mounted in the forward fuselage section of the A-7D and A-7E Airplanes. The introduction of this gun to the A-7 aircraft raised several questions regarding the effect of the gunfire induced environment on the weapon system. It is necessary to correctly describe the structural response to the gunfire excitation to be able to evaluate the effects of the vibratory environment on subsystems and components. With this requirement in mind and because of the scarcity of published information, an in-flight vibration measurement program was conducted.

Random vibration analysis methods were used to obtain a description of the statistical properties of the analog signals. It was readily apparent that the structural response to gunfire had amplitude and wave form characteristics which set it apart from the flight environment resulting from boundary-layer, buffet, and engine induced excitation. "Shotgun" plots of all firings indicated a scatter of response amplitudes too great for direct use in qualification specifications. Such scatter can be reduced to reasonable limits when the measurements are grouped according to certain airplane maneuver parameters.

This paper discusses the statistical properties of the structural response to gunfire excitation and the correlation of vibration amplitudes with airplane maneuver parameters.

An early consideration was the question of how to qualify electronic equipment to this environment. Results of analyses of the measured data led to the development of a method to simulate the gunfire induced response in the laboratory using a repeated pulse signal for shaker excitation. This technique is reported in reference 1.

INTERPRETATION OF GUNFIRE SIGNAL

Typical gunfire vibration data, measured in the vicinity of the M-61 gun muzzle is presented in Figure 1a. Reference 1 characterized the data as a train of periodic pulses. As can be seen from this figure, the vibration environment produced by the M-61 gun resembles a series of shock pulses spaced 10 milliseconds

apart. The time lapse between pulses corresponds to the time between successive rounds fired. The amplitude of the pulses increases for the first few rounds and then becomes relatively constant throughout the remainder of the steady-state firing. Since the time between successive rounds is relatively short, the airplane structural response does not decay between each independent round, but tends to average the effect of each successive pulse to establish a quasi-stable vibration level within the airplane structure as shown in Figure 1a.
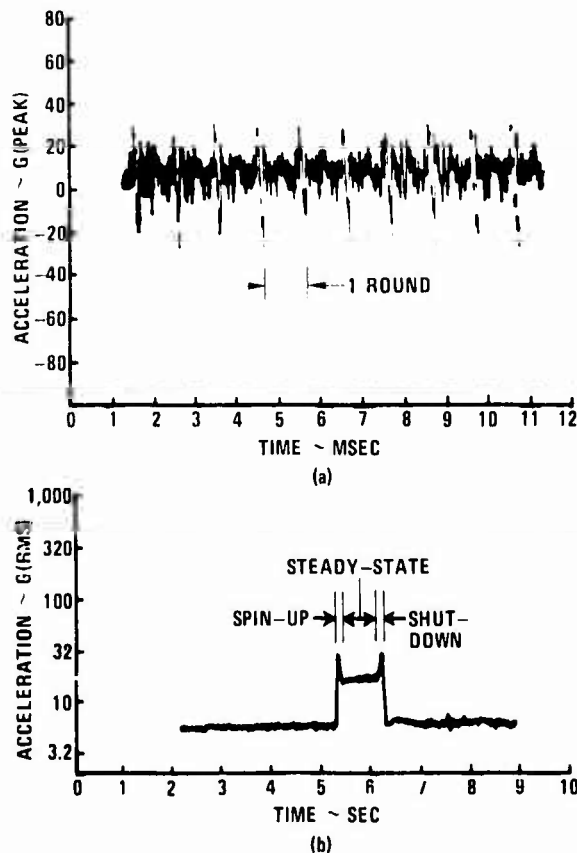
Figure 1. Time History of Flight Gunfire Environment

During normal M-61 gunfire, it requires approximately five rounds to obtain the selected firing rate and approximately five rounds are used during the gun "shutdown" process. The firing rate frequency is varying continuously between 0 and 100 Hz during both of these intervals. As can be seen in Figure 1b the amplitude of the vibration environment is unsteady during these intervals. The amount of amplitude fluctuation present in the measured gunfire data during spin-up and shut-down is dependent upon the distance from the gun muzzle and the dynamic characteristics of the airplane structure

upon which the data was measured. That is, when the fundamental frequency of the supporting structure is lower than the steady-state firing frequency, then the structure will be excited primarily during spin-up and shut-down of the gun. However, the duration of this phenomena is extremely short, less than 10 milliseconds per gunfire cycle, so the stress accumulation tends to become insignificant when compared to the stress buildup during the steady state portion of gunfire. Since the spin-up and shut-down portions of gunfire are of such short duration and do not contribute significantly to the fatigue analysis, it was decided that the first five and last five rounds of each gunfire cycle would not be included during gunfire analysis.

From correlation analysis of various gunfire signals, it was determined that the vibration measured at the majority of locations within the airplane structure is acoustically induced by the muzzle blast, rather than by the recoil of the gun itself. Hence, the maximum vibration environment induced by the gunfire is found adjacent to and forward of the gun muzzle, as one would expect based on this assumption. Typical amplitude spectra obtained from three locations in the vicinity of the M-61 gun on the A-7D airplane, are shown in Figures 2, 3, and 4. These plots were obtained from the Fourier analysis performed on the measured gunfire signal using an analyzer filter with a nominal bandwidth of 10 Hz. As was discussed in Reference 1, from an examination of these amplitude spectra, it became apparent that the gunfire environment was composed of a shaped broadband random signal with superimposed discrete
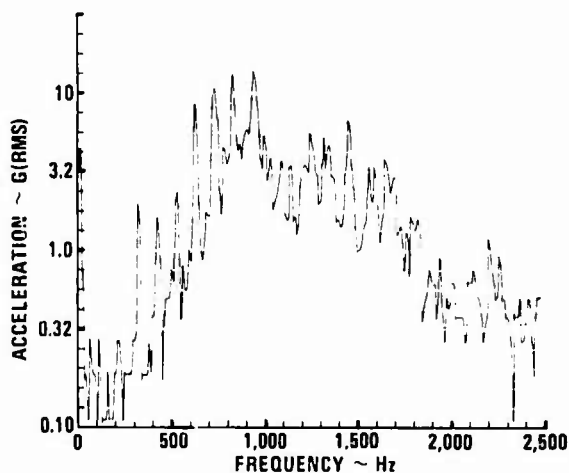
Figure 2. Amplitude Spectrum of Flight Gunfire Within 60 In. of Gun Muzzle Using 10 Hz Analysis Filter

134
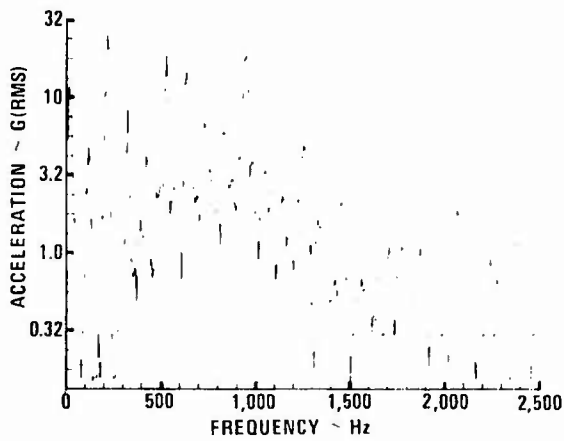
Figure 3. Amplitude Spectrum of Flight Gunfire Within 40 In. of Gun Muzzle Using 10 Hz Analysis Filter
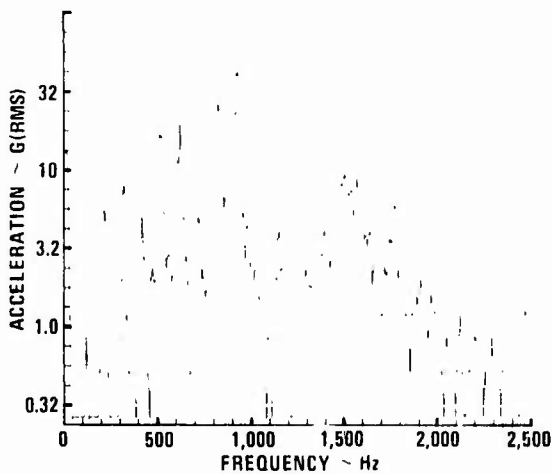
Figure 4. Amplitude Spectrum of Flight Gunfire Within 25 In. of Gun Muzzle Using 10 Hz Analysis Filter

Figure 5. Amplitude Spectrum of Flight Gunfire Within 25 In. of Gun Muzzle Using 2 Hz Analysis Filter.
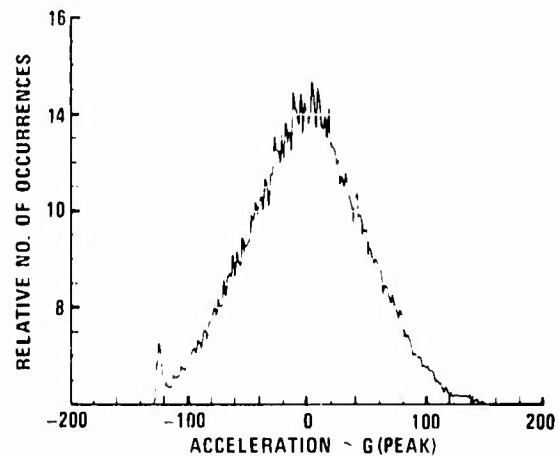
Figure 6. Amplitude Historgram of Overall Flight Gunfire Signal Within 25 In. of Gun Muzzle

signals centered at the firing rate frequency and its harmonics. When these particular gunfire signals were analyzed using a 2 Hz filter, the amplitudes of the narrowband signals did not change, indicating they are sinusoidal in nature. The results of a 2 Hz narrowband analysis are shown in Figure 5. Because of the signal's complex nature, the Fourier analysis alone does not fully describe the intrinsic properties of the gunfire signal. Therefore, amplitude histogram analyses were performed so that the peak amplitude distribution could be determined.

An amplitude histogram analysis of the broadband gunfire signal produces the curve shown in Figure 6. This curve has a Gaussian shape indicating a random amplitude distribution. However, when the gunfire signal is

prefiltered by passing it through a narrowband filter, centered at each of the discrete periodic signals present in the amplitude spectrum shown in Figure 4, the resultant amplitude histograms indicate that the lower harmonics tend toward a constant amplitude distribution in varying degrees. The amplitude histograms of these typical prefiltered signals are presented in Figure 7. From a review of these figures it can be seen that the gunfire fundamental and the first two or three harmonic frequencies indicate a rather constant amplitude distribution with the remaining higher order harmonics indicating a successively increasing random amplitude characteristic. The increase in random characteristics at the higher harmonics is due in part to the randomly distributed firing rate deviations

135
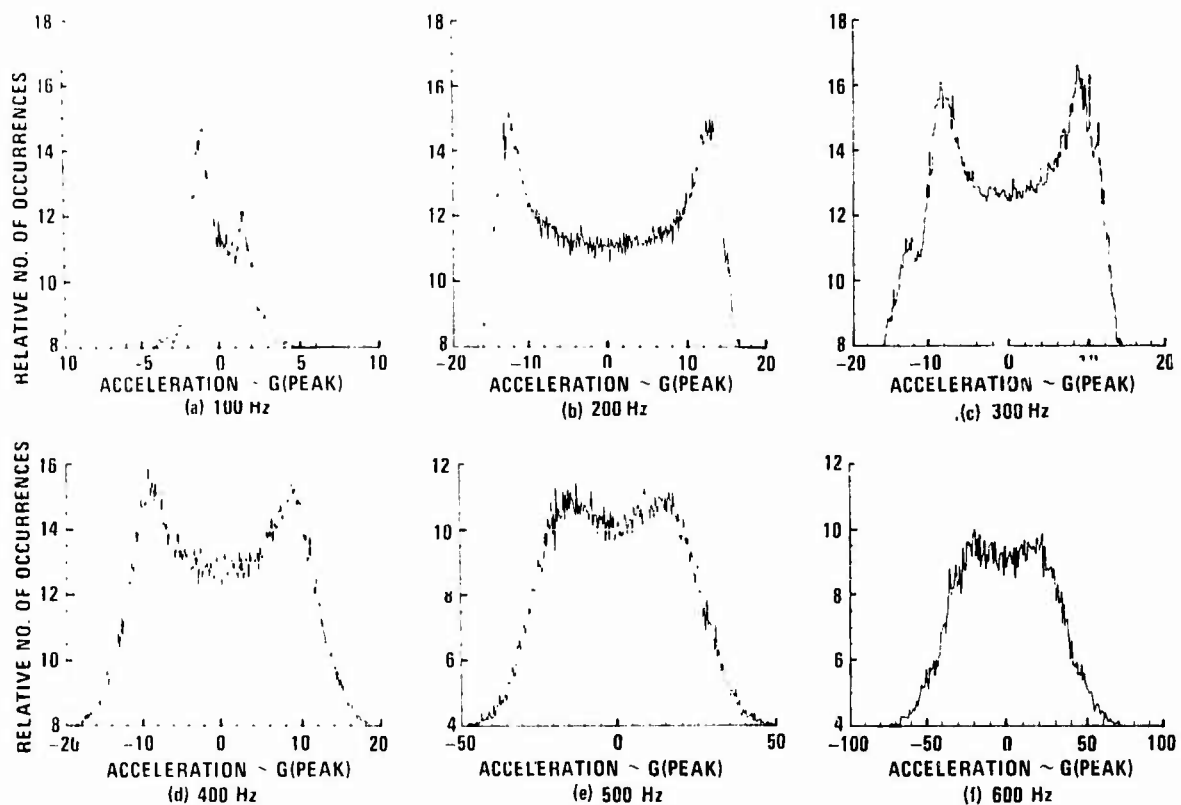
Figure 7. Amplitude Histogram of Prefiltered Flight Gunfire Using 80 Hz Filter

which produce a nominal fluctuation of 10% in the gunfire fundamental and harmonic frequencies. This is reinforced by the tuning-detuning effect of the aircraft structure resulting from the changing flight loads during the time the gunfire maneuver was being performed.

Because of the quantity of data obtained during the flight test gunfire program and the necessity to develop qualification requirements to be applied in the procurement of new avionics systems, the time was not available to perform narrowband analyses on all measured gunfire. Therefore, one-third octave band, rather than narrowband, analyses were performed on most of the data because of the relative ease and speed with which numerous records can be processed. To convert the root-mean-square (RMS) acceleration levels obtained from the one-third octave band analysis to peak acceleration levels for use in qualification requirements, it was necessary to get some ideas of the peak distributions. This was accomplished by performing amplitude histogram analyses on selected signals passed through one-third octave filters. The peak to RMS ratios obtained from these histograms for 90% and 95% confidence levels

at one location are plotted in Figure 8. It can be seen from this figure that a ratio of three should give a reasonable confidence at the higher frequencies and should be very conservative at the gunfire lower harmonic frequencies. Therefore, for the purposes of setting qualification test levels it was decided at VAD to use a ratio of 3 on the measured RMS acceleration level in obtaining the peak acceleration. Since the total gunfire lasts only a small portion of the total design life of the A-7 airplane, the duration of the gunfire qualification tests was set for the total expected in-flight gunfire exposure time.
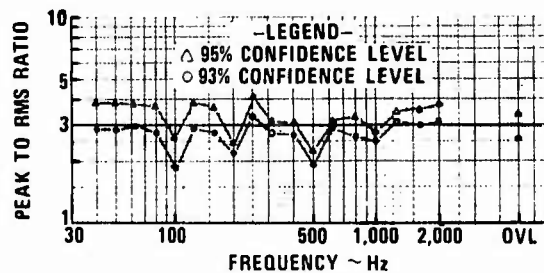
Figure 8. Peak to RMS Acceleration Ratio at Each One-Third Octave Filter Center Frequency

136

EFFECTS OF AIRPLANE FLIGHT PARAMETERS

The structural response to gunfire excitation was measured in flight at a number of locations in several A-7D and A-7E aircraft. Repeated measurements were made at selected locations to increase the statistical reliability of the data, since the data samples were of short duration. The gunfire vibration measurement program was combined with other armament demonstration programs and the number of gunfire flights were limited; therefore, to obtain the maximum number of measurements, data were recorded for each firing without regard to airplane maneuver parameters. Measurements at individual locations were initially analyzed as one data block even though they were not recorded under identical conditions.

As stated earlier, due to time limitation, complete analysis was not performed on all signals. Rather, one-third, octave pass band analysis was employed on the bulk of the data to record the maximum root-mean-square (RMS) level obtained in each filter band-pass during the quasi-stable portion of the gunfire signal. The analyzer output was entered into a digital computer for data storage and presentation in the form of amplitude versus frequency plots. A typical one-third octave amplitude plot of the aircraft structural response to the gunfire induced vibration environment is shown in Figure 9. From an examination of this figure, one can see the variation in the vibration amplitude that was experienced over a range of varied flight conditions. Presently, a commonly used method to establish the upper limit of vibration amplitudes is to multiply the maximum measured values by some scatter or uncertainty factor and envelop the products. However, in the case of gunfire, where the flight conditions can be expected to influence the overall gunfire vibration levels in varying degrees, the method of enveloping the maximum amplitude spectrum obtained during a set of varying flight conditions may yield unreliable vibration environments. That is, if the maximum vibration spectrum is obtained during a set of flight conditions only occurring at rare occasions then the resultant vibration environment may be unrealistic in terms of the design requirements of the aircraft. From a qualitative standpoint, flight parameters such as airspeed, altitude, maneuver load, etc., should influence the measured gunfire vibration level. As an example, when the aircraft is performing a high "g" maneuver, the aircraft structure experiences a subsequent increase in internal stress, thereby removing the play in structural joints. This should increase the vibration transmissability throughout the aircraft structure. Also as was stated earlier, the primary source of gunfire-induced vibration is from the muzzle blast which is acoustically transmitted and impinges upon the aircraft structure. At higher altitudes, the acoustical effects should be less due to decreasing atmospheric density.

To establish quantitative values of the effect certain independent flight parameters have on the overall gunfire vibration level, the measured data were grouped in like maneuver blocks. That is, only data recorded during the same airspeed, altitude, and maneuver load were plotted together. Results of this type of data grouping are shown in Figure 10 where the vibration data are grouped into the seven data blocks as listed in Table I.

TABLE I

Data Group	Airspeed Knots	Altitude Feet	Maneuver Load
A	424	4,500	4.1
B	435	4,600	3.8
C	282	28,600	3.4
D	437	7,500	3.1
F	252	36,800	2.0
G	270	38,000	1.0

As can be seen from this figure, the data scatter for the overall gunfire vibration level in each group of like flight parameters is approximately 4 db as compared with 20 db scatter when all data were plotted as in Figure 9. As one might expect, the airspeed, distance from the gun muzzle, and airplane maneuver load had a large influence on the overall vibration amplitude during gunfire. However, this type of procedure produces only a rough approximation of the amount each flight parameter affects the overall gunfire environment, because of the complex inter-relationship between the many possible flight parameters. Because of the coupling between the various flight parameters and the necessity to increase the accuracy in the predicted gunfire environment at locations and flight parameters where no measured data are available, a more analytical determination method was needed.
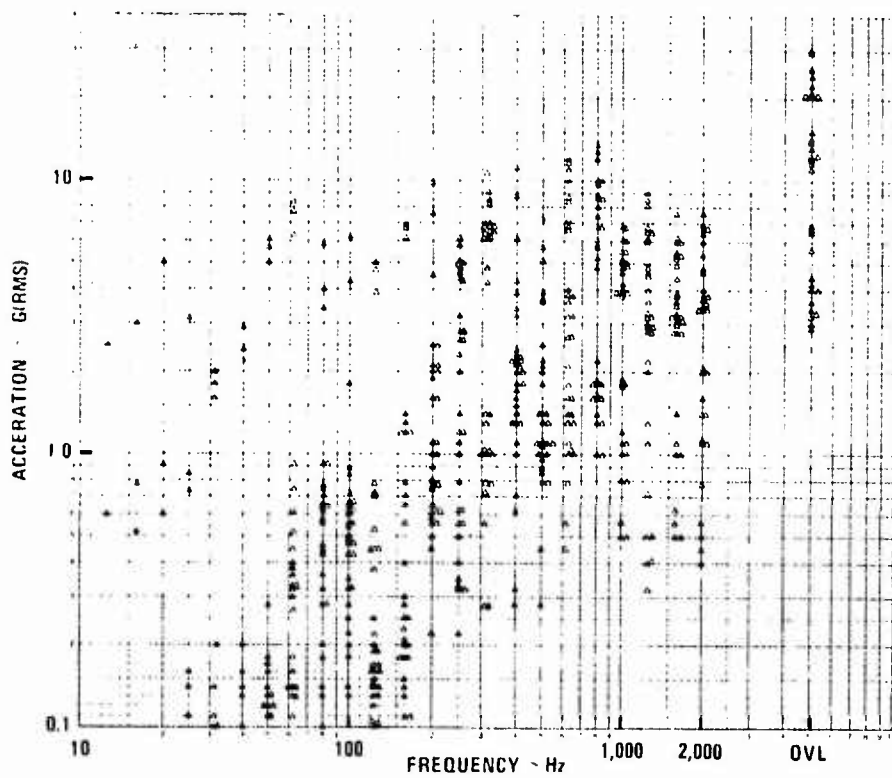
Figure 9. One-Third Octave Amplitude Spectrum of Flight Gunfire (Without Data Grouping)
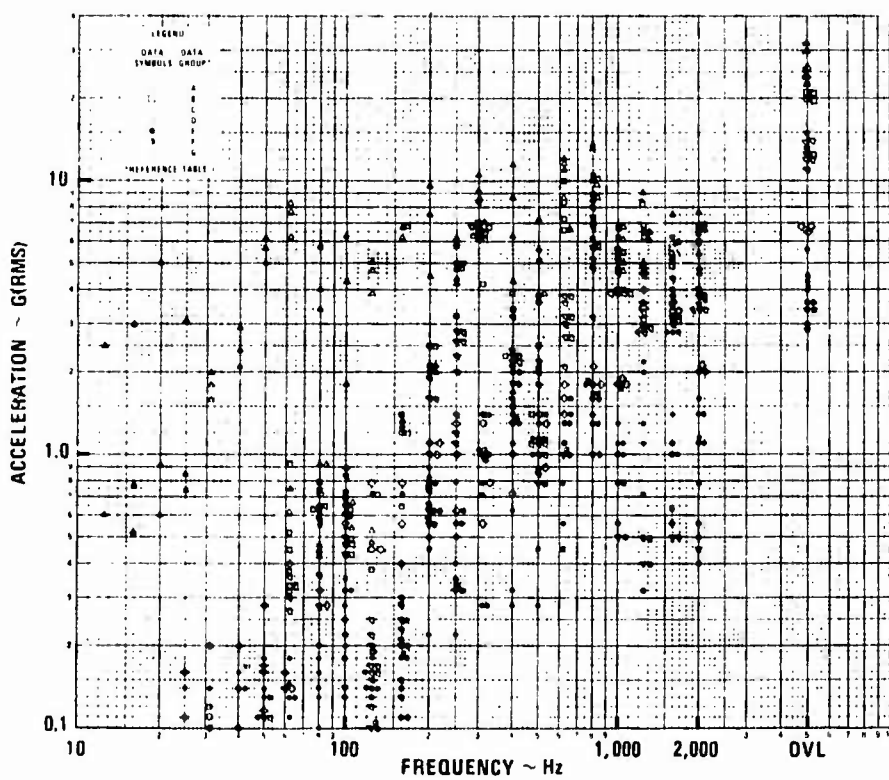
Figure 10. One-Third Octave Amplitude Spectrum of Flight Gunfire (With Data Grouping)

138

nances; they are actually due to the gunfire rate and the harmonics. Now the shape of the broadband background is influenced by the local structure or panel resonance. During a nongunfire condition the general background will be there at a much lower level.

Mr. Baker: There are pressure transducers that do have low acceleration sensitivity that might have helped if you had used them.

Mr. Ungar (Bolt Beranek and Newman): The title of your paper was the effect of flight conditions on gunfire-induced vibration environments but unless I missed something you did not really tell us what effect the flight conditions had. All I saw was a large scatter of data. Do you have any real feel of what the effects of flight conditions are? What are the physical reasons that flight conditions should affect what gunfire does to your structure?

Mr. Hutchinson: We recorded the maximum vibration levels during low altitude, high airspeed and high maneuver loads. We recorded the lowest levels during a high altitude, low airspeed, low maneuver loads. I do not want to imply this as linear with the airspeed altitude maneuver loads. It is not, and right now we are trying to determine how it is affected. We are trying to come up with a way to predict the gunfire levels at other locations where we have no measured data. Under any hypothetical flight conditions we will hopefully be able to come up with a reasonable vibration environment. Right now, I cannot tell you how the airspeed, altitudes and maneuver loads affect things.

Currently at VAD computer routines are being used to implement additional statistical evaluation methods such as described in Reference 2. This procedure describes the spectrum response level in terms of independent variables which influence the flight vibration environment. The method by which the independent variables are selected is most important, since the accuracy of the calculated spectrum levels depends upon the correct choice of the independent variables.

Initially, the information obtained from the empirical determination of the effects of flight parameters upon gunfire vibration levels are being used in selecting the form of the independent variables. Evaluation of the preliminary results, using this method, has indicated a fair degree of correlation between the predicted and measured gunfire spectrum. Further refinement in the selection of the independent variables which are to be used in this procedure is continuing.

CONCLUSIONS

The structural response to gunfire excitation results in a classic example of a complex signal, and appropriate analysis methods must be used to describe the signal. Analysis of measured gunfire response shows the unique character of the gunfire vibration which sets it apart from other flight induced excitations. It is important to remember, when interpreting vibration signals produced by a rapid-fire large caliber gun, that the Fourier analysis yields only a part of the story. Additional information

must be obtained from correlation analysis and from narrowband amplitude probability analysis on the gunfire signal. The gunfire response may be best described as a series of periodic signals with varying amplitudes occurring at the gunfire rate and its harmonics superimposed on a broad band random background. Since gunfire measurements are usually obtained for a large number of airplane flight conditions, a wide scatter in amplitudes will occur. Consequently, the flight conditions during which the gunfire data were measured must be considered when developing vibration qualification requirements.

Quantitative effects of the airplane maneuver parameters on the overall gunfire environment can be evaluated empirically through the use of measured response amplitudes. Continuing work on gunfire environment at VAD includes evaluation of weighting coefficients for the maneuver parameters and application of this information to predicting gunfire response at locations and flight conditions for which flight measurements are not available

REFERENCES

1. J. A. Hutchinson and R. N. Hancock, "A Method to Simulate Gunfire Induced Vibration Environment," 40th Shock and Vibration Bulletin, Part 6, December 1969, pages 27-35.

2. A. G. Piersol and W. F. Van der Laan, "Statistical Analysis of Flight Vibration and Acoustic Data," AFFDL-TR-68-92, Wright-Patterson AFB, Ohio, February 1970.

DISCUSSION

Mr. Baker (Southwest Research Institute): You mentioned earlier in your talk that you did use microphones. Were these located within the aircraft structure?

Mr. Hutchinson: The only one inside the aircraft structure was in the cockpit. We had them located inside the end of the duct, along the sidewalls, and down the side of the fuselage. On the ground we had them in the blastport area and stationed in the near field perpendicular to the gun.

Mr. Baker: They were essentially all outside the aircraft then?

Mr. Hutchinson: Yes, and they were flush mounted.

Mr. Baker: You did not report any data from those. Did you get pressure signals from them?

Mr. Hutchinson: We did during flight. We did not get gunfire data. Our pressure data on the ground was not very good because the signals messed up our pickups.

Mr. Baker: Your accelerometers of course showed many different frequencies in the response. Were they mounted on the inside of skin panels or where? I suspect that many of these frequencies may be resonances in local panels.

Mr. Hutchinson: Practically all that data I showed is from microphones mounted on hard load-bearing structure. The spikes are not panel reso-

THE BOX CAR DYNAMIC ENVIRONMENT

Robert W. Luebke
C&O/B&O Railroad Companies
Baltimore, Maryland

The continuous or over-the-road vibration environment within present day railroad merchandise freight car equipment is defined in terms of frequency spectrograms, power spectral density curves, and curves of peak-to-peak accelerations versus speed and load. The effects of suspension system changes being introduced in the industry are also presented. This paper is based on the results of a joint effort on the part of the C&O/B&O Railroad Companies and the Office of High Speed Ground Transportation of the U. S. Department of Transportation to define the vibration environment and the effect of its major variables.

In May of 1969, the C&O/B&O Railroad Companies and the Office of High Speed Ground Transportation of the U. S. Department of Transportation, commenced a joint effort to define the vibration environment within present day freight cars. This study was primarily concerned with the continuous over the road environment rather than the infrequent single pulse inputs which are caused by yard switching, switches, turn outs, and slack run in and run out.

The basic intent of this paper is to provide design data for packaging engineers and product designers so that realistic limits can be set on product strength and cushioning requirements. Previously submitted data has given an exaggerated vibration envelope for rail transportation. If the packaging engineer used these previous vibration envelopes, his product would have been so overprotected that the package in many cases would cost more than the product itself.

The vibration environment within present rail cars can be broken down into 3 categories: (1) Impact shock due to coupling of cars in yards; (2) Impact type inputs from road crossings, turn outs, and switches. (3) Continuous input from rail joints, ties, and subgrade. The last category comprises about 90% of the input to commodities and is the cause of resonant damage to packages. The first 2 categories, while more severe, only occur 10% of the time a package is in transit. Furthermore, these impact type shocks are considerably lower than those experienced in the material handling environment.

Because most engineers design their packages to protect products from the inputs received in the materials handling environment, the single impact type inputs from the in transit rail environment have little effect on the single package. The effect of impact and vibration inputs on stacks of packages is another story altogether.

Unfortunately, most commodities are shipped this way and little has been done by anyone except Forest Products Laboratories, Madison, Wisc. to define this problem. It is hoped that the availability of the data presented in this paper will spur additional research on the part of manufacturers to determine the effect of vibration inputs on their packages when stacked for shipment.

The basic intent of the joint effort was, therefore, to define the environment to which packages or stacks of packages were subjected for the greatest amount of time. Consequently, the over-the-road input formed the basis for the Federal Railroad Administration report "Investigation of 50' - 70 ton Box Car Vibrations". Those portions of the report which relate to the Box Car environment are the subject matter of this paper. The areas of interest are: 1) the effect of load and speed; 2) the effect of primary suspension system spring rates; 3) the effect of variable rate springs; and 4) the effects of truck designs on the vibration environment within present day freight equipment.

The tests were performed on a section of C&O railroad track just west of Huntington, W. Va. This track consisted of a vertical and a lateral test section. The vertical test section, Figure 1, was shimmed to produce a continuous vertical surface and cross elevation input with a 39-foot wave length. The lateral test section, Figure 2, was developed by jacking the track over at each joint on the south rail to produce a periodic lateral input to the equipment being tested. All tests except those designed to evaluate track input were made with the vertical section shimmed to generate staggered 1/2-inch low joint inputs every 19-1/2 feet and with the lateral section jacked over to generate a 1/4-inch misalignment input every 39 feet. These input levels were designed to generate violent actions in the equipment tested so that differences in performance would be detected. These sustained inputs

are more severe than those developed by any normal main line track and consequently can be considered the maximum, or "worst case" continuous vibrational input to a box car moving over the road.

The data required to define the environment was obtained by operating a special test train, Figure 3, over the test sections at speeds between 10 and 60 m.p.h. in 10 m.p.h. increments. The test train included a C&O GP-9 locomotive followed by a test box car, a "control" box car, and the DOT cars T-2 and T-4. Cars T-2 and T-4, Figure 4, served as the instrumentation and track measurement platforms. The load in the test box car was varied to obtain the effect of weight on the vibration environment and the load in the "control" box car remained constant at 35 tons. The control car served as a quality control device to insure that the observed variations in the test car were due to changes in test parameters and not due to an uncontrollable change in the test conditions. Track parameter measurements obtained from car T-2 served as a control measure for track geometry.

The instrumentation used to define the vibration environment comprised vertical and lateral accelerometers mounted on the unsprung truck mass, Figure 5, and on the car floor over the center plate, Figure 6.

The vibration data recorded onboard the test train at Huntington, W. Va. was processed with a filter bank-type spectral analyzer at the Signal Analysis Laboratory of Melpar, Inc., Falls Church, Virginia. The work commenced in mid-May, while the data collection was still in progress, and ended in late October, 1969.

The analog third-octave filter bank was used to develop practical and useful spectral displays for this task. The third-octave filter bank consists of 31 contiguous bandpass filters, each having a one-third octave (1.26) ratio of upper-to-lower cutoff frequencies. The lower cutoff, or half-power frequency of this bank

is 17.9 Hz and the upper half-power
frequency is 22,400 Hz.

Because the data frequencies
recorded on the FM tape recorder
(Ampex FR1300) aboard the test train
were distributed from dc (zero fre-
quency) to over 500 Hz, the data tape
was reproduced at 60 inches per sec-
ond, resulting in a speedup factor of
32 over the original 1-7/8 ips record-
ing speed. This speedup acted as a
frequency multiplier of 32, and fre-
quencies from 0.6 Hz to 700 Hz could
then be analyzed on the 20-2400 Hz
filter bank. A table of filter center
frequencies, upper and lower cutoff
frequencies, and their real time
equivalents are shown in Figure 7.

The block diagram of the filter
bank and display apparatus is shown
in Figure 8. The signal from the tape
recorder (running at 60 IPS) was fed
to the power amplifier input; the
output of this amplifier was fed into
the entire bank of 31 parallel filters.
Each filter output was rectified (peak
detected) and averaged in the RC cir-
cuit following the rectifiers. The 31
detected and smoothed outputs were
then doubly connected to a 64-pole
mercury jet scanning switch. The ro-
tor of this device spins at 3600 rpm,
sampling each filter every 8.33 milli-
seconds. In this manner, a spectral
scan occurs periodically 120 times per
second.

The output of the scanning switch
was connected via an amplifier to the
vertical deflection plates of a CRT.
This amplifier produced an output pro-
portional to the logarithm of the in-
put signal for moderate to high ampli-
tude inputs, and was amplified linear-
ly for low level inputs; hence, the
"hybrid" scale for the vertical ampli-
tude axes of the spectrograms shown
in this paper.

In order to display frequency on
the horizontal axis of the vibration
spectrogram, a 120 Hz sawtooth wave-
form, synchronized to the mercury jet
scanning switch rotor, was impressed
on the horizontal plates on the CRT.
This waveform functioned to produce a
raster, and caused the lower-to-higher

frequency filters to be displayed from
left to right on the CRT screen; the
resultant spectral displays were re-
corded on Polaroid photographs for
analysis.

These spectral displays or spec-
trograms and the resultant PSD curves
permits the basis for defining the
natural environment in present day
rail transportation equipment.

The natural frequencies program which
are the environment as environment within
present day transportation equipment are
shown in Figures 9 through 23.

Figure 9 shows the theoretical
natural frequencies of the freight car
tested while Figure 10 shows the forc-
ing frequencies available to create
resonance in commodities shipped in
rail vehicles. Figure 11 shows the
natural frequencies of common rail car
suspension systems.

Figures 12 through 17 show the
vibration spectra within a box car as
a function of the load in the car and
the speed with which it is moving.
Figures 18 through 21 show the impor-
tance of specific frequency ranges.
These Power Spectral Density curves
show that for the car tested, there
are two important frequency ranges.
These are the forcing frequency range
of 0 to 20 Hz and the car body vibra-
tion range between 50 and 100 Hz.
Other car designs will have different
body bending frequencies. The lowest
natural frequency input found is 7 Hz
and is the second vertical bending
mode of an 89 foot flat car.

Figures 22 and 23 show the peak-
to-peak accelerations on the car floor
as a function of load and speed. The
important item to note is that as the
lading weight decreases, the vibration
amplitude increases. Consequently,
the packaging protection must be great-
er for a product that will be loaded
to one half of rail car capacity than
one which will be loaded to full rail
car capacity.

Figures 24 and 25 show the peak-
to-peak vertical and lateral accelera-
tions as a function of presently

143

available rail car truck suspension spring
rates. Due to the increased stiffness
of the rail car truck suspension spring
type. Because of the change in frequency with load and the fact that the
commodity package is in direct association with the freight carrying vehicle,
the package cushion would not be sufficient to protect against the product
abuse.

The railroad industry is currently
engaged in developing new suspension
systems which reduce the frequency
range and the amplitude of vibration
within our freight equipment. One of
the methods presently under consideration to reduce the range of available
damaging frequencies is the variable
rate spring. This non-linear spring
maintains a nearly constant natural
frequency regardless of load, and consequently would reduce the damage potential of rail car suspension systems.
The performance of this type of spring
is shown in Figures 26 and 27.

In addition to the variable rate
spring, the railroad industry is developing new freight car trucks with improved ride quality for carrying fragile or sensitive commodities. The
performance of a few of these trucks is
shown in Figures 28 through 33.

These new truck data should be considered as an indication of the future
vibration environment within merchandise freight cars.

It is hoped that the data presented will enable the realistic design of
commodity packaging and cushions, and
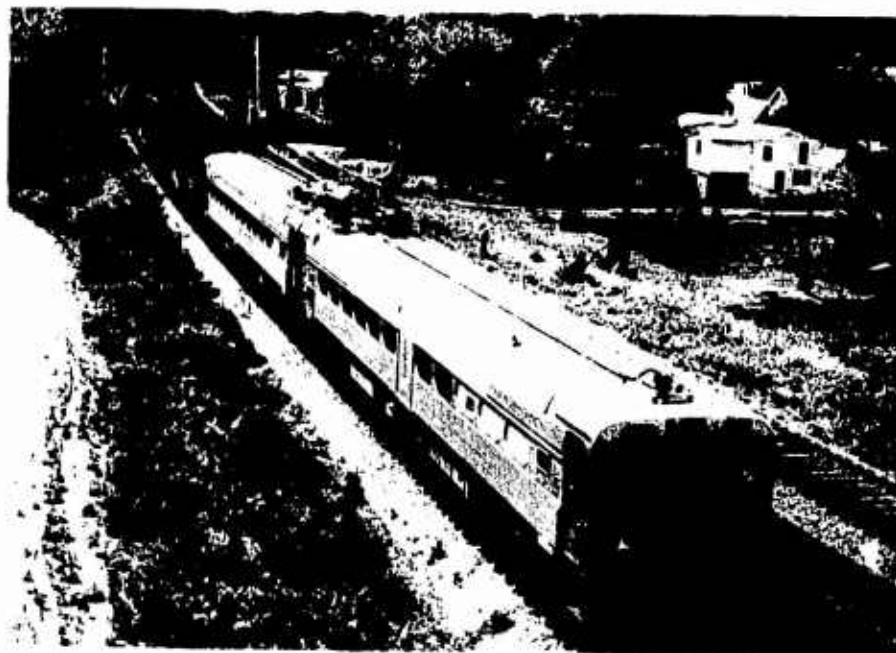thereby help reduce in-transit loss &
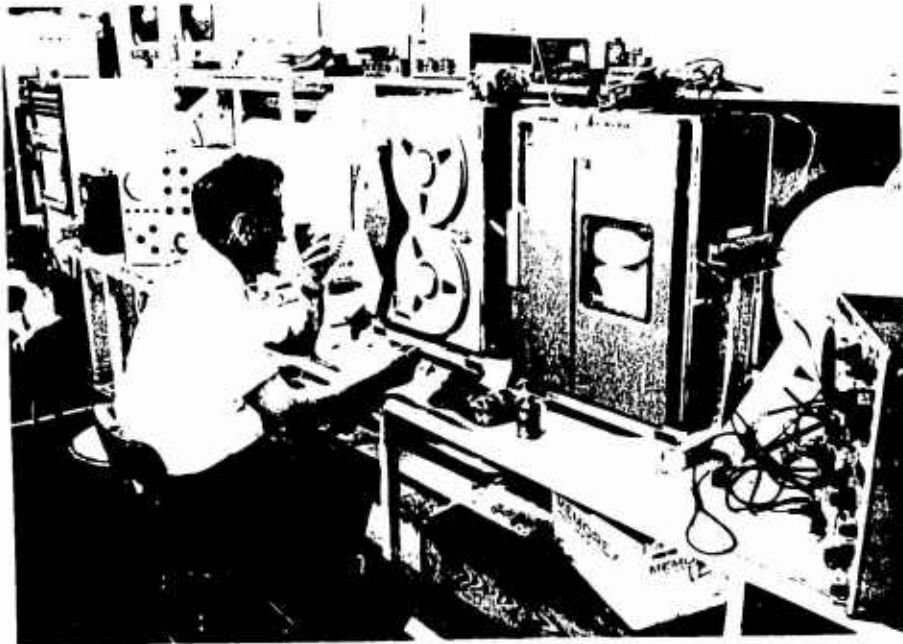damage.

MODIFIED VERTICAL TEST SECTION

FIGURE 1

144

MODIFIED LATERAL TEST SECTION.
FIGURE 2

TEST CONSIST
FIGURE 3

145

RESEARCH CAR INSTRUMENTATION
FIGURE 4

TRUCK ACCELEROMETERS
FIGURE 5

CAR BODY ACCELEROMETERS
FIGURE 6

146

TABLE OF PASSBANDS OF 1/3-OCTAVE BAND FILTERS

Actual Center Frequency	Actual Lower Cut-Off Frequency	Actual Upper Cut-Off Frequency	Equivalent* Center Frequency	Equivalent* Lower Cut-Off Frequency	Equivalent Upper Cut-Off Frequency
20	17.9	22.4	0.625	0.560	0.700
25	22.4	28.1	0.782	0.700	0.878
31.5	28.1	35.5	0.983	0.878	1.11
40	35.5	44.7	1.25	1.11	1.40
50	44.7	56.2	1.56	1.40	1.75
63	56.2	71.0	1.97	1.75	2.22
80	71.0	89.4	2.50	2.22	2.79
100	89.4	111.8	3.12	2.79	3.50
125	111.8	141.4	3.91	3.50	4.42
160	141.4	179	5.00	4.42	5.60
200	179	224	6.25	5.60	7.00
250	224	281	7.82	7.00	8.78
315	281	355	9.83	8.78	11.1
400	355	447	12.5	11.1	14.0
500	447	562	15.6	14.0	17.5
630	562	710	19.7	17.5	22.2
800	710	894	25.0	22.2	27.9
1000	894	1118	31.2	27.9	35.0
1250	1118	1414	39.1	35.0	44.2
1600	1414	1789	50.0	44.2	56.0
2000	1789	2236	62.5	56.0	70.0
2500	2236	2806	78.2	70.0	87.8
3150	2806	3556	98.3	87.8	111
4000	3556	4472	125	111	140
5000	4472	5615	156	140	175
6300	5615	7099	197	175	222
8000	7099	8944	250	222	279
10000	8944	11180	312	279	350
12500	11180	14142	391	350	442
16000	14142	17889	500	442	560
20000	17889	22361	625	560	700

FIGURE 7
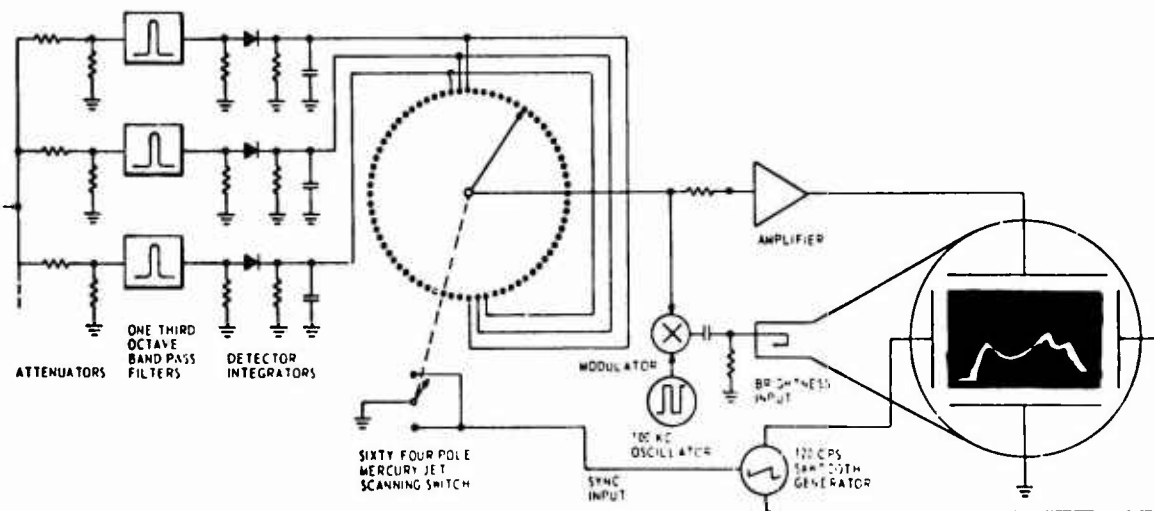
FUNCTIONAL BLOCK DIAGRAM OF
FILTER BANK AND DISPLAY
FIGURE 8

THEORETICAL NATURAL FREQUENCIES			
Suspension System		2.18 Hz	3.88 Hz
Car Body Vertical	1 wave bending		40 Hz
Car Body Vertical	2 wave bending		80 Hz
Car Body Vertical	3 wave bending		120 Hz
Car Body Vertical	4 wave bending		160 Hz
Car Body Lateral	1 wave bending		30 Hz
Car Body Lateral	2 wave bending		60 Hz
Unsprung Mass	(Vertical)		12 Hz
Unsprung Mass	(Lateral)		8.5 Hz
Wheel on Rail			6 Hz
Track Structure			73 Hz

FIGURE 9

FORCING FREQUENCY TABLE			
Speed (MPH)	Rail (Hz)	Joint (Hz)	Wheel (Hz)
10	0.38	0.76	1.7
20	0.76	1.51	3.4
30	1.13	2.26	5.1
40	1.51	3.02	6.8
50	1.88	3.77	8.5
60	2.26	4.53	10.2

FIGURE 10

SUSPENSION SYSTEM NATURAL FREQUENCIES			
Equipment	EMPTY	36 TON	70 TON
Barber - Normal Damping	Hz	Hz	Hz
2-1/2" Travel	4.25	2.93	2.40
3-1/16" Travel	3.88	2.66	2.18
3-11/16" Travel	3.54	2.45	2.02

FIGURE 11

BARBER S-2 TRUCK
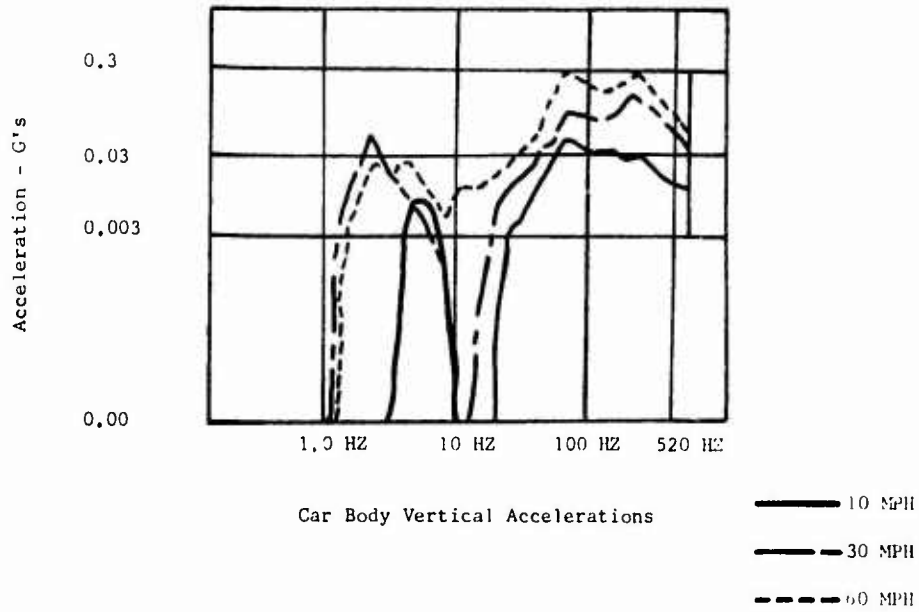3-1/16" SPRINGS
STD. SNUBBING
70 TON LOAD

Car Body Vertical Accelerations

FIGURE 12

BARBER S-2 TRUCK
3-1/16" SPRINGS
STD. SNUBBING
70 TON LOAD

Car Body Lateral Accelerations

FIGURE 13

149

BARBER S-2 TRUCK
3-1/16" SPRINGS
STD. SNUBBING
30 TON LOAD

Car Body Vertical Accelerations

10 MPH
30 MPH
60 MPH
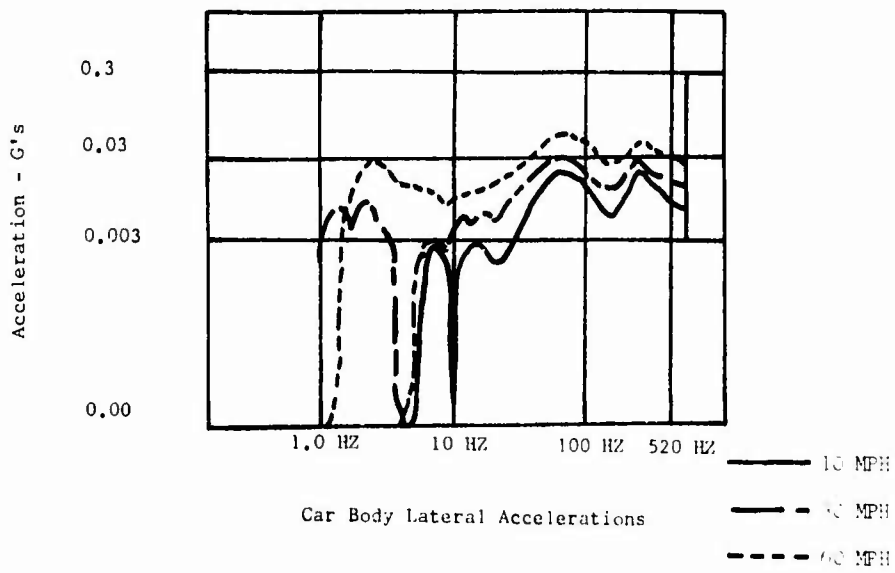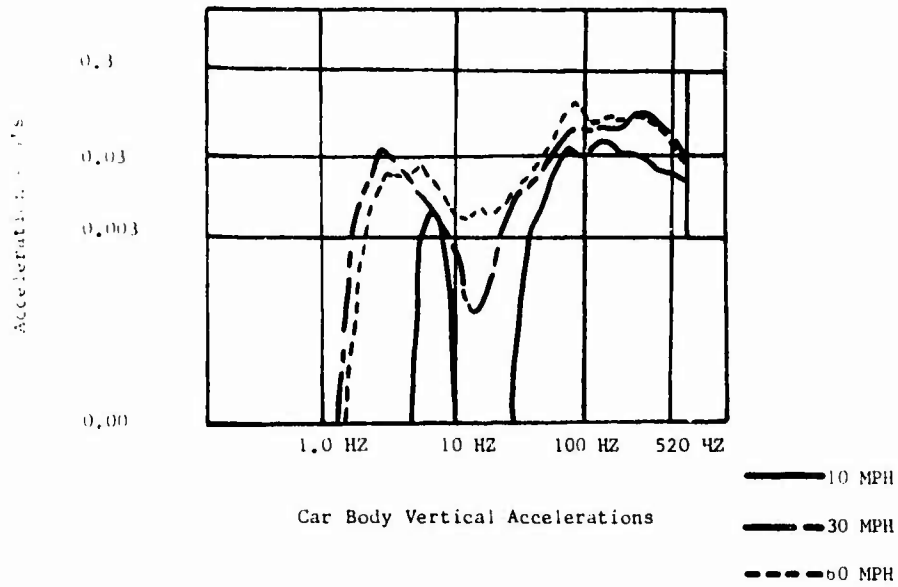
FIGURE 14

BARBER S-2 TRUCK
3-1/16" SPRINGS
STD. SNUBBING
30 TON LOAD

Car Body Lateral Accelerations

10 TON
30 MPH
60 MPH

FIGURE 15

150

Barber S-2 Truck
3-1/16" Springs
Std. Snubbing
Empty Car

Car Body Vertical Accelerations

— 10 MPH
— — 30 MPH
- - - - - 60 MPH
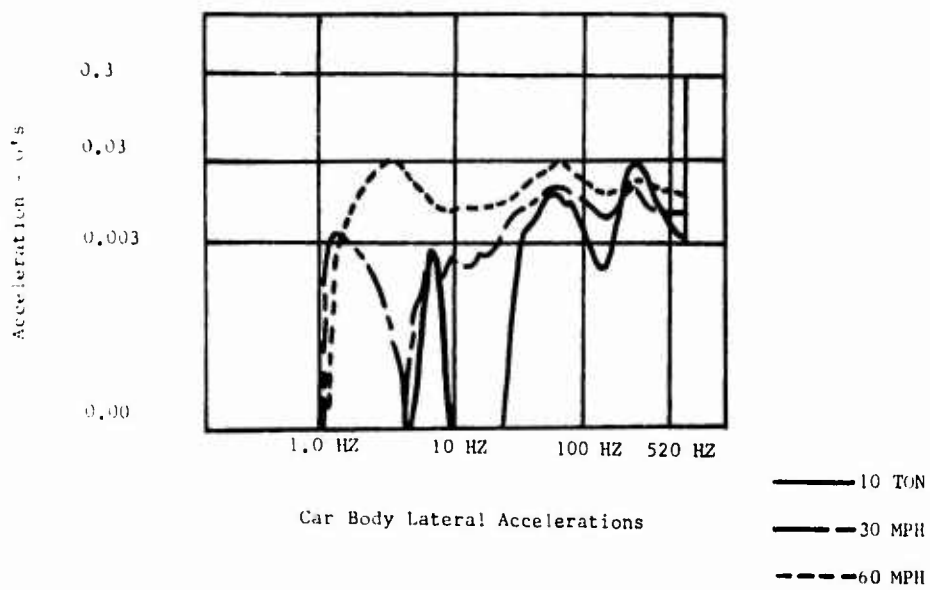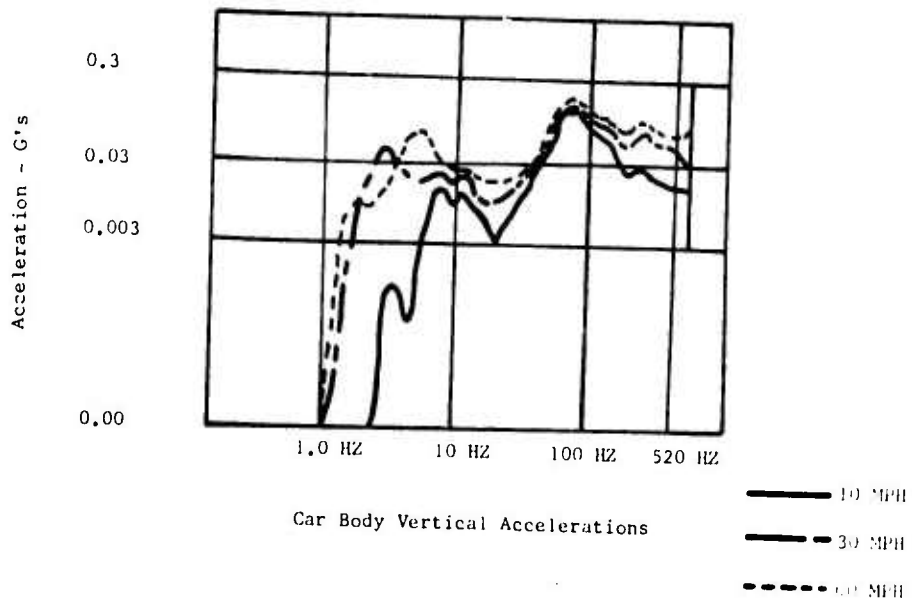
FIGURE 16

BARBER S-2 TRUCK
3-1/16" SPRINGS
STD. SNUBBING
EMPTY CAR

Car Body Lateral Accelerations

— MPH
— — MPH
- - - - MPH

FIGURE 17

151
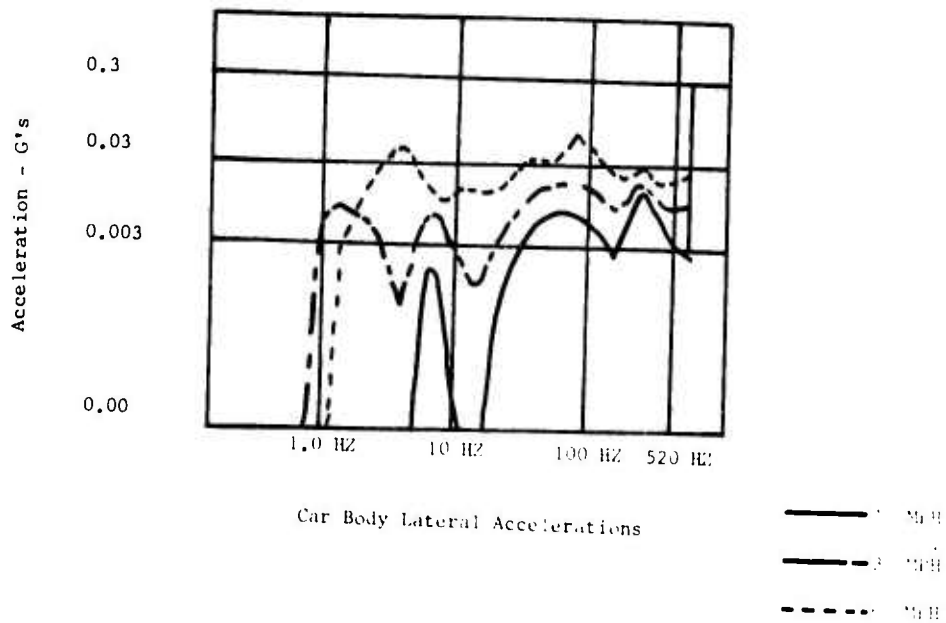
POWER SPECTRAL DENSITY

CAR BODY VERTICAL
FIGURE 18

EMPTY
36 TON
70 TON

FREQUENCY – HZ
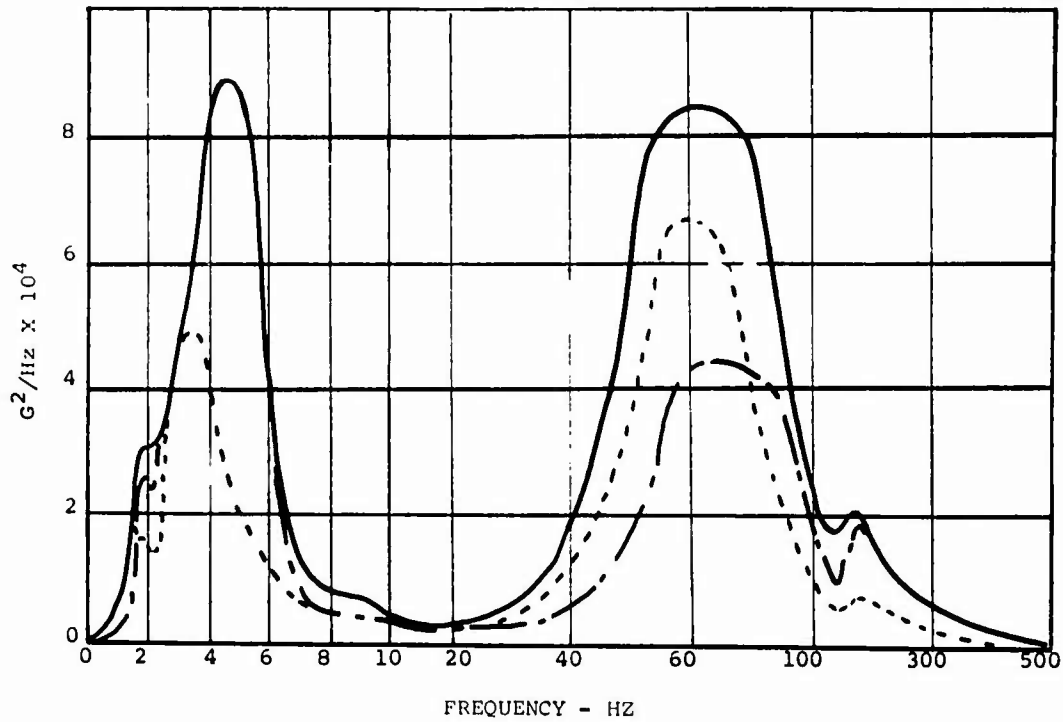
CAR BODY LATERAL
FIGURE 19

70 TON
36 TON
EMPTY

FREQUENCY – Hz

152
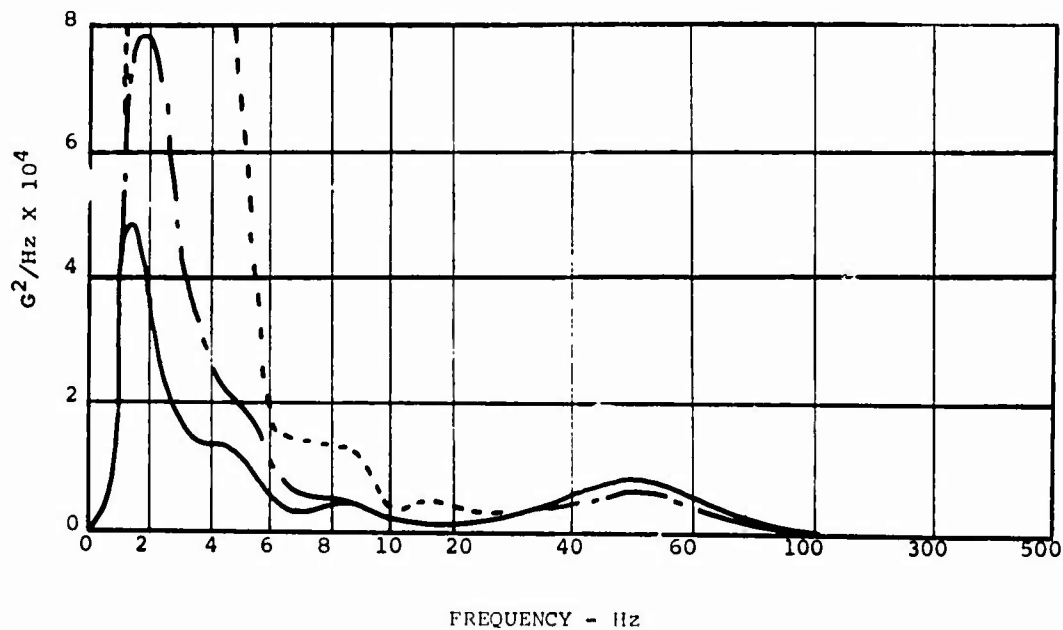
Barber S-2
3-1/16" Springs
70 Ton

CAR BODY VERTICAL
FIGURE 20

——— 60 MPH
——- 30 MPH
– – – 10 MPH

FREQUENCY - Hz
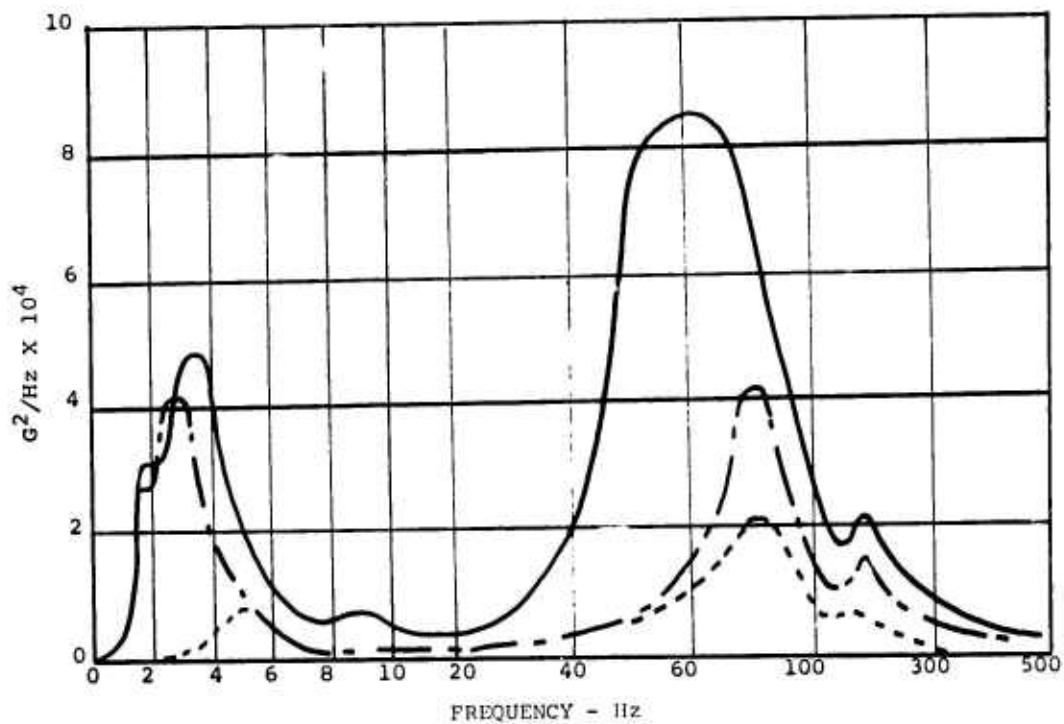
CAR BODY LATERAL
FIGURE 21

FREQUENCY - Hz

153
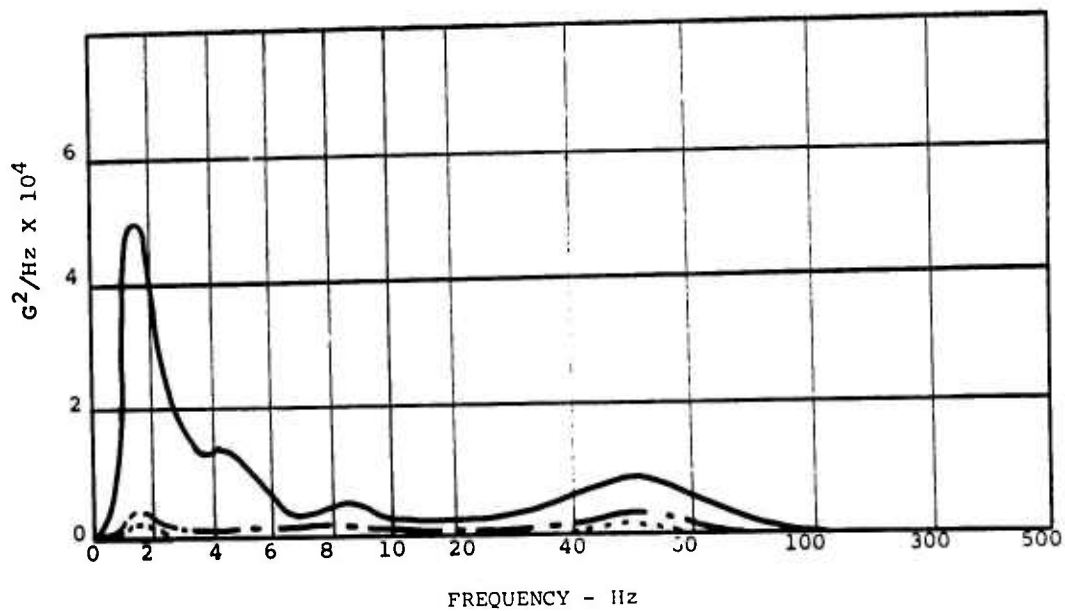
FIGURE 22   CAR BODY VERTICAL

SPEED - MPH
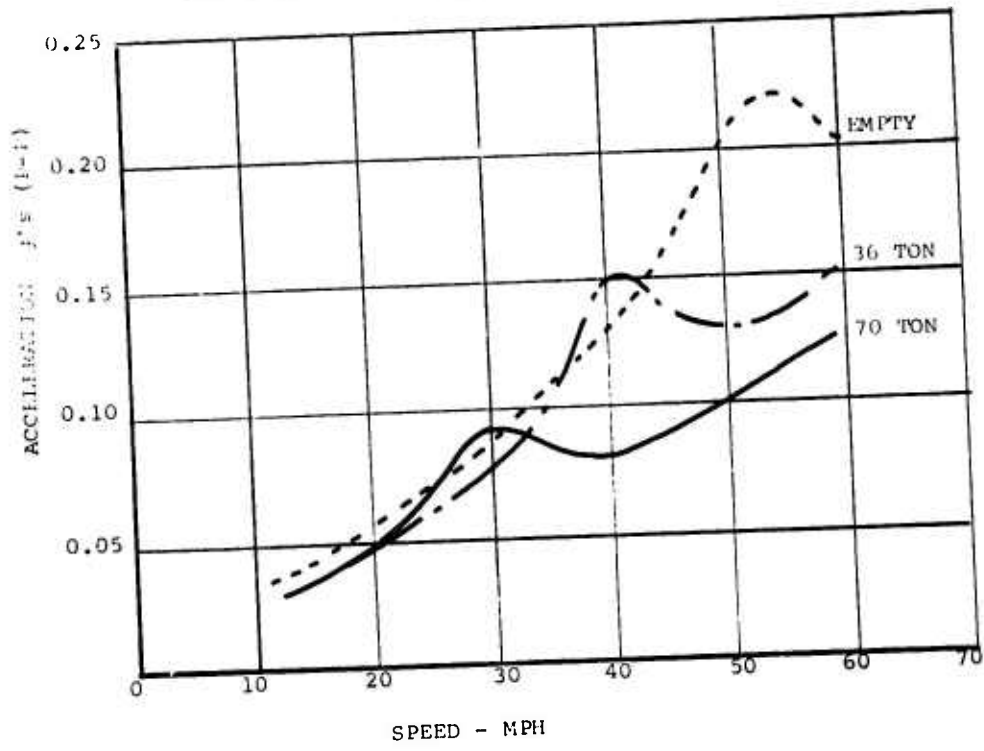
FIGURE 23   CAR BODY LATERAL

SPEED - MPH

154
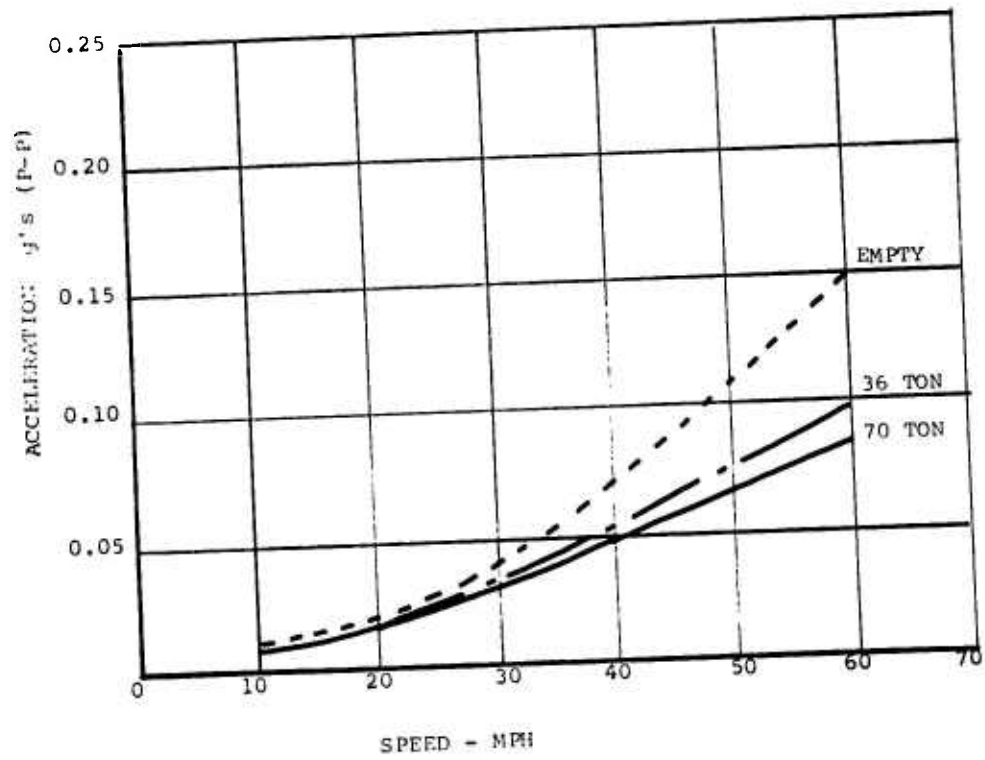
FIGURE 24   EFFECT OF PRIMARY SPRING RATE ON CAR BODY VERTICAL

SPEED - MPH
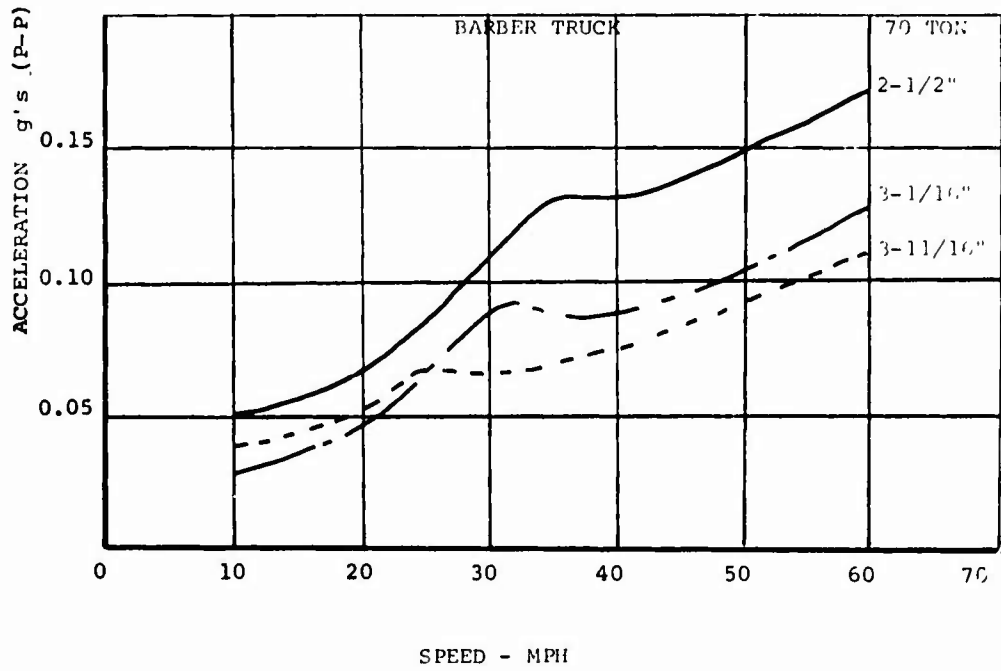
FIGURE 25   EFFECT OF PRIMARY SPRING RATE ON CAR BODY LATERAL

SPEED - MPH

155

FIGURE 26   CAR BODY VERTICAL

ASF VARI RATE SPRINGS

FIGURE 27   CAR BODY LATERAL

ASF VARI RATE SPRINGS

156
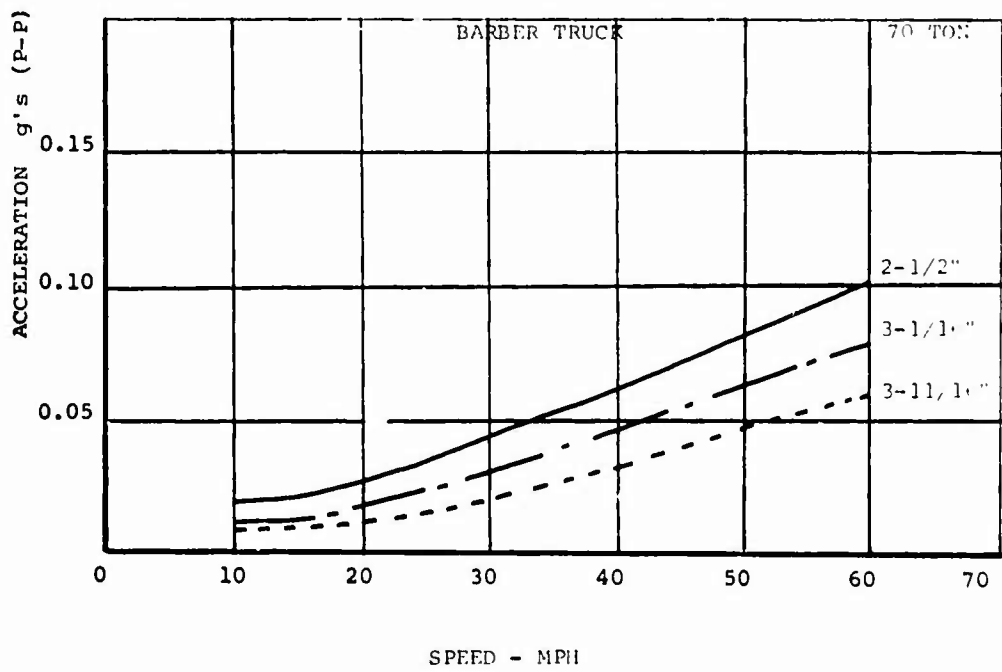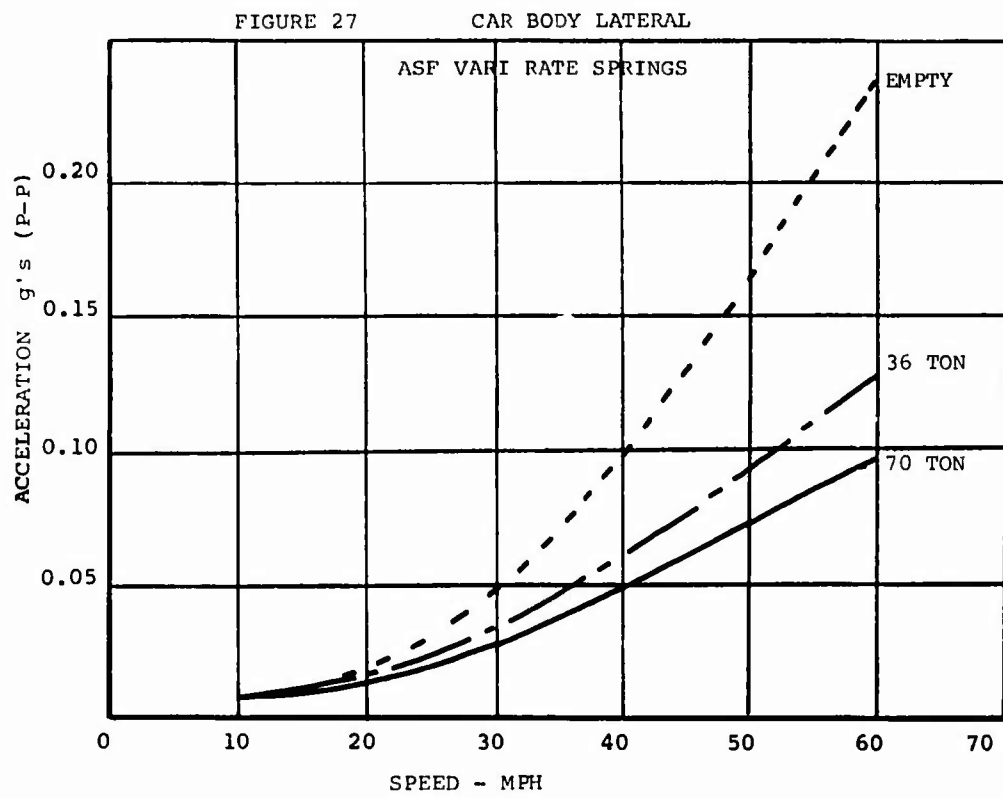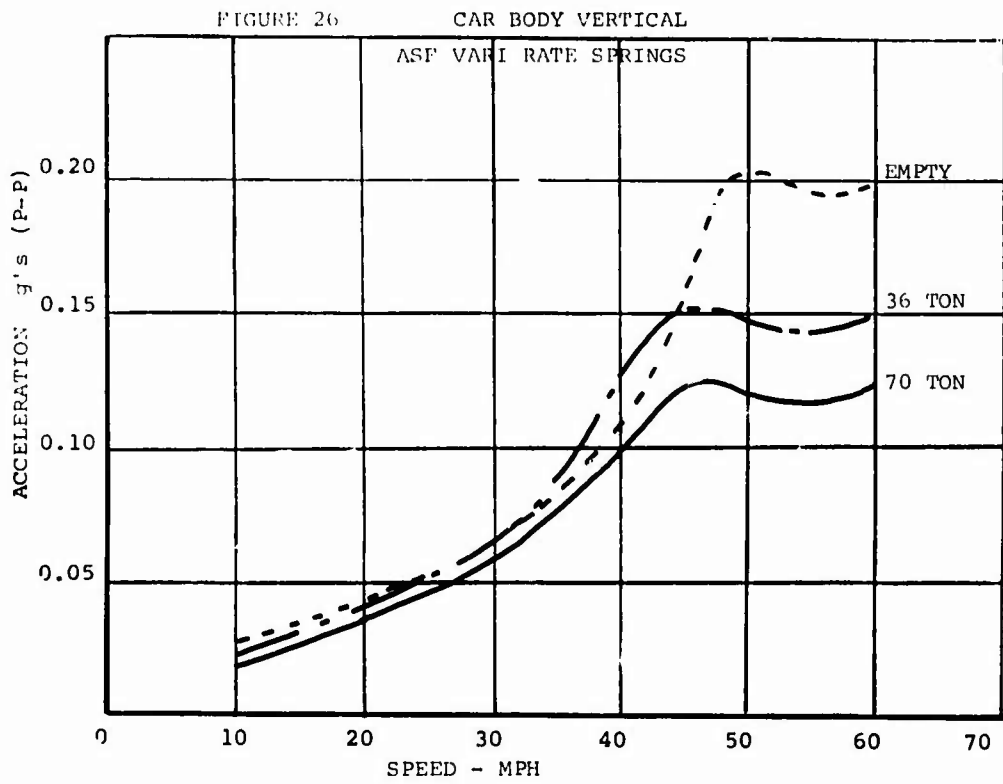
FIGURE 28   CAR BODY VERTICAL

SPEED - MPH
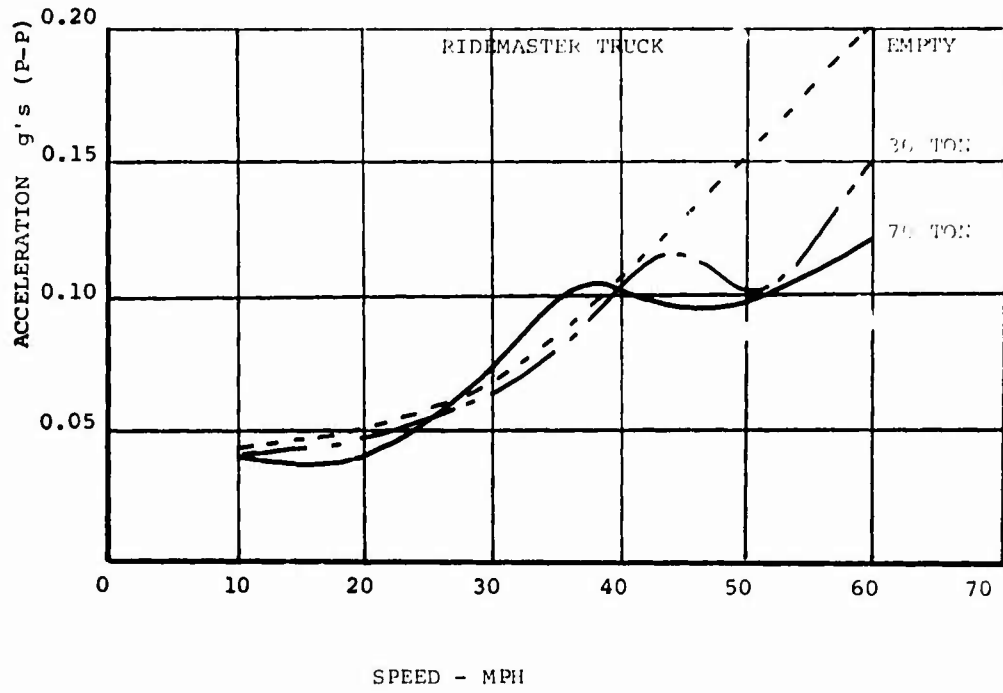
FIGURE 29   CAR BODY LATERAL

SPEED - MPH

157

FIGURE 30   CAR BODY VERTICAL

XL-70 TRUCK

ACCELERATION g's (P-P)

EMPTY
36 TON
70 TON

SPEED - MPH
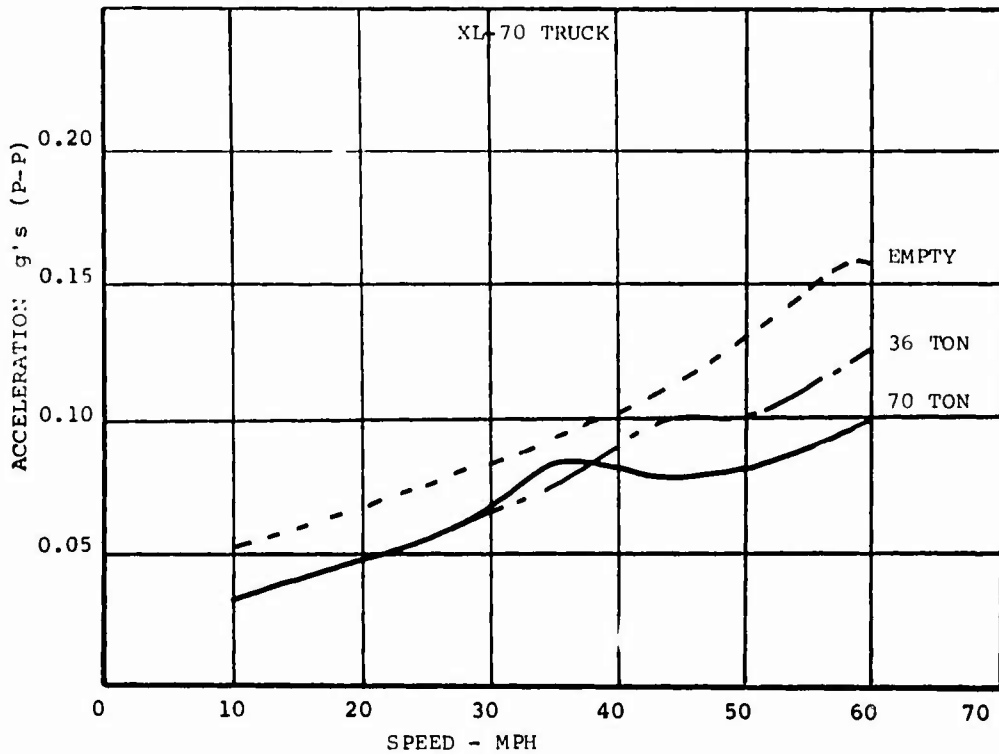
FIGURE 31   CAR BODY LATERAL

XL-70 TRUCK

ACCELERATION g's (P-P)

EMPTY
36 TON
70 TON

SPEED - MPH

158

FIGURE 32   CAR BODY VERTICAL
ROCKWELL TRUCK

FIGURE 33   CAR BODY LATERAL
ROCKWELL TRUCK

159

Mr. Parmenter (Naval Weapons Center, China Lake): On your psd analysis, what was the effective bandwidth filter?

Mr. Luebke: The data were applied on a one-third octave filter. The bandwidth varied in accordance with the center frequency. The smallest band, with a center frequency of around 1 1/2 Hz had a width of about 0.35 Hz. Out at 150 Hz the bandwidth was on the order of 100 Hz.
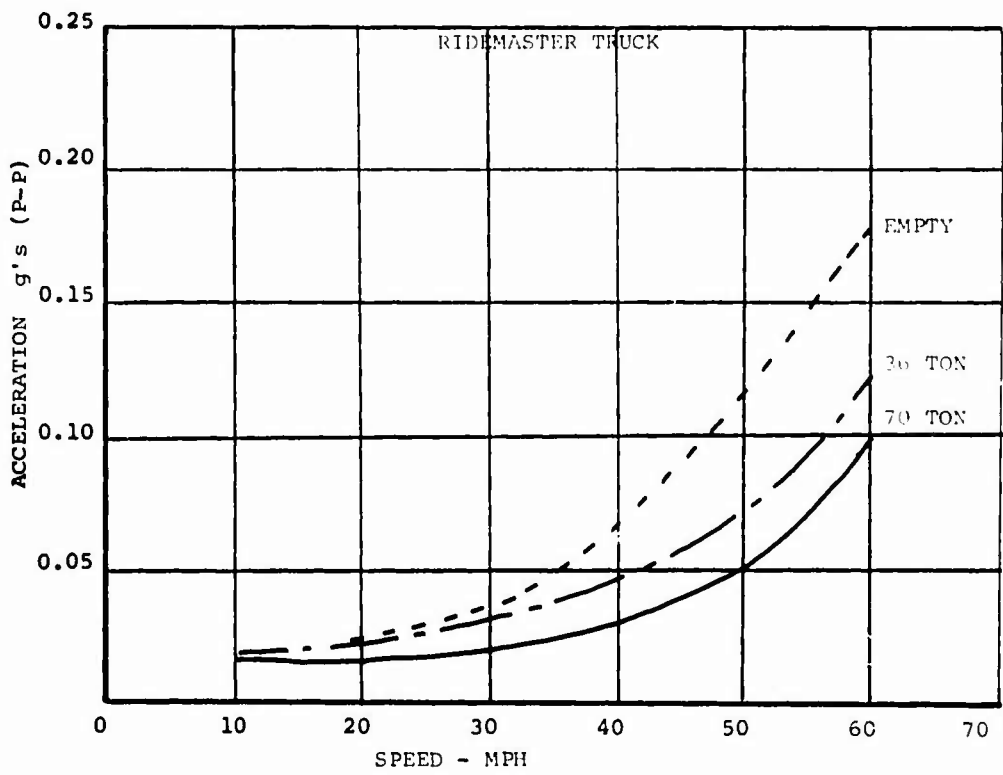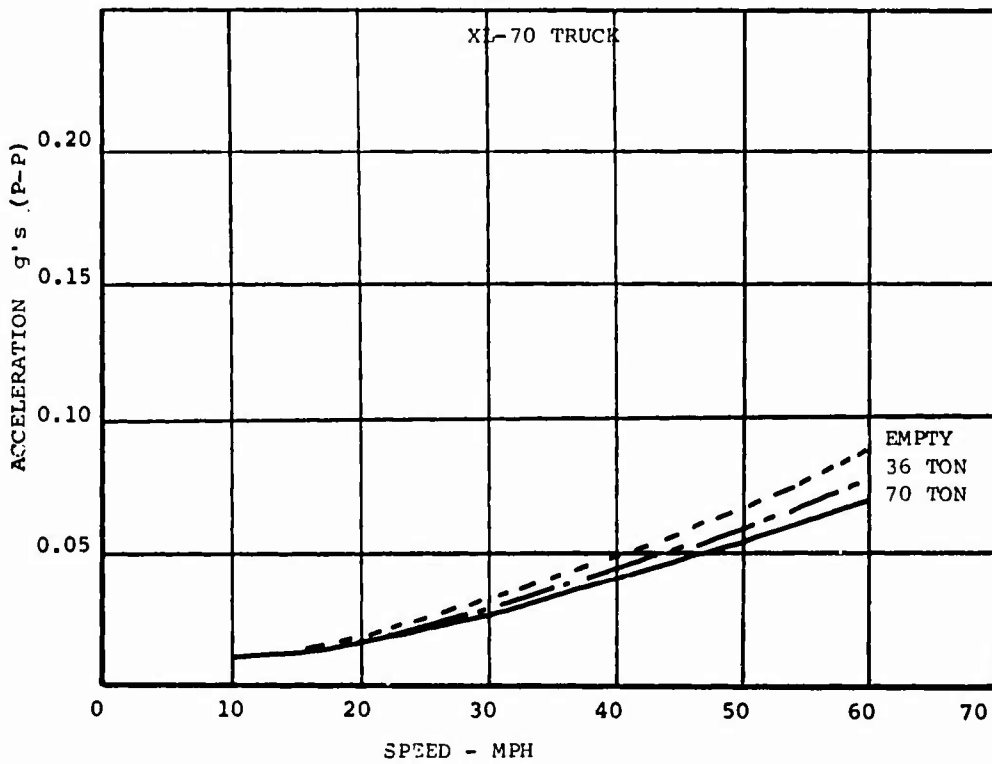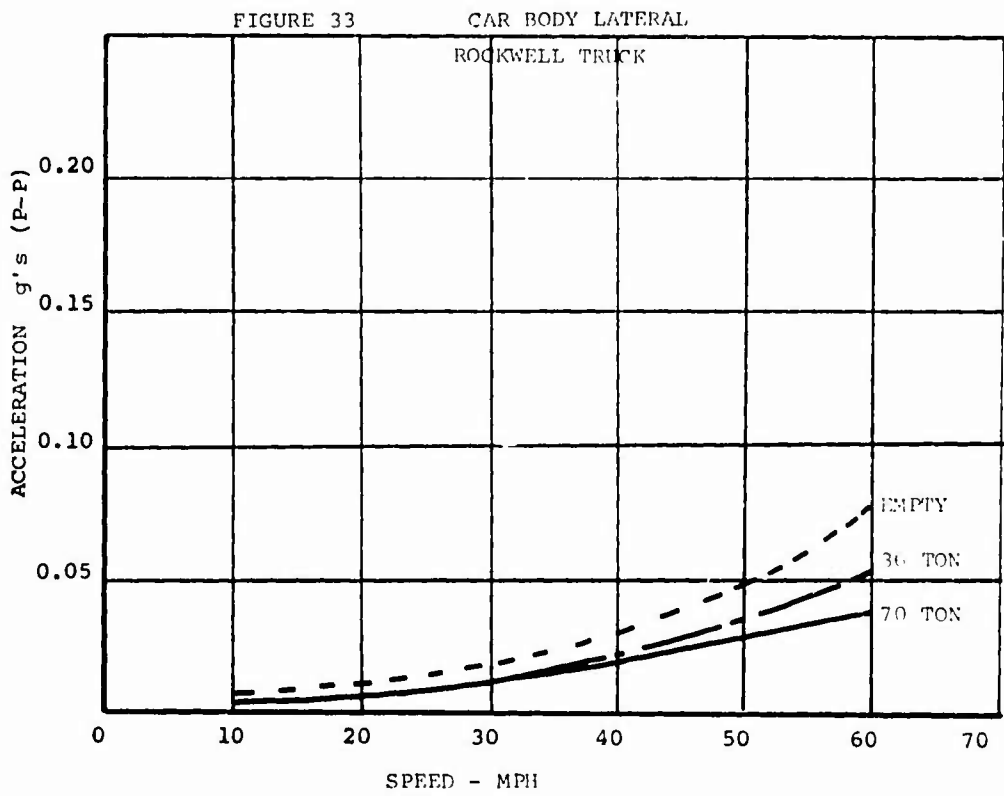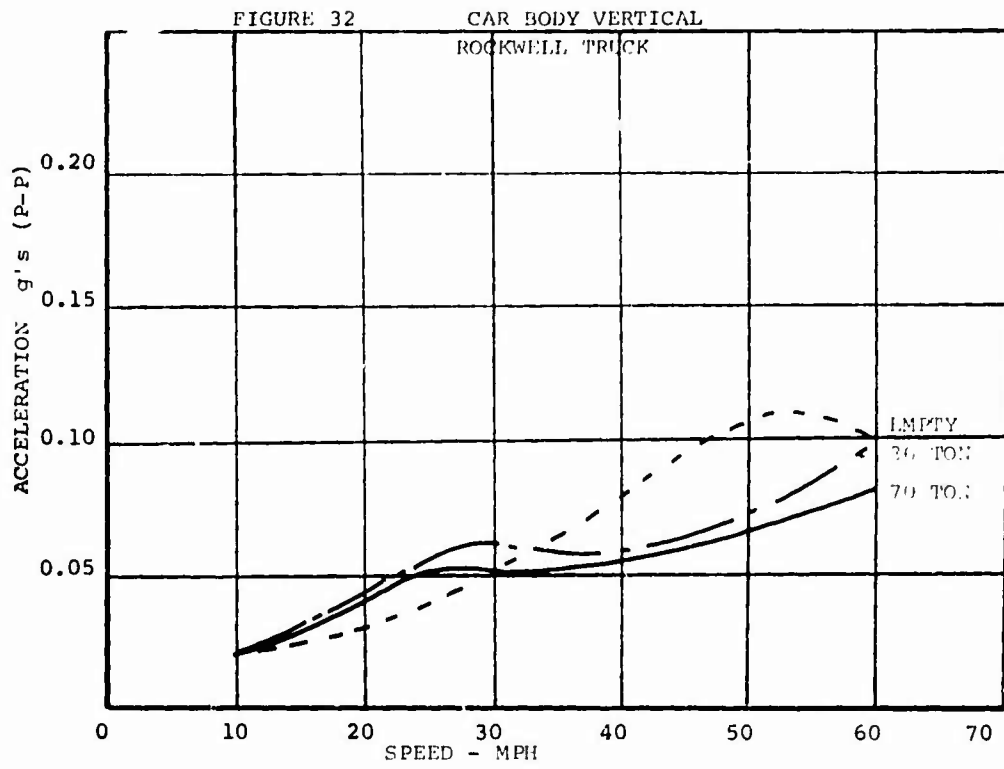
Mr. Parmenter: Were the results from this study incorporated in Mil STD-810?

Mr. Luebke: They have not been incorporated in Mil STD-810. Right now they are available from the Clearinghouse. The report is entitled "Vibrations of a fifty foot, seventy Ton Box Car".

Mr. Hughes (Naval Weapons Evaluation Facility): I was a little concerned that at higher speeds all your curves kept going up. I would have expected the energy in the frequency content to have peaked over. You mentioned some resonance, but you ended up with the tail end of the curve higher than the peak resonance.

Mr. Luebke: That is right. Three things are involved. The effect of speed on this vibration environment increases exponentially from zero. Also, the effect of track irregularities is exponential. Further, the frequency content of the spectrum increases in the same manner, however, the high frequency information is relatively constant. The data that you saw on the slides was the forcing frequency data below 10 Hz.

Mr. Galef (TRW Systems): For over 20 years now the principal, maybe the only, source of data of the type that you are presenting, has been something published by Guins. I am struck by the fact that the levels you seem to be reporting, even though you are dealing with artificially severe tracks, seem to be much much lower than that old data. Am I remembering wrong?

Mr. Luebke: No, you are quite accurate. The difference has been the technological change in freight equipment since the time Sergei Guins was running those tests back in 1948. Then the normal freight car was undamped with 1-5/8-inch-travel springs, or extremely stiff springs. The environment was indeed as rough as measured and reported at that time.

160

THE NOISE ENVIRONMENT OF A DEFLECTED-JET VTOL AIRCRAFT

S.L. McFarland and D.L. Smith
Air Force Flight Dynamics Laboratory
Wright-Patterson Air Force Base, Ohio

A noise survey conducted on a deflected-jet VTOL aircraft is
described. The test aircraft was mounted on a vertical thrust
stand with the nozzles oriented in the "hover-stop" position while
engine runs were made at different power settings. Forty-one (41)
microphones were located in the field on the port side of the air-
craft and six (6) microphones were located at positions near the
aircraft skin. The height of the field microphones was varied (5 ft,
10 ft, and 15 ft). One-third octave band spectra obtained from all
microphones and for all engine power settings were flat and did not
exhibit the "haystack" shape which is characteristic of a free jet.
Typical one-third octave band sound pressure level spectra and contours
of overall sound pressure levels are presented. Estimates of jet total
acoustic power are developed from the measurements and related to engine
operating parameters. Expressions are derived from the measurements to
predict the one-third octave band spectra at positions in the field and
on the vehicle from similarly configured aircraft for various engine
operating conditions.

INTRODUCTION

The design of VTOL aircraft structures
and the selection of their propulsion systems
will be strongly influenced by the noise
produced by the propulsion system. The in-
crease in propulsion power required for verti-
cal flight will be accompanied by an increase
in radiated acoustic energy. The radiated
acoustic pressures impinging on the aircraft
will be affected by operation of the propul-
sion system in close proximity to the ground.
Acoustic fatigue, which is generally restricted
to a small percent of structure for convention-
al aircraft, may affect nearly the entire
structure for a VTOL aircraft. Methods are
not currently available to predict the acoustic
environment from VTOL aircraft. The develop-
ment of such methods will rely heavily on
experimental data in that the mechanisms of
noise generation from candidate propulsion
systems are not completely understood. This
is especially true for a VTOL jet where the
operation in close proximity to the ground
might alter the noise source mechanisms which
exist in a free jet.

An acoustic survey was conducted at
Edwards Air Force Base on a Hawker-Siddeley
P1127 deflected-jet VTOL aircraft to provide
definition of the noise environment for this
type aircraft operating in a hover mode. The
survey and its measured results are reported
in Ref. [1]. The results are used here to
develop methods for predicting the acoustic
environment in the field and on a deflected-
jet VTOL aircraft as a function of nozzle
parameters, i.e., exhaust temperature, exhaust
Mach number, and nozzle diameter.

NOISE SURVEY

Test Aircraft

The test aircraft is shown in Fig. 1.
The propulsion system was a Bristol-
Siddeley Pegasus 5, ducted fan, lift-
thrust, jet engine. The design of this
engine for adaptation to the aircraft
incorporated four exit nozzles, two "cold"
plus two "hot", which are adjustable for
different modes of flight. This arrange-
ment results in a high vertical thrust/weight
ratio. Most of the fan discharge is fed to
two rotatable nozzles (the "cold" jets)
situated symmetrically on both sides of the
engine. The remainder of the fan discharge
passes through the high pressure compressor,
through the combustion chamber to the tur-
bines, and is exhausted through two more
rotatable nozzles (the "hot" jets) at both
sides of the rear of the engine. Rotation
of these four nozzles, which incorporate
deflecting vanes in the exit areas, enables
thrust to be directed rearward, forward, or
vertically for the desired flight mode. For
horizontal flight the nozzles are in the
positions indicated in Fig. 2. For vertical
thrust the nozzles are rotated downward 81°.
This position is designated as the "hover-stop
position". The 92.5% rpm engine setting in the
VTOL mode corresponds to the vertical takeoff
condition for this aircraft. Operational para-
meters for the engine are given in Table I.

161
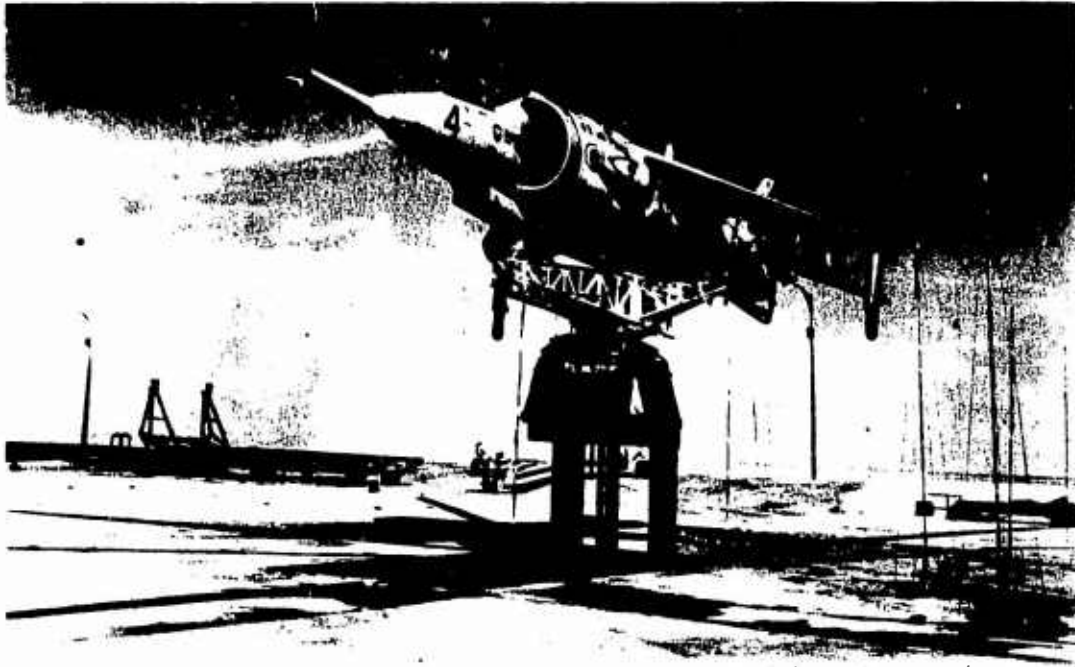
FIGURE 1, P1127 ON THE VERTICAL THRUST STAND

TABLE I

P1127 Aircraft Engine Data

Engine Condition % RPM	Gross Cold Thrust lb	Gross Hot Thrust lb	Cold Weight Flow lb/sec	Hot Weight Flow lb/sec	Cold Jet Velocity ft/sec	Hot Jet Velocity ft/sec	Cold Exit Total Temperature °R	Hot Exit Total Temperature °R	Cold Mach Nr	Hot Mach Nr
45	1600	1000	102	65	504	498				
60	3000	1900	136	92	709	664	606	1089	.606	.416
80	5500	4100	190	130	931	1014	676	1276	.767	.596
85	6300	5500	206	142	984	1223				
90	7000	6600	222	153	1014	1387				
MAX 97.5	7200	7200	230	160	1035	1447	721	1458	.832	.817

162
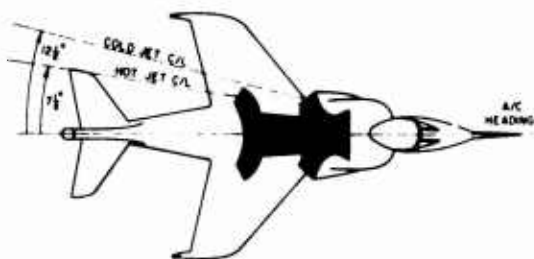
Test Setup and Run Conditions

The aircraft was mounted statically on a vertical thrust stand for all test conditions. The thrust stand stood in an open pit surrounded by a cement pad which extended at least 100 feet in all directions. The jets were directed such that the primary flow impinged on the concrete rather than into the pit. Measurements were made at the engine power settings given in Table I for aircraft heights of 10 feet and 15 feet and for field microphone heights of 5 feet, 10 feet, and 15 feet.

Forty-one (41) microphones were located on the port side of the aircraft in the field in a plane parallel to the ground as shown in Fig. 3. These microphones were positioned with respect to the centerline of the hot jet in its forward flight position as shown in Fig. 2. Six (6) microphones were positioned with their diaphragms between 2 and 4 inches from, and parallel to, the aircraft skin at the locations shown in Fig. 4.
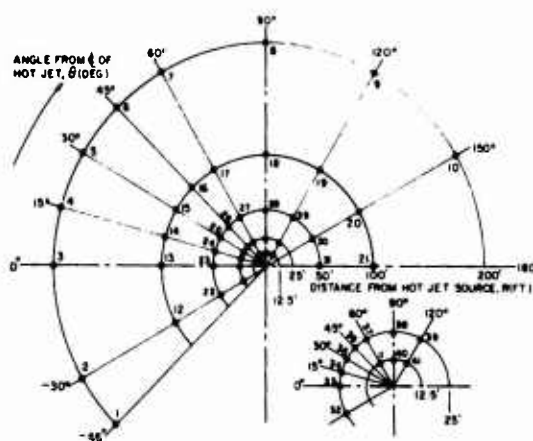
FIGURE 3 . MICROPHONE FIELD LOCATIONS AND SPOT NUMBER IDENTIFICATION
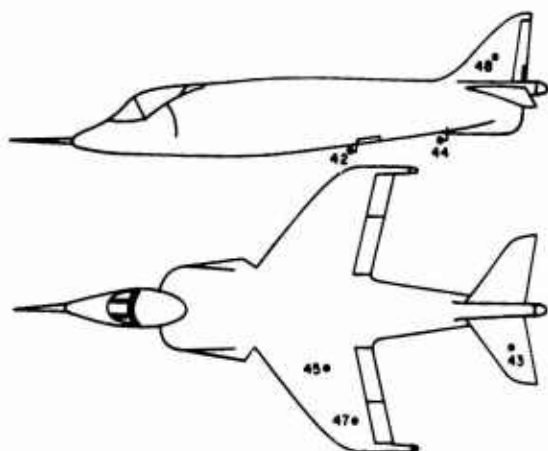
FIGURE 4, LOCATIONS OF MICROPHONES ON AIRCRAFT

Survey Results

One-third octave band spectra were obtained from each microphone, corresponding to those runs where the nozzles were set at 81°, the hover-stop position. The most notable characteristic of the data obtained from the noise survey was that these spectra were all essentially "flat" and did not exhibit the "haystack" shape characteristic of a free jet. This is illustrated by the spectra obtained from microphone 25, given in Fig. 5. Microphone 25 was located 50 feet and at 30 degrees from the centerline of the hot jet (see Fig. 3). The shape of these spectra is typical of the spectra obtained from microphones at other positions in the field and on the aircraft.

163

FIGURE 5 . 1/3 OCTAVE BAND SOUND PRESSURE LEVELS IN FIELD OF A DEFLECTED-JET VTOL AIRCRAFT WITH NOZZLES AT 81° (HOVER STOP POSITION)

Contours of equal overall sound pressure level (SPL*) for a plane parallel to and 15 feet above the ground plane are given in Fig. 6. They were faired manually from the overall SPL readings obtained at each microphone position. The contours exhibit lobes corresponding to the hot and cold nozzles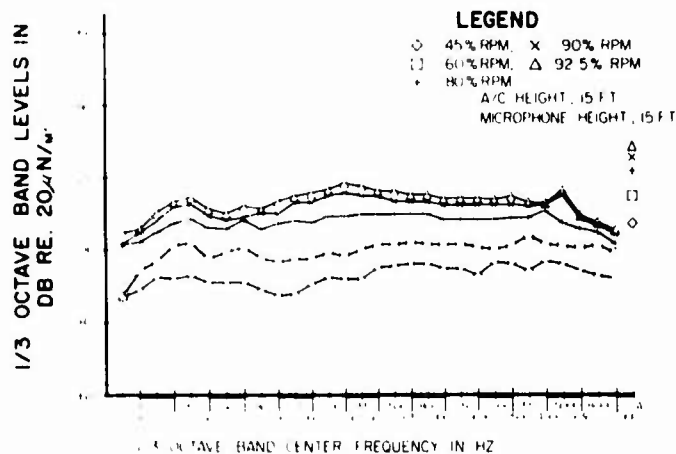 at the lower power settings; however, as the engine power setting is increased, the contours become more nearly circular.

Contours of equal overall SPL for planes vertical to the ground plane are presented in Figs. 7, 8, and 9. These figures correspond to the 60, 80, and 92.5% rpm engine operating conditions. In each figure contour plots are shown for four (4) different vertical planes at different angles (θ) referenced to the tail heading of the test aircraft from a point directly below the hot jet. The contours were faired manually through data obtained from all of the field microphones and from the microphone on the vertical stabilizer which was at a height of approximately 18 feet.

The overall SPL's obtained at the microphone positions located on the aircraft as shown in Fig. 4 are presented in Table II for the specified engine power settings with the aircraft at a height of 15 feet.

$$\overline{SPL} = 10 \log \frac{\overline{P^2}}{P_0^2}$$

where: P^2 = mean square sound pressure, N/m^2
P_0 = reference pressure = 20 $\mu N/m^2$

TABLE II

Overall Sound Pressure Levels on the P1127 Aircraft

MICROPHONE LOCATIONS	60%RPM	80% RPM	92.5% RPM
Under Wing Inboard	132 dB	141 dB	143 dB
Under Wing Outboard	132 dB	140 dB	143 dB
Under Fuselage Middle	127 dB	133 dB	138 dB
Under Fuselage Tail	126 dB	131 dB	138 dB
Under Horizontal Stabilizer	121 dB	131 dB	138 dB
On Vertical Stabilizer	116 dB	123 dB	129 dB

164

AXIAL DISTANCE FROM HOT JET, FEET

FIGURE 6. OVERALL SOUND PRESSURE LEVEL CONTOURS IN THE FIELD OF A P1127 AIRCRAFT

DISTANCE FROM HOT JET, FEET
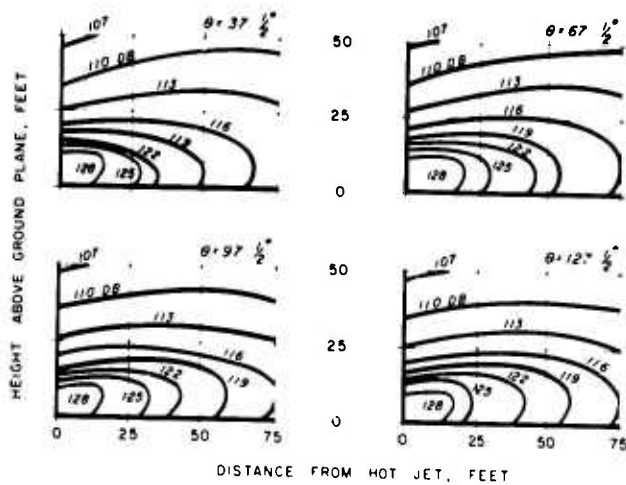
FIGURE 7. OVERALL SOUND PRESSURE LEVEL CONTOURS FOR SELECTED VERTICAL PLANES IN THE P1127 NOISE FIELD (60% RPM ENGINE SETTING)

165
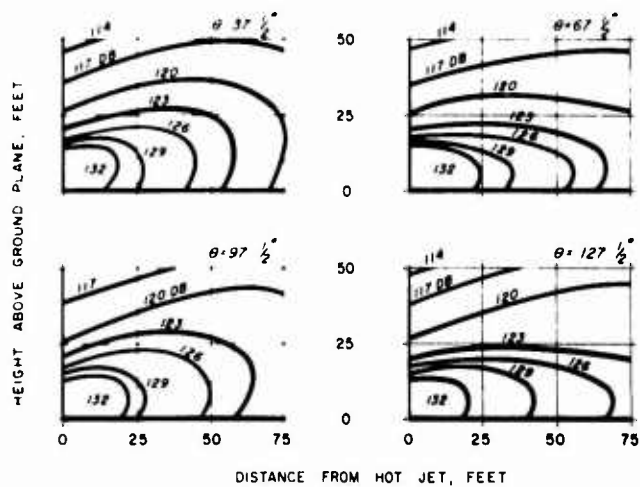
FIGURE 8, OVERALL SOUND PRESSURE LEVEL CONTOURS FOR
SELECTED VERTICAL PLANES IN THE P1127
NOISE FIELD (80% RPM ENGINE SETTING)

FIGURE 9, OVERALL SOUND PRESSURE LEVEL CONTOURS FOR
SELECTED VERTICAL PLANES IN THE P1127
NOISE FIELD (92.5% RPM ENGINE SETTING)

166

ESTIMATION OF TOTAL ACOUSTIC POWER

The aircraft can be described as a noise source from the acoustic power radiated by the jets and the associated directionality of the noise. In this section the overall SPL's measured in the field during the noise survey are used to estimate the total radiated jet acoustic power. The measured SPL's were used directly to estimate the acoustic power except where pure tone compressor noise was obviously present. When this occurred, a ca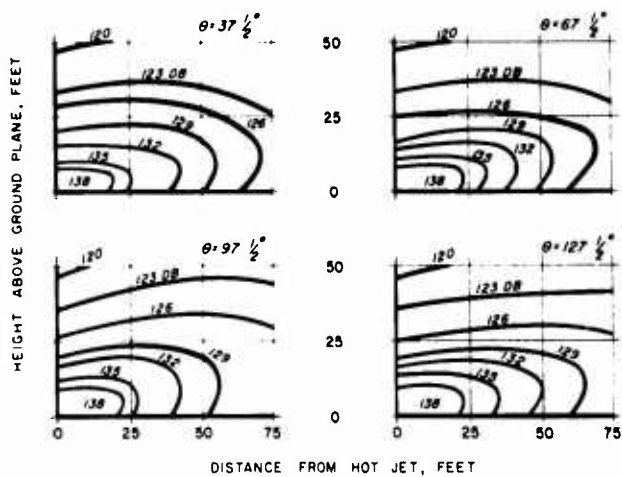lculated overall SPL was used which was obtained by subtracting the one-third octave band level containing the compressor noise from the measured overall level. In no case did this correction exceed 3 dB. No attempt was made to remove the broad band noise components generated by the compressor and other noise sources.

The total acoustic power (W) generated by a source above the ground plane can be determined by integrating the sound intensity (I) over a hemispherical area (A) centered at the source, i.e.,

$$W = \int_A I \, dA \qquad (1)$$

The sound intensity at any point in the far field of the source is given by

$$I = \frac{P^2}{\rho c} \qquad (2)$$

where I = sound intensity
P = sound pressure
ρ = density of air
c = speed of sound in air

The total acoustic power is then given by

$$W = \int_A \frac{P^2}{\rho c} \, dA \qquad (3)$$

The total acoustic power can be estimated by dividing the hemisphere into n representative areas such that the sound pressure is nearly constant over each area, calculating the acoustic power for each area, and then summing the results, i.e.,

$$W = \sum_{i=1}^{n} \left(\frac{P^2}{\rho c}\right)_i A_i \qquad (4)$$

The above procedure was used to estimate the total acoustic power generated by the aircraft. Since the sound pressure distribution was assumed to be symmetrical about the test aircraft, the total acoustic power was obtained by doubling the result determined from a quarter sphere. The quarter spheres were divided as shown in Fig. 10. They were divided circumferentially into half lunes or $\pi R^2/12$ (j = 1 through j = 12) and each half lune was divided
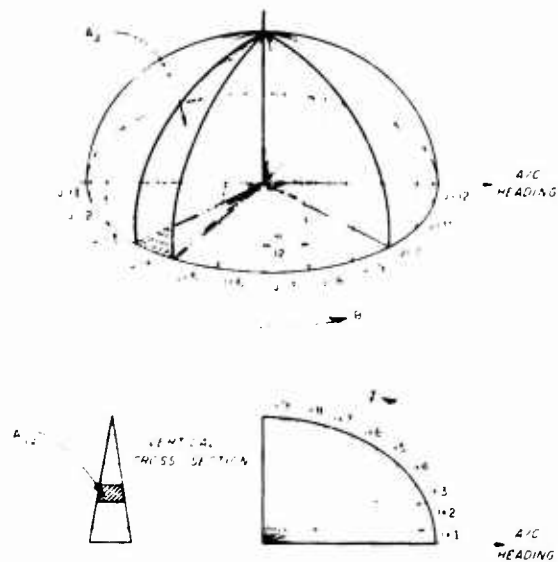
FIGURE 10. ISOMETRIC OF HEMISPHERE CENTERED ON GROUND BELOW P1127 AIRCRAFT HOT JET EXIT SHOWING AREAS, A_{ij}

into nine areas (i = 1 through i = 9) where R is the radius of the reference hemisphere. Each area A_i in one of the "j" half lunes is determined from:

$$A_i = \frac{\pi R^2}{6} (\sin \phi_i - \sin \phi_{i-1}) \qquad (5)$$

where ϕ_1 and ϕ_2 are angles of elevation relative to a point below the hot jet on the ground plane. The total acoustic power in watts can then be estimated from the following:

$$W_e = \frac{\pi R^2 P_0^2}{6 \rho c} \sum_{j=1}^{12} \left[\sum_{i=1}^{9} (\sin \phi_i - \sin \phi_{i-1}) \times \left(\text{antilog} \frac{SPL_{ij}}{10}\right) \right]_j \qquad (6)$$

where W_e = estimated total acoustic power, watts
R = radius of reference hemisphere, m
P_0 = 20 μN/m^2
ρc = 416 $\frac{\text{N-sec}}{\text{m}^3}$
ϕ_i = angle of elevation from an origin on the ground plane
SPL_{ij} = sound pressure level associated with A_{ij}

167

... [illegible text] ... jet power ... "2" half lune by ... "4" summations, sums the contributions ... of the other half lunes, and then doubles ... [illegible] ... the ... of the ... distribution. The ... corre-... N_o ... determined from ... overall ... similar to those ... 7, 8, and 9.

A ... computer was used ... all data the net total acoustic power from ... Estimates were made for engine power settings of 60, 80, and 92.5 rpm and for hemispheres of 25 and 50 foot radii. The resulting estimates given in Table III are expressed in sound power level (PWL) in dB as below:

$$PWL = 10 \log S_o/10^{-12} \quad (7)$$

where S_o is the estimated acoustic power in watts determined from Eq. (6).

TABLE III

Estimates of P1127 Jet Total
Acoustic Power Level

ENGINE POWER SETTING	Radius of Reference Hemisphere	
	25 ft	50 ft
60 RPM	148.5 dB	148.2 dB
80 RPM	155.1 dB	154.2 dB
92.5 RPM	159.5 dB	159.2 dB

The values of PWL determined from the above results which are taken as representative of the total acoustic power generated by the P1127 aircraft for 60, 80, and 92.5% rpm power settings are respectively 148, 154, and 159 dB.

NOISE FIELD PREDICTION

The noise environment of a similarly con-figured aircraft operating in the hover mode can be obtained from the P1127 noise measure-ments by relating the estimated radiated acoustic power to engine or nozzle parameters and determining the directional properties of the noise.

When operating in the VTOL mode the aircraft constitutes multiple noise sources. The pres-ence of deflecting vanes in the exits of the four (4) nozzles (2 "hot" + 2 "cold") create multiple, efficient high-frequency noise gener-ation mechanisms. Also, the vortices generated by the jet exhaust impinging on the ground plane will contribute additional noise sources. Ideally, each noise source should be identified and related to its own controlling parameters. The contribution from all sources should be summed to obtain the total acoustic power and radiated noise for each operating condition. Such an approach would require a rather complete description of the noise generation mechanisms associated with each source and would result

in complicated expressions relating the acoustic power and radiated noise to the engine or nozzle parameters. Although this comprehensive approach was not taken it was considered desirable to obtain an expression which would account for the operation of the "cold" and "hot" nozzles.

An expression for the mean square sound pressure of free jets taken from Ref. [1] was modified to obtain means for predicting the total acoustic power of a deflected-jet VTOL aircraft. The following relationship was assumed:

$$W = K \left[(T^{1.54} M^{6.34} D^2)_{HOT} + (T^{1.54} M^{6.34} D^2)_{COLD} \right]^n \quad (8)$$

where T = exit total temperature, °R
M = exit Mach number
D = exit diameter, feet

Expressed as sound power level (PWL) in db re 10^{-12} watts this equation becomes:

$$PWL = 10n \log \left[(T^{1.54} M^{6.34} D^2)_{HOT} + (T^{1.5} M^{6.34} D^2)_{COLD} \right] + 10 \log K + 120 \quad (9)$$

The PWL's determined from the measurements are plotted in Fig. 11 versus $10 \log \left[(T^{1.54} M^{6.34} D^2)_{HOT} + (T^{1.54} M^{6.34} D^2)_{COLD} \right]$. From a least square best fit it was determined that n = .74 and 10 log K = 1.6, therefore:

$$PWL = 7.4 \log \left[(T^{1.54} M^{6.34} D^2)_{HOT} + (T^{1.54} M^{6.34} D^2)_{COLD} \right] + 121.6 \quad (10)$$
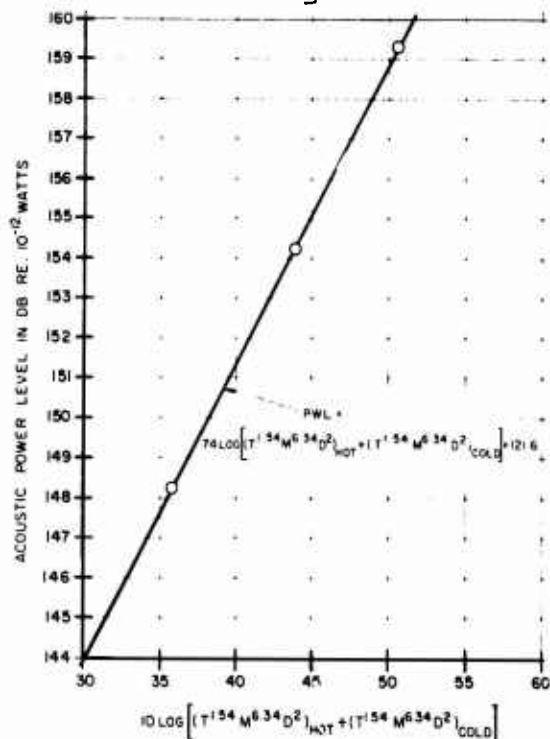

FIGURE 11, ESTIMATED TOTAL ACOUSTIC POWER VS P1127 JET NOZZLE PARAMETERS

The above expression can then be used to determine the noise environment in the field if the directional properties can be obtained. From Eq. (10) the space average SPL at any distance R can be found from:

$$SPL_S = PWL - 10 \log R^2 + 2.5 \qquad (11)$$

where SPL_S = space average SPL, dB re 20 $\mu N/m^2$
PWL = total acoustic power level, dB re 10^{-12} watts
R = distance from source to field point, feet

The SPL at any point in the field can then be determined from:

$$SPL(R,\theta,\phi) = \overline{SPL_S}(R) + DI(\theta,\phi) \qquad (12)$$

where $SPL(R,\theta,\phi)$ = SPL at field point (R,θ,ϕ), dB
$\overline{SPL_S}(R)$ = space average SPL at distance R, dB
$DI(\theta,\phi)$ = directivity index, dB

Substituting Eqs. (10) and (11) into Eq. (12) gives:

$$SPL(R,\theta,\phi) = 7.4 \log\left[(T^{1.54}M^{6.34}D^2)_{HOT} + (T^{1.54}M^{6.34}D^2)_{COLD}\right] - 10 \log R^2 + 124 + DI(\theta,\phi) \qquad (13)$$

An estimation of the directivity index $DI(\theta,\phi)$ can be made by noting that contours of equal SPL in a plane parallel to the ground become nearly circular for the higher engine power settings. This was particularly true for $22.5° \leq \theta \leq 172.5°$, where $\theta = 180°$ corresponds to the aircraft heading. Consequently, in this range it is assumed that $DI(\theta,\phi) = DI(\phi)$. Fig. 12 presents a curve for $DI(\theta,\phi)$ between $\theta = 22.5°$ and $172.5°$, and another curve for values of θ outside this range.

These curves were obtained by solving Eq. (13) for $DI(\theta,\phi)$ for all engine power conditions. The values inserted for $SPL(R,\theta,\phi)$ were those obtained from contours as given in Figs. 7, 8, and 9 at a distance of R = 50 ft. The resulting curves are approximations and differ from individual values by as much as 2 dB for $22.5° \leq \theta \leq 172.5°$ and by as much as 5 dB for θ outside this range.

Equation (13) and Fig. 12 can be used to predict the overall sound pressure level at any point in the field of a deflected-jet VTOL aircraft. The coordinates of the field point (R,θ,ϕ) are taken with respect to an origin on the ground directly below the hot jet, even though the source of noise is not located on the ground.

In order to test the accuracy of the prediction, Eq. (13) and Fig. 12 were used to obtain the predicted overall SPL for the 60, 80, and 92.5% rpm conditions at points corresponding to microphone locations 10 and 15 feet off the ground. The measured SPL was subtracted from the predicted value to determine the error. The results are summarized in Table IV which presents the mean error, the standard deviation, and the maximum and minimum

TABLE IV

Error Analysis of Noise Prediction Technique

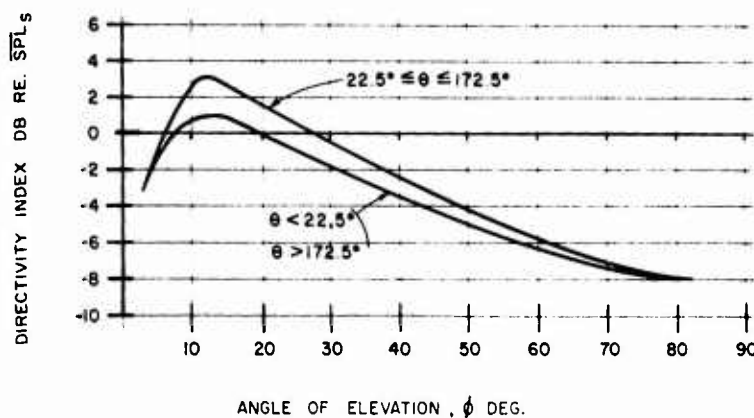| RANGE OF θ	MEAN ERROR dB	STANDARD DEVIATION dB	RANGE OF ERROR dB
$\theta < 22.5$	2.3	2.3	+6.9 -2.2
$22.5 \leq \theta \leq 172.5$	0	2	+6.2 -5.3

FIGURE 12, THE DIRECTIVITY OF THE NOISE FROM A DEFLECTED-JET VTOL AIRCRAFT
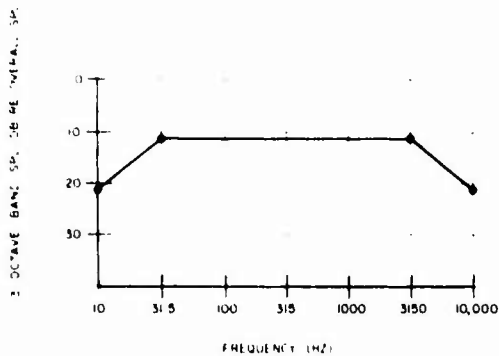
169

FIGURE 13. CHARACTERISTIC ONE THIRD OCTAVE BAND SPECTRUM FOR A DEFLECTED JET VTOL AIRCRAFT

It was pointed out previously that the one-third octave band SPL spectra obtained at all points in the P1127 noise survey were nearly flat. Consequently, a characteristic one-third octave band spectrum can be applied to all points in the field. Such a characteristic spectrum is given in Fig. 13. This spectrum is flat between 31.5 Hz and 3150 Hz where the one-third octave band level is 11 dB below the overall SPL found from Eq. (13) and Fig. 12. Consequently, not only the overall SPL but also the one-third octave band spectrum can be estimated for any position in the field given the coordinates at that location, the exhaust temperature, exhaust Mach number, and nozzle diameter.

PREDICTION OF NOISE ON AIRCRAFT

The procedures used in the previous section are limited to predicting the noise levels in the field of a deflected-jet VTOL aircraft and are not expected to apply to positions in close proximity to the aircraft skin. However, expressions can be obtained for predicting the SPL's on deflected-jet VTOL aircraft using the SPL's measured for this case.

Measurements were made in four general areas near the aircraft skin: (1) under the wing, (2) under the fuselage, (3) under the horizontal stabilizer, and (4) on the vertical stabilizer. These locations are shown in Fig. 4 and the resulting sound pressure levels are given in Table II.

The measured overall SPL's are plotted in Fig. 14 versus $10 \log \left[(T^{1.54}M^{6.34}D^2)_{HOT} + (T^{1.54}M^{6.34}D^2)_{COLD} \right]$ for each of the four areas. A least square best fit line is given in Fig. 14 for each area. The corresponding expressions are:

a. Under Wing,

$$SPL_{OA} = 7.5 \log \left[(T^{1.54}M^{6.34}D^2)_{HOT} + (T^{1.54}M^{6.34}D^2)_{COLD} \right] + 105.7 \qquad (14)$$

b. Under Fuselage,

$$SPL_{OA} = 7.7 \log \left[(T^{1.54}M^{6.34}D^2)_{HOT} + (T^{1.54}M^{6.34}D^2)_{COLD} \right] + 98.7 \qquad (15)$$
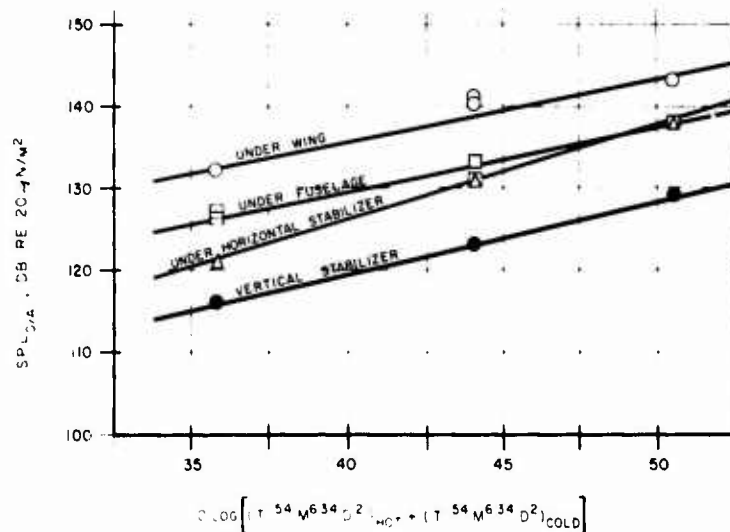

FIGURE 14. OVERALL SPL'S AT VARIOUS LOCATIONS ON A DEFLECTED-JET VTOL AIRCRAFT VS JET NOZZLE PARAMETERS

170

c. Under Horizontal Stabilizer,

$$SPL_{OA} = 11.5 \log \left[(T^{1.54}M^{6.34}D^2)_{HOT} + (T^{1.54}M^{6.34}D^2)_{COLD} \right] + 80.1 \qquad (16)$$

d. On Vertical Stabilizer,

$$SPL_{OA} = 8.7 \log \left[(T^{1.54}M^{6.34}D^2)_{HOT} + (T^{1.54}M^{6.34}D^2)_{COLD} \right] + 84.6 \qquad (17)$$

where T, M, and D are as defined in Eq. (8).

The one-third octave band spectra measured on the aircraft were also nearly flat. Consequently, it is assumed that the one-third octave band spectra for similar locations on deflected-jet VTOL aircraft can be predicted using the characteristic spectrum given in Fig. 13.

Equations (14) through (17) and Fig. 14 can be used to predict the noise in areas corresponding to the above on deflected-jet VTOL aircraft of similar configuration. Some degree of extrapolation would be required to determine the SPL's at other locations on the aircraft.

CONCLUDING REMARKS

It was found from the measurements that the spectra of the sound pressures associated with deflected-jet VTOL aircraft are nearly "flat" and do not exhibit the "haystack" shape typical of a single free jet. It is expected that this is primarily due to the presence of multiple noise sources. Also, operation in a VTOL mode may have altered the noise source mechanisms compared to operation in a free field.

Noise prediction methods have developed above for deflected-jet VTOL aircraft based on the results of this noise survey. It is expected that these methods will apply reasonably well to all aircraft of similar configuration operating in the VTOL mode. However, they should be applied judiciously where different airplane and engine configurations are being considered.

REFERENCES

1. Plumblee, H.E., Ballentine, J.R., and Passinos, B., "Near Field Noise Analysis of Aircraft Propulsion Systems with Emphasis on Prediction Techniques for Jets", AFFDL-TR-67-43, Aug. 1967

VIBRATION SIGNATURE ANALYSIS OF BEARINGS
AND ELECTRONIC PACKAGES

Charles H. Roos
General Electric Company
Aerospace Electronic Systems
Utica, New York

Vibration signature analysis methods have been developed at General Electric Aerospace Electronic Systems which can be readily and inexpensively applied to assure the quality of rolling bearings and electronic packages. These methods detect a loose item inside a package, a weak bond between a microcircuit substrate and its case, and surface defects on the balls or races of bearings. This paper presents the methods which have been developed and the results obtained in applying vibration signature analysis to the inspection of product lines.

INTRODUCTION

Aerospace Electronic Systems (AES) has developed and is successfully using vibration signature analysis* techniques to inspect and assure the quality of bearings and electronic packages. These inspections detect the following types of defects:

1) Loose or free items inside a package, subassembly, or component

2) Weak bond between a microcircuit substrate and its case

3) Surface defects (e.g., pits, scratches, spalling, foreign particles) on the balls or races of bearings.

The vibration signature analysis methods developed at AES are nondestructive, can be readily applied to product lines, and require only the equipment generally used in vibration laboratories. This paper presents the methods which have been developed and some of the results obtained in applying MSA to product line inspection.

BACKGROUND

Previous related work has been published by B. Weichbrodt and M.W. Schulz of the General Electric Research and Development Center, and by O.G. Gustafson and T. Tallian of SKF Industries Research Laboratory. Weichbrodt [1] presented a general discussion on the use of spectrum analysis, summation analysis, transient analysis, and impedance methods to detect defects in products. Schulz [2] reported on the detection of loose parts in sealed containers. Gustafson and Tallian [3] developed a method and specialized equipment for detecting damaged rolling element bearings.

In relation to the papers referenced above, the vibration signature analysis work reported in this paper makes the following contributions:

1) Simplified instrumentation and vibration fixturing is presented for detecting loose items

2) The experience gained in applying signature analysis to product lines is presented

3) New, easily applied, and sensitive, methods for detecting defective substrate bonds in microcircuit packages and for detecting surface defects in rolling element bearings are presented.

---

*Although the term vibration signature analysis is more precise, the term mechanical signature analysis (MSA) is more commonly used. In this paper, MSA will be used interchangeably with vibration signature analysis.

MSA METHOD FOR DETECTING LOOSE ITEMS

The method for detecting loose items is based on the fact that the impact of one hard object against another hard object produces stress waves in the kilohertz range. The stress waves propagate readily through a typical electronic package to a point on the exterior surface of the chassis or vibration fixture where they are detected by a piezoelectric accelerometer. So that a high ratio of stress wave signal-to-noise may be obtained, the MSA accelerometer is oriented perpendicular to the axis in which the package is vibrated. The location of the MSA accelerometer is carefully selected to assure that it is mounted on a portion of the structure (package or vibration fixture) to which the stress waves may readily be transmitted. The output of the MSA accelerometer is amplified and then filtered to pass only the high frequencies (e.g., above 10 KHz). The filtered signal is displayed on a dual trace oscilloscope above the trace of the vibration input (e.g., 2 g sine at 34 Hz) to the electronic package. The oscilloscope is triggered from the signal of this second accelerometer which senses the sinusoidal vibration input to the package. This permits the inspector to detect whether an impact is periodic (as from a partially constrained item) or nonperiodic (as from a free item). The oscilloscope pattern is photographed using a Polaroid camera. Based on the amplitude of the transients in the mechanical signature, the electronic package passes or fails the loose item test.

LOOSE ITEM DETECTION METHOD APPLIED TO QUALITY ASSURANCE

The above method for detecting loose items may be performed using only the standard vibration instrumentation shown in the block diagram, Fig. 1. This instrumentation or its equivalent is generally available in vibration laboratories. For convenience and mobility, the
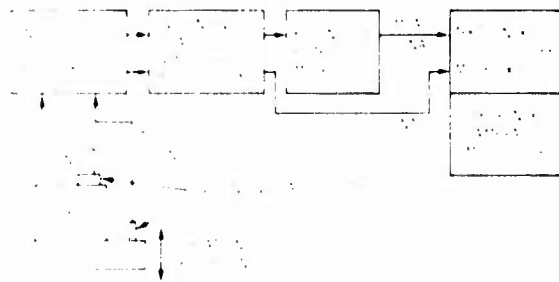

Fig. 1 - Block diagram of instrumentation

MSA instrumentation may be installed on a cart as shown in Fig. 2. The cart is especially convenient when the MSA inspections are performed outside a vibration laboratory. A fixed frequency mechanically driven shaker located in a manufacturing area is satisfactory for providing the required excitation.

Fig. 2 - Mobile MSA instrumentation system

Figs. 3 and 4 show two electronic packages mounted on rigid vibration fixtures which are hard mounted to electromagnetic shakers. This hard mounting permits performing the MSA inspection using the same vibration fixture which is used for vibration acceptance tests and qualification tests.

The vibration level required to detect loose items must, of course, be in excess of 1 g. For a given loose item, the magnitude of its signature (stress waves) is determined by its position when striking the package and its velocity relative to the package. Therefore, for a given input acceleration, the maximum signature amplitude is produced at the lowest excitation frequency. For example, if a package must pass a swept sine vibration acceptance test consisting of a constant amplitude displacement at low frequencies and a constant acceleration level at higher frequencies, then the maximum package velocity will occur at the frequency where the test specification changes from constant displacement to constant acceleration. This is the
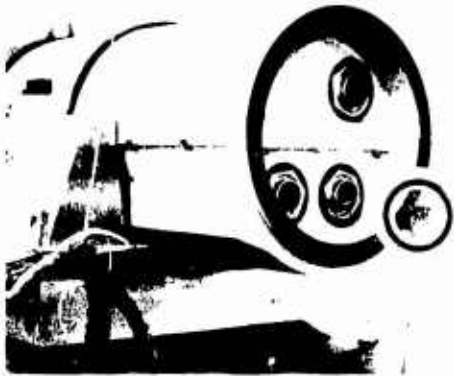
174

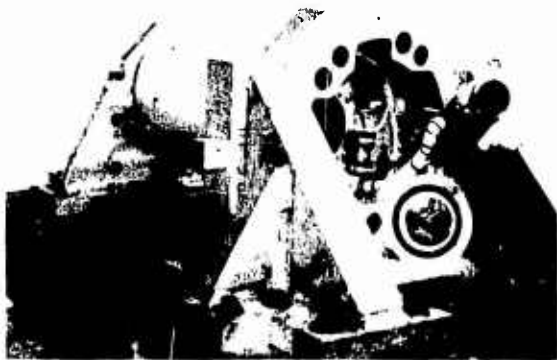Fig. 3 - MSA accelerometer attached to canister

Fig. 4 - MSA accelerometer attached to tail
cone vibration fixture

frequency and acceleration level which will produce the maximum vibration signature without exceeding the acceptance test vibration levels.

To establish an acceptance criterion for the MSA loose item inspection, the amplification of the MSA accelerometer signal is adjusted until it presents a straight trace on the oscilloscope similar to that shown in Fig. 6. Then a loose item of the desired minimum size is placed in the package and the amplitude of its signature is photographed. This amplitude is the desired acceptance criterion. Depending on the noise level of the package, its vibration fixture and the shaker, it is possible to detect items weighing as little as 0.2 milligram. Items smaller than this become difficult to detect. The problem with very lightweight items is that surface forces (e.g., adhesive and electrostatic) may overcome the small inertia force produced by vibrating the small mass of a loose

item. The acceptance criterion should of course be based on the requirements of a particular package. A criterion based on the impact of a washer for a 4-40 screw may be satisfactory for electronic packages as shown in Figs. 3 and 4, but a 0.2 milligram criterion may be required to detect solder balls inside a microcircuit container.

The electronic packages shown in Figs. 3 and 4 are produced in quantity. Each package must pass a vibration acceptance test while meeting its electrical performance requirements. The MSA inspection is performed immediately after the acceptance test. This permits detecting loose items which could cause serious damage due to arcing during the vibration acceptance test. The post-acceptance test MSA inspection detects the items which may have become loose during the acceptance test. As an example of what may be found, Fig. 5 shows an unsatisfactory mechanical signature. The package producing this signature was opened for inspection and the cause of the failure was found to be a loose nut in the power supply. After the nut was tightened, the MSA inspection produced the acceptable signature shown in Fig. 6. A loose nut is a typical cause of an MSA failure. Other typical causes are loose threaded inserts, loose cables, and pieces of broken hardware and extra hardware (metallic and nonmetallic). Prior to implementing the
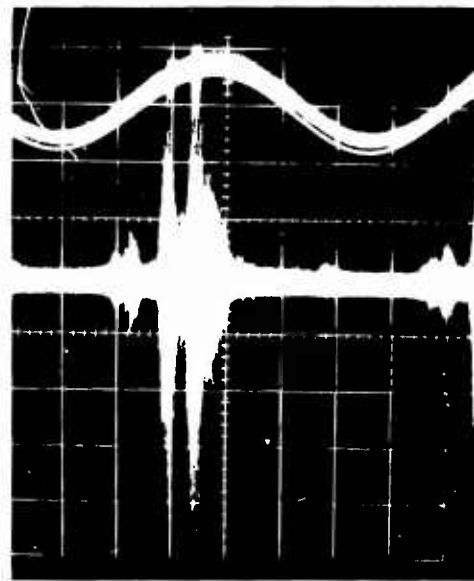

Fig. 5 - Unsatisfactory mechanical signature
produced by loose nut in the power
supply of the electronic package shown
in Fig. 3

MSA inspection station, there was little knowledge of the existence of these defects. MSA inspection provides information which is used to improve the manufacturing operations. Perhaps a bolt is loose because the proper tool was not provided, or perhaps there are broken pieces from a component which is being torqued excessively. Too, the worker on the assembly line is aware that he had better extract the item which fell into the package or it will be discovered during the MSA inspection. The graph presented in Fig. 7 illustrates the improvement in quality which can result from the use of MSA inspections.
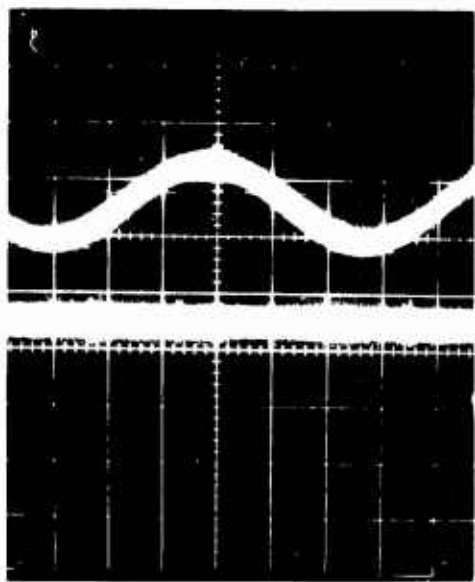

Fig. 6 - Satisfactory mechanical signature obtained after tightening loose nut referred to in Fig. 5

MSA has also been found to be useful in detecting defective purchased components. These components pass incoming inspection and electrical systems tests, but the MSA failures of completed electronic packages have been traced to loose shims inside an electronic tube or to the absence of a peening operation on a shaft inside a switch.

In comparison with visual inspection, an MSA inspection is quicker (30 seconds of vibration time) and permits finding the items hidden under or inside subassemblies, or inside a sealed package. For example, the electronic package shown in Fig. 3 is approximately 37 inches long, 10 inches in diameter, and weighs 120 pounds. It contains a maze of components,
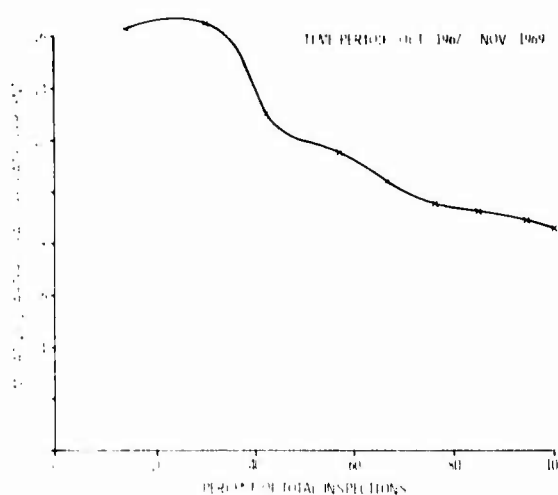

Fig. 7 - MSA inspections of canisters - loose item detection

cables, and dip-brazed subassemblies. Due to this complexity, a visual inspection of a completed package would be of little value. In fact, opening a package for visual inspection exposes the package to possible physical damage and the entrance of debris. For these reasons, an MSA inspection station has been established for this product line. Because the package must pass a vibration acceptance test, no additional manpower and very little additional time are required to perform this MSA inspection.

MSA METHOD OF DETECTING DEFECTIVE ROLLING BEARINGS

The method developed for detecting defective rolling bearings is similar to that used for detecting loose items; in fact, the instrumentation is identical. Apparently, however, there has been nothing previously published on the application of this method to rolling bearings. Although not yet tried by the author, it appears that this method is also suitable for the inspection of gears.

The similarity of the methods for inspection of bearings and detection of loose items is due to the fact that in both cases the defects result in impacts which produce stress waves in the kilohertz range and are therefore readily distinguishable from the normal, relatively low frequency excitation of a vibration exciter or the rotation of a bearing. The purpose of the bearing MSA inspection is to detect surface defects. A surface defect (e.g., pit, scratch, spalling, foreign particles) is a discontinuity in a ball or race. When this discontinuity strikes

176

a ball or race, stress waves are generated in the same manner as when a loose item strikes a portion of a vibrating package. These stress waves are above 10 KHz whereas the stress waves due to the balls rolling on the races are function of the bearing geometry but are below 2 KHz. Therefore, the out-of-balance frequency and the ball pass frequencies may be calculated (Table 1) and this portion of the signal filtered out of the MSA signal. In brief, this MSA method for detecting defective rolling bearings is as follows:

1) An accelerometer is attached to the device (e.g., gyroscope, fan) in a position such that there is a rigid structure between the accelerometer and the bearing.

2) The device is isolated from ambient vibration excitation and its power is turned on.

3) The filtered MSA signal is displayed on an oscilloscope. The oscilloscope is triggered using the transient voltage spikes in the MSA signal. The oscilloscope time base is set to display approximately one revolution of the shaft.

4) A Polaroid photograph is taken of the signal displayed on the oscilloscope. The exposure time is sufficiently long to assure a representative data sample (e.g., long enough for one hundred or more shaft revolutions).

5) The rms voltage of the MSA signal is recorded.

6) Based on the maximum instantaneous voltage amplitude of the photographed pattern and based on the rms voltage, the bearings pass or fail this inspection.

The reason for these two criteria (instantaneous voltage and rms voltage) is that a single large defect will produce a large instantaneous voltage without having much effect on the rms voltage. On the other hand, a bearing with a uniformly rough surface will produce a large rms voltage without having a large instantaneous voltage. Note that the oscilloscope is set to

TABLE 1
Ball Pass Frequencies*

f_e = frequency of impact of balls with a surface defect on the outer race

f_i = frequency of impact of balls with a surface defect on the inner race

f_b = frequency of impact of a surface defect on a ball with the inner and outer races

$$f_e = \frac{n}{2}f_r(1 - \frac{BD}{PD}\cos\beta)$$

$$f_i = \frac{n}{2}f_r(1 + \frac{BD}{PD}\cos\beta)$$

$$f_b = \frac{PD}{BD}f_r(1 - (\frac{BD}{PD})^2\cos^2\beta)$$

where:

f_r = relative speed between inner and outer race (revolutions per second)

n = number of balls

BD = ball diameter

PD = pitch diameter of ball circle

β = angle between the line of contact of a ball with the inner and outer races and the plane containing the ball circle

*Equations from B. Weichbrodt, Ref. 1.

177

trigger on the spikes in the transient voltage.
Therefore, if there is a singular defect on a ball
or race, it will produce a periodic voltage spike
on the oscilloscope. By determining the period
between impacts from the photograph and having
calculated the ball pass frequencies (see Table
1), it is possible to identify the source of the de-
fect as being on a ball, the inner race, or the
outer race. Primarily, however, this method
of inspection is used as an accept or reject
screen and not as a diagnostic tool.

QUALITY ASSURANCE OF ROLLING BEARINGS USING MSA

The above method for detecting defective
rolling bearings was developed after the suc-
cessful application of MSA to loose particle de-
tection. Although the method is very similar to
that used for loose particle detection, its appli-
cation to the quality control of product lines is
more difficult due to the work involved in estab-
lishing a failure criterion. In applying MSA to
the inspection of gyroscope spin bearings, the
first step is taken to collect signatures from a
number of gyros. The MSA inspection is per-
formed after the spin bearings are assembled
into a gyro optics unit and the gyro is attached
to a driving coil by means of a support post.
Therefore, the spin bearing mechanical signa-
ture has a transmission path through two sets
of gimbal bearings, the support post, and the
bushing attaching the support post to the head
coil.

The MSA accelerometer is attached to an
adapter plate which is bolted to the bushing in
the head coil. A photograph of a representative
spin bearing signature is shown in Fig. 8. The
maximum peak voltage is read from the photo-
graph. A plot of the distribution of these peak
voltages is presented in Fig. 9. A similar plot
is made for rms voltage versus quantity of
bearings inspected. These plots are used to
develop tentative failure criteria. For example,
a tentative failure criterion might be that volt-
age transients in excess of three times the rms
value of the collected transient data is cause for
rejection of the bearing. Rejected bearings
may then be life tested or disassembled for
visual evidence of defects. Based on the re-
sults of the life test and/or optical inspection,
the failure criterion is adjusted as needed.

Determining when a bearing has failed can
be a problem. For instance, in the case of the
gyroscope spin bearings, indications of failures
may be that the electrical noise in the guidance
system is excessive, the gyro start-up time is
excessive, or the slow-down time is too short.

Fig. 8 - Typical spin bearing signature

Fig. 9 - Amplitude distribution of gyro spin
bearing signatures

Our experience with this new method of
bearing inspection has been very satisfactory.
In applying it to the production inspection of
gyroscope spin bearings, we have found the fol-
lowing:

1) A correlation between signature am-
plitude and bearing life (see Table 2
and Fig. 10).

2) A correlation between signature am-
plitude and the magnitude of bearing
defects (e.g., contamination, brinel-
ling)(See Ref. 4.)

3) An ability to detect defective bearings
at an early stage in the production cy-
cle and thus avoid costly work which
would be wasted when the assembled
guidance system fails to perform sat-
isfactorily (see Fig. 11).
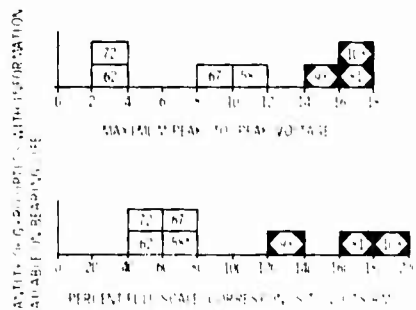
MSA INSPECTION OF MICROELECTRONIC DEVICES

AES manufactures microelectronic devices
(Super Flat Packs) which have very high relia-

178

TABLE 2
Spin-Bearing MSA and Life Data

Gyro-optics Number	MSA Inspection Data		Comments
	Volts peak-to-peak	Percent full scale*	
58	Not available		Successfully completed 300-hour reliability demonstration test. MSA data from post-reliability demonstration test: 10 V p-p, 75% f.s.
62	2.3	40	Successfully completed 300-hour reliability demonstration test.
67	9.3	60	Successfully completed 300-hour reliability demonstration test.
72	3.8	50	Successfully completed 300-hour reliability demonstration test.
81	16.7	167	Failed slow-down test after 120 hours of reliability demonstration test.
93	15.0	133	MSA data was obtained prior to the use of MSA as a quality assurance inspection. Subsequent field report stated that seeker had intermittent noisy spin bearings accompanied by excessive electrical noise.
103	17.7	183	Spin bearings failed during 20th reliability demonstration cycle (approx. 290 hours of operation).

NOTE: This table presents all available data from gyro-optics which have had an MSA inspection and have yielded information on the life of spin bearings.

*Corresponds to volts rms.

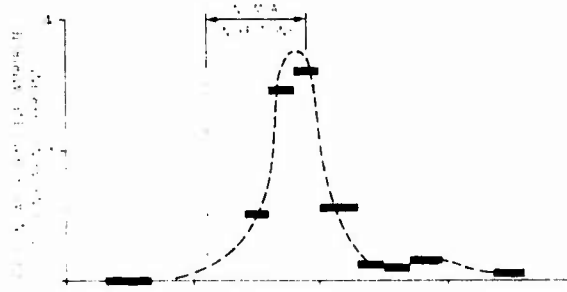Fig. 10 - Correlation between signature amplitude and bearing life

Fig. 11 - Effect of MSA spin bearing inspections on rejections at systems level

179

bility requirements. These flat packs are subjected to a rigorous series of acceptance tests which include thermal shock and acceleration (10,000 g's). It was found that a small percentage of the flat packs which pass these tests would later, when installed in a subassembly, fail due to a loose bond between the flat pack substrate and its case. Evidently, the acceptance tests would damage some flat packs which had weakly bonded substrates, but the damage was not sufficient to cause an electrical failure. Therefore, a test was needed to screen out the few flat packs with weak substrate bonds which were getting through the acceptance tests.

Structurally, a flat pack is a metal container approximately 1.1 inches long X 0.6 inch wide X 0.1 inch thick with a ceramic plate (substrate) bonded to the bottom surface of the container. The flat pack container is permanently sealed prior to the environmental testing. Initially, an effort was made to detect substrates with loose or weak bonds by use of the MSA loose item detection method. However, it was found that due to the small mass of the substrate, a weak bond could prevent the substrate from making an impact with the surrounding structure. A new MSA method was therefore required to detect loose substrates.

A review of the flat pack structure revealed that the ceramic substrate was more rigid than the bottom cover of the container to which it was bonded. It was then apparent that the resonant frequency of the bottom cover would be significantly affected if the substrate was weakly bonded to the cover. In brief, using this idea, the following inspection method was developed:

1) Attach the microcircuit package (flat pack) to a small shaker.

2) Attach an accelerometer to one end of a metal rod. Rest the other end of the rod on the center of the flat pack cover to which the substrate is attached.

3) Perform a 1-2 g peak sinusoidal vibration sweep from 400 to 2000 Hz.

4) Obtain a trace of the accelerometer response. The resonant frequency of the accelerometer, rod, and cover combination will reveal if the bond is satisfactory. For a particular container design, rod mass, and accelerometer mass, it was found that for a satisfactory bond, the resonant frequency was between 1200 and 1700 Hz but with a weak bond, the resonant frequency was as low as 500 Hz.

Note that the resonant frequency which is found is not that of the bottom cover. The resonant frequency of the bottom cover is above 3000 Hz. Therefore, the mass of the metal rod and accelerometer applied at the center of the cover reduces the measured resonant frequency to a value more easily determined with standard vibration equipment.

Fig. 12 presents the results of applying this MSA inspection method to the production of super flat packs. The cumulative failure rate was initially low but it is gradually becoming lower. Improvements in design and manufacturing processes have caused this quality improvement. However, perhaps the use of MSA to detect bonding defects, which would otherwise be undetected, has helped to focus greater attention on the critical process of bonding substrates to their container. The continued use of this MSA inspection, despite the low failure rate, is justified on the basis that the product is used in high reliability equipment and that it serves as a screen to catch any unintentional small changes in the manufacturing process which would affect the strength of the substrate bond.
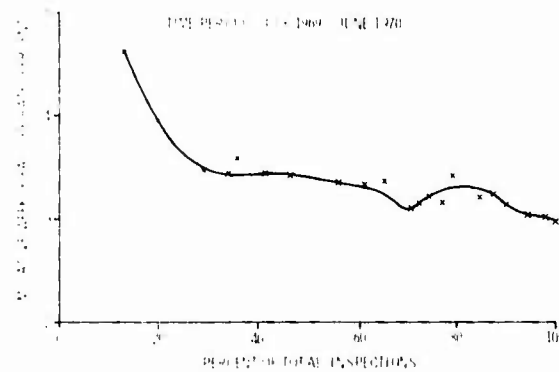

Fig. 12 - MSA inspections of microcircuit substrate bond

CONCLUSIONS

Vibration signature analysis methods have been developed at AES which can be readily and inexpensively applied to assure the quality of rolling bearings and electronic packages. These methods are being used at AES as routine methods of inspecting product lines. It is believed that the simplicity and sensitivity of the methods justify their extensive use in quality assurance and maintenance work.

ACKNOWLEDGMENTS

REFERENCES

1. B. Weichbrodt, "Mechanical Signature Analysis, a New Tool for Product Assurance and Early Fault Detection," Fifth Reliability and Maintainability Conference, July, 1966, Annals of Reliability and Maintainability, Vol. 5, "Achieving System Effectiveness," AIAA, 1966.

2. M.W. Schulz, "Detection of Loose Parts and Free Objects in Sealed Containers," Shock and Vibration Bulletin, Naval Research Laboratory, Feb. 1967.

3. O.G. Gustafson and T. Tallian, "Detection of Damage in Assembled Rolling Element Bearings," Amer. Soc. Lubr. Engr., Vol. 5, pp. 197-209, 1962.

4. A. Kern and J. Zawada, GE/AES Report on Trip to GE Research and Development Center at Schenectady, N.Y., Feb. 5, 1969.

Gordon Lester
... In-Elmer Corporation
... r , Connecticut

and

James Gay Helmuth
Chadwick-Helmuth Company, Inc.
Monrovia, California

Most vibration test levels can be adequately controlled by one feed ac loop; the signal level driving the vibration exciter is adjusted ... an AGC element whose gain is determined by vibration level as sensed by a pickup suitably located on the vibrat- ... str... on exciter head.

However, if the test program demands more than this "single loop" control, additional AGC and sensing elements may be required.

Multiple exciter testing demands and single exciter testing is implemented by multi-logic control when program criteria is desired at both the exciter drive point(s) and at the specimen.

The additional ("outer") loop also allows preliminary verifica- tion of the main ("inner") loop at low vibration level, and can be used to increase the total dynamic range of vibration control. In a multiple exciter test, the "outer" loop also serves to bring all drives up to level together.

INTRODUCTION

Most vibration tests can be adequately controlled by a single transducer located somewhere near the specimen mounting points. However, for larger specimen for which the de- sign of a fixture to fl... through out the fre- quency range of the test is not practical, or if test control criteria is required from both the test specimen and the shaker interface, a single control transducer is not suffi- cient. These require and it multi-control transducers as both the development of suitable fixtures whose acceleration inputs are a number of accelerometers, and for equipment ... scheme to maintain ... a "best" signal ... given values of several transducers.

This as proves insufficient for ... shaker specimen, even more so in single ... ... with use of multi- axis testing a loss of vibration level to ...

develop instrumentation which will provide the above control capabilities for multi-shaker testing. The Outer Loop Control was designed to fill this requirement. It has also provided some unique capabilities for single shaker applications.

GENERAL DESCRIPTION

Most multi-shaker control systems use independent level servos for each shaker and some means to control the phase relationship between each system. A monitoring transducer is mounted close to the shaker and used to de- rive the control signal. The phase control unit adjusts the shaker driving signal such that the response is maintained at a fixed phase relationship to some reference. The servo controls the amplitude at each transducer location to some predetermined level.

Although this system uses a transducer for

each shaker, it is in effect only a single point control. The controls operate to make the multi-shaker cluster perform as one large shaker by maintaining the phase and relative amplitude relationship of each shaker. Further, the control locations must be relatively close to the shaker interface to hold cross coupling effects to a minimum.

Outer loop control provides the means for using multi-control logic with multi-shaker applications. The independent servo oscillators and phase control operate to make the shakers perform as one large shaker and the Outer Loop Control provides control of the overall system.

OPERATION

Figure 1 is a block diagram of a two shaker control system using independent servo oscillators, analog multiplier phase and amplitude control, and outer loop control. The control input to the Outer Loop Control may come from conventional averagers or peak selecting instrumentation, or it may be the output from a single accelerometer.

The Outer Loop Control exerts a control over the test level in the following manner: A variable gain attenuator is placed in signal path between the oscillator and the power amplifier. A variable gain amplifier is placed in the feedback signal path between the control accelerometer and the servo input. The attenuator and amplifier gains are servoed by a common signal. The circuits are ganged such that an attenuation of the output is accompanied by an equal gain increase in the feedback signal.

Since a decrease in the output signal is accompanied with an equal increase in the servo feedback signal, the level and phase controllers perform their function independent of the overall test level. Thus relative amplitude and phase control are maintained at points close to each shaker by the servo oscillators while the absolute level is controlled by the Outer Loop Control unit.

APPLICATION

The most important function of the Outer Loop Control system for multi-shaker testing is properly its role in response limiting. Most multi-shaker tests involve rather large subsystems or complete vehicular systems. Often it has been determined from component or subsystem level testing that severe damage may result if acceleration levels in excess of some predetermined maximum are encountered at various locations on the structure. Such damage cannot be tolerated particularly if the test specimen represents deliverable hardware. Interrupting the test when a level in excess of the allowable limit is encountered may save the hardware but the objectives of the test would not be fulfilled.

By simply lowering the input level over some small frequency range to prevent the response at a given location from exceeding allowable limits the test may be continued. The test specimen is protected from unnecessary damage and uninterrupted response data from the specimen is available for studies of transmissibility, model shapes and other pertinent information.

In single exciter testing, response limiting is facilitated by the additional control dynamic range and independence of drive program provided by the use of Outer Loop Control.

TEST RESULTS

The test data shown in Figures 2 and 3 shows the ability of the Outer Loop Control to limit responses at various locations. Plots 1 through 4 of Figure 2 are the control signals from a four shaker test. Plots 5 and 6 are response of two cantilever beams. The plots in Figure 3 show the response at the same locations when a maximum acceleration level is imposed on each cantilever beam response.

Note that the two beams are limited to different acceleration levels. The resonant frequencies of the beam were adjusted to occur at frequencies having different excitation acceleration level. This was done to demonstrate that the response limiting level is independent of the test acceleration level.

The Outer Loop Control unit may also be used to provide level control from the average of several accelerometer signals. As in the peak limiting case described above, the relative amplitude and phase control is performed by the independent servo oscillators, but the Outer Loop Control signal comes from the average of transducer signals located at any desired locations.

The Outer Loop Control performs another important function in multi-shaker testing. It provides the capability to energize the shakers in a smooth and coherent manner. Since the speeds of the independent level servos differ to some extent it is not practical to use them to begin a vibration test as is usually done with single shaker operation. The Outer Loop Control provides a common servo to all systems, which brings each shaker up to level (or down) at the same rate. It also provides the capability to bring the system on line at a level 20 to 40 db below the test thus providing an opportunity to check all control functions and to establish phase control.

When used in single shaker testing, the Outer Loop Control provides the same benefits as multi-shaker use except, obviously, the rate of up/down is normally not critical.

CONCLUSIONS

The Outer Loop Control logic has provided

... . test-
.... an absolute acceler-
.... ed is applicable
... . is a .... oper-
.... le els . ssen are
.... le els . ... ed
.. .. en'. . ..
.. .. d instrument-
... . a eracers and
... ...
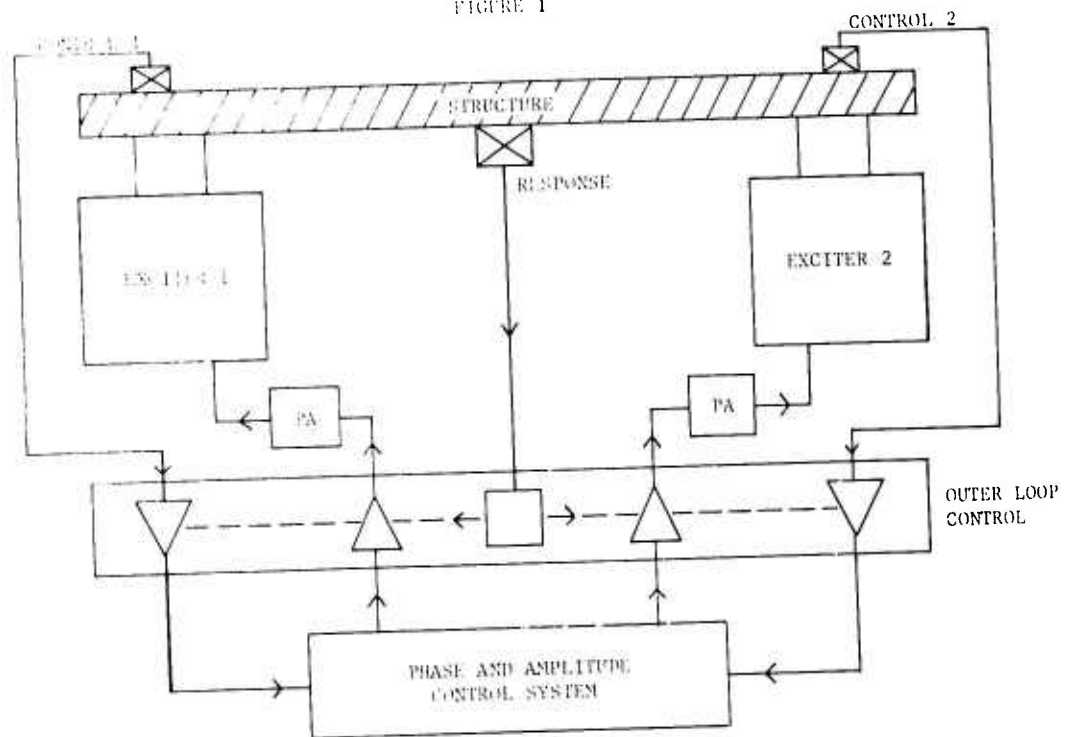
FIGURE 1

FIGURE 2 NO OUTER LOOP CONTROL
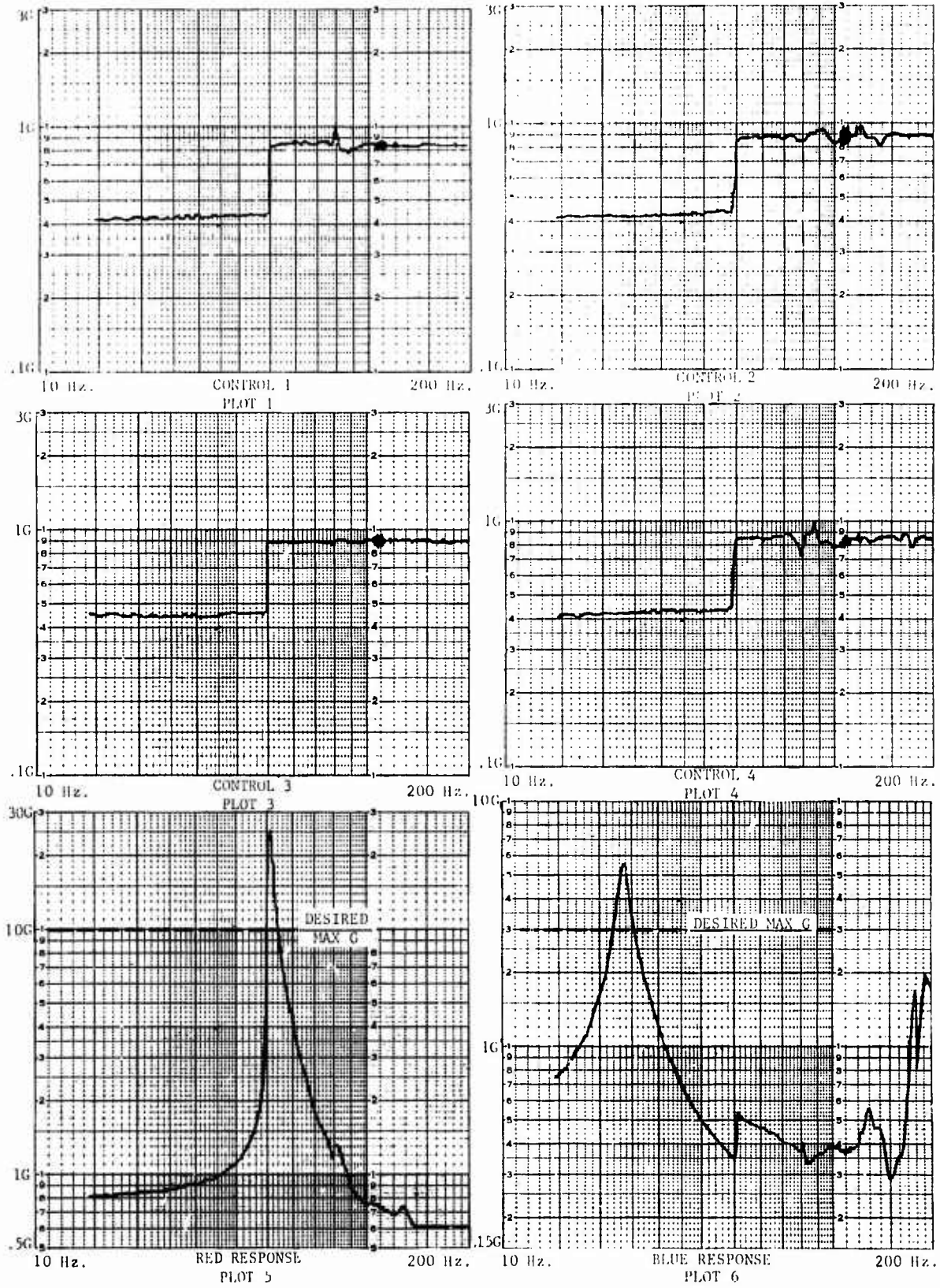
FIGURE 3 WITH OUTER LOOP CONTROL
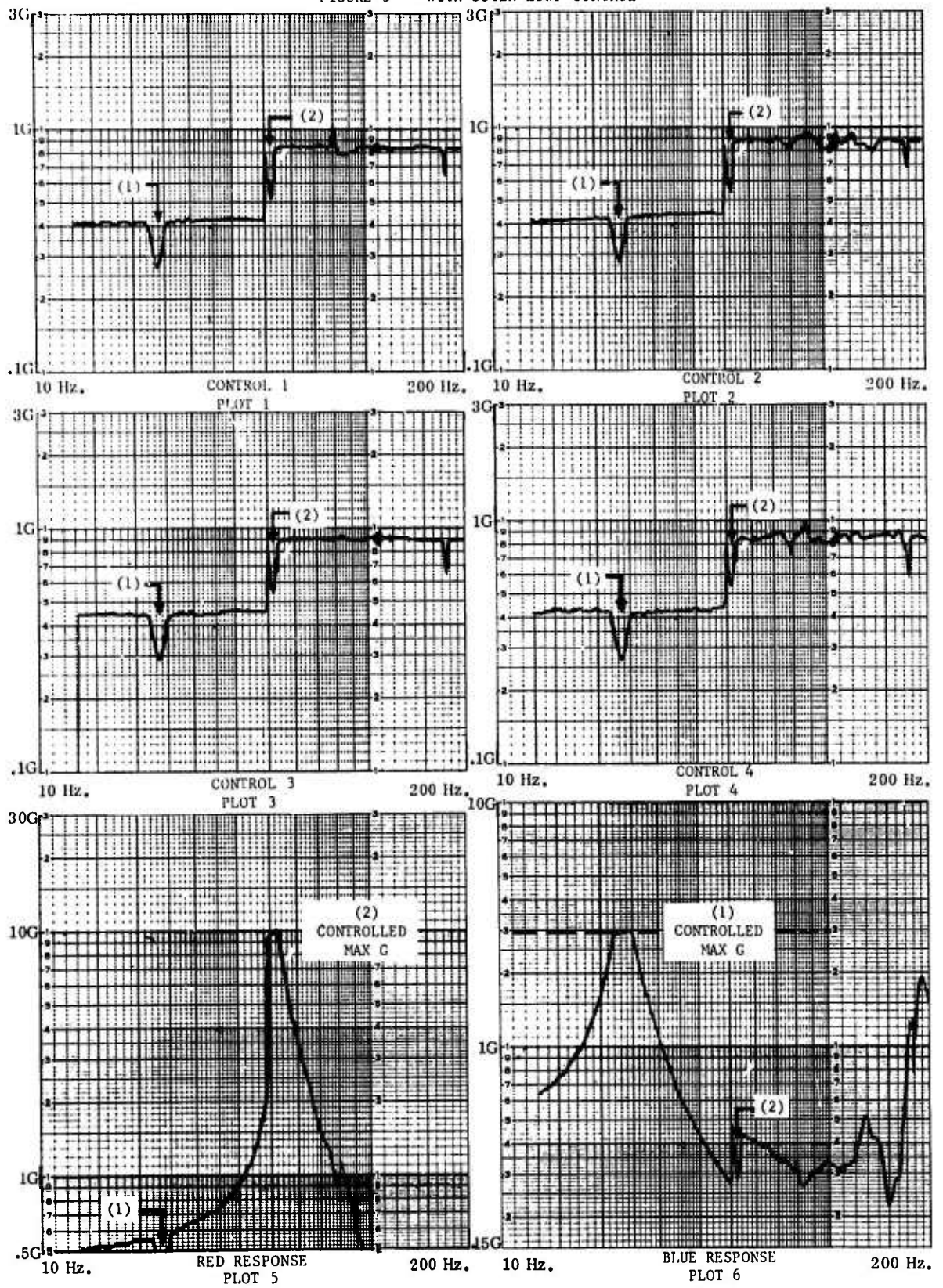
EMPIRICAL PREDICTION OF MISSILE FLIGHT RANDOM VIBRATION

A. E. Kartman
The Bendix Corporation
Mishawaka, Indiana

Purely theoretical predictions of missile flight vibration environments are precluded by complexities of the missile hardware and the environment. Complete experimental determination of the environment through extensive flight testing is undesirable and impractical. An alternative is the use of selected telemetered flight data to formulate empirical techniques for extrapolation of vibration characteristics to other areas of concern. Correlation of missile vibration with known or predictable flight parameters has permitted reasonable estimates of the environment at nearby areas. Flight vibration data acquisition, reduction and characteristics are briefly discussed; techniques derived for application of the flight data to new hardware requirements are more fully discussed.

INTRODUCTION

The TALOS missile is the second stage of a Navy two-stage, long range, high altitude, surface-to-air weapon. The first stage solid propellant rocket boosts the missile to speeds sufficient for the second stage ramjet engine to operate. Total flight time capability is in the order of several minutes. A schematic representation of the missile is shown in Figure 1. Missile electronics, hydraulic system components, and propulsion system components are contained in annular compartments formed by the missile outer skin and the ramjet diffusers and through-duct. Warhead and additional electronics are contained within the innerbody. A vibration isolated mounting platform, called the "electronics basket", is used in the electronics compartment to protect sensitive components against high amplitude vibration below approximately 600 Hz.
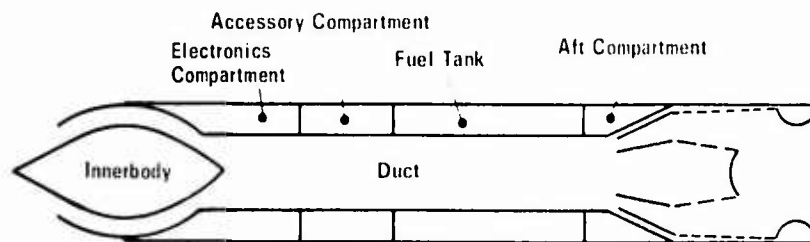

Figure 1 - Schematic of Packaging Compartments within the TALOS Ramjet Missile

189

The flight vibration environment for airborne equipment can be determined by measurement at critical locations throughout flight test vehicles. Such instrumentation, however, is expensive. In addition, it is uncommon for flight tests to yield the most stringent conditions within vehicle capabilities. It becomes necessary, then, to extrapolate flight data in predictions of the environment at unmonitored locations. In the TALOS missile program, a considerable amount of telemetered flight vibration data has provided the basis for study of the relationships between the environment and several missile flight parameters.

FLIGHT DATA

Throughout the TALOS program, much flight vibration data has been collected and analyzed. Two predominant sources of random vibration energy during flight are aerodynamic excitation over the missile external surfaces, and ramjet engine excitation due to internal airflow and fuel combustion. The vibration environment during the missile flight is measured with a piezoelectric accelerometer mounted at the point of interest. The output of the accelerometer is amplified through a calibrated system and relayed to a ground telemetry station. The RF link is an FM/FM system with a carrier frequency in the VHF range. The subcarrier frequency used for vibration information is 40 KHz or higher, and provides satisfactory frequency response in the frequency range of most interest, 20 to 2000 Hz. The telemetered signal is recorded on magnetic tape at the ground station.

The vibration environment normally is monitored continuously throughout a flight. Several locations can be monitored using the same subcarrier by means of a commutator switch carried in the airborne equipment. Commutated sample times are approximately 1.25 seconds in duration which provide a sample sufficiently long to perform a random wave power spectral density analysis. The data samples and accelerometer locations are coded for identification; data is decommutated during the analysis.

The parameters of most significance in defining the vibration environment are the acceleration spectral density function and the root mean square accelerator. The time intervals for acceleration spectral density analysis are selected in a preliminary examination of data for the entire flight. In a typical flight, three or four one-second time intervals are selected to determine characteristics during phases of flight having significantly different operating characteristics; i.e., during boost, just after missile-booster separation, during constant altitude cruise, and during the terminal phase of flight. After selecting the time intervals, the recorded telemetry data during each interval is duplicated on a tape from which a continuous loop is made for the

wave analysis. During loop playback, a 20 Hz bandpass filter with a 97 KHz center frequency is used. Other bandwidths are available and are used when special considerations are necessary, such as variations in total band being investigated. The frequency is swept at a slow rate over the entire range during successive passes of the tape loop. The calibrated filter output is plotted as a function of frequency and thus provides an estimate of spectral characteristics for a particular time period in the flight.

The information gained from the analysis of a single time interval could be quite misleading in establishing design requirements since the vibration characteristics could change considerably with changes in flight parameters. The results of the analyses for all the selected time intervals must be examined before a particular environment can be defined. Figure 2 illustrates how the vibration characteristics change with flight time at one location in the missile. To account for the vibration level shifts with frequency throughout the flight, an envelope of measured data is composed by superimposing the spectral characteristics during all the selected intervals to determine the most severe conditions throughout the flight at each frequency. The envelope is used in the derivation of a flight-equivalent spectrum.

FLIGHT EQUIVALENT SPECTRUM

The acceleration spectral density obtained in the data analysis could be applied directly as component requirements. However, it is desirable to put the data into a more convenient form. A linear approximation of the flight acceleration spectral density envelope within a particular bandwidth can be derived to achieve this. The intent in deriving this so-called equivalent spectrum is to develop vibration spectral characteristics which will yield damage potential approximately equal to that experienced in flight. The damage potential of an item can be expressed in terms of stress experienced by any element within the item when exposed to the environment. The stress is directly proportional to the acceleration response of the element. Thus, if vibration characteristics can be defined which will induce an acceleration response equal to or greater than that induced by the flight environment, then the equivalent spectrum will represent a damage potential equal to or greater than that obtained during flight.

It is assumed that the elements within an item can be adequately represented by a single degree of freedom resonator. The acceleration response, R, of the resonator as a function of frequency is:

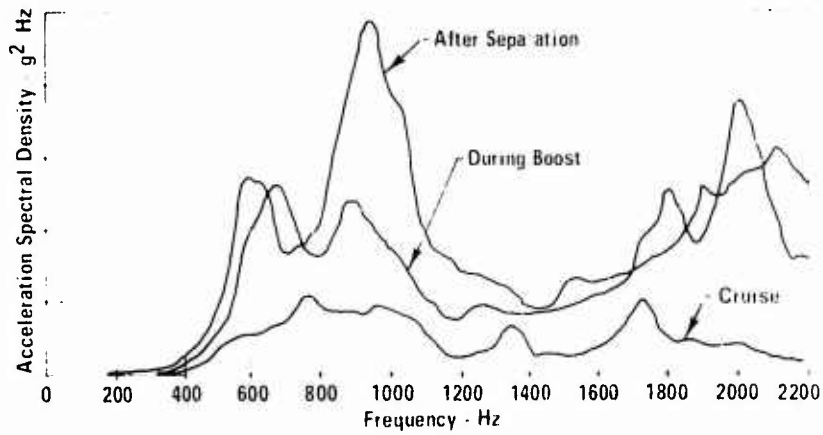$$R(f) = \left[\sum_{f=0}^{f_{max}} G(f)\, y^2\,(f)\, \Delta f \right]^{1/2} \qquad (1)$$

Figure 2 - Flight Phase Effects on Frequency Characteristics

where G(f) is acceleration spectral density as a function of frequency and y(f) is the transmissibility as a function of frequency for a damped single degree of freedom system. The resonant frequencies and transmissibilities for small elements within a module are not usually known. Therefore, it is further assumed that resonance can occur at any frequency within the 20 to 2000 Hz band. The highest transmissibilities associated with the compartment being investigated are used in response calculations. Experience shows that transmissibilities of 30 for the electronics compartment and 20 for the accessory and aft compartments are conservative maximums for TALOS.

In the derivation of an "equivalent spectrum", acceleration response to the flight environment as observed from the telemetered data is calculated. The response to the straight line equivalent spectrum

first approximation of the flight spectrum is similarly calculated. The response characteristics for the two spectra are compared and a judgment made of the adequacy of the equivalent spectrum. The criteria used in the judgment are:

1. An equivalent spectrum rms vibration level greater than the most severe measured flight vibration level at that location.

2. The response to the envelope of flight data not exceeding 20 of the response to the equivalent spectrum at any frequency.

If the equivalent spectrum does not meet these criteria, it is modified and the process is repeated. These iterative response calculations are done on a digital computer. An example of a flight acceleration spectral density envelope and its equivalent
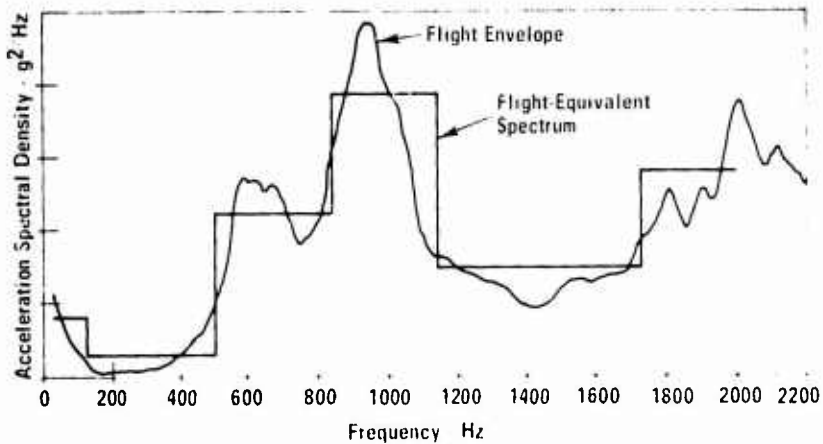
Figure 3 - Example of Flight Envelope and Its Equivalent Spectrum

191
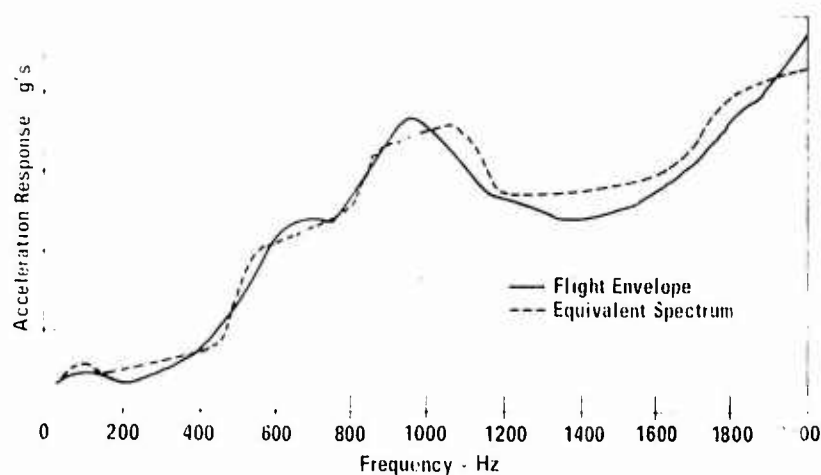
Figure 4 - System Response to Flight Envelope and Its Equivalent Spectrum

spectrum is shown in Figure 3. The corresponding system acceleration response to the flight envelope and the response to the equivalent spectrum are shown in Figure 4.

The equivalent spectrum approach tends to reduce high intensity narrow bandwidth vibration peaks and spread the vibration energy over a larger bandwidth to account for frequency shifts during flight. Comparisons of response for various spectra and transmissibilities have shown that this approach yields a condition representative of flight, without introducing severe over-design and/or over-test.

FLIGHT PARAMETER EFFECTS

The flight-equivalent spectrum provides a satisfactory means for establishing vibration requirements at a particular location for which flight data has been obtained. However, there is the need to extrapolate data to nearby locations which have not been instrumented. Investigations have been conducted to relate vibration intensities and known or predictable missile flight parameters. Telemetered flight data has shown that the intensities are affected by aerodynamic load, propulsion system characteristics such as fuel richness, rough burning and ramjet diffuser pressure oscillations, weight of the module, and location of the module within the missile. General trends have been observed in all those parameters; however, quantitative relationships have been derived only for aerodynamic loading and the module weight.

Aerodynamic Load

Aerodynamic loading is represented by free stream dynamic pressure for purposes of relating to vibration characteristics. Dynamic pressure, q, can be expressed as:

$$q = 0.7 \, pM^2 \qquad (2)$$

where p is free stream static pressure and M is free stream Mach number.

Flight data has strongly indicated a linear relationship between the average rms vibration and free stream dynamic pressure. Figure 5 shows a typical rms vibration and dynamic pressure relationship. The sharp rise from zero time occurs as the vehicle builds up speed. The dynamic pressure increases until missile-booster separation, then decreases. During high altitude cruise, the pressure remains relatively stable, then increases as the missile begins its dive. Typically, the vibration intensities also follow those characteristics.

In a recent series of flight tests, several missiles were instrumented to provide flight vibration data. The data showed that the rms vibration is generally in direct proportion to the free stream dynamic pressure. Data taken on the electronics basket resulted in a range of 5.3×10^{-4} to 6.9×10^{-4} $g/(lb/ft^2)$ throughout flight for the ratio of rms vibration to dynamic pressure. Since a large part of a long range flight will be at high altitude (low dynamic pressure), the vibration requirements representing that phase can be of correspondingly low intensity, while requirements for the initial and final phases of flight remain at the more severe intensities. This method minimizes vibration test induced stresses and still subjects the hardware to most realistic requirements.

Normally, flight tests are not designed to reach the performance limits of the vehicle. The relationship to aerodynamic load provides a method of extrapolating flight data to design performance limits. The maximum monitored rms vibration intensity is increased by the ratio of maximum perform-
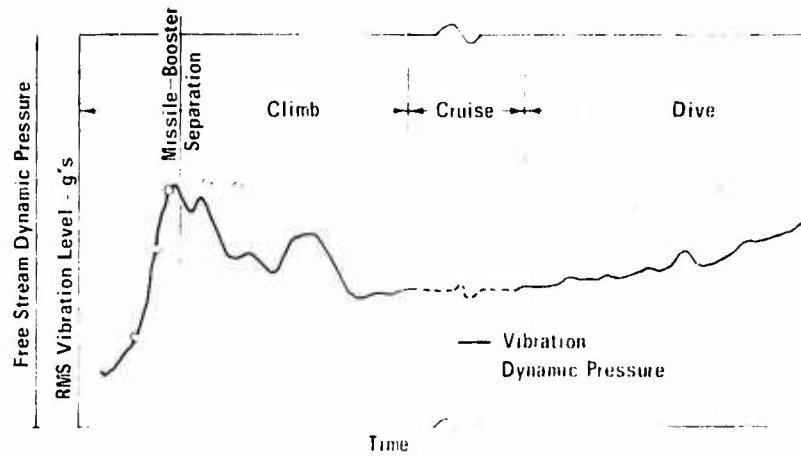
192

Figure 5 - Typical RMS Vibration and Dynamic Pressure Histories

ance dynamic pressure to the monitored flight dynamic pressure at the time of maximum pressure. Spectral characteristics of the monitored data are applied to the extrapolated data.

Propulsion

Correlation of propulsion system parameters with vibration has not been entirely successful. Fluctuations in vibration intensities, in some cases, coincide directly with fluctuations in such parameters as fuel richness and flow rates, burning peculiarities, and ramjet diffuser pressure oscillations. Several missiles have been instrumented with vibration and engine duct pressure sensors. However, inconsistencies in instrumentation and the small range of the pressure oscillations precluded quantitative correlation of the two parameters. Generally, vibration increased with increased pressure, and effects on longitudinal vibration were greater than those on radial vibration in the region of the innerbody.

Module Weight

Effects of module weight on local vibration characteristics are evident in the monitored flight data. The vibration varies inversely with the module weight. Various studies have been pursued to establish a vibration-weight relationship. These studies have concentrated on a relationship which would be applicable to hardware within the accessory compartment, since there is a wide variation in the physical characteristics of that hardware and it is mounted directly to the airframe. Electronics modules on the basket are similar to each other in configuration and extensive applicable flight data is available so that a general relationship for the electronics compartment was considered unwarranted.

In deriving the expression for vibration in terms of module weight, an initial assumption was made that there is a constant "compartment level" vibration upon which to base estimates of module environments. The "compartment level" environment was taken as that vibration measured at some point on the airframe which is unaffected by equipment loading. The straight line approximation, or equivalent spectrum, of the flight data envelope for that monitored location provides the reference for weight modified intensities. The empirical equation relating vibration to module weight is:

$$g_o = g_n - 1.5 \, [W]^{1/2} \qquad (3)$$

where g_o is the rms acceleration in g's over 20 to 2000 Hz at the point of module attachment to the airframe, g_n is the constant "compartment level" rms acceleration in g's over 20 to 2000 Hz, and W is the weight in pounds of the module plus attachment bracketry. For lightweight modules, g_o approaches the unloaded airframe intensity, g_n. The range of weights in the compartment limit the calculated g_o to a minimum of approximately 60 of g_n. In the accessory compartment, the constant g_n is 29 g's.

In using Equation (3) it is inherently assumed that the equivalent spectrum characteristics apply to other areas within the same missile compartment. This has been verified by flight instrumentation. The spectrum is adjusted to provide the rms acceleration level determined by Equation (3). The calculated vibration level and the adjusted spectrum, then, provide the estimate of the flight environment at the particular module being investigated.

Module Location

Telemetered flight data has indicated that vibration intensities and frequency characteristics change

193

with location throughout the missile. For a common reference for verification of this phenomenon, it is desirable to monitor several locations during a given flight test, since performance characteristics vary significantly between flights. Such data was obtained for the accessory and aft compartments during two flight tests. Additional data has provided the ranges of intensities for the innerbody and the electronics compartment. Table I presents representative intensities and the predominant frequency characteristics for the missile compartments. The vibration in the aft compartment is more severe than that in the accessory compartment which, in turn, is more severe than that on the electronics basket. Measured aft compartment vibration has generally been 2-1/2 to 3-1/2 times that measured on the electronics basket. The more severe environment toward the aft end of the missile is attributed primarily to the proximity to the engine combustor.

rived by the "equivalent spectrum" technique described previously, accounting for the narrow-band, high amplitude peaks, an extreme over-design or over-test condition would have resulted.

CONCLUSIONS

The relationships discussed in this paper have provided a satisfactory means of estimating TALOS flight vibration environments. While the specific relationships cited were derived for a particular missile configuration, the discussion of the general trends of vibration with the various missile parameters is intended to suggest possible areas of study of similar techniques in other types of flight vehicles.

Table I - Compartment Vibration Characteristics

Compartment	Average Measured Intensity - rms g	Predominant Frequencies Hz
Innerbody	6-8	600-800, 1500-2000
Electronics	4-7	1300-2000
Accessory	14-20	1200-1600, 1750-2000
Aft	18-22	1400-2000

SELF-GENERATED ENVIRONMENT

Occasionally, it is necessary to ascertain whether the flight data is indeed representative of the external environment at a particular location or whether it reflects some extraneous characteristics. Such characteristics caused by the data reduction process are relatively easy to detect and check. More difficult to detect and verify are those features in the data that are not actually an external environment but are self-generated within the module being monitored. Such a situation existed in data obtained in several flight tests with instrumentation on the propulsion fuel control system. In the spectral analysis of telemetered data, narrow-band, high amplitude vibrational energy appeared at several distinct frequencies throughout the 20 to 2000 Hz band. This data was considered questionable, since it was suspected that the narrow-band peaks were due to noise emanating from the fuel control system turbine/pump; but the proportion of the spectral data which could be attributed to the noise was uncertain. To resolve the uncertainty, ground tests were conducted in which the fuel control system was operated normally, with no external vibration excitation of the system. Variations in the system operating parameters were imposed for simulation of the several flight phases. In general, the agreement between the flight and ground data was excellent and indicates that the preponderance of the monitored flight environment in the immediate vicinity of the fuel control system is self-generated. If vibration requirements had been de-

SYMBOLS

B	bandwidth (Hz)
f	frequency (Hz)
$G(f)$	acceleration spectral density as a function of frequency (g^2/Hz)
g_n	compartment rms acceleration (g)
g_0	rms acceleration at module attachment (g)
M	free stream Mach number
p	free stream static pressure (lb/ft^2)
q	free stream dynamic pressure (lb/ft^2)
R	single degree of freedom system acceleration response (g)
W	module weight (lb)
$v(f)$	transmissibility as a function of frequency

194

STRUCTURAL VIBRATIONS IN THE BELL AH-1G HELICOPTER

DURING WEAPON FIRING

R. Holland
Kinetic Systems, Incorporated
Boston, Massachussetts

and

D. Marcus and J. Wiland
U.S. Army Frankford Arsenal
Philadelphia, Pennsylvania

This paper describes a test program carried out on the AH-1G Helicopter in which structural response measurements were made during firing of the minigun and the 40mm grenade launcher. Measurements were obtained on the gun turret, the aircraft structure near the gunner's station and on a wing mounted pod. The resulting data is presented both in the form of acceleration time histories and shock spectra. A discussion of the transient response due to the firing of each round is presented as well as the steady state vibration at the weapons' firing rate.

INTRODUCTION

The Frankford Arsenal is responsible for the development of a number of fire control systems for the Bell AH-1G Cobra Helicopter. In the course of insuring the suitability of these systems, various programs for measuring the dynamic environment at selected locations in the aircraft are carried out. This paper will describe one such program in which acceleration measurements were obtained during firing of the 7.62 mm minigun and the 40 mm grenade launcher, and the data reduced in the form of shock spectra [1]

The Bell AH-1G Helicopter (Figure 1) is a high speed, heavily armed aircraft specifically designed for the combat role. Its distinctive features include the long narrow fuselage, aerodynamic styling, in-line seating of the gunner and pilot, and a chin mounted gun turret. This turret can accommodate two 40 mm grenade launchers, two 7.62 mm miniguns, or a combination of one of each of these weapons as shown in Figure 2. Other armament includes the 20 mm cannon and wing mounted rockets. These weapons, combined with the associated detection, sighting and aiming equipment constitute the SMASH system (Southeast Asia Multi-Sensor Armament System for Helicopters). Important elements of this system, shown in Figure 3, are the infrared sighting system on the nose of the aircraft, and a radar pod mounted under the starboard wing.

This paper is primarily concerned with the structural response of the helicopter due to firing of the minigun and the grenade launcher, and the effect of this environment on lightweight equipment. The analyzed data is presented in the form of shock spectra.

195

Figure 1 - Bell AH-1G Helicopter with wing mounted radar pod

Figure 2 - Bell AH-1G Helicopter gun turret with 7.62 mm minigun
and 40 mm grenade launcher
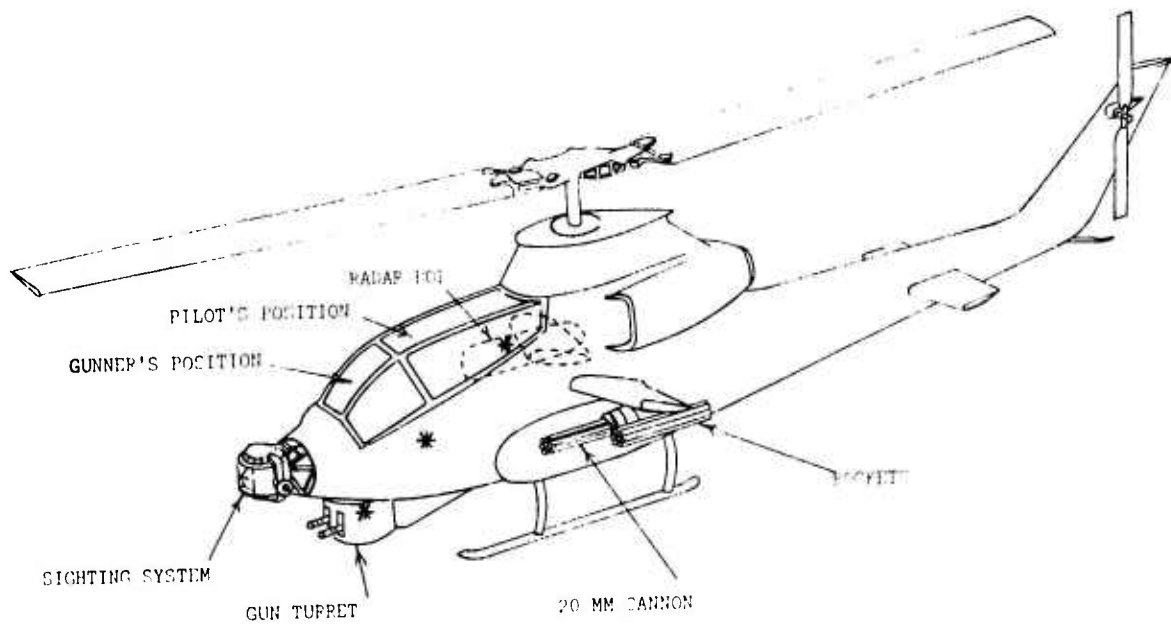
Figure 3 - Accelerometer locations in AH-1G Helicopter
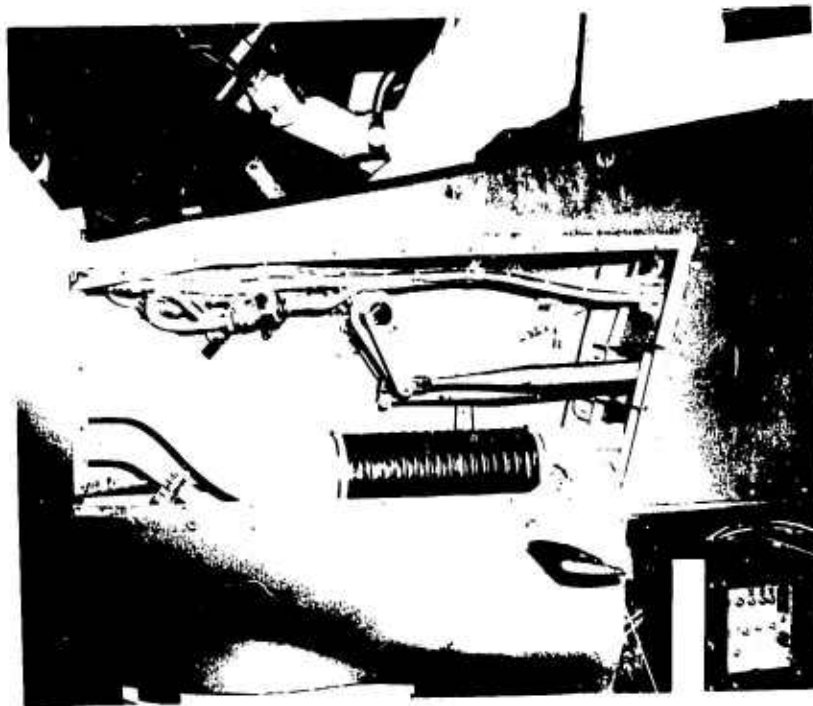
Figure 4 - Frame accelerometer position at gunner's station,
AH-1G Helicopter

197

INSTRUMENTATION

The helicopter was instrumented with Endevco Model 2264C piezo-electric accelerometers and MB Zero-Drive signal conditioning amplifiers. Recordings were obtained using a 14 channel FM airborne tape recorder operated at 7-1/2 in./sec. The accelerometers were mounted at three locations: the gun turret, on a mockup of the radar pod, and on the aircraft frame near the gunner's station. Three accelerometers were mounted at each location and were oriented to sense vibration along the three major axes of the aircraft. Figure 3 shows the accelerometer locations and portions of the SMASH system. The reader will note that in this aircraft, the gunner/copilot is seated in front of the pilot and almost directly over the gun turret. Figure 5 shows the access panel at the gunner's station where the frame accelerometers were mounted.

FIRING DATA

The firing data consisted of acceleration time-histories for a total of six firing conditions, three with the gun turret in the fore-aft position (firing head-on), and three with the turret rotated 90° (firing in the transverse direction). The three firing conditions at each turret orientation were the following: minigun firing at a rate of 4000 rounds per minute, minigun firing at a rate of 2000 rounds per minute, and the grenade launcher firing at a rate of 380 rounds per minute. Figures 5-11 show acceleration time-history records of the structural vibrations caused by the firing of the minigun and the grenade launcher. These records were obtained with the helicopter on the ground with the engine running and rotor blades turning at the normal rate.

Figures 5 and 6 show the structural response due to the minigun firing head on at its two fixed firing rates. In Figure 5 the firing rate is best defined by the vertical vibration in the gun turret. This rate is easier to see in Figure 6 where the gun is firing at its low

rate and the vibration amplitude has decayed due to structural damping before firing of the next round. The shock wave propagation from the turret to the frame can be seen in this figure. Figure 7 clearly defines the shock wave propagation from the turret to the frame and pod, and also shows the 30 Hz vertical response of the externally mounted pod. The repeated firing rate of the grenade launcher is shown in Figure 8.

Figures 9-11 show the structural responses caused by the minigun and grenade launcher firing in the transverse direction. The transverse firing data were not reduced to shock spectrum form, but are presented here to allow the reader to obtain a visual comparison between the data from the two firing directions. It should be noted that the orientation of the turret channels is relative to the bore axis of the weapon, the longitudinal axis thus being parallel to the line of fire.

DESCRIPTION OF SHOCK SPECTRUM

The acceleration time-history records of the shock motion of the helicopter structure due to the weapon firing were defined using the Shock Spectrum Method. The definition of transient shock environments by this method represents a special form of single degree of freedom response analysis. This response concept is regarded as representative of the "damaging effects" of the environment and is thoroughly documented in the technical literature. Ref. [2-5], for example, contain varied presentations of the basic concepts involved in the development of shock spectra and their application to environmental shock analysis.

In brief, the shock spectrum is a plot of the maximum relative deflection responses of many simple single degree of freedom systems presented as a function of system natural frequency.

Figure 12 presents a sample of a four coordinate shock spectrum grid. A point on this graph simultaneously
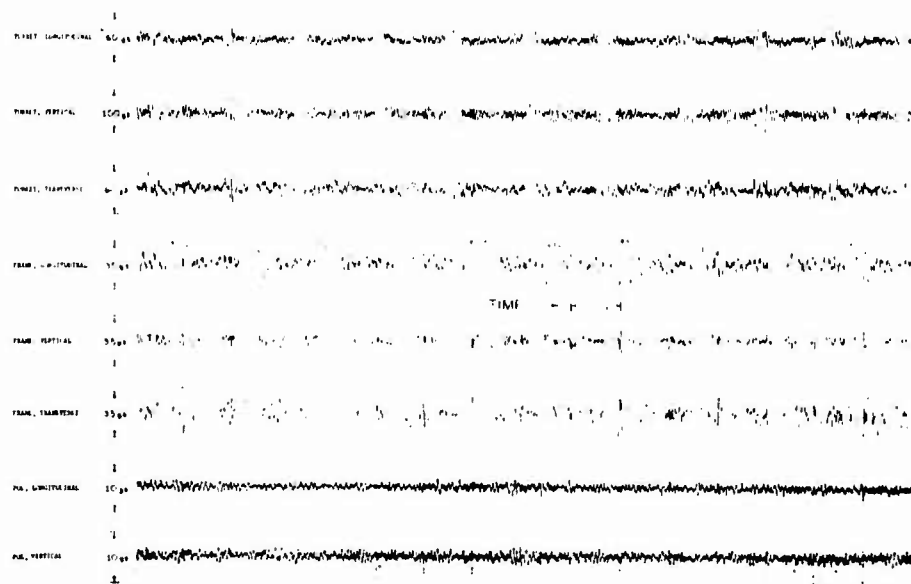
Figure 5 - Acceleration-time history due to minigun firing
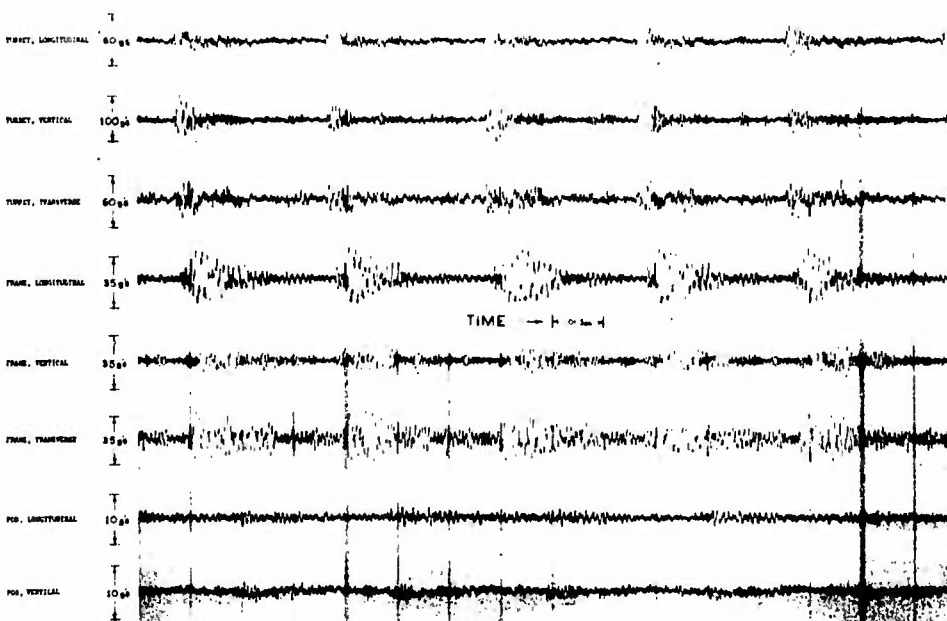head on at 4000 rounds per minute.

Figure 6 - Acceleration-time history due to minigun firing
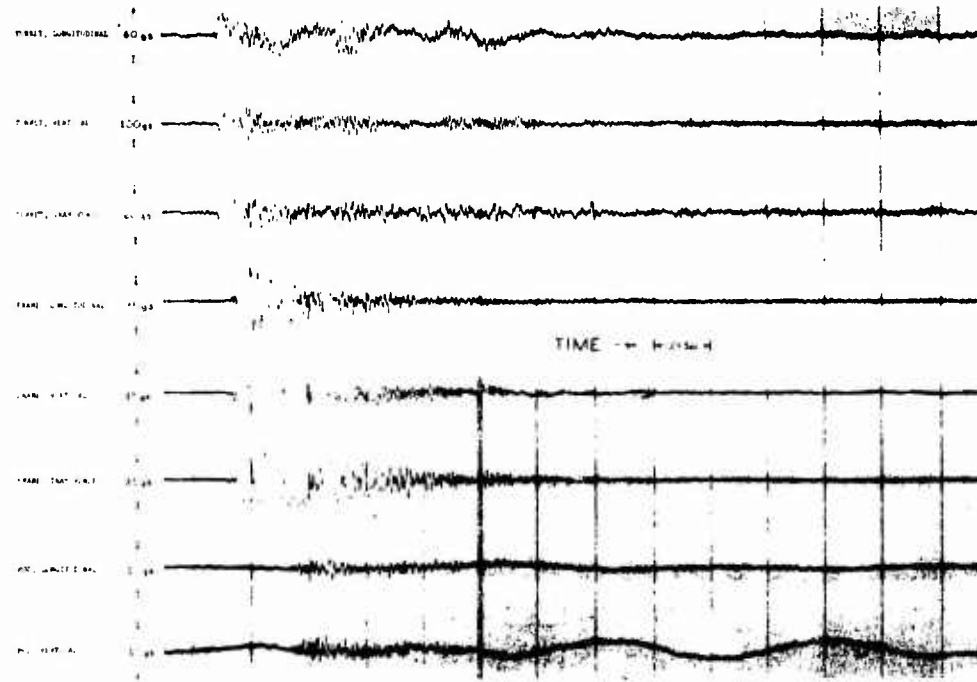head on at 2000 rounds per minute.

199

Figure 7 - Acceleration-time history due to grenade launcher
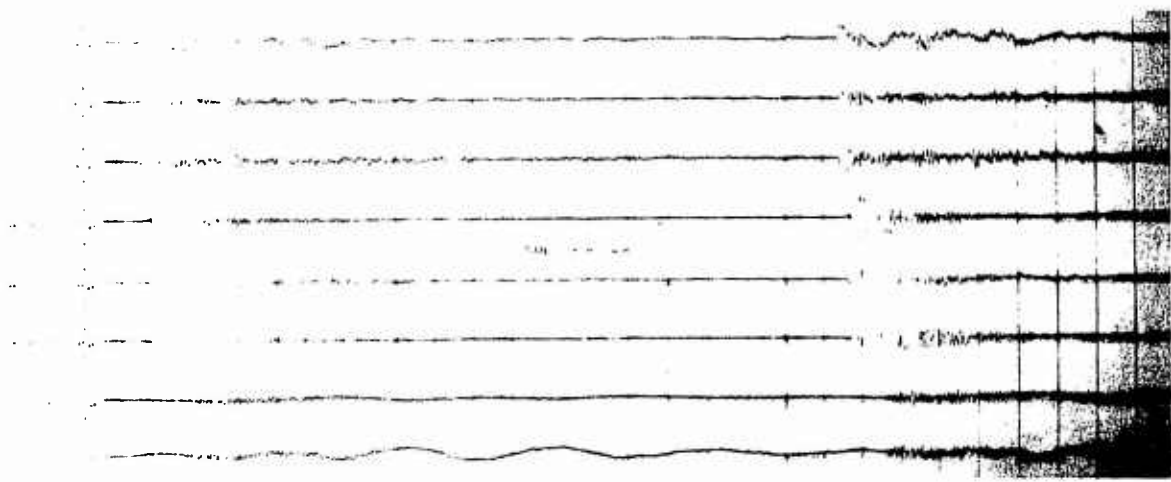firing head on at 380 rounds per minute.

Figure 8 - Acceleration-time history showing firing rate of grenade launcher.
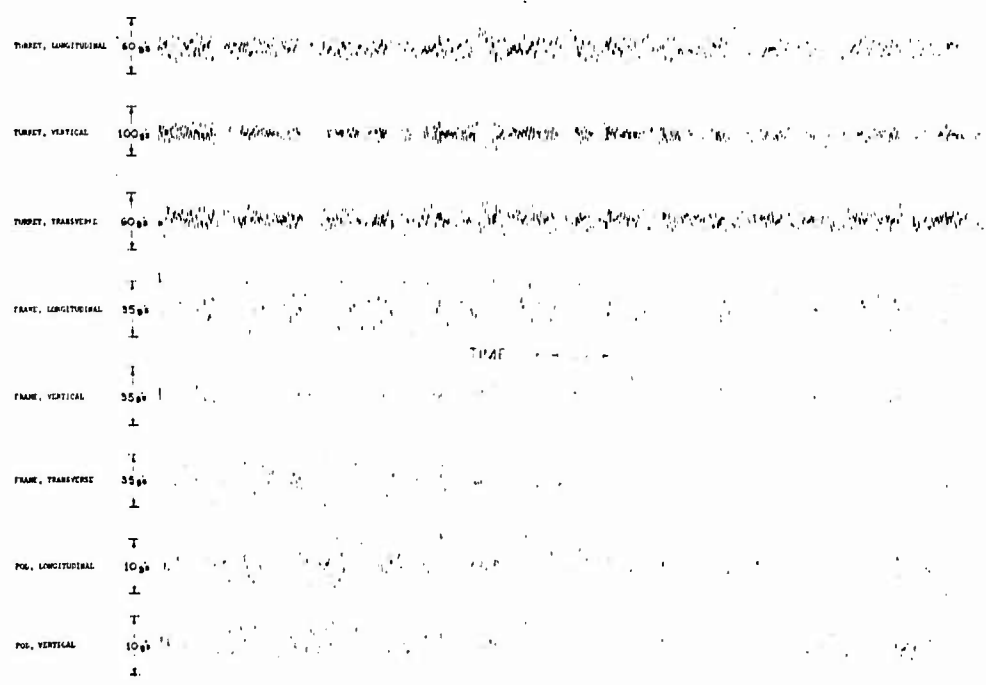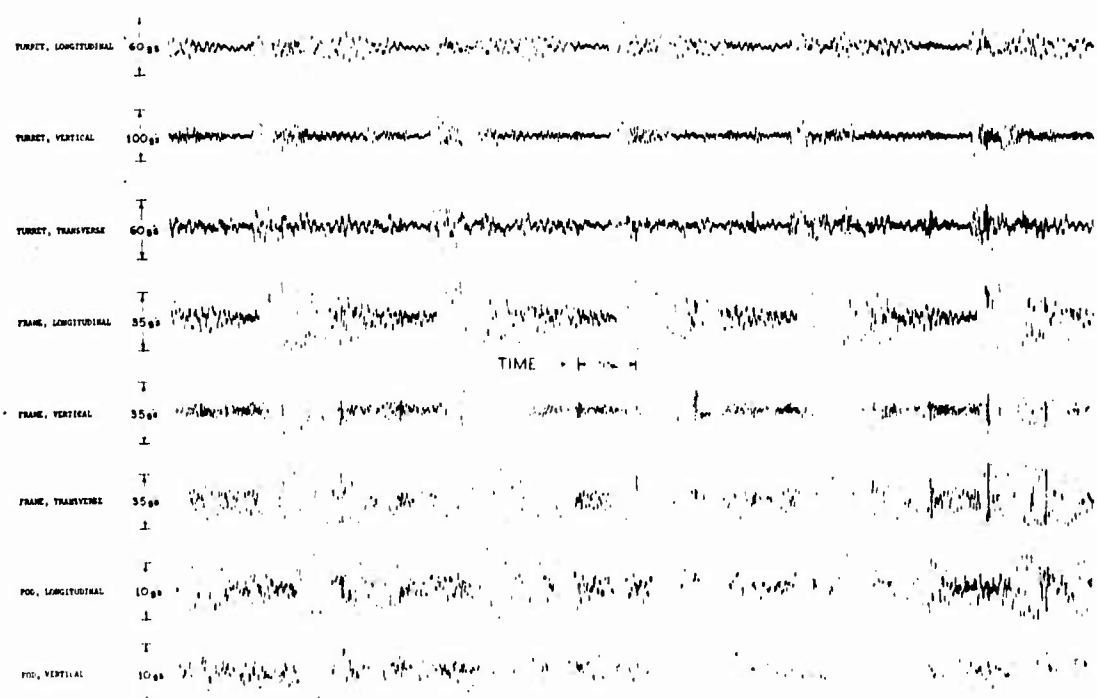
TURRET, LONGITUDINAL 60 g's

TURRET, VERTICAL 100 g's

TURRET, TRANSVERSE 60 g's

FRAME, LONGITUDINAL 35 g's

TIME

FRAME, VERTICAL 35 g's

FRAME, TRANSVERSE 35 g's

POD, LONGITUDINAL 10 g's

POD, VERTICAL 10 g's

Figure 9 - Acceleration-time history due to minigun firing at
4000 rounds per minute with turret rotated 90 .

TURRET, LONGITUDINAL 60 g's

TURRET, VERTICAL 100 g's

TURRET, TRANSVERSE 60 g's

FRAME, LONGITUDINAL 35 g's

TIME

FRAME, VERTICAL 35 g's

FRAME, TRANSVERSE 35 g's

POD, LONGITUDINAL 10 g's

POD, VERTICAL 10 g's

Figure 10 - Acceleration-time history due to minigun firing at
2000 rounds per minute with turret rotated 90 .

201
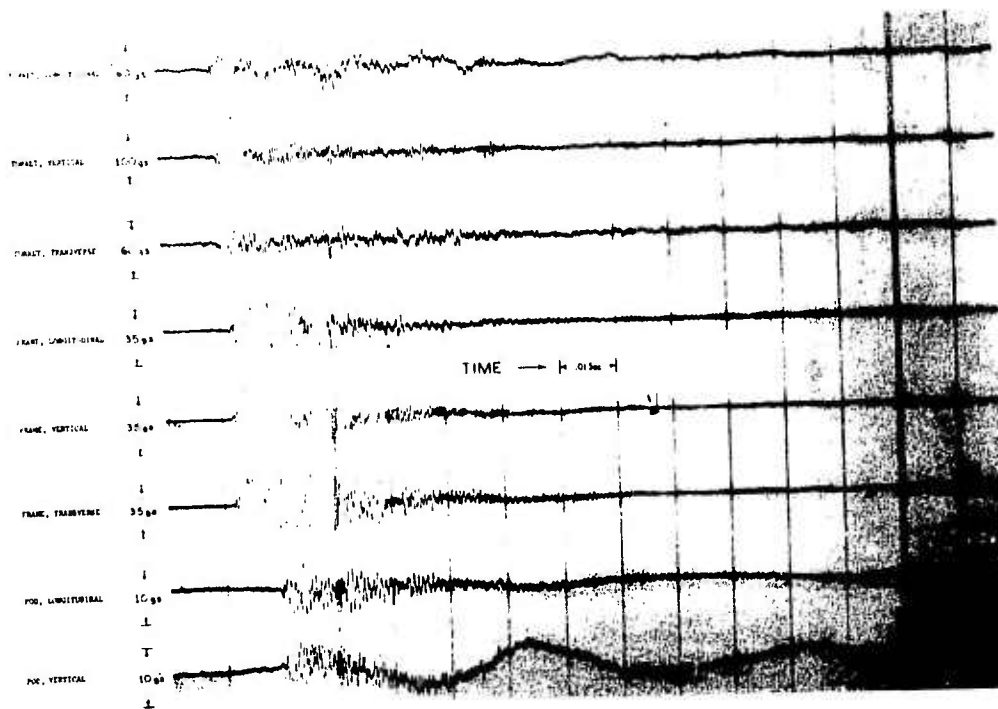
Figure 11 - Acceleration-time history due to grenade launcher
firing with turret rotated 90'.
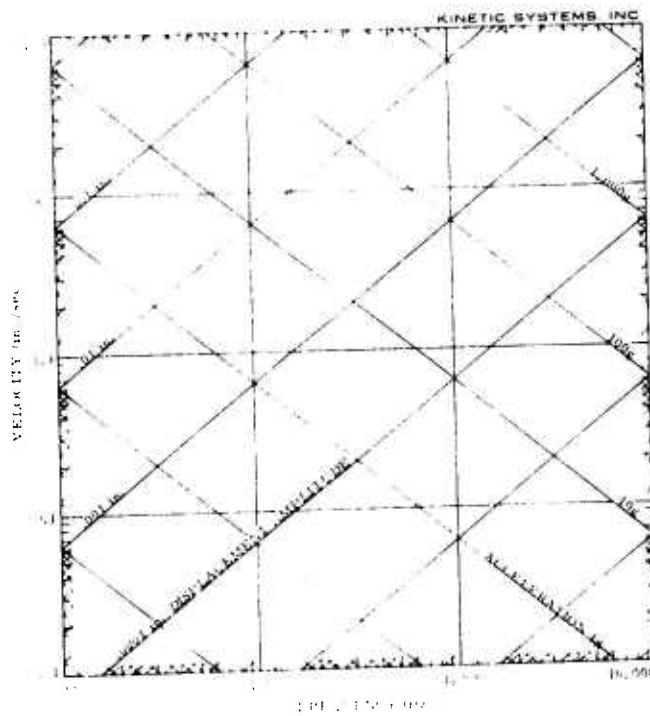
Figure 12 - Four coordinate shock spectra graph paper

presents the maximum value of the three response motions of a single degree of freedom system as a function of frequency, i.e., displacement, velocity and acceleration. The relationship between these three amplitude values and frequency are given below in Eq. (1).

$$v = \omega_n d$$
$$a = \omega_n v = \omega_n^2 d \qquad (1)$$

where d is the maximum relative deflection of a simple system response to a shock input

v is the peak velocity response

a is the peak acceleration response

and ω_n is the undamped natural frequency.

In order to utilize the data in the form of shock spectra, it is first necessary to determine the fundamental frequency of the structural component of interest. Knowing the frequency, the maximum response motion is found in terms of displacement, velocity and acceleration from the maximax shock spectrum curve.

DATA ANALYSIS TECHNIQUE

The data was analyzed and presented in the form of shock spectra using an IBM 360 Digital Computer and a Stromberg Carlson 4020 Computer Plotter, the computer program being based on the numerical procedure presented in Ref. [2]. The magnetic tape was digitized using a rate of 25,000 points per second in order to

provide the desired accuracy up to 2500 Hz [6]. Since the repeated transients for a firing condition were similar, one transient was selected from each direction at each location and for each of the firing conditions to be analyzed. In doing this, the effects of the repeated transients at the weapon's firing rate were lost and are not represented by the shock spectra. Instead, this effect is presented later as vibration data which better defines the environment. In order to obtain the resonance at the weapon firing rate in the shock spectrum, a shock record comprised of approximately ten transients would have to be analyzed. The single representative transient was selected on the basis of having a well defined initial peak which clearly indicated the beginning of the transient. Digitizing was terminated when the signal would blend into the background noise. The time durations of the digitizing process for the various records are presented in Table 1.

SHOCK ENVIRONMENT

The shock environment is representative of a single firing transient, the dynamic environment at the firing rate of the weapon is presented in the following section, "Vibration Environment". The gun firing environment of the AH-1G Helicopter, for the weapon firing head-on is presented in Figures 13-18 in the form of 3% damped shock spectra. The three curves in each figure represent the environment in the vertical, longitudinal and transverse directions. These spectra are maximax shock spectra and were computed using a value of damping of 3%. This damping value

TABLE 1
Duration of Time History Digitizing

Weapon	Firing Rate (rounds per minute)	Digitizing Duration (milliseconds)
Minigun	4000	15
Minigun	2000	30
Grenade Launcher	380	65

203
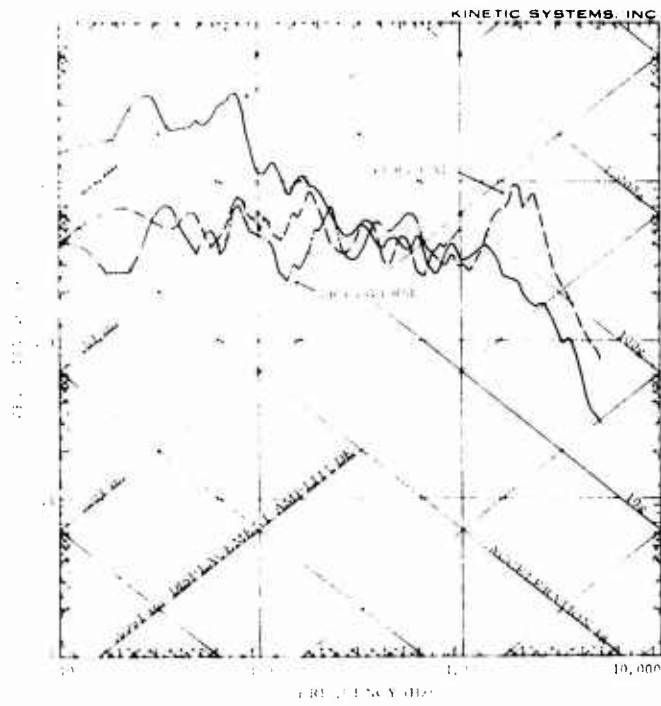
Figure 13 - Three percent damped shock spectra of turret due to grenade launcher firing.
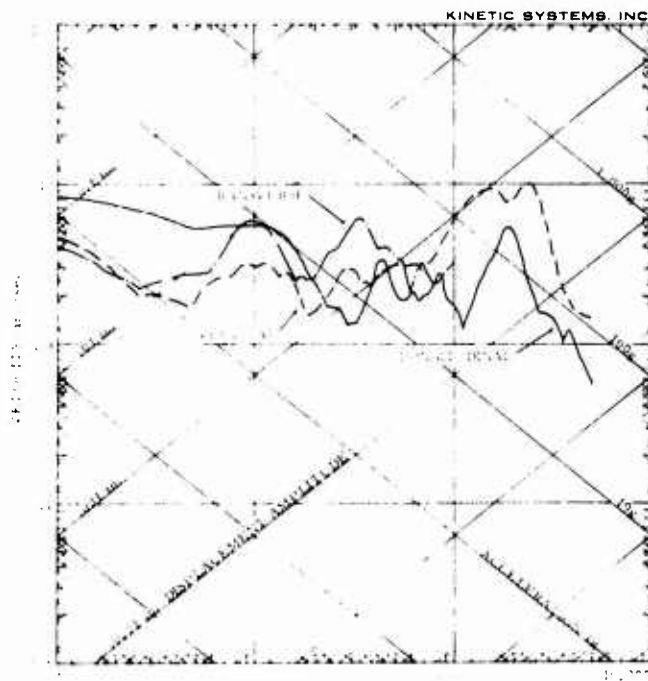
Figure 14 - Three percent damped shock spectra of turret due to minigun firing.

204
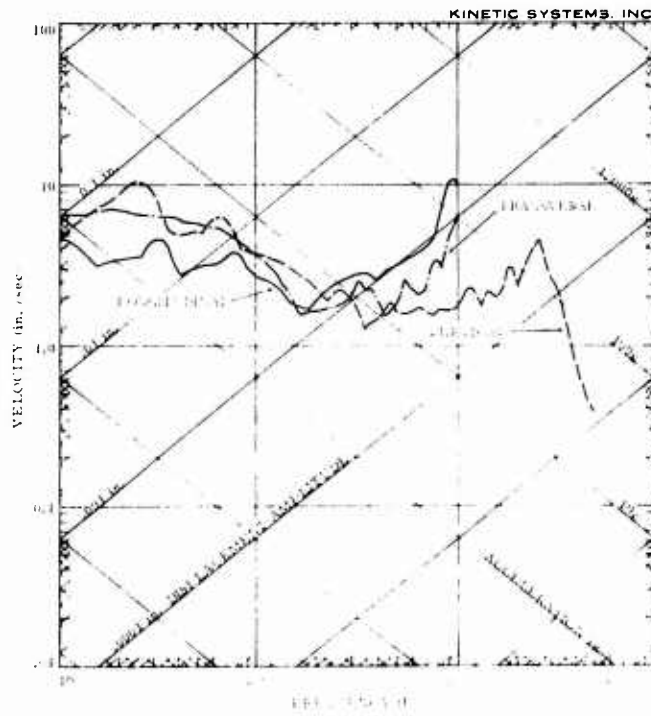
Figure 15 - Three percent damped shock spectra of frame
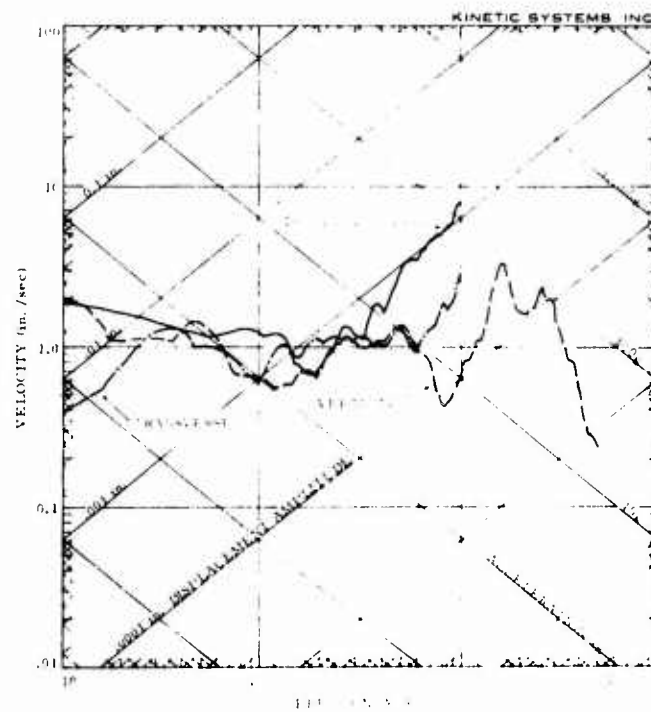near gunner's station due to grenade launcher firing.

Figure 16 - Three percent damped shock spectra of frame
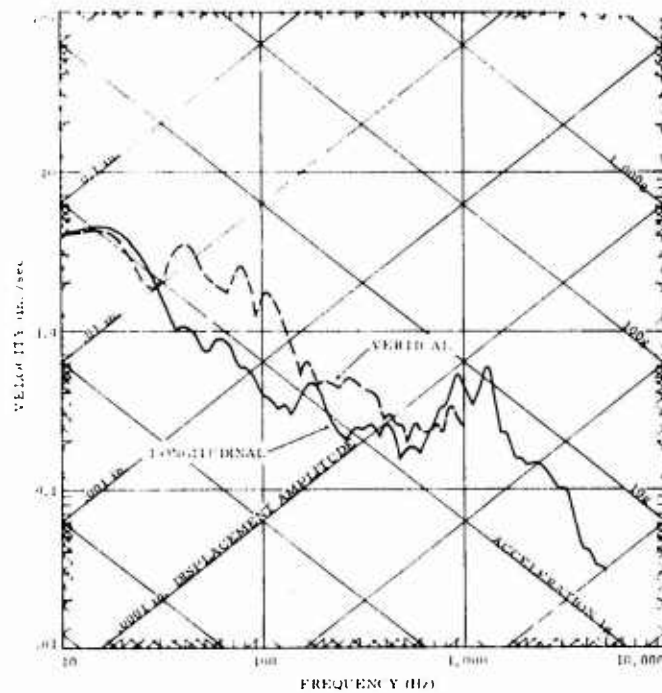near gunner's station due to minigun firing.

205

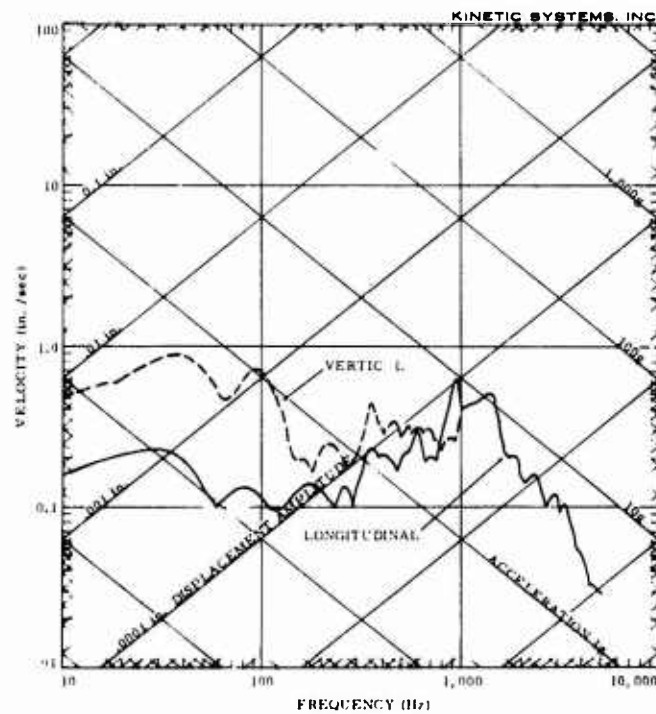Figure 17 - Three percent damped shock spectra of pod
due to grenade launcher firing.

Figure 18 - Three percent damped shock spectra of
pod due to minigun firing.

was selected since it represents a lightly damped system while significantly attenuating the undamped peak responses.

These spectra define the shock environment in the gun turret, on the aircraft's frame above the turret near the pilot/gunner's station, and in the externally mounted pod. The spectra of the minigun firing is an envelope of the environment caused by the gun firing at both its low and high firing rates. The grenade launcher spectra was not combined with this envelope since the aircraft is also supplied with two miniguns or two grenade launchers.

VIBRATION ENVIRONMENT

The vibration environment due to the repeated transients of the weapon firing was also defined via the Shock Spectrum Method. The integral of the shock time history curve represents the impulse of one transient. This is equivalent to measuring ground motion with a low frequency seismometer. This impulse is used as the peak amplitude of a simusoidal motion for a vibration test. The result is a vibration

amplitude and frequency which is representative of the gunfire environment. To the authors' knowledge, there is at present no better method of analyzing the environment of rapid firing guns. As an example, the velocity content of the turret in the longitudinal direction due to the grenade launcher firing head-on at a rate of 380 rounds per minute is 23 in./sec. This environment can be simulated by a 6.3 Hz sinusoidal velocity excitation having a peak amplitude of 23 ips, which is equivalent to a double amplitude of 1.2 in. The response of the component being tested would then be a function of its damping and natural frequency. This approach allows a simple vibration test to be specified to qualify equipment for the rapid gunfire environment.

SUMMARY

The structural vibrations of the Bell AH-1G Helicopter due to weapon firing have been measured at three locations of interest and reduced to the form of shock spectra. This data should prove useful in the design of equipment to be installed in the helicopter, and for the development of test specifications.

CHARACTERISTICS OF GUNFIRE INDUCED

VIBRATION IN HELICOPTERS

C.E. Thomas and V.C. McIntosh
Air Force Flight Dynamics Laboratory
Wright-Patterson Air Force Base, Ohio

Flight measurements of vibration induced by armament fire on three types of helicopters are described. Instrumentation and data analysis procedures are discussed briefly. Overall vibration levels as a function of distance from the gun muzzles are presented. The increase in vibration levels during gunfire over those encountered in normal flight, and the variation in vibration spectra with rate of gunfire are illustrated. Amplitude probability density curves and oscillograms of acceleration time histories are utilized to indicate the degree of randomness of armament fire vibration in various frequency bands.

INTRODUCTION

The Air Force Flight Dynamics Laboratory in cooperation with the U.S. Army Electronics Command has completed extensive vibration measurements on three helicopters. Each helicopter was equipped with one or more 7.62 millimeter machine guns whose specified (nominal) firing rates were either 2000 or 4000 SPM. A 40 millimeter grenade launcher, and 2.75 inch rocket launchers were also installed on two of the helicopters. Vibration measurements were made throughout the helicopters while the various armaments were fired. This paper reports the results of the analyses of these measurements and illustrates the spatial distribution of vibration levels, frequency spectra, and amplitude distributions.

HELICOPTER DESCRIPTIONS

The helicopter which is designated No. 1 (Figure 1) is an observation type in the 2500 pound gross weight class. A 7.62 millimeter minigun was installed externally on the left side of the helicopter with the gun muzzle approximately 12 inches outboard of the fuselage sidewall at fuselage station 70. The minigun was fired at rates of 2000 or 4000 shots per minute (SPM).

The No. 2 helicopter (Figure 2) is a utility type in the 9000 pound gross weight class. It was equipped with two 7.62 millimeter miniguns installed externally on armament mounts on each side of the helicopter. The gun muzzles were at fuselage station 105 approximately 25 inches from the fuselage sidewalls. Two seven-tube rocket launchers were installed outboard of the guns on the armament
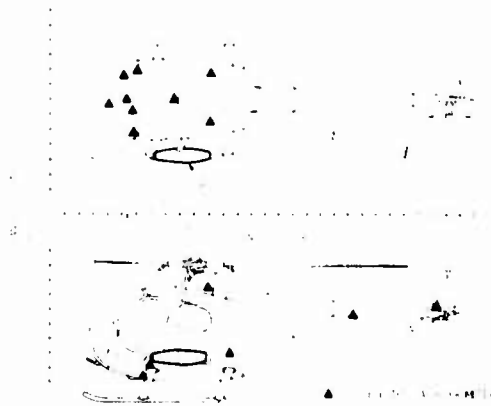
Figure 1. Armament Configuration and Transducer Locations for Helicopter No. 1
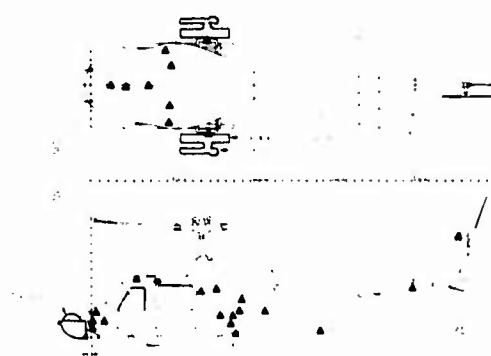
Figure 2. Armament Locations and Transducer Locations for Helicopter No. 2

209

Figure 3. Armament Configuration and Trans-
ducer Locations for Helicopter No. 3

INSTRUMENTATION AND ANALYSIS

Instrumentation consisted of (1) Endevco
2200 series crystal accelerometers bonded to
aircraft structure by epoxy cement, (2) a 12-
channel, 9-position selector switch, (3) a 12-
channel signal conditioning box utilizing
operational amplifiers with external circuitry
to obtain high input impedance and variable
gain, (4) a voice microphone, and (5) a 14-
channel, FM tape recording system utilizing
30 ips tape speed and 54 KHz carrier fre-
quencies. Accelerometers were mounted in
clusters of three to sense vibration along the
three major helicopter axes at locations
indicated in Figures 1 – 3. Recordings were
made during gunfire at 2000 and 4000 SPM and
during rocket and grenade salvo.

Flight recordings were copied in the
laboratory on continuous loops of tape for
periods of time that did not exceed the period
of armament firing (one to four seconds).
These loops were then played back and analyzed
on a Spectral Dynamics Corporation Model SD-
101A spectrum analyzer. A 10 Hz bandwidth,
one-second averaging time, and two Hz per
second sweep rate were used for frequency
analyses covering the range from 5 to 1000 Hz.
The bandwidth and sweep rate were increased to
20 Hz and four Hz per second, respectively,
for analyses covering the range from 5 to
5000 Hz.

Amplitude probability density (APD)
analyses of selected vibration recordings
were conducted using a Gulton Industries
Statistical analyzer. Controls on this
analyzer were adjusted to obtain an amplitude
range of ± 3 standard deviation units, a
smoothing time constant of three seconds, and
a scanning time of 450 seconds.

OVERALL VIBRATION LEVELS

Figure 4 illustrates overall lateral
acceleration level on Helicopter No. 1 as a
function of fuselage station during the attack
maneuver, gunfire at 2000 SPM, and gunfire at
4000 SPM. The muzzle of the single gun on
this helicopter is located at fuselage station
70. The maximum overall acceleration level of
23.4 g's was detected by an accelerometer
located at fuselage station 62, 8 inches for-
ward of the gun muzzle. Gunfire vibration
levels at fuselage stations 50 inches forward,
and aft, of the gun muzzle are less than 25%
of the maximum level. Vibration levels at
locations near the gun muzzle increase greatly
during gunfire. For example, at fuselage
station 62, the vibration level increased from
0.6 g for the attack maneuver to 23.4 g's for
gunfire at 4000 SPM. Figure 4 also shows that
the overall vibration level increased approxi-
mately 20% as the firing rate was increased
from 2000 to 4000 SPM. Overall acceleration
levels, at all locations except at fuselage
station 220, are appreciably higher during
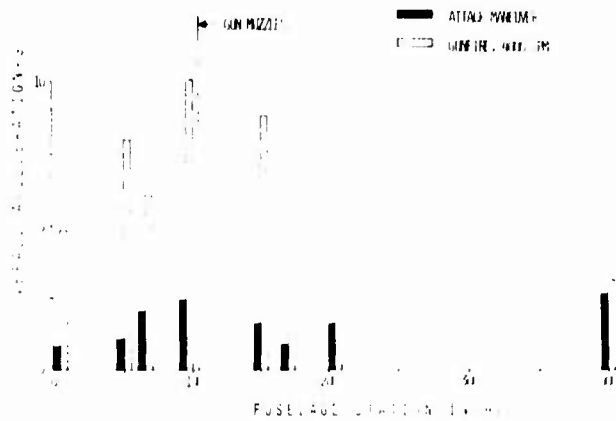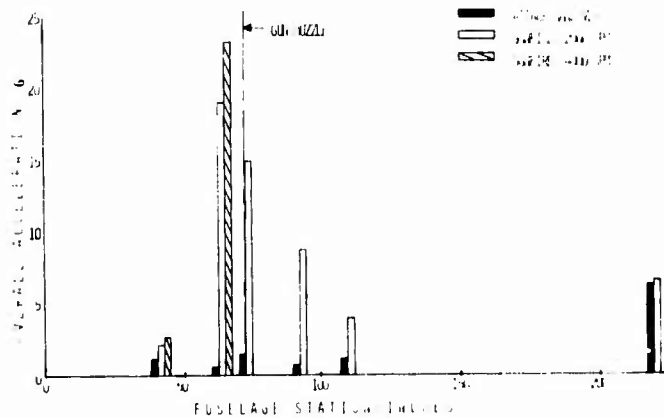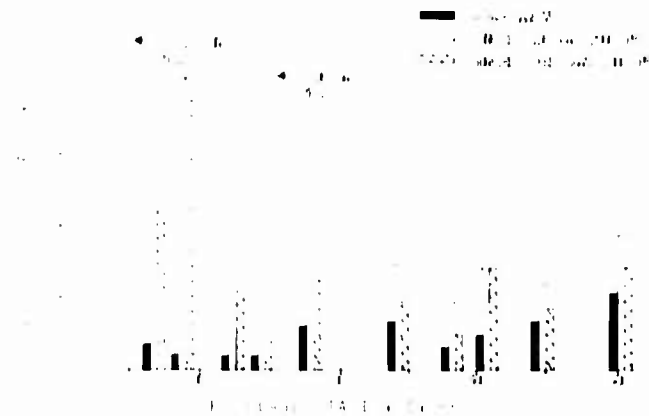gunfire than those during the attack maneuver.

Figure 4. Variation of Overall Lateral Acceleration Level with
Fuselage Station on Helicopter No. 1 During Gunfire
and Attack Maneuver

The variation of overall vertical
acceleration level with fuselage station on
Helicopter No. 2, during gunfire, is presented
in Figure 5. The maximum gunfire vibration
level (10.1 g's) was measured by an accelero-
meter located at fuselage station 95, 10 inches
forward of the gun muzzles. Gunfire effects
are somewhat less localized than they were on
Helicopter No. 1. Gunfire vibration levels at
distances of 100 inches forward, and aft, of
the gun muzzles are nearly 50% as high as the
maximum level. Overall gunfire vibration
levels are greater than 3 g's throughout the
helicopter.

Figure 5. Variation of Overall Vertical Acceleration Level with
Fuselage Station on Helicopter No. 2 During Gunfire
and Attack Maneuver

211

Vertical vibration levels at various fuse-
lage stations to the rear of both the side
and turret guns of Helicopter No. 3 are shown
... the maximum response from gunfire
... measured at
... station 160, 6 inches forward of the
gun muzzle. Remember that at an accelero-
meter located forward of the turret gun
muzzles, the maximum response to turret gunfire
gunfire was not recorded. The maximum
recorded turret gunfire level was 16.2 g's at
fuselage station 80, 20 inches aft of the
turret gun muzzles. The rate of change of
vibration level with distance from the gun
muzzle is similar to that for Helicopter No.
1, i.e., levels decrease approximately 90% in
the first 100 inches.

are obtained from three lateral accelero-
meters located in the nose compartment. All
three lateral accelerometers were located near
fuselage station 60, just forward of the gun
muzzles, but they were at different lateral
distances from the gun. The accelerometer for
the upper plot was located only 26 inches from
the gun muzzle. This spectrum shows a peak
level of approximately 4 g's at 67 Hz, the
fundamental gunfire frequency. The spectrum
then remains relatively flat to 1000 Hz except
for minor peaks at harmonics of the gunfire
frequency. The accelerometer for the center
plot was located in the center of the nose
compartment approximately 40 inches from the
gun muzzle. The lower plot is for an accelero-
meter located on the right side of the nose

Figure 6. Variation of Overall Fore and Aft Acceleration Level with
Fuselage Station on Helicopter No. 3 During
Gunfire and Attack Maneuver

Figure 7 shows a comparison of the over-
all vibration data from Helicopters No. 1 and
3. This figure illustrates major differences
in both gunfire vibration levels and the
variation of these levels with distance from
the gun muzzles. The distance of the gun
muzzles from the fuselage sidewalls for Heli-
copters No. 1 and 3, are 12 and 20 inches,
respectively. This difference certainly could
account for higher vibration levels measured
on Helicopter No. 1. Also, the gross weights
of the two helicopters are 2500 pounds for
Helicopter No. 1 and 9000 pounds for Helicopter
No. 3. This difference in gross weights and
differences in structural rigidity could result
in lower vibration response for Helicopter No.
3, and also could affect the rate of change of
gunfire levels with distance from the gun
muzzles.

FREQUENCY SPECTRA

Figure 8 shows typical frequency spectra
occurring on Helicopter No. 1 during gunfire
at 4000 SPM. The three plots in this figure

compartment approximately 56 inches from the
gun muzzle. These plots show that at all
frequencies above 400 Hz, the gunfire vibration
is attenuated as it is transmitted from the
left to the right side of the nose compartment.
At 1000 Hz, the vibration level is 1.5 g's on
the left side of the nose and only 0.11 g on
the right, or the level has decreased by a
factor greater than 10 as vibration was
transmitted through 30 inches of structure.
The overall acceleration levels for the three
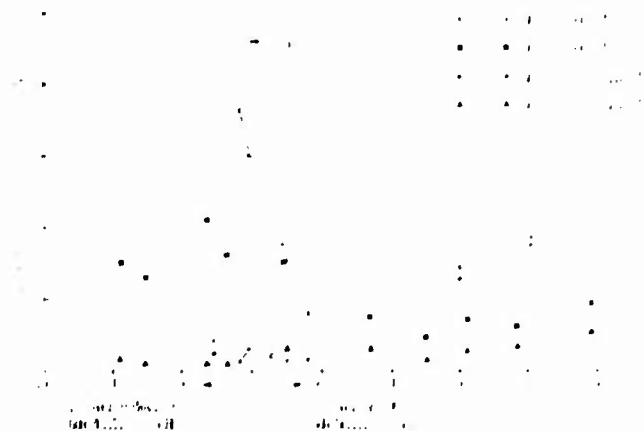locations were 23.4 g's on the left side,

Figure 7. Variation of Overall Acceleration Levels with Fore and aft Distance from Gun Muzzle for Helicopters No. 1 and 3
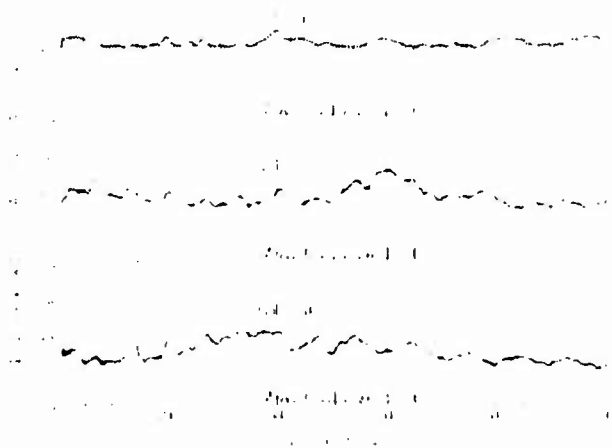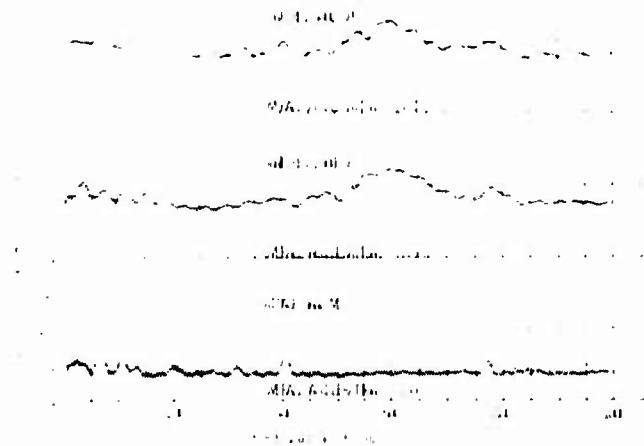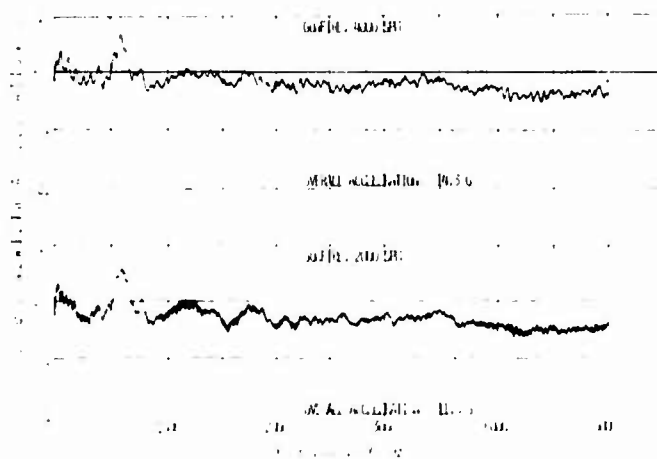

Figure 8. Lateral Vibration Spectra in Nose Compartment (F.S. 62) of Helicopter No. 1 During Gunfire at 4000 SPM from Gun Mounted on Left Side of Helicopter

14.3 g's in the center and 5.6 g's on the right side.

Figure 9 shows a comparison of vibration spectra from Helicopter No. 1 at gun firing rates of 2000 and 4000 SPM. The attack maneuver spectrum also is shown in the lower plot to indicate the decreased level of vibration existing without gunfire. The two upper plots show the first five harmonics of the fundamental gunfire frequencies (37 and 67 Hz) rather clearly, but higher harmonics are difficult to detect. Both spectra show maximum levels at 600 Hz. Spectrum levels are slightly

lower for the lower gunfire rate, and the overall acceleration level increases from 14.3 g's for 4000 SPM to 11.8 g's for 2000 SPM.

Figure 10 repeats the spectra of the two upper plots from Figure 9, except that the upper frequency limit is increased from 1000 to 5000 Hz and the analysis bandwidth is increased from 10 to 50 Hz. This figure illustrates generally higher spectra levels for the higher gunfire rate. Above 1000 Hz frequencies are too high for the peaks are higher by a factor of 2 due to the peaks in the spectrum. Note that the resonant spectra

213

Figure 9. Lateral Vibration Spectra in Nose Compartment
(F.S. 62) of Helicopter No. 1 During Gunfire at 4000 SPM,
Gunfire at 2000 SPM, and the Attack Maneuver

levels up to 1.0 g at frequencies between
1000 and 2000 Hz, and levels above 0.3 g up to
5000 Hz. These levels are low relative to the
peak of 4 g's which occurred at 600 Hz. How-
ever, the 20 Hz analyzer bandwidth may be
narrower than the response bandwidths of some
structures and equipments at frequencies above
1000 Hz, and spectrum levels obtained from the
20 Hz analysis bandwidth could be misleading.
One-third octave spectrum levels for the 4000
SPM gunfire recording varied between 3 and 4
g's in the frequency range of 1000 to 5000 Hz.
These levels could result in malfunction of
sensitive equipment.

Figure 10. Lateral Vibration Spectra in Nose Compartment
(F.S. 62) of Helicopter No. 1 During Gunfire
at 4000 and 2000 SPM

Spectra obtained from the lower nose
compartment (fuselage station 0) of Helicopter
No. 2 are shown in Figure 11. Spectra for
grenade salvo, gunfire, and the attack maneuver
are shown on the upper, center, and lower plots,
respectively. The gun firing rate was expected

to be 4000 SPM, but the center spectrum clearly shows gunfire harmonics spaced at multiples of 45 Hz and which corresponds to an actual gunfire rate of 2700 SPM. The spectrum for grenade salvo is similar to that for gunfire except for the lower gunfire harmonics. Both spectra peak at 500 Hz and are approximately the same level.
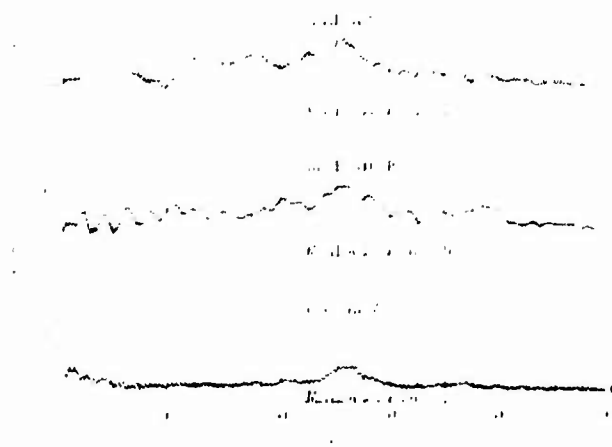
Figure 11. Vertical Vibration Spectra on Lower Shelf of Nose Compartment (F.S. 0) of Helicopter No. 2 During Grenade Salvo, Gunfire at 4000 SPM and the Attack Maneuver

Figure 12 contains spectra for the aft electronics compartment (fuselage station 173) of Helicopter No. 2 for rocket salvo, gunfire at 4000 SPM, and the attack maneuver. A check on spacing of gunfire harmonics shows that the machine gun was firing at an actual rate of 3500 SPM. The spectrum for rocket launch also is similar to that for gunfire, but the rocket salvo spectrum has higher levels below 50 Hz and above 500 Hz. The spectrum for the attack maneuver exhibits peaks in the range of 100 to 300 Hz. These peaks occur at harmonics of the tail rotor blade passage frequency (56 Hz). The vibration induced by the tail rotor also contributes to corresponding peaks in the gunfire and rocket salvo spectra. Apparently, the peaks in the response at frequencies above 300 Hz are determined more by structural resonant frequencies than by the excitation from armament fire, since gunfire, rocket fire, and grenade fire produce very similar spectra.

Spectrum plots for the aft electronics compartment (fuselage station 310) of Helicopter No. 3 during grenade salvo, rocket salvo, and gunfire at 4000 SPM from the nose turret guns are contained in Figure 13. This location is 255 inches aft of the turret gun and grenade launcher muzzles. Overall acceleration levels due to gunfire and grenade salvo are below 0.1 g. The overall level during the attack maneuver is relatively high (0.62 g's) and tends to mask the effects of the armament fire in the frequency range below 400 Hz. The spectrum for rocket salvo shows considerably higher levels at frequencies above 400 Hz. One reason for this may be that the rocket exhaust excitation is much closer to the aft electronics compartment than the turret guns or grenade launcher, and the higher frequencies are not much attenuated by the structure as they have been for the sources of excitation near the nose.

Figure 14 compares the gunfire vibration spectrum at 4000 SPM firing rate with the spectrum for 2000 SPM. The plot for the higher firing rate indicates two distinct fundamental firing frequencies at 67 Hz and the second and fourth harmonics, but other harmonics are not clearly defined. The first four harmonics at the lower firing rate are clearly indicated. The two spectra contrast similar frequency peaks above 200 Hz although increased spectrum levels are encountered at the higher firing rate. This is especially true for frequencies above 500 Hz. Corresponding overall acceleration levels were 0.5 g's for 4000 SPM and 0.49 g's for 2000 SPM. The increase in vibration levels with gunfire rate would be expected since the excitation energy increases directly with the firing rate.
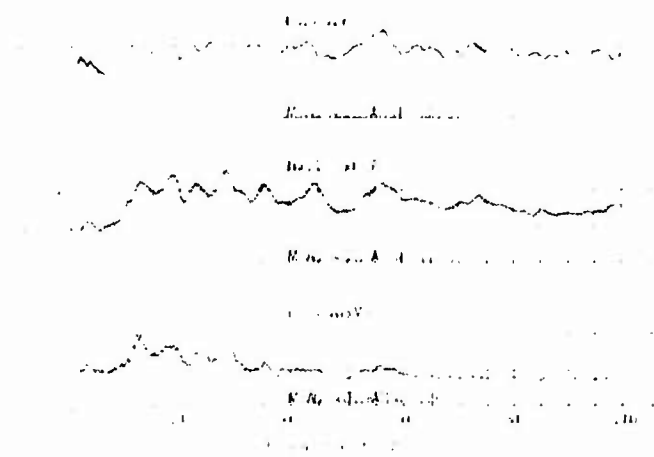
215

Figure 12. Vertical Vibration Spectra on Structure Near Fuselage Station 173 in Helicopter No. 2 During Rocket Salvo, Gunfire at 3500 SPM, and Attack Maneuver
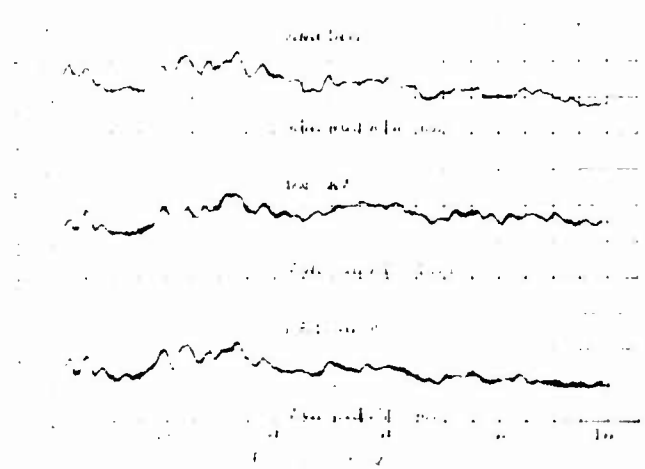

Figure 13. Vertical Vibration Spectra in Aft Electronics Compartment (F.S. 310) of Helicopter No. 3 During Grenade Salvo, Rocket Salvo, and Gunfire from Turret Guns at 4000 SPM
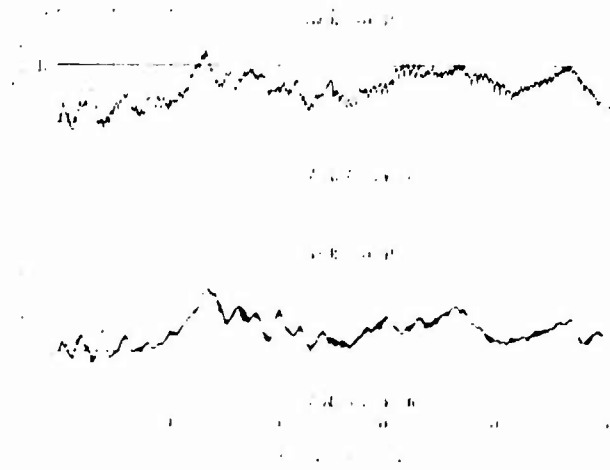
216

Figure 14. Vertical Vibration Spectra at Nose Turret Interface
(F.S. 69) of Helicopter No. 3 During Turret Gunfire at 2000 and 4000 SPM

ACCELERATION PROBABILITY DENSITY

Amplitude probability density (APD) analyses were conducted on filtered (10 Hz bandwidth) acceleration time histories during gun, rocket, and grenade firing. Oscillograms of the filtered acceleration data also were obtained. The degree of randomness of the vibration is illustrated by both the APD plots and the oscillograms.

Figure 15 illustrates APD plots and oscillograms of 10 Hz bands of acceleration time histories from Helicopter No. 3 during gunfire of the two nose turret guns at a combined rate of 4000 SPM. The accelerometer was located at the nose turret interface. The 63 Hz center frequency illustrated is the fundamental firing rate of the miniguns (slightly below 4000 SPM). In this frequency band, the acceleration is largely sinusoidal. The APD plot and the oscillogram for the 264 Hz center frequency illustrates random vibration with essentially Gaussian distribution. Although not included herein, a large number of APD analyses were performed on other gunfire time histories. In general, these analyses confirm the results illustrated by Figure 15. In frequency bands below 200 Hz, gunfire vibration generally is more nearly sinusoidal than random, and above 200 to 300 Hz gunfire vibration is predominantly random with essentially Gaussian probability density.

Both rocket and grenade salvo occur at rates of four to six shots per second. The corresponding vibration response is a series or train of transient vibrations which have broad band frequency content and decay approximately to initial conditions between firings. Figure 16 shows APD plots and

oscillograms of 10 Hz bands of acceleration time histories during grenade salvo in helicopter No. 2. The accelerometer was located in the nose compartment near the grenade launcher. The 65 Hz and 150 Hz center frequencies correspond to peaks in the grenade salvo spectrum. The APD plot for the 65 Hz center frequency shows higher probability density near zero acceleration because of the relatively long period between grenade salvos as shown by the oscillogram above the APD plot. Also, the probability density for acceleration levels two to three times the RMS level is higher than that for a Gaussian distribution. The APD plot for the higher center frequency of 150 Hz deviates even further from the Gaussian distribution, i.e., probability densities for accelerations near zero and for levels two to three times the RMS level are higher than those for the 65 Hz center frequency. These two plots are representative of other plots obtained for rocket and grenade salvo that also showed distributions very different in shape obtained from either sinusoidal or random Gaussian signals.
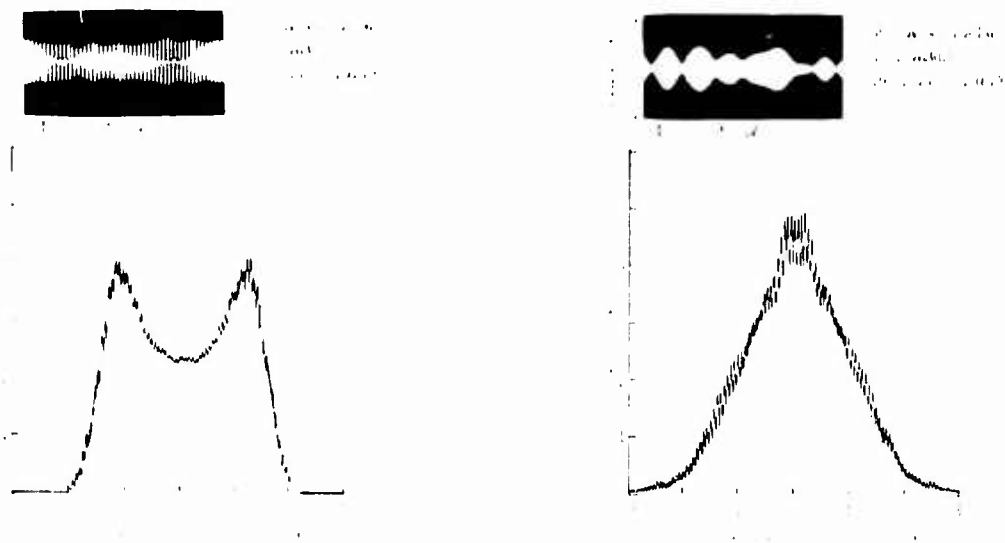
217

Figure 15. Acceleration Probability Density at Nose Turret Interface (F.S. 69) During Firing of Turret Guns on No. 3 Helicopter at 4000 SPM
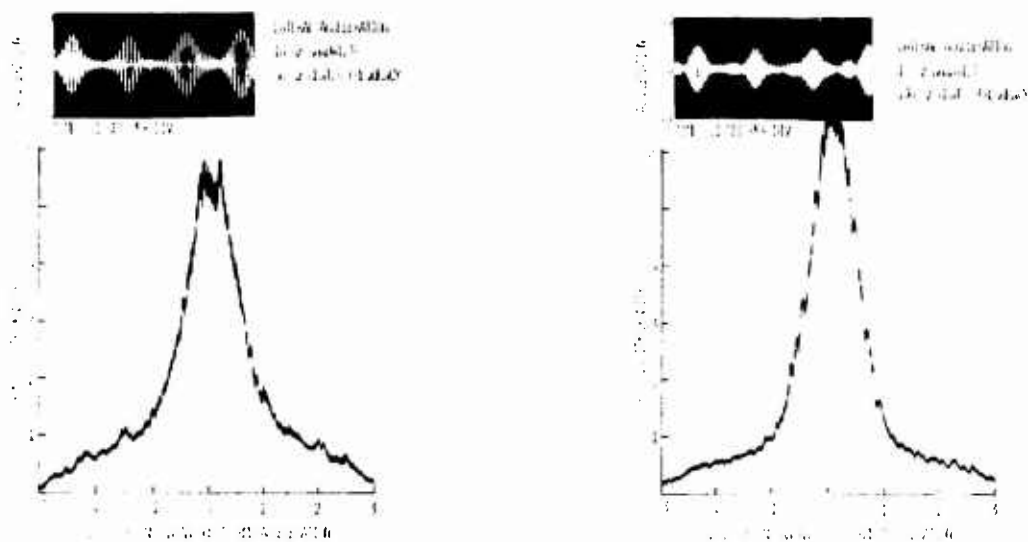

Figure 16. Acceleration Probability Density in Nose Compartment at F. S. 0 of Helicopter No. 2 During Grenade Salvo

SUMMARY

The maximum helicopter vibration response to firing of externally mounted, 7.62 milli- meter machine guns occurs within a distance of 35 inches forward of the gun muzzles. High level gunfire vibration in excess of 5 g's is localized to within 100 inches forward, and 50 inches aft, of the gun muzzles. At distances greater than 100 inches aft of the gun muzzles, gunfire vibration levels generally are not significantly greater than the levels without gunfire.

218

The maximum overall acceleration levels during gunfire are greatly influenced by the distance of the gun muzzles from the fuselage sidewalls. Maximum levels measured on Helicopter No. 1 where the gun muzzle was 12 inches from the sidewall were twice as great as the levels measured on Helicopters No. 2 and 3, where the gun muzzles were 25 and 20 inches, respectively, from the sidewalls.

Based on 16 measurements within 50 inches of the gun muzzles on three helicopters, the average ratio of overall acceleration level during gunfire to that during the attack maneuver without gunfire was 12.5. The maximum ratio obtained from measurements on three helicopters was 39.

Based on the average of 42 measurements on two helicopters, overall acceleration levels during gunfire at 4000 SPM are 36% greater than overall acceleration levels during gunfire at 2000 SPM. Increased acceleration levels occur throughout most of the frequency range at the higher gunfire rate, but the increase is more pronounced at frequencies above 500 Hz.

The frequency spectra of helicopter acceleration induced by 7.62 millimeter gunfire are characterized by well defined peaks at the fundamental gunfire frequency and the first five harmonics of the fundamental. At frequencies above 200 to 300 Hz, harmonic peaks are less pronounced, indicating more continuous spectra and more random vibration that usually is associated with continuous spectra. Maximum acceleration levels due to all types of armament fire occur in the frequency range of 250 to 600 Hz, but

appreciable acceleration levels exist at frequencies up to 5000 Hz.

At locations near the grenade launcher or rocket exhausts, vibration levels during grenade or rocket salvo may be higher than those produced by gunfire.

Helicopter vibration response to grenade and rocket salvo is characterized by a series of transient vibrations with three band frequency contents. The transients decay in accordance to the initial condition existing at a rate where the accelerance of rocket transients and that of vibration transients associated with rocket frequency bands and harmonics thereof. Acceleration levels are not equivalent in the vertical and cylinder direction, however, is quite different from that of random transient vibrations.

DISCUSSION

McCaskell (Bell Helicopter): I judge from your conclusions that you are implying that basically the helicopter vibrations are influenced more by muzzle blast than by recoil of the systems.

Mr. McIntosh: Yes sir, very definitely.

Mr. McCaskell: You covered a tremendous amount of ground in your work and it is going to be a tremendous help to us. Did you, in fact, on ship number 3 for instance do off-angle firing?

Mr. McIntosh: We did, however, none of that data is included in this paper.

Phyllis G. Bolds and John L. Ash
Air Force Flight Dynamics Laboratory
Wright-Patterson Air Force Base, Ohio

The Air Force Flight Dynamics Laboratory has obtained inflight vibration
and acoustic data on a series of helicopters for upgrading of environ-
mental design criteria and verification of dynamic prediction techniques.
These data, acquired from several helicopters, are discussed in detail.
The individual and collective characteristics of these helicopters are
determined as a function of dynamic measurement levels. These levels are
then related to sources, i.e., rotor, aerodynamics, and engine; and
performance characteristics, i.e., hover, take off, and speed range. The
spatial distribution from vehicle to vehicle are also considered. The
measured data used in this study covers jet engine powered helicopters.
The data was examined to determine whether it is generally random (dis-
tribution of amplitudes) or sinusoidal in nature. The specifications
relating to personnel and equipment for vehicles of these general types
were examined, and changes were recommended as indicated by these data.

INTRODUCTION

Human discomfort and equipment malfunction
are occurring in military aircraft operating
under combat conditions. This indicates
either an inaccurate assessment of the envi-
ronment or the use of data that is not current
to prepare personnel comfort and equipment
specifications. To obtain this needed infor-
mation for current helicopters the Air Force
Flight Dynamics Laboratory and the Army
Electronics Command (AMSEL) participated in a
joint effort to determine helicopter dynamic
characteristics under simulated combat condi-
tions, including gunfire. This program is
part of a continuing effort by the Air Force
Flight Dynamics Laboratory to acquire com-
prehensive vibration and noise data on all
available aircraft and missiles.

The objective of this paper is to discuss
the non-gunfire portion of these results: to
show the measured dynamic response of each
test vehicle as a function of performance and
station; to compare these data with existing
environmental specifications, i.e., MIL-STD-
810B(1), relating to helicopter equipments,
MIL-A-8806A, relating to the sound pressure
level in aircraft, and MIL-H-8501A, vibration
specifications relating to helicopter per-
sonnel.

TEST VEHICLE DESCRIPTIONS

Helicopter A, shown in Fig. 1, is a single-
engine aircraft in the 9000 pound weight class..
The aircraft missions are to transport per-
sonnel and equipment, medical evacuation, and
ambulance service. When equipped with armament,
it may be used to deliver point target and area
fire power. Helicopter B, shown in Fig. 2, is
a light-weight, single engine, four-place heli-
copter. Primary mission of this helicopter are
observation, target acquisition, reconnaissance,
and command control. When equipped with an
armament subsystem it is capable of defense
against ground based fire from automatic
weapons and small arms. Helicopter C, shown
in Fig. 3, is an armed tactical vehicle with
two seats and weighs approximately 5000
pounds empty and grosses at 9500 pounds. The
primary mission of Helicopter C is fire support.
General data for the three test vehicles are
listed in Table 1.

FIELD MEASUREMENT AND ANALYSIS

The flight instrumentation consisted of an
average of 64 piezoelectric accelerometers for
each of the three surveys, 12 crystal micro-
phones, 12 low frequency accelerometers (0 to
160 Hz), a 13-channel signal conditioning unit
containing operational amplifiers with external
circuitry for continuously adjustable gain, a
voice microphone, and a 14-channel FM magnetic

GENERAL DATA ON TEST VEHICLES

					Main Rotor				Tail Rotor		
				Dia-ft	Type	RPM	N_1-Hz	Dia-ft	Type	RPM	N_1-Hz
				44.2	2-blade	324	11	8.5	2-blade	1650	55.0
				26.5	4-blade	475	52	4.2	2-blade	3020	100.6
				44.0	2-blade	324	11	8.5	2-blade	1700	59.0
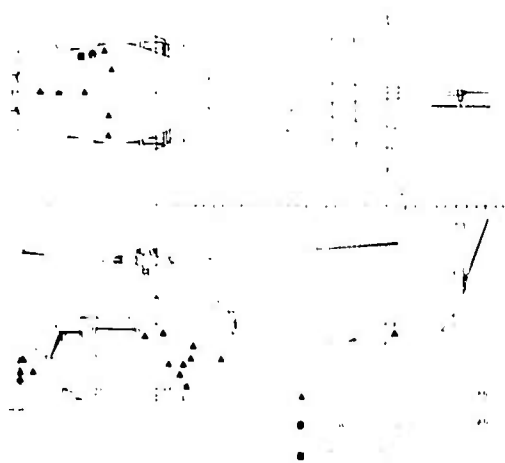
Figure 1. Selected Transducer Location - Helicopter A

Figure 2. Selected Transducer Location - Helicopter B

Figure 3. Selected Transducer Location - Helicopter C

tape recorder utilizing 30 ips tape speed and 54 KHz center frequency FM record amplifiers. Figure 4 shows a block diagram of the data acquisition system. The piezoelectric accelerometers were mounted usually in groups of three and oriented to sense vibration along the major axes of the helicopter. Microphones were mounted externally along the longitudinal axis and on the upper surface of the helicopter to sense blade passage excitation, externally on the armament mount and internally on the pilot and co-pilot's helmets, rear cabin, cabin bulkhead and avionics compartment. Low frequency accelerometers were mounted on the instrument panel, right and left side of the cabin floor, fuselage-tail section interface and tail boom. All pickups were calibrated in the laboratory using the same cables, connections and mounting brackets used during flight measurements. The accuracy limitations of the flight measurement systems are a summation of errors contributed by transducer, signal conditioning equipment and tape recorder. The maximum error of any one of these elements is unlikely to exceed +5% of full scale output. A reasonable estimate of

the maximum overall error is the root-mean-square of the errors of the three contributors or $\pm 8.7\%$ of full scale output.
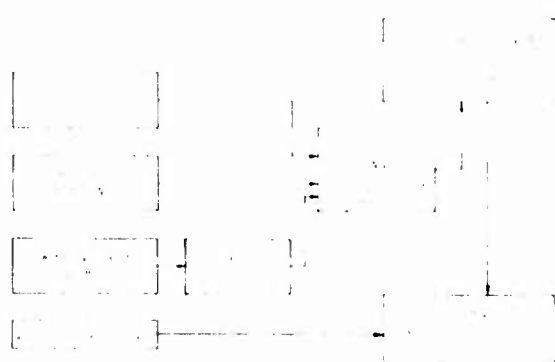
Figure 4. Block Diagram of Data Acquisition System

Measurements were taken during ground runup, take off, climb, level flights at various speeds and altitudes, hover, descent, autorotation, combat approach to landing, turns, sideward flight, and rearward flight. For each flight condition, a 12-channel data sample of 20 seconds duration was generally recorded for each of the nine selector switch positions. Recorded flight information included altitude, airspeed, rate of climb or descent, pitch angle, roll angle, engine speed, main rotor speed, torque pressure, fuel weight, outside air temperature and tail pipe temperature.

TABLE II

FREQUENCY ANALYSIS PARAMETERS

Effective Bandwidth (Hz)	Frequency Range (Hz)	True Averaging Time (Sec)	Scan Rate (Hz/Sec)
5	$^\circ$ 160	5	0.2
15	0-500	4.4	1.6
35	501-1000	2.0	7.0
75	1001-6000	1.0	22.0

The data reduction procedures consisted of playing back all records on a tape record/reproduce system and measuring overall rms

levels on a level recorder. Data samples necessary to establish maximum, minimum, and average levels, and to indicate variation in environmental levels with flight parameters, were selected and analyzed in detail. A list of the selected performance characteristics of the analyzer are contained in Table II. Table III presents a summary of the flight test conditions for which detailed analog analyses were made. The data resulting from the analog analysis were processed using an IBM 7011/7094 computer system. The computed data were sorted into the desired order and then plotted by an automatic plotter having tape input capability. A block diagram of the data analysis system is shown in Figure 5.
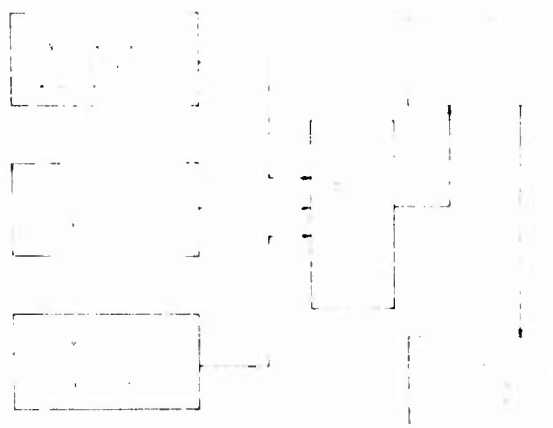
Figure 5. Block Diagram of Data Analysis System

DATA PRESENTATION

Approximately 15% of the analyzed data is presented in this paper. Figures 1 through 5 show transducer locations selected for presentation for Helicopters A, B, and C, respectively.

Four piezoelectric vibration transducers were selected from each helicopter survey at similar locations in each of the following areas: (a) nose section, (b) instrument panel (c) cargo area, and (d) tail boom. Helicopter B has no comparable transducer in the nose section since the vehicle is small and the instrument panel is in the extreme forward part of the fuselage (fuselage station 59). The vibration data were projected on a normalized fuselage scale as a function of the measured overall acceleration levels in g-units. Data are presented for the four selected vibration transducers which were oriented to sense vibration in the vertical direction. These data are presented in Figures 6 through 12. In addition, data are presented for these four transducers in Figures 13 through 16 to show the variation in overall acceleration

223

level with flight condition.

TABLE III

SELECTED FLIGHT CONDITION

Condition	Helicopter A		Helicopter B		Helicopter C	
	IAS (Knots)	ALT (Feet)	IAS (Knots)	ALT (Feet)	IAS (Knots)	ALT (Feet)
Ground Runup	0	0	0	0	0	0
Hover in ground effects	0	0	0	0-10	0	0
Level Flight	20-110	500	20-120	500	20-150	500
Level Flight	20-110	5000	20-110	5000	20-145	5000
Level Flight		-	20-100	8000	20-125	10,000
Take off	0	0-500	0	0-500	0	0
Max Climb	60	500	35	500-700	90	500
Standard Descent	120	7000-0	58	4000-0	-	-
Combat Approach (Swing)	95	5000-0	120	2500-0	-	-
Combat Approach (Spiral)	60	7000-0	100	5000-0	150	5000-0
Autorotation	45	5000-0	68	4000-0		5000-0
Right Turn, 55°	-	-	60	500	-	-
Right Turn, 45°	60	500	-	-	-	-
Right Turn, 30°	55	500	55	500	-	-
Left Turn, 60°	-	-	50	500	120	500
Left Turn, 45°	65	500	-	-	-	-
Left Turn, 30°	60	500	50	500	120	500
Hover	0	5000	-	-	-	-
Sideward Flt to Left	10	10	-	-	-	-
Attack Maneuver	120	500-2000	110	500	-	-

The maximum double amplitude levels measured from all vibration transducers located in the nose and the cargo area are presented in Figures 17 through 22. These plots represent the maximum levels measured in the three orthogonal directions for all of the flight conditions listed in Table III. Figure 23 is a summary plot showing the maximum double amplitude levels measured for each of the helicopters.

Figures 24 through 26 are plots of the maximum vibration levels obtained from two low frequency accelerometers orientated in the vertical and lateral direction and located on the cabin floor of each of the three helicopters for the flight conditions listed in Table III.

amplitude probability density curve of the main rotor fundamental frequency puted for data measured in the nose on of each helicopter during a combat approach configuration. The APD was constructed from -3σ to +3σ using the analysis parameters listed in Table IV. In addition, APD's were computed for the same flight condition for peaks in the spectrum which occurred between 200-400 Hz and 1000-1200 Hz. These APD curves were superimposed on the plot for

224

each helicopter and are presented in Figures
27 through 29.
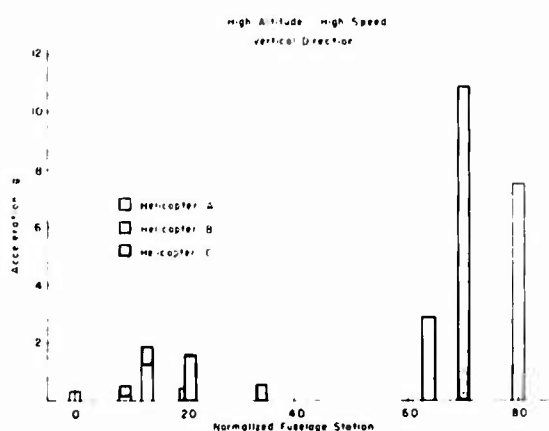
Figure 6. Spatial Distribution for High
Altitude/High Speed Flight Condition
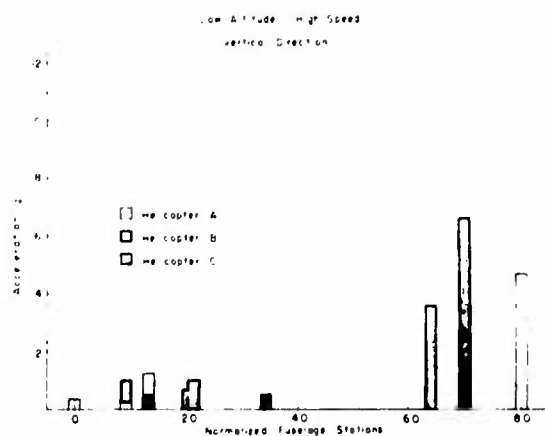
Figure 8. Spatial Distribution for Low Alti-
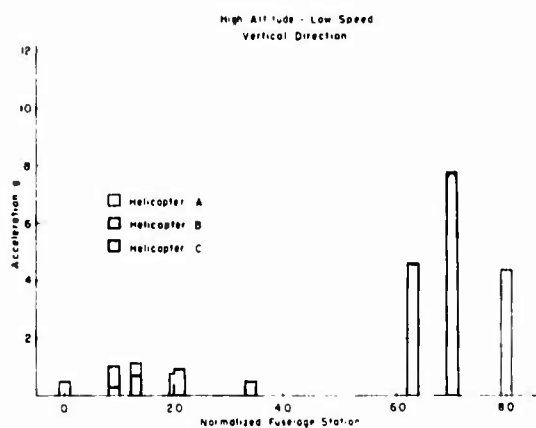tude/High Speed Flight Condition

Figure 7. Spatial Distribution for High
Altitude/Low Speed Flight Condition

Figure 9. Spatial Distribution for Low Alti-
tude Low Speed Flight Condition

The acoustic data recorded from the
microphones attached to the pilot's helmet
in each aircraft are shown in Figures 30 and
31. The graphs are maximum one-third octave
data levels recorded under the flight
conditions contained in Table III.

RESULTS

The results of this study consist of a
discussion of the figures outlined in the
Data Presentation section of this paper.

Figures 6 through 12 indicate that the
overall g-levels measured in the tailboom are
5 to 10 times higher than the g-levels meas-
ured in the nose and center section of the
three helicopters.

Figures 13 through 16 indicate little vari-
ation (less than 1.5g) in overall g-levels
(from 5 to 5KHz) measured at similar locations
in each of the three test vehicles for the
seven flight conditions considered. Figure
16, however, indicates variations of greater
magnitude (5g) measured in the tail boom. The

225
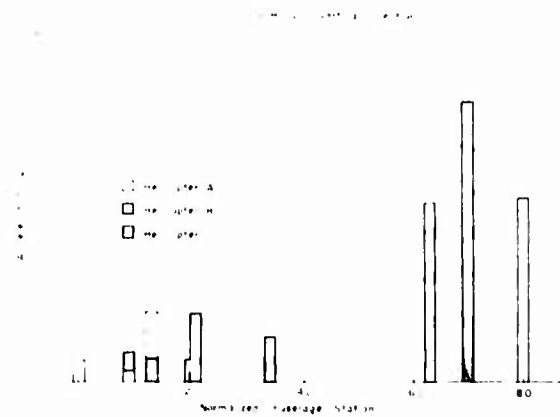
Figure 10. Spatial Distribution for Ground Runup Flight Condition
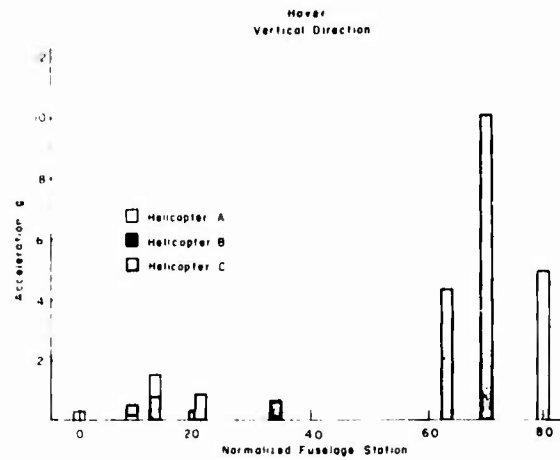
Figure 12. Spatial Distribution for Hover Flight Condition
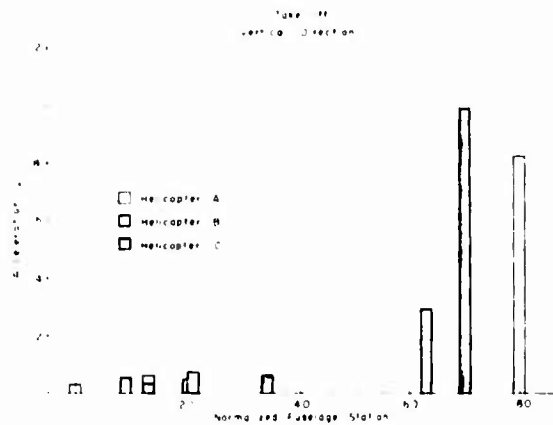
Figure 11. Spatial Distribution for Take Off Flight Condition
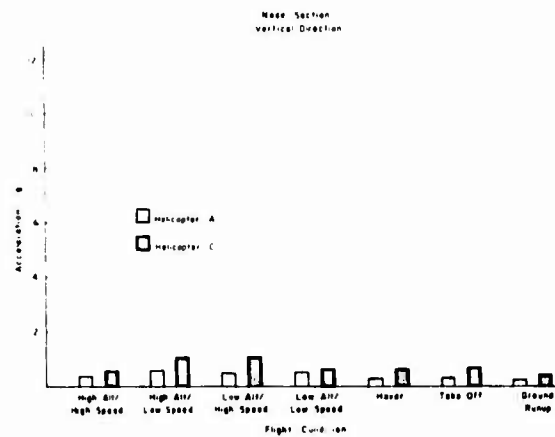
Figure 13. Helicopter Response to Selected Flight Conditions in the Nose Section

overall g-levels measured in Helicopter B are consistently higher than the overall g-levels measured in Helicopter A or C.

The vibration test curve (sinusoidal) from Ref. 1, MIL-STD-810B(1) Curve M for equipment designed for helicopter applications has been included on Figures 17-22. These figures show that in the frequency range of 5 to 500 Hz where the test curve applies, data generally fall below the test curve for all three test vehicles. However, Figures 17 and 18 contain data from Helicopter A which exceeds the test curve at frequencies between 5 and 10 Hz. Figures 19 and 20 contain data from Helicopter B which fall just below and slightly above the test curve at frequencies between 5 and 10 Hz. Figures 21 and 22 contain data from Helicopter C which exceeds

the test curve at frequencies between 5 and 35 Hz and fall only slightly below the test curve between 35 and 500 Hz. It should be noted that although the test curve does not extend beyond 500 Hz, significant levels of vibration exist up to at least 5000 Hz on all three helicopters. The maximum vibration levels measured in the main body of each of the three test vehicles is summarized in Figure 23. A recommended sinusoidal test curve for use in design and test of helicopter equipment is superimposed on Figure 23.

Typical amplitude probability density plots are shown in Figures 27 through 29. These data and a considerable amount of additional data not shown in this paper indicate a definite trend toward randomness above a frequency of
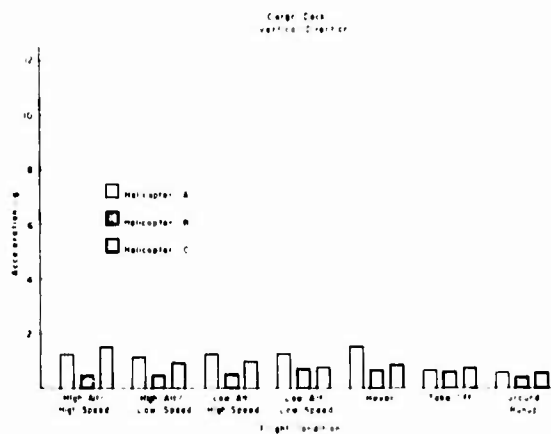
226

Figure 14. Helicopter Response to Selected Flight Conditions on the Instrument Panel

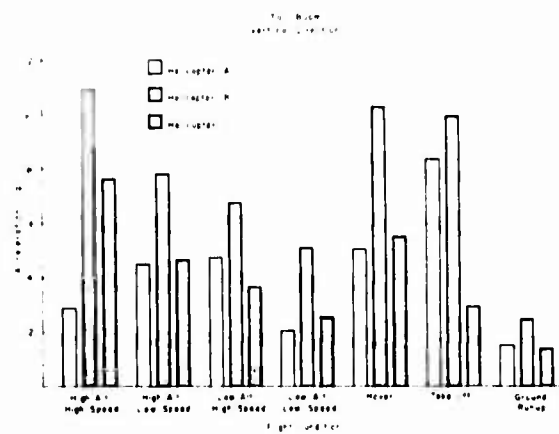Figure 15. Helicopter Response to Selected Flight Conditions in the Cargo Area

TABLE IV

APD ANALYSIS DATA - FIGURES 27-29

Heli-copter	CF-Hz	BW-Hz	St-Sec.	TC
A	11	2	400	5
A	200	10	900	5
A	1195	20	900	5
B	32	5	900	5
B	200	10	900	5
B	582	20	900	5
C	11	2	900	5
C	1000	20	1400	5

Figure 16. Helicopter Response to Selected Flight Conditions in the Tail-boom

approximately 300 Hz. The data were converted to power spectral density (PSD) and an envelope, for the maximum levels of acceleration measured, was computed. The data indicate that a PSD level of approximately 0.1 G²/Hz, over the frequency range of 300 to 5,000 Hz, would encompass the maximum levels measured. It should be noted that within the basic fuselage of the test vehicle, this envelope tends to roll off above a frequency of approximately 1,000 Hz.

During linear acceleration or deceleration from any speed to any other speed within the design flight envelope, the maximum vibration

at personnel stations in helicopters should not exceed the level specified in MIL-H-8501A, Para. 3.7.1(c), ref. 2. The specification curve is included in Figures 23 through 26 for reference. The maximum levels measured on the cabin floor of Helicopter B and C exceed the test curve in the frequency range of 30-50 Hz and 10-50 Hz, respectively as shown in Figures 25 and 26. Otherwise vibration levels fall below MIL-H-8501A requirements (as referenced).

MIL-A-8806A, Table IIIA, reference 5, lists the sound pressure level (SPL) not to be exceeded in aircraft where personnel must wear
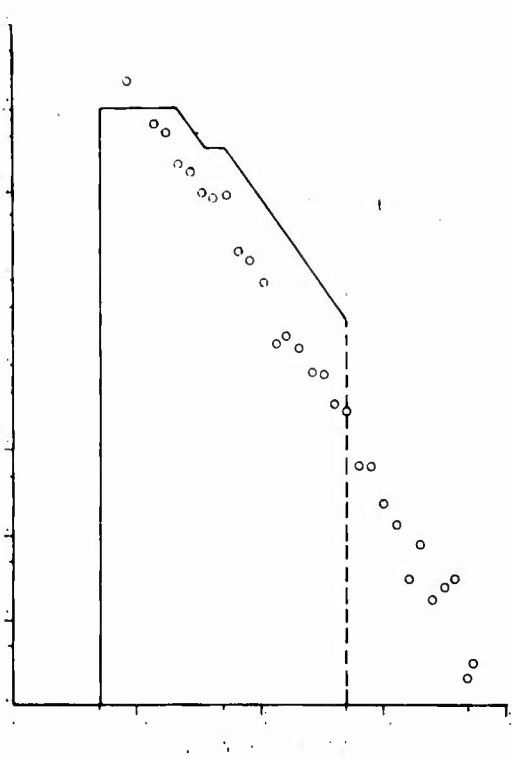
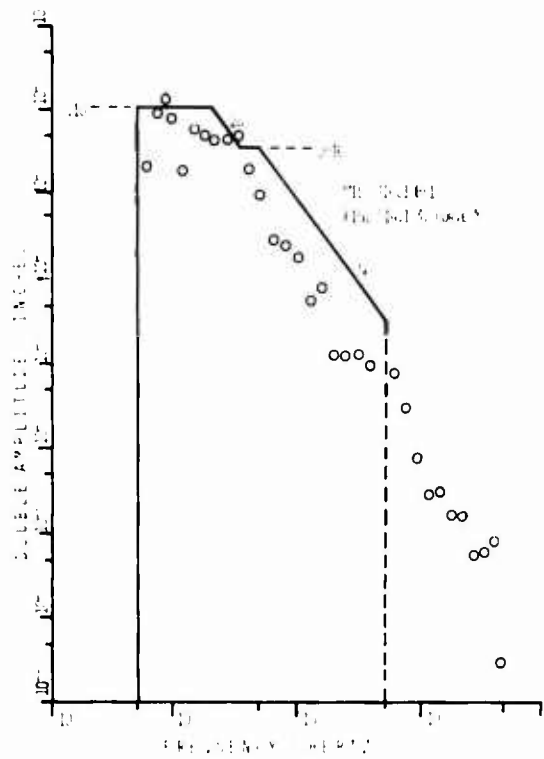Figure 17. Forward Quarter, Helicopter A

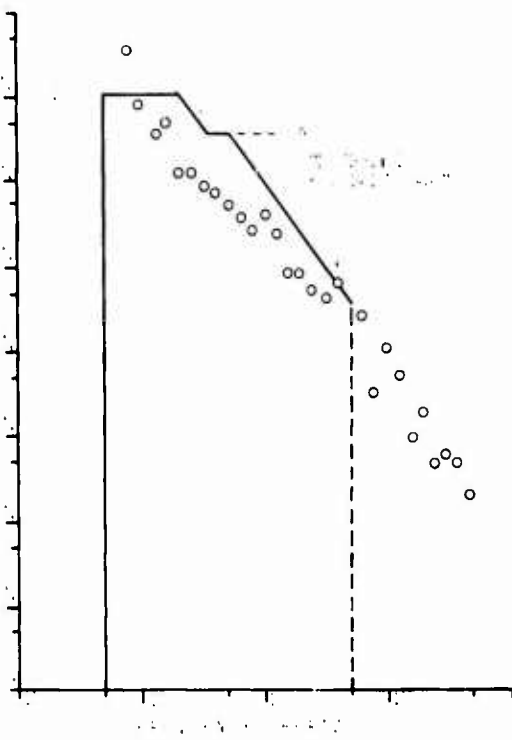Figure 19. Forward Quarter, Helicopter B

Figure 18. Center Half, Helicopter A

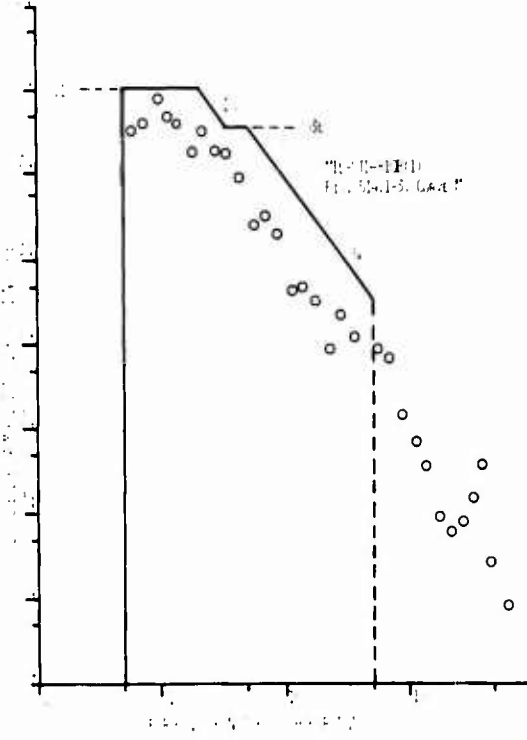Figure 20. Center Half, Helicopter B

Figure 21. Forward Quarter, Helicopter C
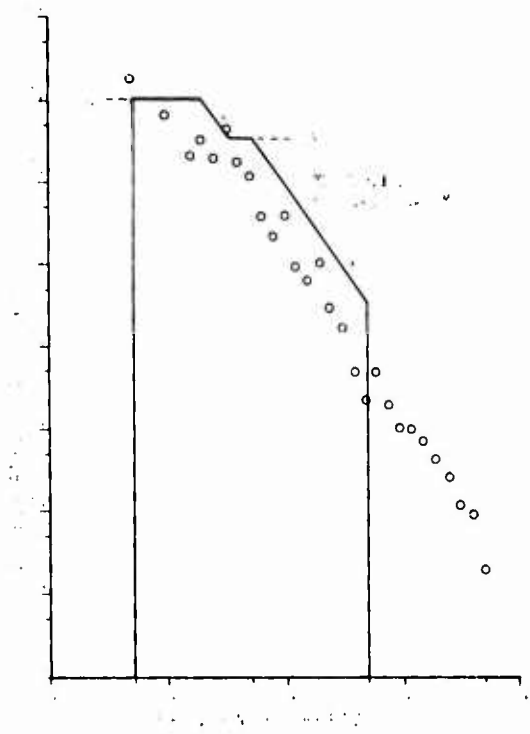

Figure 23. Summary Plot
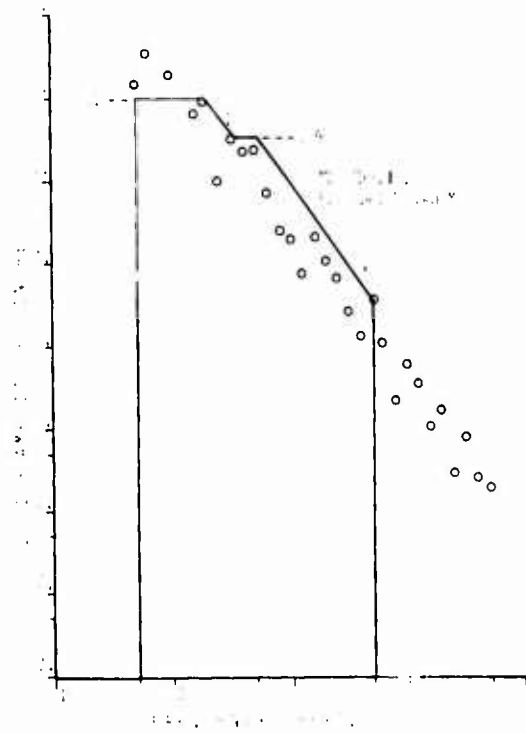

Figure 22. Center Half, Helicopter C
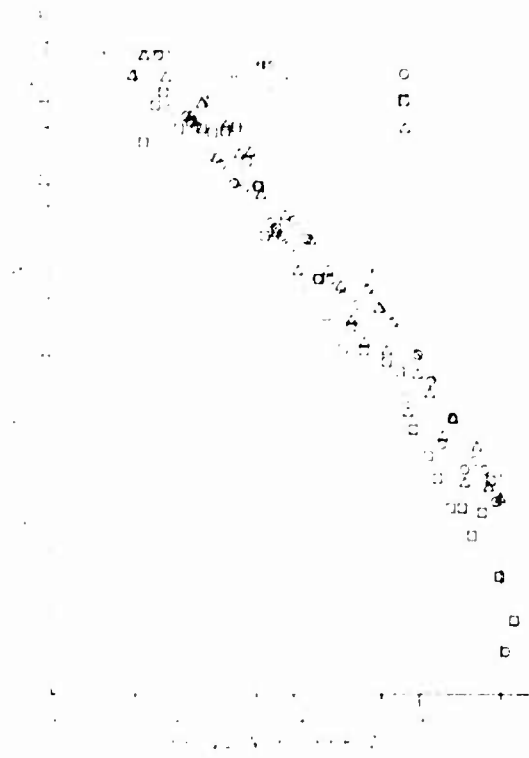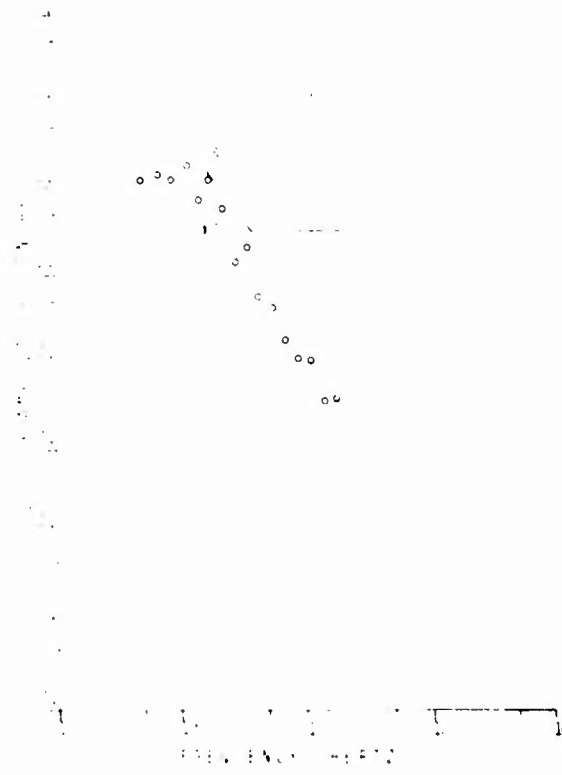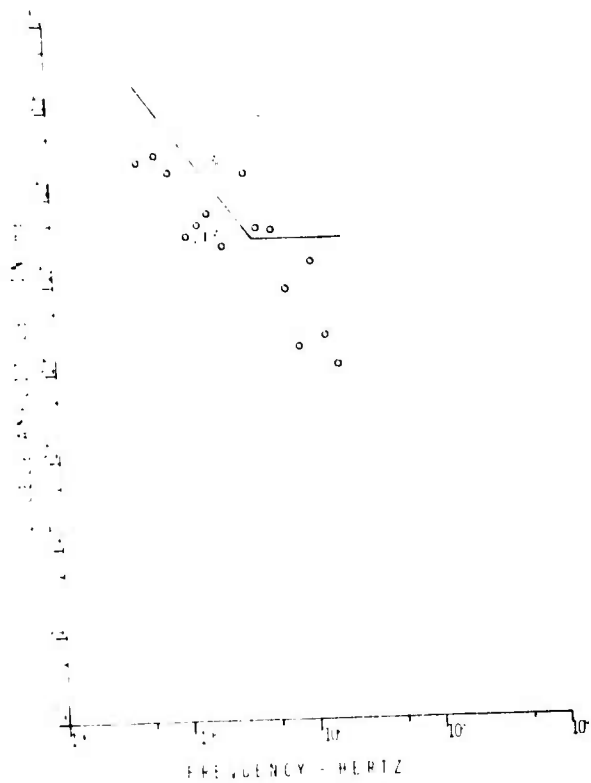

Figure 24. Low Frequency Vibratory Data, Helicopter A

229

Figure 25. Low Frequency Vibration Data, Helicopter B
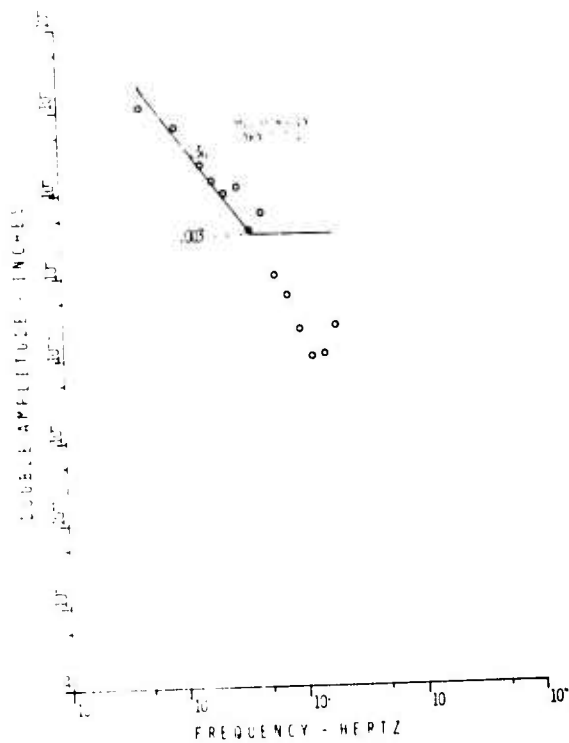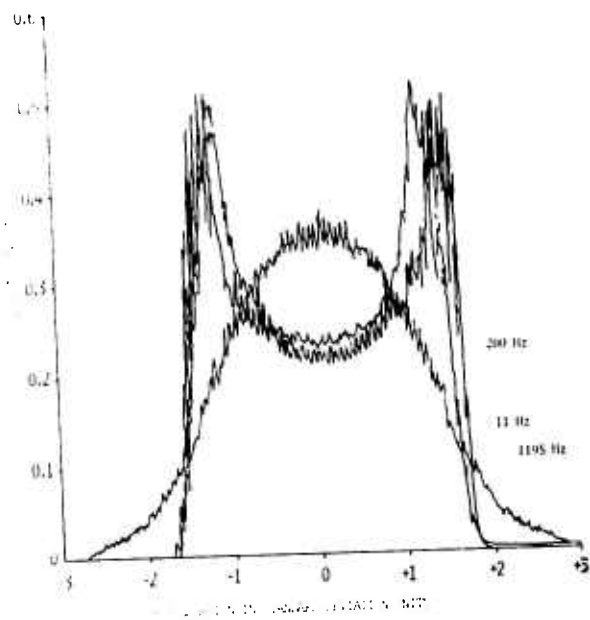

Figure 26. Low Frequency Vibratory Data, Helicopter C

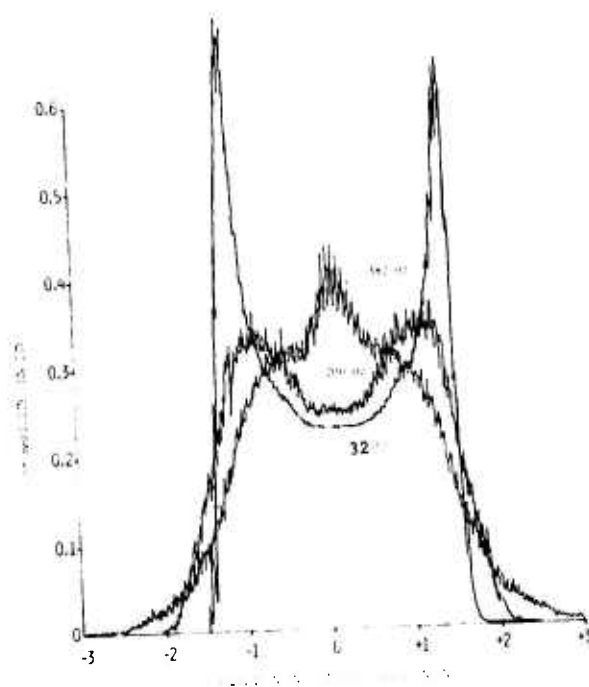Figure 27. Amplitude Probability Density Analysis, Helicopter C

Figure 28. Amplitude Probability Density Analysis, Helicopter B

helmets at all times and communicate by electronic means. For the purpose of comparison with the measured data, the specified levels were converted from octave band SPL to one-third octave band SPL and are included on Figures 30 and 31. The measured SPL for
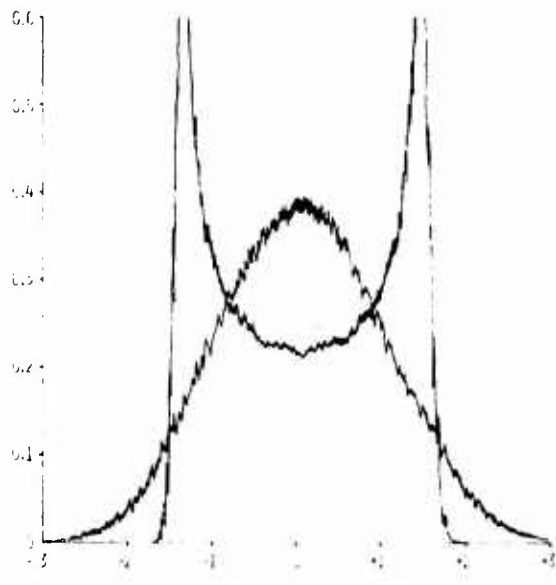
Figure 29. Amplitude Probability Density Analysis, Helicopter C
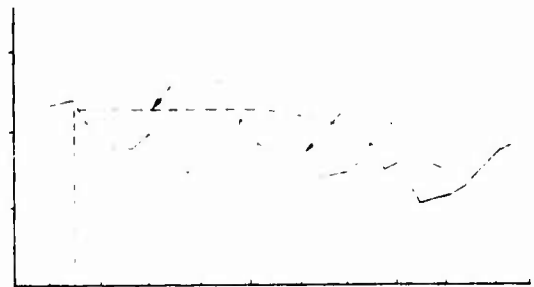

Figure 30. Noise Data, Helicopters A and B

Figure 31. Noise Data, Helicopter C

Helicopters A and C generally fall below the test curve as shown in Figures 30 and 31. The levels measured in Helicopter B exceed the test curve in frequency bands 31.5 to 400 Hz by 2 to 5 dB and as much as 12 dB in frequency bands above 1600 Hz as shown in Figure 30.

CONCLUSIONS:

1. The test level specified in MIL-STD-810B (1) Helicopter Vibration Test Curve M is inadequate for use in design and test of equipment to be located in helicopters. Measured data from this study indicate that the test curve should be changed both amplitude and frequency range. The failure to design and test helicopter equipment to the proper levels of vibration in the 5 to 10 Hz range and a complete lack of test and design criteria in the 500 to 5000 Hz range, may account for many of the equipment failures and malfunctions that now occur in field use. The following envelope curve is considered to be more realistic for use in design and test of equipment to be located in helicopters: 5-10 Hz, 0.40 in. double amplitude, and 10-28 Hz ±2g, 28-44 Hz, 0.05 in. double amplitude, and 44-5000 Hz ±5g.

2. The increase in randomness of the vibration data above 500 Hz indicates that in addition to sinusoidal vibration testing of equipment mounted in helicopters, there exists the requirement for random vibration testing in the 300 to 5000 Hz frequency range. Use of an appropriate random vibration test criteria for helicopter equipment would improve the service reliability of helicopter systems.

3. Sound pressure levels in the cockpit area of helicopters exceed levels specified in MIL-A-8806A, Table III, by 2 to 12 dB in several frequency bands. The sound pressure levels are not considered to be of a high enough magnitude to cause damage to equipment located within the helicopter fuselage. However, difficulty in communication by
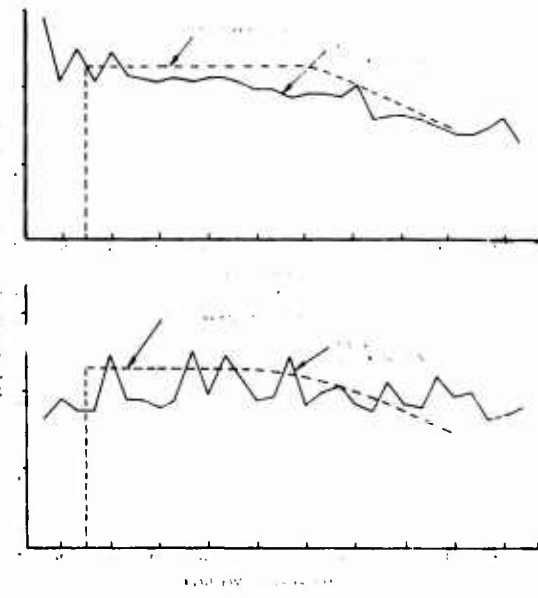
231

electronic noise will probably be encountered.
Improved analog processing might alleviate this
problem.

5. Measured data indicate that the tolerance
curves for personnel states in helicopters
MIL-A-8806A, Para 3.12.1.2 is marginal to
inadequate. Crew and/or passenger discomfort
might result from prolonged exposures.

6. In general, the variations of vibration
levels for non-structure data with flight condi-
tions are negligible compared to the vari-
ations with transducer location.

REFERENCES

1. "Military Standard Environmental Test
Methods," MIL-STD-810B, Notice-1, October 1969

2. "Military General Specification for Sound
Pressure Levels in Aircraft," MIL-A-8806A,
July 1966

3. "Helicopter Flying and Ground Handling
Qualities; General Requirements for MIL-H-
8501A," November 1961

BIBLIOGRAPHY

1. Leo L. Beranek, "Noise Reduction,"
McGraw-Hill, New York, 1960

2. R. E. Barbiere and W. Hall, "Electronic
Design's Shock and Vibration Guide for
Airborne Application," WADC Tech. Rept.
58-363, Dec. 1958

DISCUSSION

Mr. Smith (Bell Aerospace): This is a general
question aimed at the session rather than the last
speaker. I am puzzled at the need for the apparently
large amounts of analysis done on amplitude density
curves. I would have thought that in any compound
spectrum, if you know the ratio between the local sin-
usoidal part of the signal and the spectrum level in the
local one-third octave band, then you can sketch out
the amplitude density curve without going to the
trouble of doing an analysis. In any case, is there
any physical significance in the amplitude probability
density curve of a part of a compound signal? Per-
haps any or all of the previous speakers might like to
comment on that.

Mr. Thomas (AF Flight Dynamics Laboratory):
We feel it is essential, if you are going to look at
this data to define rather closely its characteristics.
This must be done to devise a specification which in
some measure will reproduce the effects, not perhaps
the environment. As to the need for looking at one-
third octave data and then at narrow band and
arriving at the conclusion that you may or may not
have random data, I would tend to disagree with you
there. If you have non-phase-correlated sinusoids
which fall within a given one-third octave, and that
is quite possible on these helicopters using one-third
octave data, it would tend to give a random distri-
bution. The object here was to eliminate that
possibility. Does that get to your point at all?

Mr. Smith: I think what you say is true but I
still think you can draw the answer without doing an
analysis.

Mr. Thomas: You may be able to do this. We
do not believe that it is quite as conclusive as
actually showing the data. The best test in my
estimation for the randomness of data is successively
narrowing the bandwidth until you get no change.
Then you know whether or not you have random data.
You may have sinusoids very closely spaced. Any
other approach to doing this would tend to indicate
randomness.

Mr. Clevenson (NASA Langley Research
Center): I would like to commend you, Mrs Bolds,
on a fine paper. You gave a wealth of information
and I am sure we are all appreciative of it. My
question pertains to the analysis in which you show
the amplitudes as a function of frequency and com-
pared them to the Mil-STD-810 specification. I
wonder what analysis you used to get all of these
amplitudes that you have shown and whether you
showed only the peak amplitude?

Mrs. Bolds: We sampled data at every 20 cycles
in the lower frequencies and we spaced them further
apart as we go up in frequency. We also measure the
data at the difference peaks in between. These data
are then run through the digital computer and we
compute acceleration, double amplitude, and so forth.
We take these data then and plot them, combining
them in frequency bands approximating one-third
octaves. That is what you see here.